

Washington University in St. Louis
Washington University Open Scholarship

All Theses and Dissertations (ETDs)

12-2-2013

Iron Isotope Cosmochemistry

Kun Wang

Washington University in St. Louis

Follow this and additional works at: <https://openscholarship.wustl.edu/etd>



Part of the [Earth Sciences Commons](#)

Recommended Citation

Wang, Kun, "Iron Isotope Cosmochemistry" (2013). *All Theses and Dissertations (ETDs)*. 1189.
<https://openscholarship.wustl.edu/etd/1189>

This Dissertation is brought to you for free and open access by Washington University Open Scholarship. It has been accepted for inclusion in All Theses and Dissertations (ETDs) by an authorized administrator of Washington University Open Scholarship. For more information, please contact digital@wumail.wustl.edu.

WASHINGTON UNIVERSITY IN ST. LOUIS

Department of Earth and Planetary Sciences

Dissertation Examination Committee:

Frédéric Moynier, Chair

Thomas J. Bernatowicz

Robert E. Criss

Bruce Fegley, Jr.

Christine Floss

Bradley L. Jolliff

Iron Isotope Cosmochemistry

by

Kun Wang

A dissertation presented to the
Graduate School of Arts and Sciences
of Washington University in
partial fulfillment of the
requirements for the degree
of Doctor of Philosophy

December 2013

St. Louis, Missouri

Copyright © 2013, Kun Wang

All rights reserved.

Table of Contents

LIST OF FIGURES	vi
LIST OF TABLES.....	ix
ACKNOWLEDGEMENTS.....	x
ABSTRACT OF THE DISSERTATION	xii
CHAPTER 1 : INTRODUCTION	1
1.1. Overview.....	2
1.2. Meteorite Classification	4
1.3. Nucleosynthesis of Iron Isotopes	9
1.4. Iron Isotope Mass-dependent Fractionation.....	12
1.5. Anion-exchange Chromatographic Separation for Iron.....	18
1.6. MC-ICP-MS Analysis for Iron Isotopes	24
Copyright and Permissions	28
References.....	29
CHAPTER 2 : ^{58}Fe AND ^{54}Cr IN EARLY SOLAR SYSTEM MATERIALS.....	33
Abstract.....	34
2.1. Introduction.....	35
2.2. Samples and Analytical Procedures.....	38
2.2.1. Sample Treatments.....	38
2.2.2. Isotopic Measurements	41
2.3. Results.....	42
2.4. Discussion	45
References.....	48
CHAPTER 3 : HOMOGENEOUS DISTRIBUTION OF FE ISOTOPES IN THE EARLY SOLAR NEBULA	51
Abstract.....	52
3.1. Introduction.....	53
3.2. Methods.....	56

3.2.1. Sample Descriptions	56
3.2.2. Sample Preparation and Chemical Purification of Fe.....	57
3.2.3. Fe Isotope Analyses	58
3.3. Results.....	61
3.4. Discussion	66
3.4.1. Fe Isotopic Homogeneity of the Early Solar Nebula	66
3.4.2. Fe Isotope Fractionation between Chondritic Components.....	67
3.5. Conclusions.....	74
References.....	75
 CHAPTER 4 : THE FE ISOTOPE COMPOSITION OF ENSTATITE METEORITES: IMPLICATIONS FOR THEIR ORIGIN AND THE METAL/SULFIDE FE ISOTOPIC FRACTIONATION FACTOR	80
Abstract	81
4.1. Introduction.....	83
4.2. Samples and Method.....	86
4.2.1. Sample Description	86
4.2.2. Analytical Methods	86
4.3. Results.....	88
4.3.1. Iron Isotope Compositions of the Whole-rock Meteorites	88
4.3.2. Iron Isotope Compositions of the Separated Mineral Phases	91
4.4. Discussion	98
4.4.1. The Homogeneous Iron Isotope Composition of Enstatite Chondrites	98
4.4.2. Implications on Bulk Earth Fe Isotope Composition.....	101
4.4.3. Iron Isotope Fractionation in EL6 Chondrites	107
4.4.4. Iron Isotope Fractionation in Enstatite Chondrite Impact Melts	111
4.4.5. Iron Isotope Fractionation in Aubrites	112
4.4.6. Iron Isotope Fractionation between Metal and Sulfide in Enstatite Meteorites....	115
4.5. Conclusions.....	119
References.....	121
 CHAPTER 5 : FE ISOTOPE FRACTIONATION IN PLANETARY CRUSTS.....	129

Abstract	130
5.1. Introduction	131
5.2. Samples and Method	134
5.2.1. Sample Descriptions	134
5.2.2. Analytical Methods	136
5.3. Results	146
5.3.1. Earth and Moon	146
5.3.2. Martian meteorites	147
5.3.3. HED Meteorites	147
5.3.4. Angrites	148
5.4. Discussion	152
5.4.1. Redox-controlled Iron Isotope Fractionation on the Angrite Parent-body	152
5.4.2. Iron Isotope Fractionation on the HED Parent-body	154
5.4.3. Iron Isotopes and Fluid-rock Interactions on Asteroidal Bodies	156
5.5. Conclusion	159
References	160
Appendix	168

CHAPTER 6 : IRON ISOTOPE FRACTIONATION DURING SULFIDE-RICH FELSIC PARTIAL MELTING ON EARLY PLANETESIMALS	170
Abstract	171
6.1. Introduction	173
6.2. Samples and Method	176
6.2.1. Sample Description	176
6.2.2. Experimental and Analytical Method	178
6.3. Results	185
6.3.1. Iron Isotope Compositions of GRA 06128/9, Brachinites and Brachinite-Like Achondrites	185
6.3.2. Iron Isotope Compositions of Metal, Sulfide and Silicate Fractions of Ordinary Chondrites	185
6.4. Discussion	188
6.4.1. Sulfide Control on Enrichment of Light Iron Isotopes in GRA 06128/9	188

6.4.2. Formation of Sulfide-rich Felsic Partial-melts in Planetesimals	189
6.4.3. Implications for Highly Siderophile Element Fractionation during Melting.....	193
6.4.4. Planetary Crust Comparisons.....	195
6.5. Conclusions.....	198
References.....	199
 CHAPTER 7 : IRON ISOTOPE FRACTIONATION DURING EVAPORATION AND THE ORIGIN OF THE NANOPHASE METALLIC IRON IN LUNAR REGOLITH	204
Abstract.....	205
7.1. Introduction.....	206
7.2. Material and Method.....	210
7.2.1. Sample Treatment	210
7.2.2. Isotopic Measurements	212
7.3. Results.....	214
7.4. Discussion	217
7.5. Conclusions.....	226
References.....	227
Appendix.....	233
 CURRICULUM VITAE.....	235
 PUBLICATION LIST	236

LIST OF FIGURES

Figure 1-1. Solar system abundance of elements.....	3
Figure 1-2. Meteorite classification diagram showing major meteorite groups	5
Figure 1-3. Iron three-isotope plots showing calculated equilibrium and kinetic fractionation lines.....	15
Figure 1-4. The mole fractions of different Fe species in HCl solutions.....	21
Figure 1-5. Distribution coefficient D increases exponentially with increasing molarity of [HCl]	23
Figure 1-6. Schematic diagram showing that the Fe stable isotopes' peaks are clearly separated from the Ar based interferences in Neptune Plus MC-ICP-MS	27
Figure 2-1. $\varepsilon^{54}\text{Cr}$ in leaching fractions from Orgueil, Murchison, and Semarkona chondrites ...	43
Figure 2-2. $\varepsilon^{54}\text{Cr}$ vs. $\varepsilon^{58}\text{Fe}$ in leaching fractions from Orgueil, Murchison, and Semarkona chondrites.....	44
Figure 2-3. Iron and chromium overabundances (defined as mass fraction, X , relative to the initial mass fraction in the star, X_i) as a function of interior mass coordinate in a 25 solar mass supernova ejecta, stellar model s25a28d	47
Figure 3-1. Photograph of the Antarctic L5 ordinary chondrite GRO 95540 broken up into five pieces using a Para-film sealed hand hammer.....	58
Figure 3-2. The bulk iron isotope compositions of the CI and ordinary chondrites from this study	60
Figure 3-3. The ranges of iron isotope compositions of CI and ordinary chondrites from this study.....	62
Figure 3-4. The ranges of iron isotope compositions of chondritic components (chondrules, matrix, CAIs and metals) and bulk chondrites	64
Figure 3-5. Cartoon showing iron isotope composition evolution in the early Solar System	70
Figure 3-6. Modeling of the bulk iron isotope compositions of ordinary chondrites by mixing chondritic components with varying chondrule type II/I ratios	71
Figure 4-1. Iron isotope compositions of all samples analyzed in this study, shown in three-isotope ($\delta^{57}\text{Fe}$ vs. $\delta^{56}\text{Fe}$) space	89
Figure 4-2. Iron isotope variations of different subgroups of enstatite meteorites	90

Figure 4-3. Iron isotope fractionation between magnetic (metal) and non-magnetic (silicate and sulfide) phases in enstatite chondrites and achondrites	92
Figure 4-4. Iron isotope variations of the different subgroups of enstatite chondrites and comparison with the iron isotope frequency distributions of previously reported terrestrial peridotites and chondrites	99
Figure 4-5. The $\delta^{56}\text{Fe}$ depth profiles of the Earth based on modeling	106
Figure 4-6. $\delta^{56}\text{Fe}$ vs. $1/\text{[Fe]}$ for (A) enstatite chondrites and (B) aubrites analyzed in this study and in the literature	109
Figure 4-7. $\Delta^{56}\text{Fe}_{(\text{metal-sulfide})}$ vs. temperature (K).....	118
Figure 5-1. Iron isotope results of the samples that were purified independently by three different purification chemistries.....	149
Figure 5-2. Mass-dependent isotope fractionation of all samples in this study, shown in a $\delta^{56}\text{Fe}$ - $\delta^{57}\text{Fe}$ space.....	150
Figure 5-3. Iron isotope compositions of martian meteorites, HEDs, and angrites	151
Figure 5-4. $\delta^{56}\text{Fe}$ vs. La, Hf, TiO_2 and $\text{FeO}_{\text{total}}/\text{MgO}$	158
Figure 6-1. Iron isotope compositions of all samples analyzed in this study, shown in three-isotope ($\delta^{57}\text{Fe}$ vs. $\delta^{56}\text{Fe}$) space	180
Figure 6-2. Iron isotope compositions for GRA 06128/9, brachinites and brachinite-like achondrites.....	186
Figure 6-3. Iron isotope compositions for magnetic (metal), non-magnetic (sulfide) and non-magnetic (silicate) fractions of three ordinary chondrites measured in this study	187
Figure 6-4. Ternary diagram showing the iron isotope compositions of melts composed of varying proportions of silicate, metal and sulfide phases from chondritic precursors	193
Figure 6-5. Average density of Fe-S-rich melts.....	194
Figure 6-6. Schematic diagram showing iron isotope fractionations in three different types of early Solar System planetary crusts.....	197
Figure 7-1. Iron isotope compositions expressed in delta notation ($\delta^{56}\text{Fe}$) relative to IRMM-014 vs. etching depth profile	211
Figure 7-2. Iron isotope compositions expressed in epsilon notation ($\varepsilon^{56}\text{Fe}$) after mass-dependent fractionation corrections	216
Figure 7-3. Solar wind Fe isotope compositions measured by spacecraft vs. Fe isotope compositions measured in lunar regolith plagioclase surface etching solutions	220

Figure 7-4. Iron isotope fractionation during thermal escape from the high-velocity-tail of Maxwell-Boltzmann distribution..... 224

Figure 7-5. The Fe isotope compositions of nanophase Fe measured in this study could be explained by fractionation during preferential thermal escape 225

LIST OF TABLES

Table 1-1. Petrologic types of chondrite groups	8
Table 1-2. Solar abundances of iron isotopes	9
Table 1-3. Certified isotopic ratios of reference material IRMM-014.....	13
Table 1-4. Mass differences of stable isotopes of selected elements	16
Table 1-5. Technical information of Bio-Rad AG 1-X8 200-400 mesh anion-exchange resin ...	18
Table 1-6. Isobar interferences of iron isotopes.....	24
Table 1-7. Positions of collectors (Faraday cups) for iron isotope analysis in MC-ICP-MS	25
Table 2-1. Iron and chromium isotope compositions of leaching meteorites	39
Table 3-1. Iron isotope compositions of CI and ordinary chondrite	65
Table 3-2. Parameters and values used in the modeling of the bulk iron isotope compositions of ordinary chondrites by mixing chondritic components	72
Table 4-1. Iron isotope compositions of enstatite meteorites.....	93
Table 4-2. Iron isotope compositions of mineral fractions of aubrites and enstatite chondrites..	96
Table 4-3. Mass-balance models of Fe isotopic compositions of the structures of the Earth....	100
Table 5-1. Iron isotope compositions of Earth/Moon rocks and martian, HED and angrite meteorites.....	139
Table 5-2. Comparison of the three iron purification chromatography protocols used in this study	145
Table 6-1. Iron isotope compositions of GRA 06128/9, brachinites and brachinite-like achondrites.....	181
Table 6-2. Iron isotope compositions of magnetic (metal), non-magnetic (sulfide) and non-magnetic (silicate) fractions of three ordinary chondrites	183
Table 6-3. The modal bulk iron isotope compositions of ordinary chondrites	184
Table 6-4. Parameters and values used in the non-modal melting modeling of ordinary chondrites.....	190
Table 6-5. Major element mixing model of GRA 06128/9	192
Table 7-1. Iron isotope compositions of etched plagioclase in Apollo 16 lunar regolith	215

ACKNOWLEDGEMENTS

This dissertation would not be possible without the genuine support of many professors, classmates, friends and family. First of all, I am especially indebted to my Ph.D. advisor Frédéric Moynier for his kind and patient mentoring throughout my four years of study and research. I really appreciate his guidance not only in matters of science, but also in professional development. I also want to thank all the other members of my Ph.D. committee for their assistance, including Profs. Thomas J. Bernatowicz, Robert E. Criss, Bruce Fegley, Jr., Christine Floss and Bradley L. Jolliff.

Thanks to my collaborators and coauthors in several papers that constitute part of this dissertation. They are Profs. Jean-Alix Barrat, Nicolas Dauphas, James Day, Randy Korotev, Frank Podosek, and Drs. Paul Craddock, Julien Foriel, Randal Paniello, Paul Savage, Corliss Sio and Ryan Zeigler, and Mr. Cole Bishop, Mr. Jean-Gabriel Fraboulet, and Ms. Charlotte Weinstein. Thanks to them for collaboration on various research projects we have successfully completed together.

I enjoyed and benefited so much from the support of my peer classmates, lab mates and friends in Washington University during my study and time in St. Louis. They are Heng Chen, Ecaterina Oana Coman, Gabrielle Coutrot, Abigail Fraeman, Pierre Haenecour, Chizu Kato, Jon Lewis, J. Garrecht Metzger, Emily Pringle, Maxwell Thiemens, Maria Valdes, Yuanyuan Wang, Teresa Wong and many others.

In addition, this dissertation and my four-years of study were financially supported by several academic institutes and agencies. Thanks to Washington University in St. Louis for a

tuition waiver and providing teaching opportunities. I would also like to thank NASA for awarding me an Earth and Space Science Fellowship (NNX12AL84H) that provided two years of financial support. I also appreciate the travel grant provided by Lunar and Planetary Institute for the 43th Lunar and Planetary Science Conference.

Last but not least, I would like to thank my parents, who raised me and provided much love in all these years. This dissertation is dedicated to them.

ABSTRACT OF THE DISSERTATION

IRON ISOTOPE COSMOCHEMISTRY

by

Kun Wang

Doctor of Philosophy in Earth and Planetary Sciences

Washington University in St. Louis, 2013

Professor Frédéric Moynier, Chair

Iron is the most abundant element in the Earth and the 4th most abundant in the crust and mantle; Fe is involved in every stage of planetary formation and differentiation. Iron isotope ratios are robust process tracers used to understand the origin of the Solar System, planetary formation, and differentiation processes such as the moon-forming giant impact, core-mantle segregation, and crust formation. In this dissertation, I report the most complete dataset of high-precision iron isotope compositions of a wide range of extraterrestrial samples including carbonaceous, ordinary, and enstatite chondrites, aubrites, brachinites, HED meteorites (howardites, eucrites and diogenites), martian meteorites, angrites, lunar meteorites, lunar regolith and ungrouped meteorites. I discuss iron isotope fractionations among these extraterrestrial materials in term of solar nebular processing, asteroidal parent-body processing, planetary differentiation (core-mantle differentiation and crust formation), magmatism, and planetary surface processing.

In Chapter 1, I introduce some basic knowledge about the meteorites and lunar samples, which comprise the research objectives in following chapters. In addition, the general concepts

of the nucleosynthesis of Fe isotopes and mass-dependent Fe isotope fractionation mechanisms are also discussed. At last, I review the technique of high precision isotopic analyses of iron using anion-exchange chromatography and MC-ICP-MS.

In Chapter 2, I focus on the non-mass-dependent fractionation of Fe isotopes and examine the possible isotopic anomalies in some of the oldest meteorites in the Solar System, which could help in understanding the stellar building blocks of our Solar System. The solar nebula was made of materials from the nucleosynthesis of older generation stars. The solar nebula was initially thought to have been chemically and isotopically well mixed. However, since late 1960s, isotopic anomalies have been observed in both bulk meteorite and mineral scales. These isotopic anomalies are relic signals of the original building blocks of our Solar System, surviving from the mixing of early solar nebula. With the instrumental advances such as the application of MC-ICP-MS, smaller and smaller scale isotopic anomalies can be identified in meteorite samples. By looking at these anomalies, we could acquire information about the original building blocks of our Solar System. I reexamined the ^{54}Cr anomalies (discovered in the 1980s and for which the origin is still debated) by investigating the collateral effects on ^{58}Fe nuclide. These neutron-rich nuclides are expected to be produced together in Type II supernovae or Type Ia supernovae. Even though these ^{54}Cr anomalies have been long observed, the carrier phases and the stellar origin had not been identified until our research. By measuring ^{58}Fe , I put constraints on the nucleosynthetic origins (most probably Type II supernovae).

From Chapter 3 to 7, I emphasize mass-dependent fractionations of Fe isotopes. First, in Chapter 3, I present the most complete Fe isotope dataset of CI chondrites using large sample masses (~ 1 g). CI chondrites have been recognized as the meteorite group whose composition resembles the (non-volatile elemental) bulk composition of the solar nebula. The Fe isotope

compositions of five different stones of Orgueil, one of Ivuna and one of Alais are highly homogeneous. I propose that this average represents the best estimate of bulk Fe isotope composition of our Solar System, and that the homogeneity of CI chondrites reflects the initial Fe isotopic homogeneity of the well-mixed solar nebula. In contrast, larger Fe isotopic variations have been found between separate ~1g pieces of the same ordinary chondrite samples. As shown in the mass-balance calculation in the paper, the Fe isotopic heterogeneities in ordinary chondrites are controlled by the abundances of chondritic components, specifically chondrules, whose Fe isotope compositions have been fractionated by evaporation and re-condensation during multiple heating events. Due to this Fe isotopic heterogeneity exhibited in ordinary chondrites, caution should be taken when interpreting the Fe isotope data from small masses of samples.

In Chapter 4, I report the most comprehensive Fe isotope database for the enstatite meteorite group (EH, EL, aubrite-main group and Shallowater). In addition to bulk samples, I also analyzed mineral phases separated from enstatite meteorites to assess the Fe isotope budget of the metal/silicate/sulfide components of enstatite meteorite parent bodies and, more generally, to estimate the Fe isotopic fractionation between metal and sulphide that can be applied to any type of material. I find that all enstatite chondrites (with the exception of EL6) have the same Fe isotopic composition, which is identical with that of the carbonaceous and ordinary chondrites. Relatively larger Fe isotopic fractionation in EL6 chondrites and aubrite achondrites are discussed in terms of the origins of these meteorites with metal/sulfide/silicate differentiation. Finally, I provide a new estimate of the Fe isotopic fractionation factor between metal and sulfide at the equilibrium temperature range of aubrites, which agrees well with the theoretical equilibrium fractionation between Fe-metal and troilite reported previously.

In Chapter 5, I investigate the Fe isotope compositions of the crustal materials from several planets or asteroidal bodies, including the Moon, Mars, 4 Vesta, and the angrite parent-body. The Earth-Moon system is widely accepted to have formed in the aftermath of the Giant Impact event, and the elevated Fe isotope composition of lunar rocks when compared to chondrites was once proposed as the first isotopic evidence of the Giant Impact. However, my studies on these planetary crusts have shown that the Moon and the Earth are not the only planetary system having heavier Fe isotope compositions compared to chondrites. These isotopic fractionations shown in planetary crusts are more likely to be formed during magmatic processes, such as fractional crystallization or partial melting controlled by oxygen fugacities, instead of previously proposed evaporative fractionation during the Giant Impact.

In Chapter 6, I study the Fe isotope compositions of Graves Nunataks (GRA) 06128 and 06129, the oldest felsic crustal material known in the Solar System, and brachinites, a group of ultramafic meteorites genetically linked with GRA. The formation of felsic continental crust on the Earth is closely associated with plate tectonics and is unique among all known Solar System materials. However, the recent identification of meteorites GRA 06128/9 as evolved felsic crustal materials has challenged the canonical view that the earliest planetary crusts were dominantly basaltic in composition. Here, I show that GRA meteorites are isotopically different from the terrestrial continental crust. I then propose that GRA meteorites were formed as Fe -S-rich felsic melts by preferential melting of sulfides during partial melting of precursor chondritic source materials. The proposed origin for GRA therefore contrasts strongly with the continental crust formation on Earth and represents a paradigm shift in our understanding of felsic crust formation in the absence of plate tectonics and even before core formation in the early Solar System history.

In Chapter 7, I examine the Fe isotope fractionation during evaporation and the formation mechanism of the nanophase metallic iron widely observed in lunar regolith. All planetary bodies are under continuous bombardment by cosmic ray radiation, solar wind sputtering, and meteorite impacts. For those planetary bodies that lack protective atmospheres, these bombardments could alter the optical features of their surface in a process called space weathering. Two leading theories have been proposed to explain the nanophase metallic iron formed by space weathering: (1) the solar wind reduction model, and (2) the vapor recondensation model. I implemented stepwise leaching experiments on Apollo regolith and have successfully isolated the isotopic signature of nanophase metallic iron on the surface of minerals. My results provide strong isotopic support for the vapor recondensation model and further reveal the isotopic effect of the space weathering mechanism.

CHAPTER 1 : INTRODUCTION

1.1. Overview

Meteorite research is important for us in understanding the origin of the Solar System and the formation of the Earth. The chemical and isotopic compositions of the Solar System and the Earth provide us a fundamental reference for planetary comparison. Primitive (undifferentiated) meteorites, especially CI carbonaceous chondrites, have the closest chemical composition (with the exception of some volatile elements such as H, C, N, O and noble gases) to the solar photosphere (Anders and Grevesse, 1989). Since the Sun comprises 99.9% of the mass of our Solar System, primitive meteorites are the best available samples to estimate the bulk elemental and isotopic composition of our Solar System. In addition, differentiated meteorites (from the Moon, Mars, 4-Vesta and other asteroids) represent direct samples from planetary bodies other than the Earth. These extraterrestrial materials were formed under a wide range of temperatures, pressures and redox conditions. They are valuable samples for us to understand the physical and chemical conditions during the formation and differentiation of terrestrial planets. Meteorite samples, either primitive or differentiated, provide valuable samplings of different stages of inner Solar System evolution.

In the past decade, the development of MC-ICP-MS has allowed high precision isotopic measurements (<100 ppm per atomic mass unit) of “non-traditional” stable isotopes (*e.g.*, Fe, Ni, Cu and Zn) to be possible. With this improvement in the analytical technique, small but distinct isotopic variations of Fe among Solar System materials have been widely observed (*e.g.*, Poitrasson et al., 2004; Weyer et al., 2005; Schoenberg et al., 2006; Dauphas et al., 2009a). Iron is the ninth most abundant element in the Solar System (see Figure 1-1), and the second most abundant one in terrestrial planets. Iron acts like a siderophile (metal-loving), lithophile (rock-loving) and chalcophile (sulfur-loving) element and is widely involved in the processes of

planetary formation, core-mantle differentiation and crust evolution. The isotopic variability of Fe among Solar System materials results from a number of processes, such as 1) stellar nucleosynthesis or early solar activity; 2) cosmic ray spallation; and 3) mass-dependent fractionation mechanisms either during nebular processing or during planetary differentiation (Moon-forming Giant Impact, core-mantle segregation or magmatic differentiation). Studies of these isotopic fractionations can help to reveal the processes producing these variations and indicate the history and conditions during the formation of the Solar System and planets.

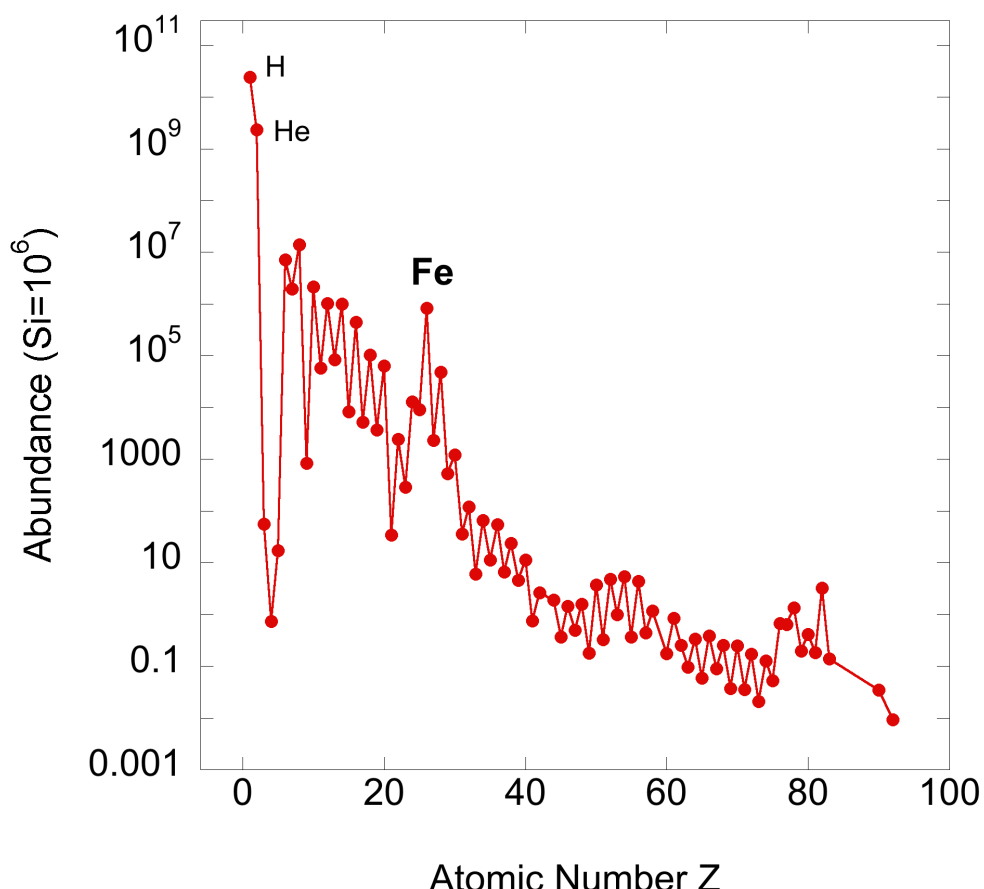


Figure 1-1. Solar system abundance of elements (Lodders, 2003).

1.2. Meteorite Classification

According to The Meteoritical Society's Meteoritical Bulletin Database, 46,323 verified meteorites have been found on the Earth (as of September, 2013). More than a century of studies on meteorites have provided an enormous amount of information about the formation and evolution of the Solar System at various spatial and temporal scales. This dissertation study of iron isotope cosmochemistry has greatly benefited from many of these previous meteorites studies. Here, I give a brief summary of the basic knowledge of meteorites. The detailed descriptions of specific meteorites used in this dissertation research are provided in corresponding chapters (marked in **bold** letters).

As shown in Figure 1-2, meteorites can be divided into two major categories based on their bulk composition and texture (Weisberg et al., 2006): undifferentiated meteorites (chondrites) and differentiated meteorites. Some meteorites have chondritic bulk composition but igneous textures similar to differentiated meteorites. They are categorized as primitive achondrites, and are independent from either chondrites or differentiated meteorites.

Chondrites (undifferentiated meteorites) are those meteorites that have the closest composition to the Sun, and formed from asteroids/comets which did not experience igneous differentiation (Weisberg et al., 2006). Chondrites are named because of the typically millimeter-sized spheres (chondrules) observed in most of them. Chondrites include three major classes: carbonaceous (see **Chapters 2 and 3**), ordinary (see **Chapters 2 and 3**) and enstatite chondrites (see **Chapter 4**). These three chondrite classes can be further divided into 14 chondrite groups (Krot et al., 2007): carbonaceous (CI, CM, CB, CO, CV, CK, CR and CH), ordinary (LL, L and H), enstatite (EL and EH) and R-K chondrites.

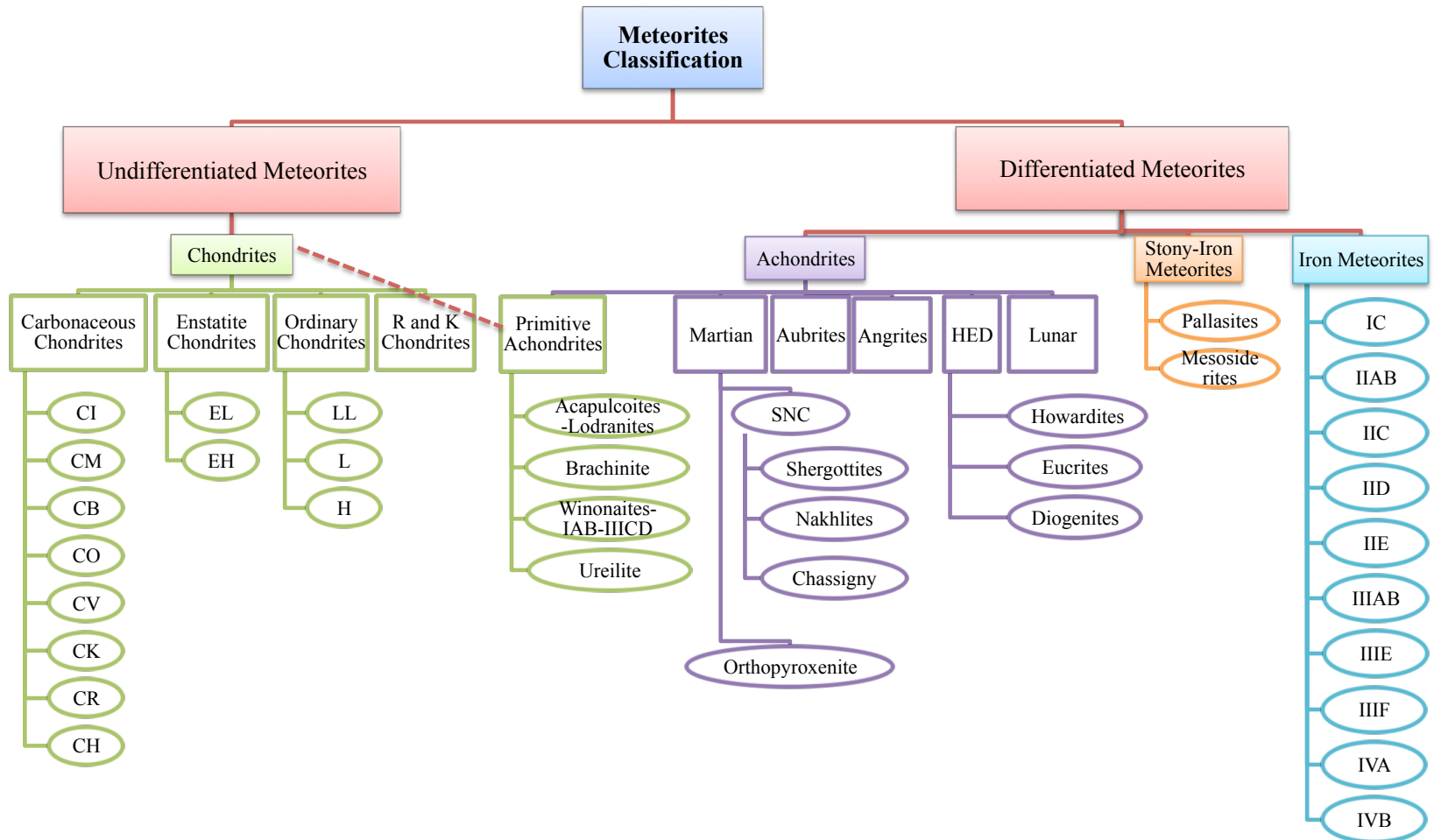


Figure 1-2. Meteorite classification diagram showing major meteorite groups.

Differentiated meteorites are those meteorites exhibiting textures of partial or complete melting, and they are from asteroids or planets that have chemically differentiated into core, mantle and crust. Differentiated meteorites actually comprise three kinds of chemically different meteorites: (stony) achondrites, stony-iron meteorites and iron meteorites. Achondrites include angrites (see **Chapter 5**), aubrites (see **Chapter 4**), HED meteorites (see **Chapters 5**), martian meteorites (see **Chapter 5**) and lunar meteorites (see **Chapter 5**). In addition to lunar meteorites, six U.S. Apollo and three Soviet Luna programs have collected and brought back 382 kg of lunar rock and soil samples (Hiesinger and Head, 2006). These Apollo samples are discussed in **Chapter 7**. Because of their high Fe concentration, the stony-iron and iron meteorites are among the first samples thoroughly examined by many previous Fe isotope studies (Zhu et al., 2001; Zhu et al., 2002; Weyer et al., 2005; Poitrasson et al., 2005; Schoenberg and von Blanckenburg, 2006; Williams et al., 2006; Moynier et al., 2007). These frequently studied types are hence not covered in this dissertation.

Primitive achondrites are those meteorites having bulk compositions similar to chondrites but exhibiting igneous textures. Primitive achondrites include acapulcoites-lodranites, brachinites (see **Chapter 6**), ureilite, winonaites, and silicate inclusions in IAB and IIICD iron (Weisberg et al., 2006). They are probably formed by ultra-metamorphism of chondrites or residues of very-low-degree partial melting (Krot et al., 2007).

Common descriptive parameters of meteorites used in this dissertation are explained here:

Falls/finds: *Falls* are those meteorites being observed falling through the atmosphere and recovered shortly after landing; while *finds* are those discovered without definitive observations

of falling (Hutchison, 2007; Krot et al., 2007). Only ~2% of meteorites in the world are observed *falls* according to the statistics of Meteoritical Bulletin Database (as of September, 2013). The “freshness” of meteorites is important to the meteorite studies. The possibility of terrestrial contamination and weathering effects need to be carefully examined for many *finds*.

Petrologic type: a secondary classification scheme first defined by van Schmus and Wood (1967) has been widely used to describe the textural and mineralogical properties of chondrites. The scales vary from 1 to 6, with 3 as the most primitive (unequilibrated) type. From type 2 to 1, the degree of low-temperature aqueous alteration increases; while from type 4 to 6, the degree of thermal metamorphism and chemical equilibrium escalates. Table 1-1 shows the petrologic type for each chondrite group (Weisberg et al., 2006). Generally speaking, CI, CM and CR chondrites are all aqueously altered (types 1 to 2), while other types of chondrites are more inclined to have been subjected to thermal alterations (types 4 to 6). Unequilibrated type 3 ordinary chondrites (and CV and CO chondrites in some cases) can be further assigned to subtypes between 3.0 to 3.9 based on their sensitivity to induced thermoluminescence (Sears et al., 1980). For example, Semarkona is LL3.0.

Shock metamorphism stage: In addition to the petrologic type, the degree of shock metamorphism is a tertiary classification scheme for ordinary and enstatite chondrites (Stöffler et al., 1991; Rubin et al., 1997). This scheme varies from S1 (unshocked) to S6 (very strongly shocked) based on the shock effects observed in minerals such as olivine, pyroxene and plagioclase.

Degree of terrestrial weathering: For meteorite *finds*, it is useful to indicate semi-quantitatively the degree of terrestrial weathering. Two classification schemes are widely used

and also adopted in this dissertation. Weathering index A, B or C represents “minor”, “moderate” or “severe” rustiness, respectively. An additional letter “e” represents evaporite minerals visible. This scheme is mainly used for hand specimens for Antarctic meteorites. In general, for thin-section samples of meteorites, the weathering scale W0 (fresh) to W6 (most weathered) is applied, based on the oxidation of metals, sulfides and silicates (Wlotzka, 1993). The weathering properties of meteorites are important to the research of Fe isotopes, since terrestrial weathering effects on Fe isotopic fractionation have been recognized among those highly weathered *finds* (Saunier et al., 2010).

Table 1-1. Petrologic types of chondrite groups

Types	1	2	3	4	5	6
	Aqueous alteration	←	Pristine	→	→	Thermal metamorphism
CI	✓					
CM	✓	✓				
CB			✓			
CO			✓			
CV			✓			
CK			✓	✓	✓	✓
CR	✓	✓				
CH			✓			
EL			✓	✓	✓	✓
EH			✓	✓	✓	✓
LL			✓	✓	✓	✓
L			✓	✓	✓	✓
H			✓	✓	✓	✓
R			✓	✓	✓	✓
K			✓			

After Weisberg (2006)

1.3. Nucleosynthesis of Iron Isotopes

Isotopes are nuclides which have the same number of protons, but different numbers of neutrons. Except H and He, which formed mostly by Big Bang nucleosynthesis, all other elements including iron have their isotopes formed during various stellar nucleosynthesis processes. Iron has four stable isotopes (^{54}Fe , ^{56}Fe , ^{57}Fe and ^{58}Fe) and one notable extinct radioactive isotope (^{60}Fe). The solar abundances and physical properties of the iron isotopes are listed in Table 1-2.

Table 1-2. Solar abundances of iron isotopes

Isotope	Mass ^a	Half-life (decay product) ^b	Solar percent ^a	Solar abundance per 10^6 Si Atoms ^b
^{54}Fe	53.9396147	Stable	5.845	5.22×10^4
^{56}Fe	55.9349418	Stable	91.754	8.25×10^5
^{57}Fe	56.9353983	Stable	2.119	1.98×10^4
^{58}Fe	57.9332801	Stable	0.282	2520
^{60}Fe		1.49 Ma (^{60}Ni)	extinct	extinct

^a in a.m.u. (atomic mass unit). Data from de Laeter et al. (2003);

^b Data from Clayton (2003).

^{54}Fe is the 2nd most abundant isotope of iron (5.845% of all Fe in solar abundance), and 21st most abundant nuclide in the universe (Clayton, 2003). The solar abundance of ^{54}Fe is the result of the mixing from two sources (Clayton, 2003): the quasi-equilibrium established during explosive silicon burning (higher $^{54}\text{Fe}/^{56}\text{Fe}$ ratio than the solar ratio) and the quasi-equilibrium formed during alpha-rich freezeout (lower $^{54}\text{Fe}/^{56}\text{Fe}$ ratio than the solar ratio).

^{56}Fe is not only the most abundant isotope of iron (91.754% of all Fe in solar abundance), but also the 10th most abundant nucleus in the universe (Clayton, 2003). ^{56}Fe exhibits significantly higher abundance than the adjacent nuclides, a phenomenon commonly recognized

as “iron peak” (see Figure 1-1). ^{56}Fe has very high binding energy per nucleon, close to the maximum binding energy of ^{62}Ni (Pagel, 2009). ^{56}Fe is the decay product of ^{56}Co (half life=77.2 days), which itself decayed from ^{56}Ni (half life=6.077 days). ^{56}Ni is synthesized through the quasi-equilibrium transmutation (net reaction: $^{28}\text{Si} + ^{28}\text{Si} \rightarrow ^{56}\text{Ni}$) established by either explosive silicon burning or alpha-rich freezeout during either thermonuclear explosions of accreting white dwarfs (Type Ia supernova) or Type II core collapse supernova (Clayton, 2003). These two sources provided comparable amounts of ^{56}Fe in our Solar System.

^{57}Fe is the 3rd most abundant isotope of iron (2.119% of all Fe in solar abundance) and ranks the 27th most abundant in the universe (Clayton, 2003). It is primarily the decay product of ^{57}Co (half life=272 days), which decayed from ^{57}Ni (half life=35.6 hours). ^{57}Ni is synthesized together with ^{56}Ni by silicon burning or alpha-rich freezeout during either Type Ia or Type II supernova (Clayton, 2003). Similar to ^{56}Fe , both Type Ia and Type II supernova contributed comparable amounts of ^{57}Fe to our Solar System. Other than these two major sources of ^{57}Fe , the *s-process* $^{56}\text{Fe}(n, \gamma)^{57}\text{Fe}$ in neutron-rich environments could form limited amounts of ^{57}Fe . This process doesn’t contribute significantly to the solar abundance; however it is important for explaining the higher $^{57}\text{Fe}/^{56}\text{Fe}$ ratios observed in presolar grains from AGB stars (Marhas et al., 2008; Floss et al., 2012; Ong et al., 2012; Trappitsch et al., 2012; Ong and Floss, 2013).

^{58}Fe is the least abundant isotope of iron (0.282% of all Fe in solar abundance) and ranks the 39th most abundant in the universe (Clayton, 2003). Approximately two-thirds of ^{58}Fe is formed by the neutron capture of existing ^{56}Fe and ^{57}Fe , and one-third by equilibrium processes of stellar nucleosynthesis (Clayton, 2003). Like ^{57}Fe , the neutron-rich isotope ^{58}Fe is also an interesting subject for the study of the *s-process* in presolar grains. However, owing to the

extremely low abundance of ^{58}Fe , the precise measurement is still challenging (*e.g.*, Ong and Floss, 2013).

^{60}Fe is an extinct short-lived radioactive isotope (half life=1.49 Myr) which decays to its daughter nucleus ^{60}Ni . The ^{60}Fe nucleus is formed either by the neutron capture of previously formed lighter Fe isotopes or by a rare neutron-rich equilibrium process of stellar nucleosynthesis (Clayton, 2003). ^{60}Fe has been a research focus by many studies due to its ability to possibly test the supernova trigger hypothesis of the origin of the Solar System (Wasserburg et al., 1998). The Tang and Dauphas' (2012) recent study has shown that no ^{60}Ni excesses have been observed, and they concluded that ^{60}Fe was homogeneously distributed in the early Solar System.

1.4. Iron Isotope Mass-dependent Fractionation

Isotope fractionation means the unequal distribution of two or more isotopes of an element between two reservoirs, and is the enrichment or depletion of one isotope relative to another due to chemical or physical processes. The basic principles of isotope fractionation have been long established by Bigeleisen, Mayer, and Urey during the gilded age of isotope discovery in the early and middle 20th century. Isotope geochemists have since been applying these principles and rules to isotope systems such as H, C, N, O, and S, but have recently extended them to uncharted waters, including Fe and other non-traditional transition metal isotopes. The isotope fractionation of Fe, resulting in the variation of isotope abundances observed in many extraterrestrial materials studied in this dissertation, is governed by these principles and rules. Here, I will give a brief summary of the essential concepts and principles closely related to this study. More detailed theoretical discussions can be found in previous works (*e.g.*, Criss, 1999; Schauble, 2004).

Isotopic ratio (R): The ratio of the numbers of two isotopes in one unique species, for example,

$$R^{56/54} = \frac{^{56}\text{Fe}}{^{54}\text{Fe}} \quad \text{Eq.1-1}$$

Isotope fractionation factor (α): the isotopic ratio of two isotopes in species A divided by the isotopic ratio in species B, which is

$$\alpha_{A-B}^{56/54} = \frac{R_A^{56/54}}{R_B^{56/54}} \quad \text{Eq.1-2}$$

The delta value (δ): the deviation from a standard, which is commonly used to represent an isotope composition. The delta value is used in isotope geochemistry because it is relatively easier to determine the difference between samples and standards than to determine the absolute value of isotopic ratios. Because the fractionation is usually very small, the unit of the delta value is per mil (‰), which is one part per thousand. $\delta^{56}\text{Fe}$, $\delta^{57}\text{Fe}$ and $\delta^{58}\text{Fe}$ are used in this dissertation, and are defined as,

$$\delta^x\text{Fe} = \left[\frac{\left({}^x\text{Fe} / {}^{54}\text{Fe} \right)_{\text{sample}}}{\left({}^x\text{Fe} / {}^{54}\text{Fe} \right)_{\text{standard}}} - 1 \right] \times 1000 \quad \text{Eq.1-3}$$

In the above equation $x=56$, 57 or 58 and IRMM-014 is the standard. IRMM-014 is made of 99.99% pure metallic iron. It is an isotopic reference provided by the Institute for Reference Materials and Measurements (Table 1-3) and has been used as the standard for Fe isotope studies by most of the laboratories in the world (Beard and Johnson, 2004).

Table 1-3. Certified isotopic ratios of reference material IRMM-014

<i>Isotopic ratio</i>	<i>Value</i>
${}^{56}\text{Fe} / {}^{54}\text{Fe}$	15.69859
${}^{57}\text{Fe} / {}^{54}\text{Fe}$	0.362575
${}^{58}\text{Fe} / {}^{54}\text{Fe}$	0.048210

Data from Institute for Reference Materials and Measurements.

Mass-dependent fractionation: The magnitude of isotope fractionation depends on the relative mass differences among different isotopes of one element. Hence, they are large for light elements such as H, C, N and O (see Table 1-4). It was traditionally thought that Fe and other transition metal isotopes are too heavy to fractionate at a resolvable level, and it was difficult, if not impossible, to detect using analytical techniques prior to MC-ICP-MS. All *equilibrium isotope fractionations* and *many kinetic isotope fractionations* are mass-dependent fractionations.

Equilibrium fractionation is the isotope exchange between species in thermodynamic equilibrium. Kinetic fractionation is defined as the isotope fractionation during fast, incomplete and unidirectional physicochemical processes such as evaporation, diffusion and many biological reactions (Hoefs, 2009). Equilibrium and kinetic isotope fractionation are governed by different fractionation laws (*e.g.*, Criss, 1999; Young et al., 2002):

$$\alpha_{57/54} = \alpha_{56/54}^\beta \quad \text{Eq.1-4}$$

$$\text{For equilibrium fractionation: } \beta = \frac{1/m_{54} - 1/m_{57}}{1/m_{54} - 1/m_{56}} = 1.475 \quad \text{Eq.1-5}$$

$$\text{For kinetic fractionation: } \beta = \frac{\ln\left(\frac{m_{54}}{m_{57}}\right)}{\ln\left(\frac{m_{54}}{m_{56}}\right)} = 1.488 \quad \text{Eq.1-6}$$

Figure 1-3 shows these two equilibrium and kinetic fractionation curves on a plot of ^{57}Fe against ^{56}Fe . All the meteorite data acquired in this dissertation research have also been plotted in Figure 1-3 (A). Since the fractionations among all the meteorite samples in this dissertation are very small ($\delta^{56}\text{Fe} \sim -0.338$ to $0.240\text{\textperthousand}$), the equilibrium and kinetic fractionation curves cannot be distinguished within the current analytical uncertainties. Figure 1-3 (B) plots the meteorite sample with the largest fractionation ever reported (Mullane et al., 2005); however, it is still too small to distinguish equilibrium from kinetic fractionation effects. Only fractionation larger than 5\textperthousand can effectively distinguish the two mass-dependent fractionation effects at our present level of precision as shown in Figure 1-3 (C).

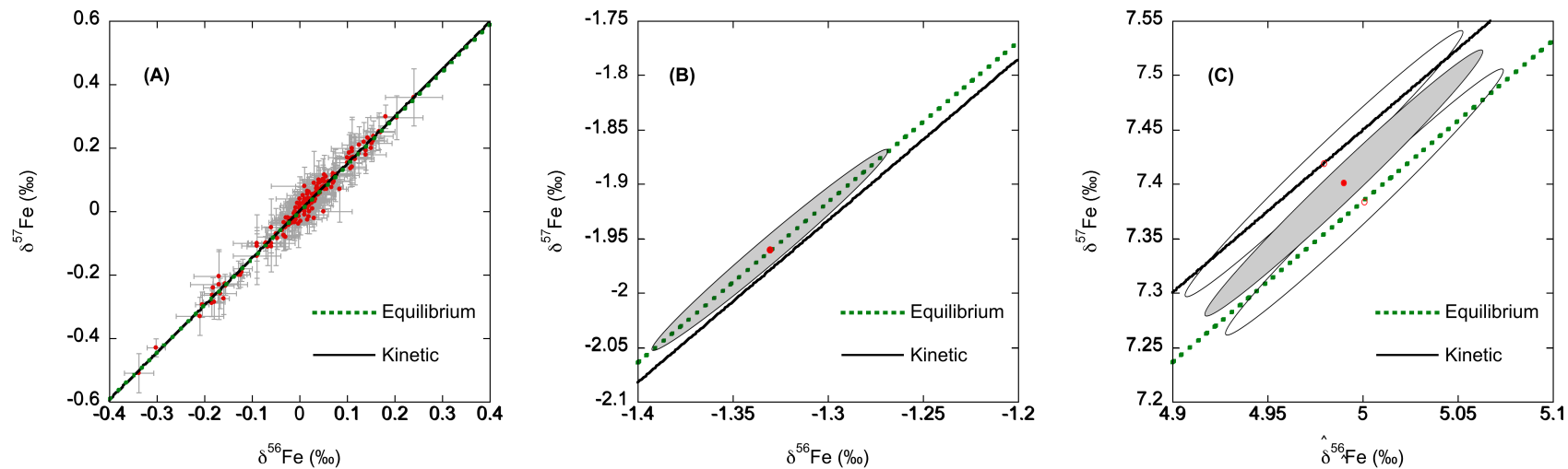


Figure 1-3. Iron three-isotope plots (Hulston and Thode, 1965) showing calculated equilibrium and kinetic fractionation lines. (A) All meteorite data in this dissertation. Equilibrium and kinetic fractionation laws cannot be distinguished within the uncertainties (2 standard errors). (B) The reported meteorite sample with the largest fractionation (Mullane et al., 2005). This chondrule separated from the Allende meteorite cannot distinguish the equilibrium and kinetic fractionation laws with the 95% confidence level error ellipse. (C) Only fractionation larger than 5 per mil can distinguish the equilibrium and kinetic fractionation laws with the 95% confidence level error ellipses in current analytical uncertainties. The 95% confidence level error ellipses are calculated from the maximum reproducibility in this dissertation research ($\pm 0.03\text{\textperthousand}$ 1 σ for $\delta^{56}\text{Fe}$ and $\pm 0.05\text{\textperthousand}$ 1 σ for $\delta^{57}\text{Fe}$; and 0.987 for the correlation coefficient).

Table 1-4. Mass differences of stable isotopes of selected elements

Element	Stable isotopes	Mass (a.m.u.) ^a	Mass difference ^b
Hydrogen	¹ H	1.0078250319	495.74
	² H (D)	2.0141017779	
Carbon	¹² C	12.0000000000	6.43
	¹³ C	13.003354838	
Nitrogen	¹⁴ N	14.0030740074	4.75
	¹⁵ N	15.000108973	
Oxygen	¹⁶ O	15.9949146223	6.96
	¹⁷ O	16.99913150	
	¹⁸ O	17.9991604	
Iron	⁵⁴ Fe	53.9396147	1.28
	⁵⁶ Fe	55.9349418	
	⁵⁷ Fe	56.9353983	
	⁵⁸ Fe	57.9332801	

^a in a.m.u. (atomic mass unit). Data from de Laeter et al. (2003);

^b The mass difference is expressed as $(m_H - m_L)/m_H m_L \times 1000$, where m_H and m_L are the mass of the heaviest or lightest isotopes, respectively.

The specific fractionation effects relevant to the different groups of meteorite samples in this dissertation are thoroughly discussed in the following chapters; however, several general qualitative rules are summarized here (Schauble, 2004):

1) The magnitude of equilibrium isotope fractionation rapidly decreases as temperature increases ($\sim 1/T^2$); however, the magnitude of kinetic isotope fractionation in general does not decrease. For example, Fe isotope fractionations among high-temperature igneous rock samples show a narrow variation (<<1 per mil) of $\delta^{56}\text{Fe}$, but fractionation in low-temperature systems can vary up to several per mil (Beard and Johnson, 2004).

2) At equilibrium, the heavy isotopes of an element tend to be enriched in those phases where the element is in the stiffest bonds. For example, Fe^{3+} mineral phases are in general enriched in heavy Fe isotopes compared to the Fe^{2+} phases (Polyakov and Mineev, 2000).

3) In kinetic fractionation, light isotopes of an element are more reactive; hence they are enriched in the products of the reaction. For example, during evaporation, heavy Fe isotopes are concentrated in the residues (Wang et al., 1994).

In addition to mass-dependent fractionation, *mass-independent* fractionation has been discovered, notably for the O isotope system (*e.g.*, Thiemens and Heidenreich, 1983). However, it is beyond the scope of this dissertation on Fe isotopes and is not mentioned further.

1.5. Anion-exchange Chromatographic Separation for Iron

The MC-ICP-MS technique of Fe isotope analysis used in this dissertation requires separation and purification of Fe prior to loading on the instrument; hence anion-exchange chromatography has been used during the meteorite sample preparation (Strelow, 1980). Here I summarize the principles of this chemical separation technique for Fe. Specific methods and customized protocols used for different groups of meteorite samples are presented in the sample treatment/preparation sections of the following chapters.

The basic idea of anion-exchange chromatographic separation for Fe is that the partition coefficient of Fe with anion-exchange resin depends on the HCl molarity of the solution. In highly concentrated HCl, Fe forms strong anion chloride complexes, and hence is retained on the resin and separated from matrix elements in the samples. In low molarity of HCl, Fe detaches from the resin, can be eluted from the chromatography column. Bio-Rad Analytical Grade (AG) 1-X8 200-400 mesh anion-exchange resin (see Table 1-5 for the technical information) is used in this dissertation.

Table 1-5. Technical information of Bio-Rad AG 1-X8 200-400 mesh anion-exchange resin

Parameter	Value
Ionic form	Chloride
Cross-linking	8%
Dry mesh size	200-400
Wet bead diameter (μm)	45-106
Capacity (mEq/mL)	1.2
Nominal density (g/mL)	0.75

Data from Bio-Rad AG 1, AG MP-1 and AG 2 Strong Anion Exchange Resin Instruction

Manual.

The theoretical principle is demonstrated as follows.

When Fe^{3+} and Cl^- form complex,



$$K_1 = \frac{[\text{FeCl}^{2+}]}{[\text{Fe}^{3+}][\text{Cl}^-]} \quad \text{Eq.1-11}$$

$$K_2 = \frac{[\text{FeCl}_2^+]}{[\text{FeCl}^{2+}][\text{Cl}^-]} \quad \text{Eq.1-12}$$

$$K_3 = \frac{[\text{FeCl}_3^-]}{[\text{FeCl}_2^+][\text{Cl}^-]} \quad \text{Eq.1-13}$$

$$K_4 = \frac{[\text{FeCl}_4^-]}{[\text{FeCl}_3^-][\text{Cl}^-]} \quad \text{Eq.1-14}$$

Therefore,

$$[\text{FeCl}^{2+}] = K_1 [\text{Fe}^{3+}][\text{Cl}^-] \quad \text{Eq.1-15}$$

$$[\text{FeCl}_2^+] = K_1 \cdot K_2 [\text{Fe}^{3+}][\text{Cl}^-]^2 \quad \text{Eq.1-16}$$

$$[\text{FeCl}_3^-] = K_1 \cdot K_2 \cdot K_3 [\text{Fe}^{3+}][\text{Cl}^-]^3 \quad \text{Eq.1-17}$$

$$[\text{FeCl}_4^-] = K_1 \cdot K_2 \cdot K_3 \cdot K_4 [\text{FeCl}_3^-][\text{Cl}^-]^4 \quad \text{Eq.1-18}$$

Because,

$$[\Sigma Fe] = [Fe^{3+}] + [FeCl^{2+}] + [FeCl_2^+] + [FeCl_3^-] + [FeCl_4^-] \quad \text{Eq.1-19}$$

Substitute equation 1-15, 1-16, 1-17 and 1-18 into equation 1-19,

$$\begin{aligned} [\Sigma Fe] &= [Fe^{3+}] + K_1[Fe^{3+}][Cl^-] + K_1 \cdot K_2[Fe^{3+}][Cl^-]^2 \\ &\quad + K_1 \cdot K_2 \cdot K_3[Fe^{3+}][Cl^-]^3 + K_1 \cdot K_2 \cdot K_3 \cdot K_4[Fe^{3+}][Cl^-]^4 \end{aligned} \quad \text{Eq.1-20}$$

Therefore, the mole fractions of Fe^{3+} , $[FeCl^{2+}]$, $[FeCl_2^+]$, $[FeCl_3^-]$ and $[FeCl_4^-]$ can be calculated by the following equations, respectively.

$$\frac{[Fe^{3+}]}{[\Sigma Fe]} = \frac{1}{1 + K_1[Cl^-] + K_1 \cdot K_2[Cl^-]^2 + K_1 \cdot K_2 \cdot K_3[Cl^-]^3 + K_1 \cdot K_2 \cdot K_3 \cdot K_4[Cl^-]^4} \quad \text{Eq.1-21}$$

$$\frac{[FeCl^{2+}]}{[\Sigma Fe]} = \frac{K_1[Cl^-]}{1 + K_1[Cl^-] + K_1 \cdot K_2[Cl^-]^2 + K_1 \cdot K_2 \cdot K_3[Cl^-]^3 + K_1 \cdot K_2 \cdot K_3 \cdot K_4[Cl^-]^4} \quad \text{Eq.1-22}$$

$$\frac{[FeCl_2^+]}{[\Sigma Fe]} = \frac{K_1 \cdot K_2[Cl^-]^2}{1 + K_1[Cl^-] + K_1 \cdot K_2[Cl^-]^2 + K_1 \cdot K_2 \cdot K_3[Cl^-]^3 + K_1 \cdot K_2 \cdot K_3 \cdot K_4[Cl^-]^4} \quad \text{Eq.1-23}$$

$$\frac{[FeCl_3^-]}{[\Sigma Fe]} = \frac{K_1 \cdot K_2 \cdot K_3[Cl^-]^3}{1 + K_1[Cl^-] + K_1 \cdot K_2[Cl^-]^2 + K_1 \cdot K_2 \cdot K_3[Cl^-]^3 + K_1 \cdot K_2 \cdot K_3 \cdot K_4[Cl^-]^4} \quad \text{Eq.1-24}$$

$$\frac{[FeCl_4^-]}{[\Sigma Fe]} = \frac{K_1 \cdot K_2 \cdot K_3 \cdot K_4[Cl^-]^4}{1 + K_1[Cl^-] + K_1 \cdot K_2[Cl^-]^2 + K_1 \cdot K_2 \cdot K_3[Cl^-]^3 + K_1 \cdot K_2 \cdot K_3 \cdot K_4[Cl^-]^4} \quad \text{Eq.1-25}$$

Bjerrum and Lukes (1986) provided values for K_1 , K_2 , K_3 , and K_4 are 30, 4.5, 0.15 and 0.0078 respectively. The mole fractions of different Fe species in HCl solutions are plotted in Figure 1-4. This result is consistent with Fujii et al. (2006).

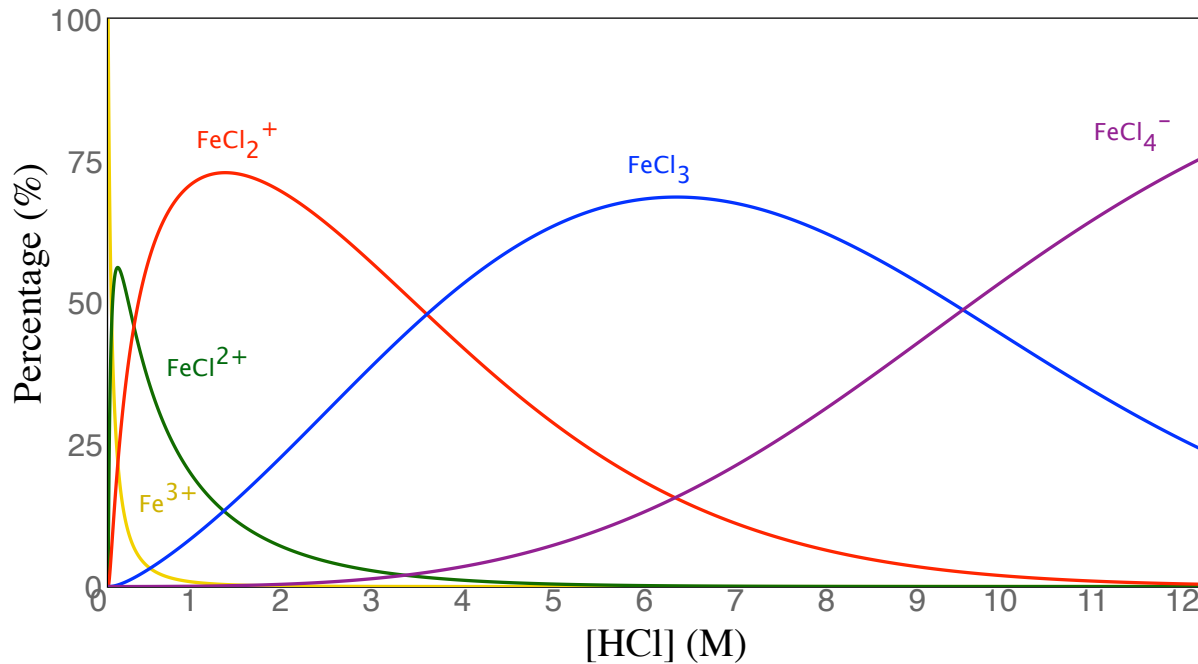
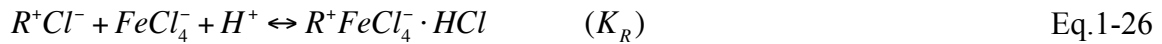


Figure 1-4. The mole fractions of different Fe species in HCl solutions.

Fe is adsorbed as FeCl_4^- by substituting the Cl^- in the resin $R^+\text{Cl}^-$.



$$K_R = \frac{[R^+\text{FeCl}_4^- \cdot \text{HCl}]}{[R^+\text{Cl}^-][\text{FeCl}_4^-][\text{H}^+]} \quad (\text{Eq.1-27})$$

Because, $[R^+\text{Cl}^-] \gg [R^+\text{FeCl}_4^- \cdot \text{HCl}]$, so $[R^+\text{Cl}^-] \approx N$, which is the capacity of resin,

then

$$K_R = \frac{[R^+FeCl_4^- \cdot HCl]}{N[FeCl_4^-][H^+]} \quad \text{Eq.1-28}$$

$$[R^+FeCl_4^- \cdot HCl] = K_R \cdot N[FeCl_4^-][H^+] \quad \text{Eq.1-29}$$

Because

$$D_{Fe} = \frac{[R^+FeCl_4^- \cdot HCl]}{[\Sigma Fe]} \quad \text{Eq.1-30}$$

Substitute equation 1-29 into equation 1-30,

$$D_{Fe} = \frac{K_R \cdot N[FeCl_4^-][H^+]}{[\Sigma Fe]} \quad \text{Eq.1-31}$$

Substitute equation 1-25 into equation 1-31,

$$D_{Fe} = \frac{K_R \cdot N \cdot K_1 \cdot K_2 \cdot K_3 \cdot K_4 [Cl^-]^4 [H^+]}{1 + K_1 [Cl^-] + K_1 \cdot K_2 [Cl^-]^2 + K_1 \cdot K_2 \cdot K_3 [Cl^-]^3 + K_1 \cdot K_2 \cdot K_3 \cdot K_4 [Cl^-]^4} \quad \text{Eq.1-32}$$

Because the $[H^+] = [Cl^-]$,

$$D_{Fe} = \frac{K_R \cdot N \cdot K_1 \cdot K_2 \cdot K_3 \cdot K_4 [Cl^-]^5}{1 + K_1 [Cl^-] + K_1 \cdot K_2 [Cl^-]^2 + K_1 \cdot K_2 \cdot K_3 [Cl^-]^3 + K_1 \cdot K_2 \cdot K_3 \cdot K_4 [Cl^-]^4} \quad \text{Eq.1-33}$$

The capacity of AG1-X8 is 1.2 mEq/ml, so $N=1.2$ mol/L. There is no experimentally-determined value of K_R ; however, it can be estimated from the literature (Moore and Kraus, 1950; Fujii et al., 2006). The partition coefficient D can be calculated by substituting these values into equation 1-33, The result is shown in Figure 1-5. It shows that the partitioning of Fe

to anion-exchange resin is strongly dependent on the molarity of HCl in the solution, which is the fundamental concept of the anion-exchange chromatographic separation for Fe.

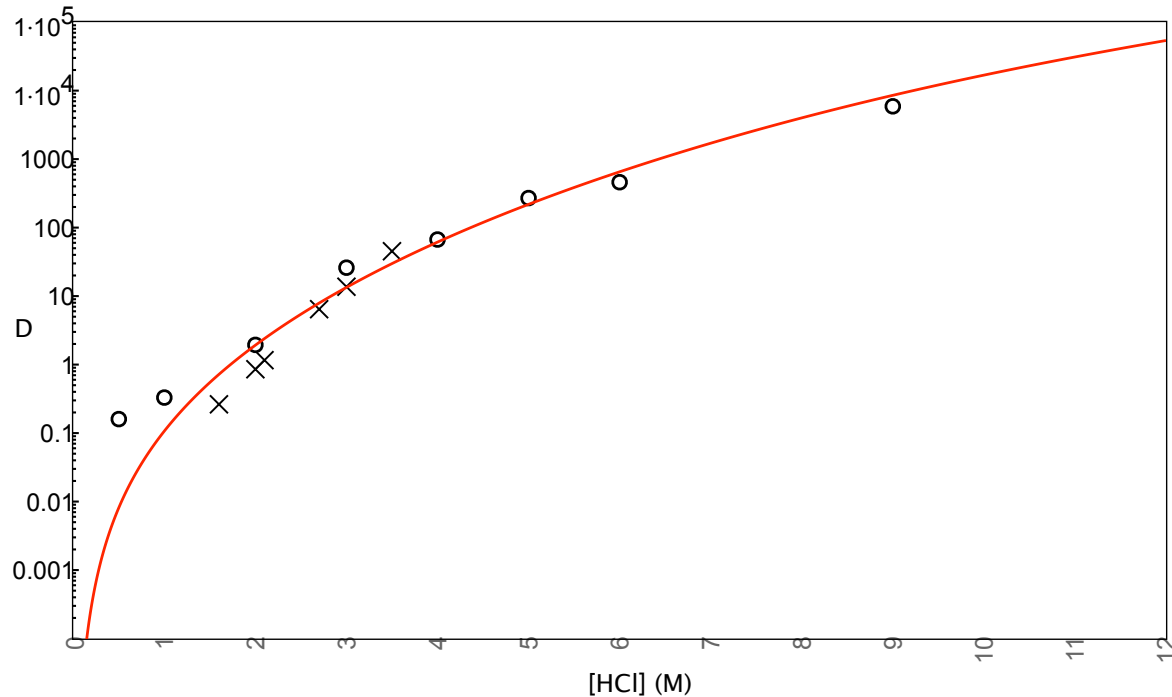


Figure 1-5. Distribution coefficient D increases exponentially with increasing molarity of [HCl]. The cross points come from Fujii et al. (2006) whereas the circle points are from Moore and Kraus (1950). The theoretical calculation fits very well with the experimental data.

1.6. MC-ICP-MS Analysis for Iron Isotopes

The earliest attempts to measure Fe isotopes using Thermal Ionization Mass Spectrometry (TIMS) have shown that it is challenging to resolve any Fe isotopic variation among terrestrial and extraterrestrial igneous rocks (*e.g.*, Beard and Johnson, 1999). The advent of Multi-Collector Inductively-Coupled-Plasma Mass-Spectrometry (MC-ICP-MS) in the early 2000s has greatly improved the analytical precision and made it possible to measure Fe isotopes with an analytical uncertainty as small as $\sim 0.03\text{\textperthousand}$ in $\delta^{56}\text{Fe}$ (*e.g.*, Dauphas et al., 2009). Compared to TIMS, MC-ICP-MS has the advantages of high ionization efficiency and rapid sample analysis (Beard and Johnson, 2004). However, isobar interferences in MC-ICP-MS analysis are substantial, and it is necessary to correct for instrumental fractionation in order to obtain true Fe isotope ratios.

Important isobar interferences for the four isotopes of Fe are ^{54}Cr and $^{40}\text{Ar}^{14}\text{N}$ for ^{54}Fe ; $^{40}\text{Ar}^{16}\text{O}$ for ^{56}Fe ; $^{40}\text{Ar}^{16}\text{O}^1\text{H}$ for ^{57}Fe ; and ^{58}Ni for ^{58}Fe . A more comprehensive list of possible isobar interferences is tabulated in Table 1-6.

Table 1-6. Isobar interferences of iron isotopes

<i>Isotope</i>	<i>Interference</i>
^{54}Fe	$^{54}\text{Cr}^+$, $^{40}\text{Ar}^{14}\text{N}^+$, $^{37}\text{Cl}^{16}\text{O}^1\text{H}^+$, $^{38}\text{Ar}^{15}\text{N}^1\text{H}^+$, $^{36}\text{Ar}^{18}\text{O}^+$, $^{38}\text{Ar}^{16}\text{O}^+$, $^{36}\text{Ar}^{17}\text{O}^1\text{H}^+$, $^{36}\text{S}^{18}\text{O}^+$, $^{35}\text{Cl}^{18}\text{O}^1\text{H}^+$, $^{37}\text{Cl}^{17}\text{O}^+$
^{56}Fe	$^{40}\text{Ar}^{16}\text{O}^+$, $^{40}\text{Ca}^{16}\text{O}^+$, $^{40}\text{K}^{16}\text{O}^+$, $^{40}\text{Ar}^{15}\text{N}^1\text{H}^+$, $^{38}\text{Ar}^{18}\text{O}^+$, $^{38}\text{Ar}^{17}\text{O}^1\text{H}^+$, $^{37}\text{Cl}^{18}\text{O}^1\text{H}^+$
^{57}Fe	$^{40}\text{Ar}^{16}\text{O}^1\text{H}^+$, $^{40}\text{Ca}^{16}\text{O}^1\text{H}^+$, $^{40}\text{Ar}^{17}\text{O}^+$, $^{38}\text{Ar}^{18}\text{O}^1\text{H}^+$, $^{38}\text{Ar}^{19}\text{F}^+$
^{58}Fe	$^{58}\text{Ni}^+$, $^{40}\text{Ar}^{18}\text{O}^+$, $^{40}\text{Ar}^{17}\text{O}^1\text{H}^+$

After May and Wiedmeyer (1998)

The elemental isobars ^{54}Cr and ^{58}Ni are eluted from Fe during sample preparation through the chromatographic separation procedure before loading on the MC-ICP-MS. In case of any possible trace amount of ^{54}Cr and ^{58}Ni remaining in the solution, ^{53}Cr and ^{60}Ni are always monitored during measurements (see Table 1-7 for the positions of Faraday cups). Any addition of ^{54}Fe and ^{58}Fe “signals” due to ^{54}Cr and ^{58}Ni interferences need to be subtracted. Because mass spectrometers favor transmission of heavy isotopes, this mass bias has to be first corrected by using the exponential law (Marechal et al., 1999):

$$r \approx R \left(\frac{M}{M'} \right)^\beta \quad \text{Eq.1-34}$$

In equation 1-34, r and R are the measured and true isotopic ratios; M and M' are the atomic masses of the two isotopes; and β is the element-dependent fractionation coefficient.

$$\beta_{\text{Fe}}^{57/56} = \frac{\ln \left(\frac{r^{57/56}}{R^{57/56}} \right)}{\ln \left(\frac{m^{57}}{m^{56}} \right)} \quad \text{Eq.1-35}$$

$r^{57/56}$ is the measured ratio of ^{57}Fe and ^{56}Fe . $R^{57/56}$ is the true ratio, m^{57} and m^{56} are the atomic masses of ^{57}Fe and ^{56}Fe , which are 0.02309, 56.9353983, 55.9349418, respectively (see Table 1-2; de Laeter et al., 2003).

Table 1-7. Positions of collectors (Faraday cups) for iron isotope analysis in MC-ICP-MS

Cup Number	L4	L3	L2	L1	C	H1	H2	H3	H4
Isotope		^{53}Cr	^{54}Fe		^{56}Fe	^{57}Fe	^{58}Fe		^{60}Ni

Assuming $\beta_{\text{Fe}}^{57/56} = \beta_{\text{Cr}}^{54/53} = \beta_{\text{Ni}}^{60/58}$ and using the true ratios and atomic masses of $^{54}\text{Cr}/^{53}\text{Cr}$ and $^{60}\text{Ni}/^{58}\text{Ni}$ (de Laeter et al., 2003), the “measured” ratios of $^{54}\text{Cr}/^{53}\text{Cr}$ and $^{60}\text{Ni}/^{58}\text{Ni}$ can be calculated. From there, the interferences caused by ^{54}Cr and ^{58}Ni on ^{54}Fe and ^{58}Fe can be evaluated and corrected. For all the results from this dissertation study, all the ^{54}Cr and ^{58}Ni interferences are negligible effects.

For the argide interferences, several techniques have been used to minimize, if not entirely eliminate, this effect (Dauphas et al., 2009). These techniques include: 1) using high concentrations of Fe and hence increasing Fe/argide ratio; 2) using collision cell technology to break down argide molecules; 3) using cold plasma operating conditions during MC-ICP-MS analysis to suppress the formation of argide; and 4) using the medium/high resolution mode of new-generation MC-ICP-MS instruments to separate the Fe isotope signals from the argide interferences. In this dissertation, I use the high resolving power of the Thermo Scientific Neptune Plus MC-ICP-MS to separate the argide from Fe. As shown in Figure 1-6, the signals of Fe isotopes and argides are effectively separated. All the measurements have been done on the Fe “shoulder” peak plateau to avoid the interferences.

To correct for the instrumental mass fractionation introduced by MC-ICP-MS, standard-sample bracketing is used. The concentrations of Fe in the solutions of samples and standards are measured previously and matched before the isotopic analysis. Each sample/standard is measured for 30 cycles with 8.389 s integration time per cycle. Every sample is repeated ~10 times with standard-sample bracketing and the average is reported as the final data for each sample.

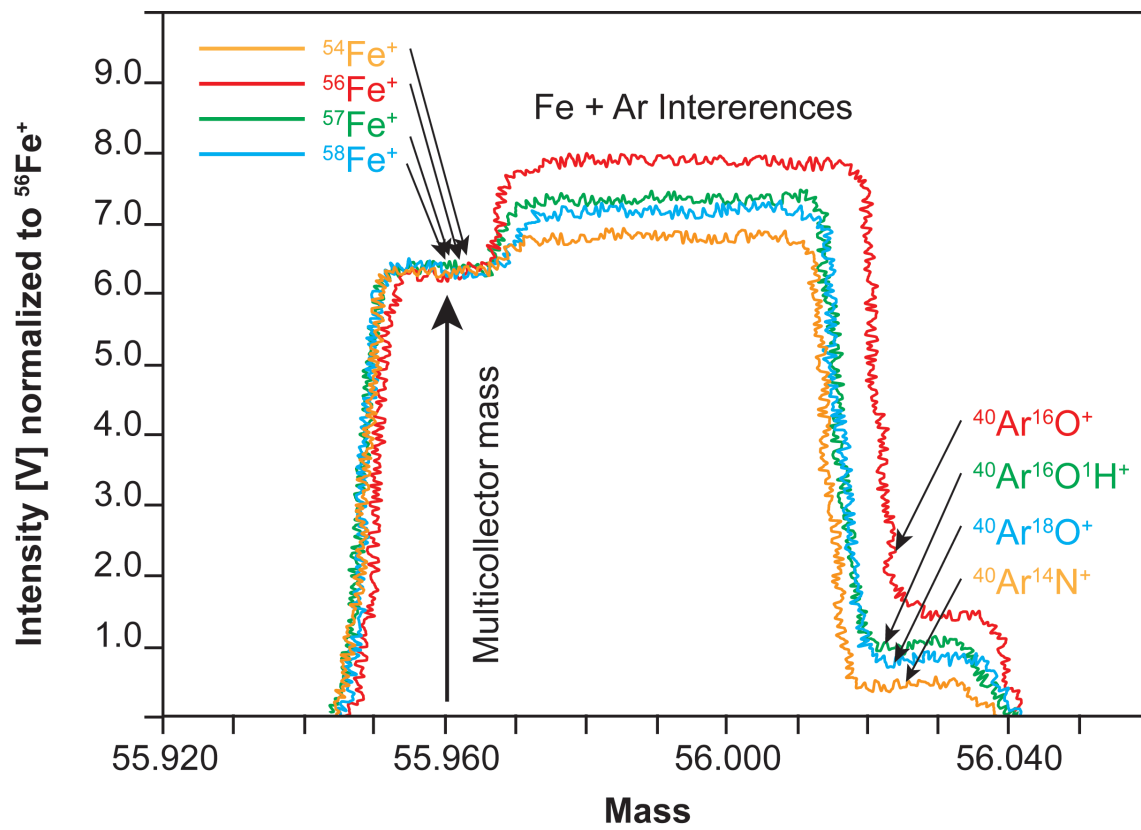


Figure 1-6. Schematic diagram showing that the Fe stable isotopes' peaks are clearly separated from the Ar-based interferences in the Neptune Plus MC-ICP-MS.

Copyright and Permissions

The journals *The Astrophysical Journal Letters*, *Meteoritics & Planetary Sciences*, *Geochimica et Cosmochimica Acta*, and *Earth and Planetary Sciences Letters* explicitly give permission for authors to reproduce their work in dissertation, as long as the original publication is cited. Please see the following websites for statements of official policies:

<http://iopscience.iop.org/2041-8205/page/Copyright%20&%20permissions>

[http://onlinelibrary.wiley.com/journal/10.1111/\(ISSN\)1945-5100/homepage/Permissions.html](http://onlinelibrary.wiley.com/journal/10.1111/(ISSN)1945-5100/homepage/Permissions.html)

<http://www.elsevier.com/journal-authors/author-rights-and-responsibilities>

The co-authors cited in this dissertation give permission for the works they are associated with to be reprinted in my dissertation.

References

- Anders E. and Grevesse N. (1989) Abundances of the elements: Meteoritic and solar. *Geochim. Cosmochim. Acta* **53**, 197–214.
- Beard B. L. and Johnson C. M. (2004) Fe isotope variations in the modern and ancient earth and other planetary bodies. In *Geochemistry of Non-Traditional Stable Isotopes, Reviews in Mineralogy & Geochemistry* (eds. C. M. Johnson, B. L. Beard, and F. Albarede). pp. 319–357.
- Beard B. L. and Johnson C. M. (1999) High precision iron isotope measurements of terrestrial and lunar materials. *Geochim. Cosmochim. Acta* **63**, 1653–1660.
- Bjerrum J. and Lukes I. (1986) The iron (III)-chloride system. A study of the stability constants and of the distribution of the tetrachloro species between organic solvents and aqueous chloride solutions. *Acta Chem. Scand. A* **40**, 31–40.
- Clayton D. (2003) *Handbook of Isotope in the Cosmos: Hydrogen to Gallium.*, Cambridge University Press, New York.
- Criss R. E. (1999) *Principles of Stable Isotope Distribution.*, Oxford University Press, New York.
- Dauphas, N., Craddock, P.R., Asimow, P.D., Bennett, V.C., Nutman, A.P. and Ohnenstetter, D. (2009a) Iron isotopes may reveal the redox conditions of mantle melting from Archean to Present. *Earth Planet. Sci. Lett.* **288**, 255–267.
- Dauphas N., Pourmand A. and Teng F.-Z. (2009b) Routine isotopic analysis of iron by HR-MC-ICPMS: How precise and how accurate? *Chem. Geol.* **267**, 175–184.
- Floss C., Ong W. J. and Gyngard F. (2012) Fe isotopic compositions of presolar silicate grains from Acfer 094. *75th Annu. Meet. Meteorit. Soc.* #5031(abstr.).
- Fujii T., Moynier F., Telouk P. and Albarede F. (2006) Isotope fractionation of iron(III) in chemical exchange reactions using solvent extraction with crown ether. *J. Phys. Chem. A* **110**, 11108–11112.
- Hiesinger H. and Head J. W. I. (2006) New views of lunar geoscience: an introduction and overview. In *New Views of the Moon, Reviews in Mineralogy and Geochemistry* (eds. B. L. Jolliff, M. A. Wieczorek, C. K. Shearer, and C. R. Neal). Mineralogical Society of America. pp. 1–81.
- Hoefs J. (2009) *Stable Isotope Geochemistry.*, Springer.
- Hulston J. R. and Thode H. G. (1965) Variations in the S³³, S³⁴, and S³⁶ contents of meteorites and their relation to chemical and nuclear effects. *J. Geophys. Res.* **70**, 3475–3484.

- Hutchison R. (2007) *Meteorites: A Petrologic, Chemical and Isotopic Synthesis.*, Cambridge University Press.
- Krot A. N., Keil K. and Scott E. R. D. (2007) Classification of Meteorites. In *Meteorites, Comets and Planets, Treatise on Geochemistry* (ed. A. M. Davis).
- De Laeter J. R., Böhlke J. K., De Bièvre P., Hidaka H., Peiser H. S., Rosman K. J. R. and Taylor P. D. P. (2003) Atomic weights of the elements. Review 2000 (IUPAC Technical Report). *Pure Appl. Chem.* **75**, 683–799.
- Lodders K. (2003) Solar system abundances and condensation temperatures of the elements. *Astrophys. J.* **591**, 1220–1247.
- Marechal C. N., Telouk P. and Albarede F. (1999) Precise analysis of copper and zinc isotopic compositions by plasma-source mass spectrometry. *Chem. Geol.* **156**, 251–273.
- Marhas K. K., Amari S., Gyngard F., Zinner E. and Gallino R. (2008) Iron and nickel isotopic ratios in presolar SiC grains. *Astrophys. J.* **689**, 622–645.
- May T. W. and Wiedmeyer R. H. (1998) A table of polyatomic interferences in ICP-MS. *At. Spectrosc.* **19**, 150–155.
- Moore G. E. and Kraus K. A. (1950) Adsorption of iron by anion exchange resins from hydrochloric acid solutions. *J. Am. Chem. Soc.* **72**, 5792–5793.
- Moynier F., Blichert-Toft J., Telouk P., Luck J. M. and Albarede F. (2007) Comparative stable isotope geochemistry of Ni, Cu, Zn, and Fe in chondrites and iron meteorites. *Geochim. Cosmochim. Acta* **71**, 4365–4379.
- Mullane E., Russell S. S. and Gounelle M. (2005) Nebular and asteroidal modification of the iron isotope composition of chondritic components. *Earth Planet. Sci. Lett.* **239**, 203–218.
- Ong W. J. and Floss C. (2013) Fe isotope nucleosynthesis: constraints from Fe isotopic analyses of presolar silicate grains from Acfer 094. *Lunar Planet. Sci. Conf. XLIV. Lunar Planet. Inst.* #1163(abstr.).
- Ong W. J., Floss C. and Gyngard F. (2012) Negative secondary ion measurements of $^{54}\text{Fe}/^{56}\text{Fe}$ and $^{57}\text{Fe}/^{56}\text{Fe}$ in presolar silicate grains from Acfer 094. *Lunar Planet. Sci. Conf. XLIII. Lunar Planet. Inst.* #1864(abstr.).
- Pagel B. E. J. (2009) *Nucleosynthesis and Chemical Evolution of Galaxies.*, Cambridge University Press.
- Poirrasson F., Halliday A. N., Lee D. C., Levasseur S. and Teutsch N. (2004) Iron isotope differences between Earth, Moon, Mars and Vesta as possible records of contrasted accretion mechanisms. *Earth Planet. Sci. Lett.* **223**, 253–266.

- Poitrasson F., Levasseur S. and Teutsch N. (2005) Significance of iron isotope mineral fractionation in pallasites and iron meteorites for the core-mantle differentiation of terrestrial planets. *Earth Planet. Sci. Lett.* **234**, 151–164.
- Polyakov V. B. and Mineev S. D. (2000) The use of Mossbauer spectroscopy in stable isotope geochemistry. *Geochim. Cosmochim. Acta* **64**, 849–865.
- Rubin A. E., Scott E. R. D. and Keil K. (1997) Shock metamorphism of enstatite chondrites. *Geochim. Cosmochim. Acta* **61**, 847–858.
- Saunier G., Poitrasson F., Moine B., Gregoire M. and Seddiki A. (2010) Effect of hot desert weathering on the bulk-rock iron isotope composition of L6 and H5 ordinary chondrites. *Meteorit. Planet. Sci.* **45**, 195–209.
- Schauble E. A. (2004) Applying stable isotope fractionation theory to new systems. In *Geochemistry of Non-Traditional Stable Isotopes, Reviews in Mineralogy & Geochemistry* (eds. C. M. Johnson, B. L. Beard, and F. Albarede). Mineralogical Soc America, Washington. pp. 65–111.
- Van Schmus W. R. and Wood J. A. (1967) A chemical-petrologic classification for the chondritic meteorites. *Geochim. Cosmochim. Acta* **31**, 747–765.
- Schoenberg R. and von Blanckenburg F. (2006) Modes of planetary-scale Fe isotope fractionation. *Earth Planet. Sci. Lett.* **252**, 342–359.
- Sears D. W., Grossman J. N., Melcher C. L., Ross L. M. and Mills A. A. (1980) Measuring metamorphic history of unequilibrated ordinary chondrites. *Nature* **287**, 791–795.
- Stöffler D., Keil K. and Edward R.D S. (1991) Shock metamorphism of ordinary chondrites. *Geochim. Cosmochim. Acta* **55**, 3845–3867.
- Strelow F. (1980) Improved separation of iron from copper and other elements by anion-exchange chromatography on a 4% cross-linked resin with high concentrations of hydrochloric acid. *Talanta* **27**, 727–732.
- Tang H. and Dauphas N. (2012) Abundance, distribution, and origin of ^{60}Fe in the solar protoplanetary disk. *Earth Planet. Sci. Lett.* **359-360**, 248–263.
- Thiemens M. H. and Heidenreich J. E. I. I. I. (1983) The mass-independent fractionation of oxygen: A novel isotope effect and its possible cosmochemical implications. *Science* **219**, 1073–1075.
- Trappitsch R., Savina M. R., Willingham D. G., Liu N., Pellin M. J., Dauphas N. and Davis A. M. (2012) Iron isotopic abundances in presolar grains. *Lunar Planet. Sci. XLIII*. Lunar Planet. Inst. #2497(abstr).

- Wang J., Davis A. M., Clayton R. N. and Mayeda T. K. (1994) Kinetic isotopic fractionation during the evaporation of the iron oxide from liquid state. *Lunar Planet. Sci. XXV*. Lunar Planet. Inst. #1459(abstr.).
- Wasserburg G. J., Gallino R. and Busso M. (1998) A test of the supernova trigger hypothesis with ^{60}Fe and ^{26}Al . *Astrophys. J.* **500**, L189–L193.
- Weisberg M. K., Mccoy T. J. and Krot A. N. (2006) Systematics and evaluation of meteorite classification. In *Meteorites and the Early Solar System II* (eds. D. S. Lauretta and H. Y. J. McSween). University of Arizona Press, Tucson. pp. 19–52.
- Weyer S., Anbar A. D., Brey G. P., Munker C., Mezger K. and Woodland A. B. (2005) Iron isotope fractionation during planetary differentiation. *Earth Planet. Sci. Lett.* **240**, 251–264.
- Williams H. M., Markowski A., Quitte G., Halliday A. N., Teutsch N. and Levasseur S. (2006) Fe isotope fractionation in iron meteorites: New insights into metal-sulphide segregation and planetary accretion. *Earth Planet. Sci. Lett.* **250**, 486–500.
- Wlotzka F. (1993) A weathering scale for the ordinary chondrites. *Meteoritics* **28**, 460.
- Young E. D., Galy A. and Nagahara H. (2002) Kinetic and equilibrium mass-dependent isotope fractionation laws in nature and their geochemical and cosmochemical significance. *Geochim. Cosmochim. Acta* **66**, 1095–1104.
- Zhu X. K., Guo Y., O’Nions R. K., Young E. D. and Ash R. D. (2001) Isotopic homogeneity of iron in the early solar nebula. *Nature* **412**, 311–313.
- Zhu X. K., Guo Y., Williams R. J. P., O’Nions R. K., Matthews A., Belshaw N. S., Canters G. W., de Waal E. C., Weser U., Burgess B. K. and Salvato B. (2002) Mass fractionation processes of transition metal isotopes. *Earth Planet. Sci. Lett.* **200**, 47–62.

CHAPTER 2 :

^{58}Fe AND ^{54}Cr IN EARLY SOLAR SYSTEM MATERIALS

This chapter has been published in *The Astrophysical Journal Letters*:

Wang, K., Moynier, F., Podosek, F. and Foriel, J. (2011). ^{58}Fe and ^{54}Cr in Early Solar System Materials. *The Astrophysical Journal Letters*, **739**, L58.

Abstract

Stepwise dissolution of primitive meteorites exhibits large ^{54}Cr anomalies but no collateral effects on ^{58}Fe and ^{48}Ca , two other neutron-rich nuclides from the iron peak. These results suggest that ^{54}Cr must have been produced in particular zones of the rare Type Ia supernovae or that ^{48}Ca and/or ^{58}Fe were produced together in Type II supernovae and were chemically separated into some mineral phase that favors Cr over Ca and Fe, and it is the dissolution properties of that phase that is driving the isotopic effect in leaching. The recent findings of nanometer-size oxide grains with very large ^{54}Cr excesses favored the latter scenario for the origin of the mono-isotopic Cr isotopic effect. In addition, the absence of isotopic variations in the $^{58}\text{Fe}/^{54}\text{Fe}$ ratio at the mineral scale confirms that the short-lived nuclide ^{60}Fe ($T_{1/2} = 2.62$ Myr) was homogeneously distributed to a less than 15% dispersion in the early solar nebula.

2.1. Introduction

CI carbonaceous chondrites are among the most primitive samples of our Solar System's materials available for laboratory examinations. They have incorporated presolar solids relatively unmodified by nebular processes. For example, carbonaceous chondrites are hosts for several types of circumstellar grains (diamond, graphite, silicon carbide, corundum, silicon nitride, and silicates; Anders and Zinner, 1993; Zinner, 1997; Nagashima et al., 2004; Nguyen and Zinner, 2004; Zinner et al., 2011). These grains are identified as presolar because of the very large isotopic anomalies they carry which are attributable to nucleosynthesis in specific stellar environments. The known types of presolar grains constitute only a very small fraction of total meteorite mass and their identification and characterization relies on their efficient isolation from other meteoritic constituents. The first grains discovered were thermally refractory and very resistant to chemical reagents that dissolve most of the other phases in the meteorite; the latter feature in particular has been crucial in their successful isolation. But there are also cases in which presolar materials are carried in phases that are not chemically resistant, as first revealed in simple acid leaching of whole rock meteorites (Rotaru et al., 1992; Podosek et al., 1997; Trinquier et al., 2007), and more recently identified in cosmic dust particles (Messenger et al., 2002) and later in carbonaceous chondrites (Nguyen and Zinner, 2004; Nagashima et al., 2004; Mostefaoui and Hoppe, 2004).

The different leaching fractions of Orgueil (CI1 chondrite) show large isotopic anomalies in ^{54}Cr (Rotaru et al., 1992; Podosek et al., 1997; Trinquier et al., 2007). Initial treatment with acetic and nitric acids was found to dissolve most of the Cr (and other cations as well); the Cr thus dissolved is nearly uniform in composition but deficient (with respect to the normal composition) in ^{54}Cr by some 5–6 ε (per ten thousand). Further treatments with hydrochloric acid

and then other reagents liberate the remainder of the Cr, which can have variable compositions, mostly with excess ^{54}Cr (up to more than 200 ϵ).

There is no known way to generate such isotopic variations within the Solar System; this effect must be interpreted in terms of isotopic anomalies, *i.e.*, non-homogenization of distinct presolar nucleosynthetic components. Recently, Dauphas et al. (2010) and Qin et al. (2011) have shown presolar spinel grains as possible carrier phases for these anomalies.

Dense Type Ia supernovae provide the neutron-rich, low-entropy environment thought responsible for the neutron-rich iron-group isotopes (*e.g.*, Meyer et al., 1996). Collateral isotopic effects on other elements associated with the ^{54}Cr enrichment would provide compelling evidences to refine the nucleosynthetic origin of the ^{54}Cr anomalies. For example, no Ca isotopic anomalies have been found in leachates from the CI1 chondrite Orgueil containing large ^{54}Cr anomalies (Moynier et al., 2010). This absence of ^{48}Ca anomalies suggests that the ^{54}Cr anomalies must be produced either in massive stars during *s*-process nucleosynthesis without accompanying ^{48}Ca or in particular zones in a rare Type Ia supernovae (Moynier et al., 2010). On the other hand, ^{50}Ti enrichment is correlated with ^{54}Cr in Orgueil leachates (Trinquier et al., 2009), which has led the authors to suggest a common carrier phase for these two anomalies. However, the difference in volatility between Cr ($T_c = 1296\text{ K}$) on the one hand and the refractory elements Ti ($T_c = 1582\text{ K}$) and Ca ($T_c = 1517\text{ K}$) on the other hand (see Lodders, 2003 for T_c , the 50% condensation temperature) may lead to fractionation and decoupling between these elements during thermal events within the Solar System. Therefore, it would be very important to compare the ^{54}Cr excesses with another element with similar volatility such as Fe ($T_c = 1334\text{ K}$).

Fe is composed of four stable isotopes: ^{54}Fe (5.84%), ^{56}Fe (91.76%), ^{57}Fe (2.12%), and ^{58}Fe (0.28%). The different Fe isotopes are formed by different nucleosynthetic mechanisms in stars. ^{54}Fe , ^{56}Fe , and ^{57}Fe are formed by nuclear statistical equilibrium (NSE) while the neutron-rich ^{58}Fe (as well as other neutron-rich isotopes from the Fe peak) are formed by neutron-rich version of the equilibrium process in Type Ia or Type II supernovae (Clayton, 2003). The neutron-rich ^{60}Fe ($T_{1/2} = 2.62$ Myr) is produced by neutron capture in Type II supernovae or asymptotic giant branch (AGB) stars. However, the probability of having both a passing AGB star and a molecular cloud is very low (Kastner and Myers, 1994) and AGB stars are usually not considered as viable sources of the live ^{60}Fe in the early Solar System (Huss et al., 2009). Early measurements of Fe isotopic ratios for most chondritic materials yield a normal Fe composition (at a resolution of $\approx 0.3 \epsilon$ -units, 2 standard error, 2SE; Dauphas et al., 2004, 2008; Tang et al., 2009), except for effects in rare FUN inclusions that contain Fractionated isotopic compositions and Unusual Nuclear isotopic effects (Voelkening and Papanastassiou, 1989). Here, we report the relative isotopic abundances of Fe and Cr isotopes in leaching CI1 chondrite Orgueil, CM2 chondrite Murchison, and LL3 chondrite Semarkona to search for possible collateral effects and document the Cr isotopic composition of leachates from ordinary chondrites. Another motivation for this work is to use the variability of the ^{58}Fe to evaluate the extent of the heterogeneity within the solar nebula of the extinct nuclide ^{60}Fe ($T_{1/2} = 2.62$ Myr), which is formed in the same stellar environments.

2.2. Samples and Analytical Procedures

In keeping with the nomenclature system used by Podosek et al. (1997), each starting whole rock sample is designated by a letter and a Roman numeral. Letters O, M, and S designate Orgueil, Murchison, and Semarkona, respectively. Samples processed for this work are O-IV, M-II, and S-I for Cr and Fe isotopes. Successive leaching fractions of each whole rock sample are further identified by an Arabic numeral following the Roman numeral (*e.g.*, Table 2-1).

2.2.1. Sample Treatments

All starting whole rock samples (see Table 2-1 for masses of starting materials) were crushed and then subjected to a series of leaches in different reagents. After each leaching step the sample was centrifuged and the supernatant decanted by pipette; the sample was then washed with water, centrifuged again, and similarly decanted. The washing procedure was repeated twice more, and all supernatants were combined to form the solution for that leaching step. In most cases these solutions were split, part being taken for the isotopic analysis and part reserved for other uses. In a few cases, a very small fraction of the solid residue was also removed for other studies.

The sequences of reagents applied to the various samples were similar but not identical. In general, the first reagent was 50% acetic acid. The treatment after the acetic acid was 25% nitric acid (HNO_3), then multiple steps with hydrochloric acid (HCl), finally further with hydrofluoric acid (HF) to obtain as complete dissolution as possible.

Since the principal interest in the further analyses herein reported was constraining the nature of the HCl-soluble carrier phase with the largest excesses of ^{54}Cr , the Murchison samples were not processed beyond HCl treatment.

Table 2-1. Iron and chromium isotope compositions of leaching meteorites

Sample	Type	Treatment	$\varepsilon^{56}\text{Fe}^{\text{a}}(\pm 2\text{SE})$	$\varepsilon^{58}\text{Fe}^{\text{a}}(\pm 2\text{SE})$	$\varepsilon^{57}\text{Fe}^{\text{b}}(\pm 2\text{SE})$	$\varepsilon^{58}\text{Fe}^{\text{b}}(\pm 2\text{SE})$	n ^c	$\varepsilon^{53}\text{Cr}^{\text{d}}(\pm 2\text{SE})$	$\varepsilon^{54}\text{Cr}^{\text{d}}(\pm 2\text{SE})$
<i>Semarkona (536mg)</i>									
S-I-2	LL3	50% Acetic acid, RT ^e	-0.04±0.21	-0.75±1.79	0.06±0.31	-0.67±1.96	5	0.99±0.16	-6.2±0.4
S-I-3	LL3	25% HNO ₃ , RT	-0.10±0.08	0.04±0.79	0.15±0.11	0.24±0.76	5	0.44±0.15	-1.4±0.3
S-I-4	LL3	6N HCl RT	-0.02±0.09	0.67±1.25	0.02±0.13	0.70±1.40	5	0.14±0.15	-3.4±0.3
S-I-5	LL3	6N HCl 40°C	-0.06±0.15	-0.48±0.76	0.09±0.23	-0.36±0.75	5	0.19±0.23	4.4±0.5
S-I-6	LL3	6N HCl 80°C	0.07±0.15	3.5±0.3
S-I-7	LL3	Conc. HF/HCl 100°C	-0.19±0.14	0.68±0.55	0.28±0.21	1.06±0.71	5	0.38±0.15	1.0±0.3
S-I-8	LL3	Conc. HF/HNO ₃ RT	0.03±0.09	0.50±0.78	-0.05±0.14	0.44±0.80	5	-0.15±0.15	-0.5±0.3
<i>Orgueil IV (59.5mg)</i>									
O-IV-2	CI1	50% Acetic acid, RT	-0.22±0.10	-1.45±2.14	0.33±0.15	-1.01±2.11	7	1±1	-4±2
O-IV-3	CI1	25% HNO ₃ , RT	-0.99±1.73	0.35±0.70	0.19±0.36	0.48±0.81	7	0±1	-5±2
O-IV-4	CI1	6N HCl RT	0.07±0.13	0.69±0.80	-0.06±0.20	-0.15±0.64	8	0±1	-5±2
O-IV-5	CI1	6N HCl 40°C	0.16±0.28	-0.43±2.00	-0.24±0.41	-0.74±1.89	7	0±1	8±2
O-IV-6	CI1	6N HCl 80°C	-1±1	71±2
O-IV-7	CI1	9N HCl 80°C	-2±2	98±4
O-IV-8	CI1	Conc. HF/HCl 100°C	-0.18±0.30	-2.63±4.33	0.27±0.45	-2.27±4.14	4	-1±2	33±2
<i>Murchison II (550mg)</i>									
M-II-2	CM2	50% Acetic acid, RT	-0.07±0.13	-0.48±1.06	0.11±0.20	-0.34±1.03	6	0.3±0.3	-15.5±0.7
M-II-3	CM2	25% HNO ₃ , RT	-0.05±0.15	0.37±1.24	0.08±0.22	0.48±1.20	6	0.4±0.4	-2.5±0.4
M-II-5	CM2	6N HCl RT	-0.31±0.20	-0.31±0.91	0.47±0.30	0.31±0.98	5	0.0±0.4	14.5±1.0
M-II-6	CM2	6N HCl 40°C	0.1±0.5	34.2±1.2
M-II-7	CM2	6N HCl 80°C	-0.29±0.28	-0.10±1.01	0.43±0.42	0.47±1.24	7	0.1±0.4	21.1±0.7
BCR-2	(basalt)	(Bulk)	-0.04±0.15	0.21±1.48	0.06±0.22	0.29±1.60	5
BIR-1	(basalt)	(Bulk)	-0.07±0.22	0.37±1.48	0.10±0.28	-0.20±1.92	8
BHVO-2	(basalt)	(Bulk)	-0.05±0.07	-1.03±0.89	0.02±0.13	-1.55±1.47	7	-	-

^a x Fe/⁵⁴Fe normalized to ⁵⁷Fe/⁵⁴Fe = 0.362566. x = 56 and 58.

^b x Fe/⁵⁴Fe normalized to ⁵⁶Fe/⁵⁴Fe = 15.69786. x = 57 and 58.

^c Number of sample measurements.

^d x Cr/⁵²Cr normalized to ⁵⁰Cr/⁵²Cr = 0.051859. x = 53 and 54.

^e Room temperature.

2.2.2. Isotopic Measurements

Prior to the mass-spectrometric analysis, Cr and Fe were purified by ion-exchange chromatography following procedures described previously (Podosek et al., 1997 and Moynier et al., 2007 for Cr, and Dauphas et al., 2004 for Fe). In order to minimize the Ni isobaric interference on the ^{58}Fe , the samples have been passed up to four times through the ion-exchange columns.

The Cr isotopic data reported here have been analyzed by TIMS Micromass Sector 54 at Washington University in St Louis (WUSTL), following the protocol described in Podosek et al. (1997). Fe isotopic data were measured using the MC–ICP–MS (Thermo-Finnigan Neptune Plus) at WUSTL. The Fe isotopic samples were introduced into the mass spectrometer using an Apex-Q+Spiro inlet system and a $100 \mu\text{L minute}^{-1}$ PFA nebulizer. The measurements were done in medium-resolution mode on the peak shoulder in order to resolve the isobaric interferences of $^{40}\text{Ar}^{14}\text{N}$ with ^{54}Fe , $^{40}\text{Ar}^{16}\text{O}$ with ^{56}Fe , and $^{40}\text{Ar}^{16}\text{OH}$ with ^{57}Fe . The intensities of masses 53, 54, 56, 57, 58, and 60 were measured on the Faraday cups L3, L2, central, H1, H2, and H4, respectively.

2.3. Results

Cr and Fe isotopic data are given in Table 2-1 and in Figures 2-1 and 2-2 as epsilon units (deviation in parts per 10,000 relative to the composition of the Cr SRM 986 and Fe IRMM014 standards) after internal normalization to $^{50}\text{Cr}/^{52}\text{Cr}$ of 0.051859 and $^{57}\text{Fe}/^{54}\text{Fe}$ of 0.362566 using the exponential law (Marechal et al., 1999). For Fe, we report an alternative normalization to $^{56}\text{Fe}/^{54}\text{Fe} = 15.69786$. The errors are reported as 2SE of the replicated measurements.

All of the samples analyzed in this study are found to have Fe isotope compositions similar to the terrestrial standard within the level of analytical precision of 30 ppm for the $^{56}\text{Fe}/^{54}\text{Fe}$ and of 150 ppm for the $^{58}\text{Fe}/^{54}\text{Fe}$ for a normalization to $^{57}\text{Fe}/^{54}\text{Fe}$. All samples also have a terrestrial Fe isotopic composition when normalized to $^{56}\text{Fe}/^{54}\text{Fe}$ (Table 2-1). The fractions Semarkona I-6, Orgueil IV-6 and 7, and Murchison II-6 did not have enough iron to perform an isotopic measurement. The Cr isotopic compositions of Murchison and Semarkona show a similar pattern with Orgueil, in the sense that at least most of the Cr in these meteorites have anomalous relative abundance of ^{54}Cr . The sizes of the anomalies in Murchison and Semarkona are smaller (although still well resolved analytically) than in Orgueil, and the pattern in which the anomalies appear is different (Figure 2-1), but the essential features of the isotopic effects in Murchison and Semarkona are fundamentally similar to those in Orgueil: a HCl-soluble phase bears Cr with excess ^{54}Cr and other Cr carriers are deficient in ^{54}Cr . These results are in good agreement with Trinquier et al. (2007); Qin et al. (2010) for Murchison and the recent report of Cr isotopic data in leachates from the ungrouped carbonaceous chondrite Tagish Lake (Petitat et al., 2011). In addition, some fractions of Semarkona show ^{53}Cr excesses, which are agreement with data on ordinary chondrites, which have small ^{53}Cr excesses (Trinquier et al., 2007; Yin et

al., 2007; Qin et al., 2010). To our knowledge, this study reports the first leaching experiment on an ordinary chondrite and shows that ordinary chondrites contain small ^{54}Cr anomalies.

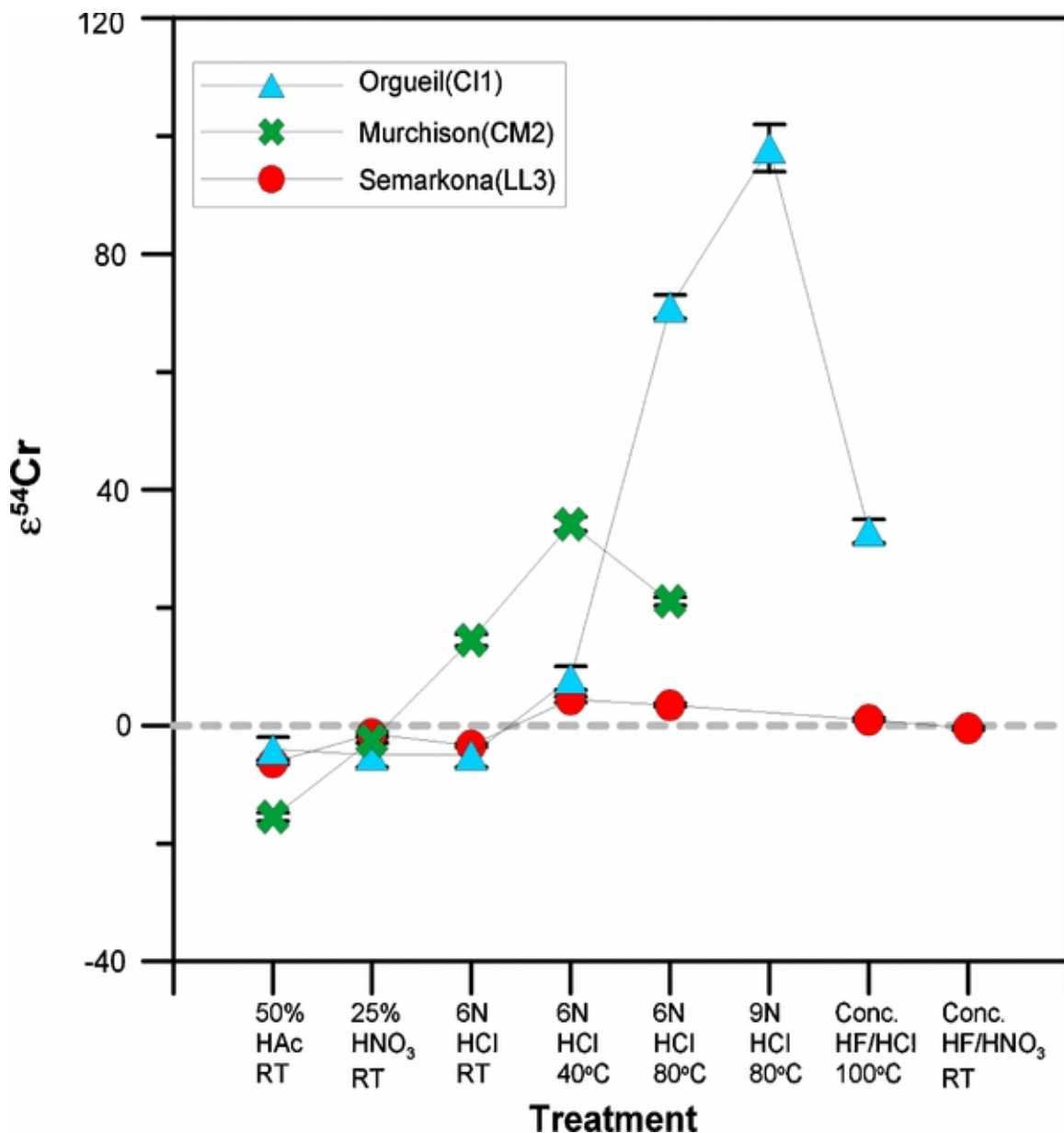


Figure 2-1. $\epsilon^{54}\text{Cr}$ in leaching fractions from Orgueil, Murchison, and Semarkona chondrites. Please refer to Table 2-1 for the exact data. HAc stands for acetic acid and RT for room temperature.

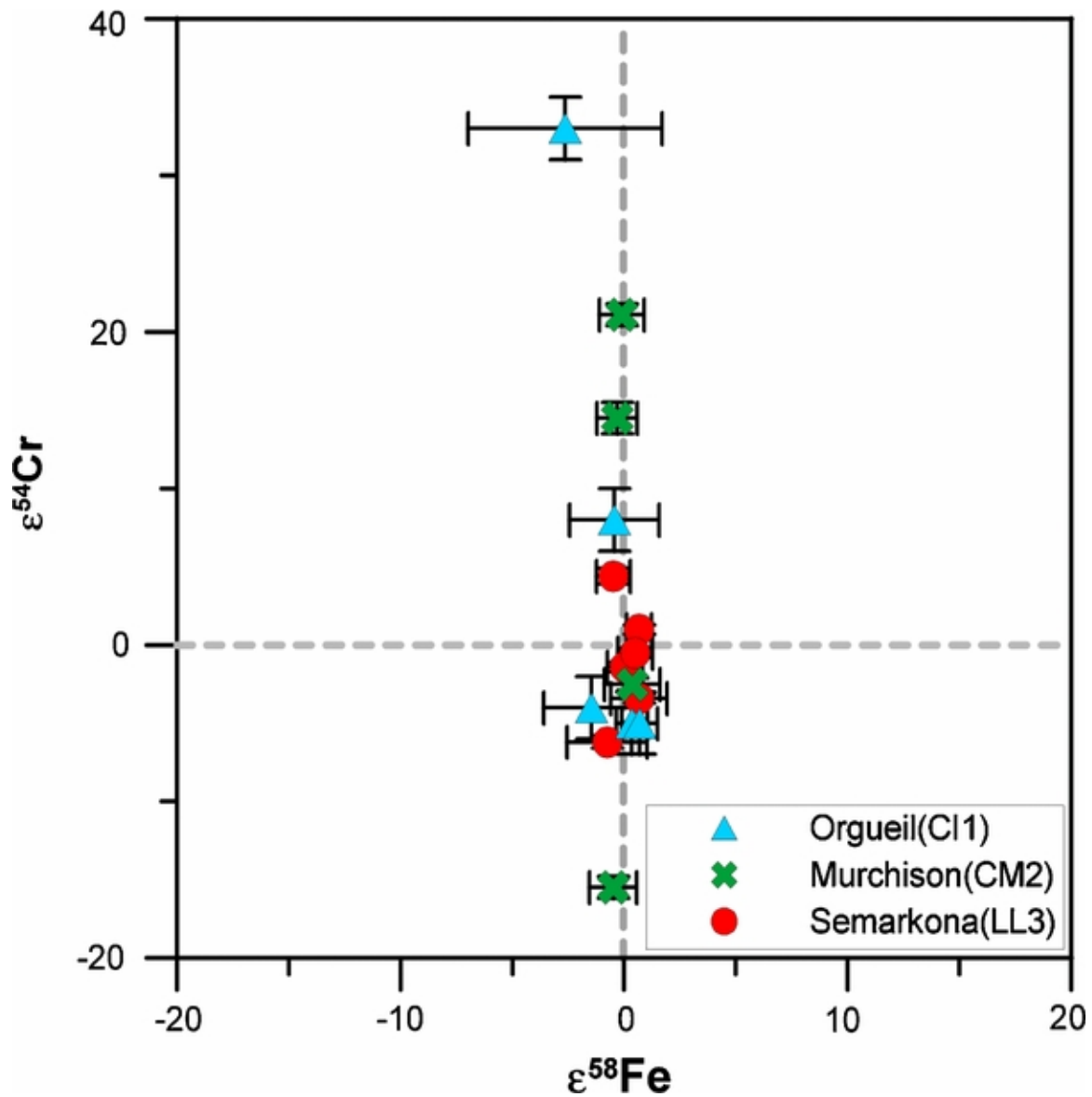


Figure 2-2. $\epsilon^{54}\text{Cr}$ vs. $\epsilon^{58}\text{Fe}$ in leaching fractions from Orgueil, Murchison, and Semarkona chondrites. Please refer to Table 2-1 for the exact data.

2.4. Discussion

The ^{54}Cr excess observed here is nucleosynthetic in origin as no known or plausible isotopic fractionation mechanism, energetic particle reaction (*i.e.*, spallation), or short-lived nuclide progenitor (in particular ^{54}Mn) can account for the magnitude and mono-isotopicity of this effect. The only known stellar sites expected to produce significant excesses of ^{54}Cr are either the *s*-process in Type II supernovae (The et al., 2007) or particularly rare massive Type Ia supernovae that achieve significant neutron-richness during the NSE followed by the low entropy freezeout, often producing other Fe-group elements with neutron-rich excesses, in particular ^{48}Ca , ^{50}Ti , ^{58}Fe , ^{64}Ni , and ^{70}Zn (Cameron, 1979; Hartmann et al., 1985; Woosley et al., 1986, 1995; Meyer et al., 1996; Woosley, 1997). Only about 15% of the Solar System's supply of ^{54}Cr is formed in Type II supernovae by *s*-process (The et al., 2007).

Correlated enrichments and depletions of the neutron-rich isotopes of Ca, Ti, Cr, Fe, and Zn have indeed been measured in a variety of inclusions, in particular FUN CAIs as well as in carbonaceous chondrites. These correlated variations have been attributed to material having formed under NSE conditions (Lee et al., 1978; Niederer et al., 1980; Niederer and Papanastassiou, 1984; Papanastassiou, 1986; Papanastassiou and Brigham, 1989; Voelkening and Papanastassiou, 1989). While the effects in CAIs and in the ^{54}Cr -rich phase may be related, the carrier-phase does not contain excesses in either ^{48}Ca (Moynier et al., 2010) or in ^{58}Fe isotopes (this study), and the ^{54}Cr -rich carrier resides in a low-density and/or small grain size in a mineral soluble in HCl, unlike the higher density, more refractory phases present in CAIs. It has been recently proposed that the carrier phase of the ^{54}Cr anomalies measured in the stepwise leaching of Orgueil and Murchison may be related to nanoparticles (most likely spinels; Dauphas et al., 2010; Qin et al., 2011) with nucleosynthetic origins.

The absence of ^{58}Fe anomalies in the leaching fractions of carbonaceous chondrites with large ^{54}Cr effects can be used to refine the nucleosynthetic origin of the ^{54}Cr . Based on the absence of ^{48}Ca anomalies in the Orgueil leachates O-I, Moynier et al. (2010) proposed that the ^{54}Cr must have been synthesized either in the oxygen-rich, *s*-process enhanced ejecta from massive stars or in particular zones in the rare Type Ia supernovae. In the former origin, the grains should be enriched in ^{58}Fe with a $^{58}\text{Fe}/^{54}\text{Cr}$ overabundance of $\sim 4\text{--}5$ (Figure 2-3). Therefore our data suggest that the ^{54}Cr anomalies are either produced by rare Type Ia supernovae or ^{54}Cr was indeed co-synthesized with ^{58}Fe in Type II supernovae, but it was chemically separated into some mineral phase that favors Cr over Fe, and it is the dissolution properties of that phase that is driving the isotopic effect in leaching. From our data it is not possible to tell which star produced the mono-isotopic ^{54}Cr excesses. Dauphas et al. (2010) and Qin et al. (2011) found nanoparticles with very large ^{54}Cr enrichments. Based on the oxygen-rich composition of these grains and on the rarity of Type Ia supernovae able to produce such ^{54}Cr excesses, Type II supernovae are the most likely origin for the ^{54}Cr isotopic anomalies (Dauphas et al., 2010; Qin et al., 2011).

Finally, the lack of large ^{58}Fe anomalies in leachates of Orgueil and Murchison confirm that Fe isotopes were homogeneously distributed in the early solar nebula (Dauphas et al., 2008), not only at the bulk rock scale but also at the mineral scale. These results confirm that the short-lived nuclide ^{60}Fe ($T_{1/2} = 2.62$ Myr) was homogeneously distributed to less than 15% dispersion in the early solar nebula (Dauphas et al., 2008; Moynier et al., 2009).

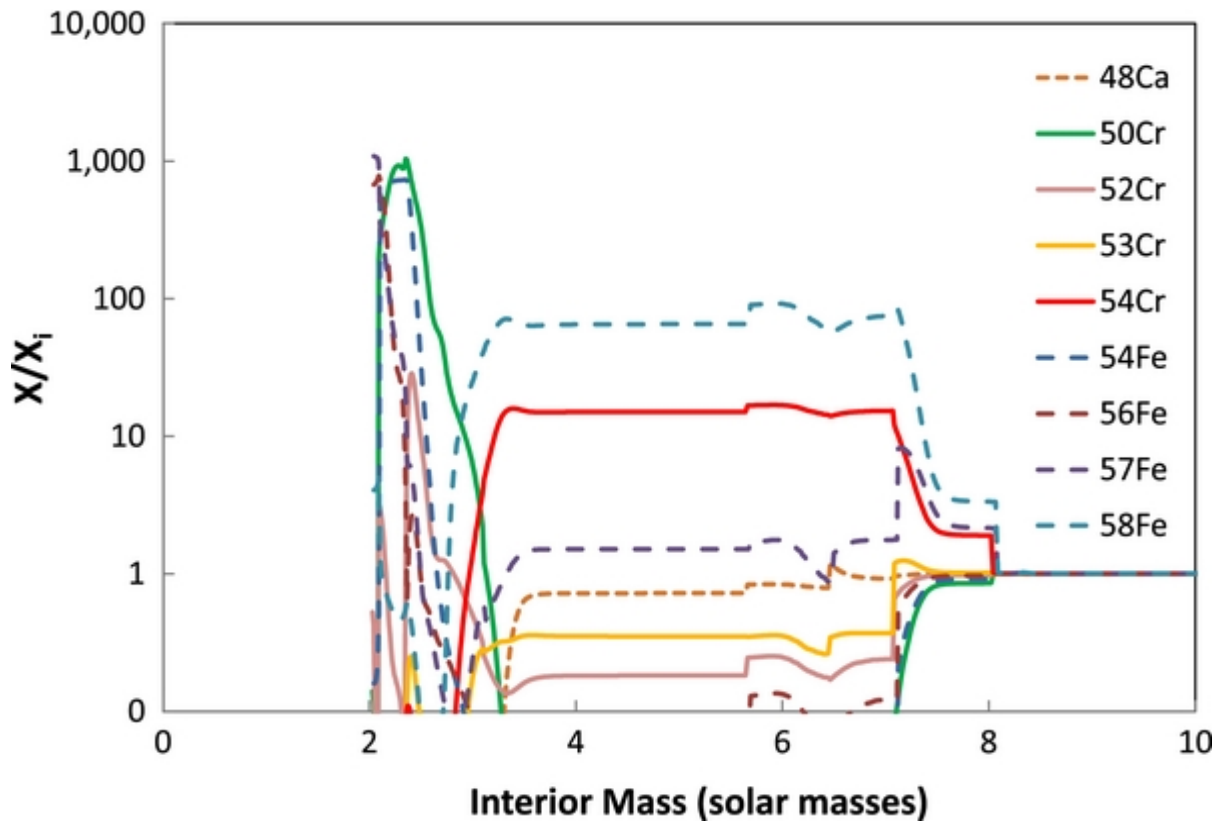


Figure 2-3. Iron and chromium overabundances (defined as mass fraction, X , relative to the initial mass fraction in the star, X_i) as a function of interior mass coordinate in a 25 solar mass supernova ejecta, stellar model s25a28d (figure generated from data of Rauscher et al., 2002). While most of the Fe and Cr isotopes are produced in the innermost supernova regions ($\leq 3 M_\odot$), the neutron-rich, ^{54}Cr , and ^{58}Fe are enriched in the mass range ≈ 3 to ≈ 8 solar masses. This is the material that experienced helium and some carbon burning. The other isotopes of Cr and Fe are either little changed or are depleted in these layers.

References

- Anders E. and Zinner E. (1993) Interstellar grains in primitive meteorites: diamond, silicon carbide, and graphite. *Meteoritics* **28**, 490–514.
- Cameron A. G. W. (1979) The neutron-rich silicon-burning and equilibrium processes of nucleosynthesis. *Astrophys. J.* **230**, L53.
- Clayton D. (2003) *Handbook of Isotope in the Cosmos: Hydrogen to Gallium*. Cambridge University Press, New York.
- Dauphas N., Cook D. L., Sacarabany A., Fröhlich C., Davis A. M., Wadhwa M., Pourmand A., Rauscher T. and Gallino R. (2008) Iron 60 evidence for early injection and efficient mixing of stellar debris in the protosolar nebula. *Astrophys. J.* **686**, 560–569.
- Dauphas N., Janney P. E., Mendybaev R. A., Wadhwa M., Richter F. M., Davis A. M., van Zuilen M., Hines R. and Foley C. N. (2004) Chromatographic separation and multicollection-ICPMS analysis of iron. Investigating mass-dependent and -independent isotope effects. *Anal. Chem.* **76**, 5855–5863.
- Dauphas N., Remusat L., Chen J. H., Roskosz M., Papanastassiou D. A., Stodolna J., Guan Y., Ma C. and Eiler J. M. (2010) Neutron-rich chromium isotope anomalies in supernova nanoparticles. *Astrophys. J.* **720**, 1577–1591.
- Hartmann D., Woosley S. E. and El Eid M. F. (1985) Nucleosynthesis in neutron-rich supernova ejecta. *Astrophys. J.* **297**, 837.
- Huss G. R., Meyer B. S., Srinivasan G., Goswami J. N. and Sahijpal S. (2009) Stellar sources of the short-lived radionuclides in the early solar system. *Geochim. Cosmochim. Acta* **73**, 4922–4945.
- Kastner J. H. and Myers P. C. (1994) An observational estimate of the probability of encounters between mass-losing evolved stars and molecular clouds. *Astrophys. J.* **421**, 605.
- Lee T., Papanastassiou D. A. and Wasserburg G. J. (1978) Calcium isotopic anomalies in the Allende meteorite. *Astrophys. J.* **220**, L21.
- Lodders K. (2003) Solar system abundances and condensation temperatures of the elements. *Astrophys. J.* **591**, 1220–1247.
- Marechal C. N., Telouk P. and Albarede F. (1999) Precise analysis of copper and zinc isotopic compositions by plasma-source mass spectrometry. *Chem. Geol.* **156**, 251–273.
- Messenger S., Keller L. P., Stadermann F. J., Walker R. M. and Zinner E. (2003) Samples of stars beyond the solar system: silicate grains in interplanetary dust. *Science* **300**, 105–108.
- Meyer B. S., Krishnan T. D. and Clayton D. D. (1996) ^{48}Ca production in matter expanding from high temperature and density. *Astrophys. J.* **462**, 825.

- Mostefaoui S. and Hoppe P. (2004) Discovery of abundant in situ silicate and spinel grains from red giant stars in a primitive meteorite. *Astrophys. J.* **613**, L149–L152.
- Moynier F., Dauphas N. and Podosek F. A. (2009) A search for ^{70}Zn anomalies in meteorites. *Astrophys. J.* **700**, L92–L95.
- Moynier F., Simon J. I., Podosek F. A., Meyer B. S., Brannon J. and De Paolo D. J. (2010) Ca isotope effects in Orgueil leachates and the implications for the carrier phases of ^{54}Cr anomalies. *Astrophys. J.* **718**, L7–L13.
- Moynier F., Yin Q. and Jacobsen B. (2007) Dating the first stage of planet formation. *Astrophys. J.* **671**, L181–L183.
- Nagashima K., Krot A. N. and Yurimoto H. (2004) Stardust silicates from primitive meteorites. *Nature* **428**, 921–924.
- Nguyen A. N. and Zinner E. (2004) Discovery of ancient silicate stardust in a meteorite. *Science* **303**, 1496–1499.
- Niederer F. R. and Papanastassiou D. A. (1984) Ca isotopes in refractory inclusions. *Geochim. Cosmochim. Acta* **48**, 1279–1293.
- Niederer F. R., Papanastassiou D. A. and Wasserburg G. J. (1980) Endemic isotopic anomalies in titanium. *Astrophys. J.* **240**, L73.
- Papanastassiou D. A. (1986) Chromium isotopic anomalies in the Allende meteorite. *Astrophys. J.* **308**, L27.
- Papanastassiou D. A. and Brigham C. A. (1989) The identification of meteorite inclusions with isotope anomalies. *Astrophys. J.* **338**, L37.
- Petitat M., Birck J.-L., Luu T. H. and Gounelle M. (2011) The chromium isotopic composition of the ungrouped carbonaceous chondrite Tagish Lake. *Astrophys. J.* **736**, 23.
- Podosek F. A., Ott U., Brannon J. C., Neal C. R., Bernatowicz T. J., Swan P. and Mahan S. E. (1997) Thoroughly anomalous chromium in Orgueil. *Meteorit. Planet. Sci.* **32**, 617–627.
- Qin L., Alexander C. M. O., Carlson R. W., Horan M. F. and Yokoyama T. (2010) Contributors to chromium isotope variation of meteorites. *Geochim. Cosmochim. Acta* **74**, 1122–1145.
- Qin L., Nittler L. R., Alexander C. M. O., Wang J., Stadermann F. J. and Carlson R. W. (2011) Extreme ^{54}Cr -rich nano-oxides in the CI chondrite Orgueil – Implication for a late supernova injection into the solar system. *Geochim. Cosmochim. Acta* **75**, 629–644.
- Rauscher T., Heger A., Hoffman R. D. and Woosley S. E. (2002) Nucleosynthesis in massive stars with improved nuclear and stellar physics. *Astrophys. J.* **576**, 323–348.
- Rotaru M., Birck J. L. and Allègre C. J. (1992) Clues to early Solar System history from chromium isotopes in carbonaceous chondrites. *Nature* **358**, 465–470.

- Tang H., Dauphas N. and Craddock P. R. (2009) High precision iron isotopic analyzes of meteorites and terrestrial rocks: ^{60}Fe distribution and mass fractionation laws. *Lunar Planet. Sci. XL*. Lunar Planet. Inst., Woodlands. #1903(abstr.).
- The L., El Eid M. F. and Meyer B. S. (2007) s -process nucleosynthesis in advanced burning phases of massive stars. *Astrophys. J.* **655**, 1058–1078.
- Trinquier A., Birck J. and Allègre C. J. (2007) Widespread ^{54}Cr heterogeneity in the inner Solar System. *Astrophys. J.* **655**, 1179–1185.
- Trinquier A., Elliott T., Ulfbeck D., Coath C., Krot A. N. and Bizzarro M. (2009) Origin of nucleosynthetic isotope heterogeneity in the solar protoplanetary disk. *Science* **324**, 374–376.
- Voelkening J. and Papanastassiou D. A. (1989) Iron isotope anomalies. *Astrophys. J.* **347**, L43.
- Woosley S. E. (1997) Neutron-rich nucleosynthesis in carbon deflagration supernovae. *Astrophys. J.* **476**, 801–810.
- Woosley S. E., Taam R. E. and Weaver T. A. (1986) Models for type I supernova. I - detonations in white dwarfs. *Astrophys. J.* **301**, 601.
- Woosley S. E., Weaver T. A. and Hoffman R. D. (1995) Rare neutron-rich nucleosynthesis in type IA supernovae. In *AIP Conf. Proc. 327, Nuclei in the Cosmos III* (eds. M. Busso, R. Gallino, and C. M. Raiteri). AIP, Melville, NY. p. 463.
- Yin Q., Jacobsen B., Moynier F. and Hutcheon I. D. (2007) Toward consistent chronology in the early Solar System: high-resolution ^{53}Mn - ^{53}Cr chronometry for chondrules. *Astrophys. J.* **662**, L43–L46.
- Zinner E. (1997) Presolar material in meteorites: an overview. In *AIP Conf. Proc. 402, Astrophysical implications of the laboratory study of presolar materials* (eds. T. J. Bernatowicz and E. K. Zinner). AIP, Melville, NY. pp. 3–26.
- Zinner E. K., Moynier F. and Stroud R. M. (2011) Laboratory technology and cosmochemistry. *PNAS* **108**, 19135–19141.

CHAPTER 3 :

HOMOGENEOUS DISTRIBUTION OF FE ISOTOPES IN THE EARLY SOLAR NEBULA

This chapter has been published in *Meteoritics & Planetary Sciences*:

Wang, K., Moynier, F., Barrat, J-A., Zanda, B., Paniello, R.C. and Savage, P.S. (2013)
Homogeneous Distribution of Fe Isotopes in the Early Solar Nebula. *Meteoritics & Planetary Sciences*, **48**, 354-364.

Abstract

To examine the iron (Fe) isotopic heterogeneities of CI and ordinary chondrites, we have analyzed several large chips ($\sim 1\text{g}$) from three CI1 chondrites and three ordinary chondrites (LL5, L5 and H5). The Fe isotope compositions of five different samples of Orgueil, one from Ivuna and one from Alais (CI1 chondrites) are highly homogeneous. This new dataset provides a $\delta^{56}\text{Fe}$ average of $0.02 \pm 0.04\text{\textperthousand}$ (2SE, $n=7$), which represents the best available value for the Fe isotopic composition of CI chondrites and likely the best estimate of the bulk Solar System. We conclude that the homogeneity of CI1 chondrites reflects the initial Fe isotopic homogeneity of the well-mixed solar nebula. In contrast, larger (up to $0.26\text{\textperthousand}$ in $\delta^{56}\text{Fe}$) isotopic variations have been found between separate $\sim 1\text{g}$ pieces of the same ordinary chondrite sample. The Fe isotope heterogeneities in ordinary chondrites appear to be controlled by the abundances of chondritic components, specifically chondrules, whose Fe isotope compositions have been fractionated by evaporation and re-condensation during multiple heating events.

3.1. Introduction

The CI chondrites are primitive samples of the Solar System that display the closest chemical composition (with the exception of some volatile elements such as H, C, N, O and noble gases) to the solar photosphere (Anders and Ebihara, 1982; Anders and Grevesse, 1989; Lodders, 2003). Since the sun comprises 99.9% of the mass of our Solar System, CI chondrites are the best available samples to estimate the bulk elemental and isotopic composition of our Solar System. To date, there are only nine recognized specimens of CI chondrites and only five of them are observed falls: Orgueil (14,000 g), Alais (6,000 g), Ivuna (700 g), Tonk (10 g), and Revelstoke (1 g). Most of the chemical and isotopic compositions reported for CI chondrites come from the same single stone of Orgueil (see Lodders et al., 2009 and references therein). Barrat et al. (2012) have recently reported major and trace elements and Cu and Zn isotopic compositions from six large chips (~1 g each) of five different stones of Orgueil, from one stone of Alais and one Ivuna stone. This study provides the best available average chemical composition of CI chondrites today. Here, we report the Fe isotopic compositions of the same eight large chips studied by Barrat et al. (2012).

The first and main objective of this study is to precisely determine the average Fe isotope composition of CI chondrites in order to provide a bulk Solar System value for inter-planetary comparison. In the past decade, with the application of MC-ICP-MS (Multiple Collector-Inductively Coupled Plasma-Mass Spectrometry), high precision Fe isotopic measurements have been routinely performed (*e.g.*, Zhu et al., 2001; Poitrasson et al., 2004; Weyer et al., 2005; Anand et al., 2006; Schoenberg and von Blanckenburg, 2006; Dauphas et al., 2009b; Millet et al., 2012) and it has been discovered that planetary materials from different parent bodies have distinct Fe isotope compositions (*e.g.*, Poitrasson et al., 2004; Poitrasson and Freydier, 2005;

Weyer et al., 2005; Schoenberg et al., 2006; Dauphas et al., 2009a; Wang et al., 2012a). In particular, terrestrial oceanic and continental crusts, lunar rocks and angrites ($\delta^{56}\text{Fe} \sim 0.1\text{-}0.2\text{\textperthousand}$) are enriched in the heavier isotopes of Fe compared to chondrites, martian and HED meteorites ($\delta^{56}\text{Fe} \sim 0.0\text{\textperthousand}$). Whether these variations are due to distinct solar nebular reservoirs of these planetary bodies or fractionation processes (volatilization, core-mantle segregation or magmatic differentiation) on these planetary bodies is still a debated issue (*cf.*, Weyer, 2008; Poitrasson, 2009). The precise determination of the Fe isotopic composition of CI chondrites could help us to fully understand where this planetary-scale variation within our Solar System originally stems from.

Another goal of this study is to examine the possible heterogeneities of CI and ordinary chondrites. Chondrites are composed of four main components: chondrules, CAI (Calcium-Aluminum-rich Inclusions), metals and matrix (Scott and Krot, 2005; 2007) and it has been shown that these components have distinct Fe isotopic compositions (Mullane et al., 2005; Theis et al., 2008; Needham et al., 2009; Hezel et al., 2010). The proposed possible causes for the observed Fe isotopic fractionations between chondritic components are that the Fe of these components is 1) inherited from isotopically distinct solar nebular reservoirs; 2) fractionated as a result of nebular evaporation/condensation processing; or 3) fractionated as a result of asteroidal processing on parent bodies, such as aqueous alteration and thermal metamorphism. In order to better understand the origin of the Fe isotopic variability within chondritic meteorites, we focused on two groups of chondrites: CI and ordinary chondrites, which have very different modal proportions of chondritic components and have experienced contrasting secondary processing effects (aqueous alteration or thermal metamorphism) on their parent bodies.

To this end, we report high precision Fe isotopic compositions of seven individual stones of CI chondrites (five Orgueil, one Ivuna and one Alais) and several large chips of three ordinary chondrites (L, LL, and H), and discuss the heterogeneities of these early Solar System materials and their implications for the Fe isotopic reservoirs in the early solar nebula and on nebular/parent-body processing.

3.2. Methods

3.2.1. Sample Descriptions

Eight large (~1 g each) pieces from three CI carbonaceous chondrites (six Orgueil, one Alais and one Ivuna) have been used in this study. Orgueil, Alais and Ivuna are the only three CI chondrite falls with a mass >10 g. The six samples of Orgueil are from five different stones. All the CI chondrites are fine-grained regolith breccias and are composed of more than 95% matrix, lacking chondrules or CAIs (Krot et al., 2007). They have been classified as petrologic type 1 due to almost complete aqueous alteration on their parent body (Scott and Krot, 2007). Petrological descriptions as well as major and trace element compositions and Cu and Zn isotopic ratios of these CI samples are reported by Barrat et al. (2012).

In addition, large chips (~3g each) of three Antarctic ordinary chondrites have been disaggregated to study the possible Fe isotopic heterogeneity of these meteorites. Lewis Cliff 85320 (LEW 85320) is an H ordinary chondrite, Grosvenor Mountains 95540 (GRO 95540) is an L ordinary chondrite, and Dominion Range 03194 (DOM 03194) is a LL ordinary chondrite. All three have been classified as petrologic type 5 due to high-level thermal metamorphism in their parent bodies. Even though the peak temperature could reach more than 700°C (Huss et al, 2006) for type 5 thermal metamorphism, re-equilibration among large grains is prohibitively slow (*e.g.*, Poitrasson et al., 2005) and will not be considered hereafter. Chondrites GRO 95540 and DOM 03194 display “A” grade (minor) weathering. LEW 85320 is designated as having undergone “B” grade (moderate) weathering, as magnesium carbonates (terrestrial weathering products) have been observed (Jull et al., 1988; Grady et al., 1989; Velbel et al., 1991). Terrestrial weathering could affect the Fe isotopic composition of “find” meteorites from hot deserts (Saunier et al., 2010), while Antarctic “find” meteorites are usually considered less altered and better candidates

for bulk isotopic cosmochemical studies (Crozaz and Wadhwa, 2001). We carefully removed all of the fusion crusts and only chose the “fresh” inner parts for analysis, to minimize terrestrial contamination.

3.2.2. Sample Preparation and Chemical Purification of Fe

For all carbonaceous chondrites, large (~1g) chips of samples were already powdered for the study of Barrat et al. (2012). About 10 mg of the well-mixed powders were used for Fe isotope analysis (see Table 3-1 for the mass of each sample). For the three ordinary chondrites, large fresh chips of samples were broken into four to seven large chips with a Parafilm-covered hand hammer (see Figure 3-1). The mass of each individual chip ranges from several hundred mg to ~1g (Table 3-1). Each chip was finely ground using an agate pestle and mortar, and no visible large metal grains were identified. About 10 mg of the well-mixed powders were digested with concentrated HF/HNO₃ (4:1 v/v) under heat lamps for three days. Fully dissolved samples were dried and re-digested with double-distilled 6 M HCl.

Anion exchange chromatography for the purification of Fe was applied to all samples following the procedures described by Dauphas et al. (2004; 2009b); such procedures are routinely utilized in our laboratory (*e.g.*, Wang et al., 2011; 2012a; 2012b). Samples were loaded on to columns filled with 1 mL AG1-X8 200-400 mesh anion-exchange resin. Matrix elements were eluted in 6 M HCl and Fe was subsequently eluted in 0.4 M HCl. The ion chromatography procedures were repeated for maximum purification. The yield of the procedure is close to 100% (Dauphas et al., 2009b). Two geostandards (BCR-2 and BHVO-2) were subjected to the same chemical treatment and analyzed as external standards to monitor for any fractionation induced due to the chemistry.



Figure 3-1. Photograph of the Antarctic L5 ordinary chondrite GRO 95540 broken up into five pieces using a Para-film sealed hand hammer.

3.2.3. Fe Isotope Analyses

The Fe isotopic compositions of samples were measured on a Thermo Scientific NEPTUNE Plus MC-ICP-MS (Multiple Collector-Inductively Coupled Plasma-Mass Spectrometry) at Washington University in St. Louis. Samples were introduced into the plasma ion source via a 100 $\mu\text{L}/\text{min}$ PFA MicroFlow nebulizer and a cyclonic spray chamber. The intensities of ^{54}Fe , ^{56}Fe , ^{57}Fe were measured on Faraday cups L2, C and H1, respectively. Isobaric interference of ^{54}Cr and ^{58}Ni were monitored by measuring the intensities of ^{53}Cr and ^{60}Ni on Faraday cups L3 and H4. Measurements were performed on the Fe peak shoulder to avoid polyatomic interferences from $^{40}\text{Ar}^{14}\text{N}^+$, $^{40}\text{Ar}^{16}\text{O}^+$ and $^{40}\text{Ar}^{16}\text{O}^1\text{H}^+$, running the instrument at medium resolution (resolving power $M/\Delta M \sim 8500$; Weyer and Schwieters, 2003). Instrumental

mass bias was corrected for using sample-standard bracketing. All results are reported as $\delta^{56}\text{Fe}$ and $\delta^{57}\text{Fe}$, calculated by the following equation.

$$\delta^x\text{Fe} = \left[\frac{\left({}^x\text{Fe} / {}^{54}\text{Fe} \right)_{\text{sample}}}{\left({}^x\text{Fe} / {}^{54}\text{Fe} \right)_{\text{standard}}} - 1 \right] \times 1000$$

In the above equation $x=56$ or 57 , and IRMM-014 is the standard. Analytical uncertainties are reported as $2 \times$ standard errors (2SE) of repeated measurements. As shown in Figure 3-2, the $\delta^{56}\text{Fe}$ and $\delta^{57}\text{Fe}$ of all of the meteorite and terrestrial samples display an excellent linear correlation (slope ~ 1.41), which is in good agreement with the expected mass-dependent fractionation lines (see Figure 3-2), and implies that our samples do not contain mass-independent Fe isotopic anomalies.

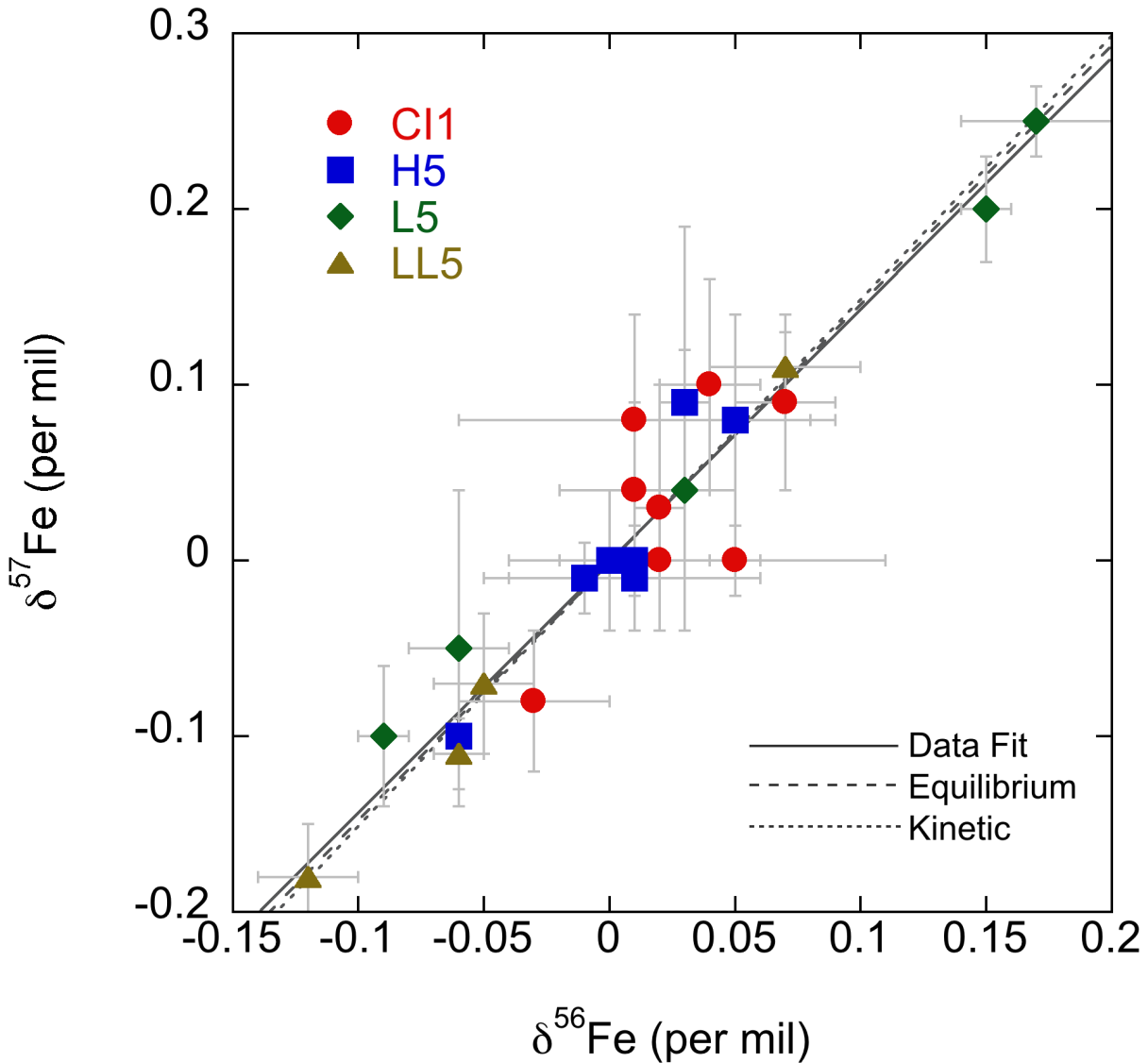


Figure 3-2. The bulk iron isotope compositions of the CI and ordinary chondrites from this study (see also Table 3-1). The least squares regression of the data, theoretical equilibrium and kinetic mass-dependent fractionation lines are shown in solid, dashed and dotted lines, respectively (see Young et al., 2002).

3.3. Results

All isotopic data are listed in Table 3-1 and shown in Figure 3-2. The Fe isotopic compositions of the two basaltic geostandards BCR-2 ($\delta^{56}\text{Fe} = 0.12 \pm 0.04\text{\textperthousand}$) and BHVO-2 ($\delta^{56}\text{Fe} = 0.10 \pm 0.02\text{\textperthousand}$) agree well with published data (~0.1; *e.g.*, Poitrasson et al., 2004; Weyer et al., 2005; Schoenberg and von Blanckenburg, 2006; Dauphas et al., 2009a; Craddock and Dauphas, 2011; Millet et al., 2012). Such analyses suggest that our analytical methods are robust, and provide a good evaluation of the accuracy of Fe isotope analysis in this study.

All of the Orgueil pieces have identical Fe isotopic compositions within error. Orgueil-6 is different from the five others based on its elemental abundances of Zn and REE, as previously reported by Barrat et al. (2012). This difference is probably due to local redistribution of these elements by aqueous fluids on the CI parent body (Barrat et al., 2012). Following Barrat et al. (2012), that excluding Orgueil-6 from the calculation of averages, we did not use Orgueil-6 in the calculation of the average Fe isotopic composition. The five other chips from four different Orgueil stones define an average $\delta^{56}\text{Fe}$ of $0.01 \pm 0.04\text{\textperthousand}$ (2SE). This average is consistent with previous studies of one Orgueil stone (*e.g.*, $-0.02 \pm 0.07\text{\textperthousand}$; Craddock and Dauphas, 2011).

The two other carbonaceous chondrites, Alais and Ivuna, have the same Fe isotopic composition as Orgueil, and all of the CI carbonaceous chondrite data define a very limited range (average $\delta^{56}\text{Fe} = 0.02 \pm 0.04\text{\textperthousand}$; range from -0.03 to $0.05\text{\textperthousand}$; see Figure 3-3). The Fe isotopic composition of CI chondrites is well homogenized. In addition to this isotopic homogeneity, our study also confirms that CI chondrites, on average, have $\delta^{56}\text{Fe} \sim 0.00\text{\textperthousand}$, which agrees with previous reports (Zhu et al., 2001; Kehm et al., 2003; Poitrasson et al., 2004; Schoenberg and von Blanckenburg, 2006; Craddock and Dauphas, 2011). We propose that $\delta^{56}\text{Fe} = 0.02 \pm 0.04\text{\textperthousand}$ is the best value for the average Fe isotopic composition of CI chondrites. This new average for

CI chondrites also supports the previous observations that all carbonaceous chondrites (CI, CM, CO and CV) have indistinguishable Fe isotopic compositions (-0.01 ± 0.01 ; see Craddock and Dauphas, 2011 and references therein) within current analytical precisions.

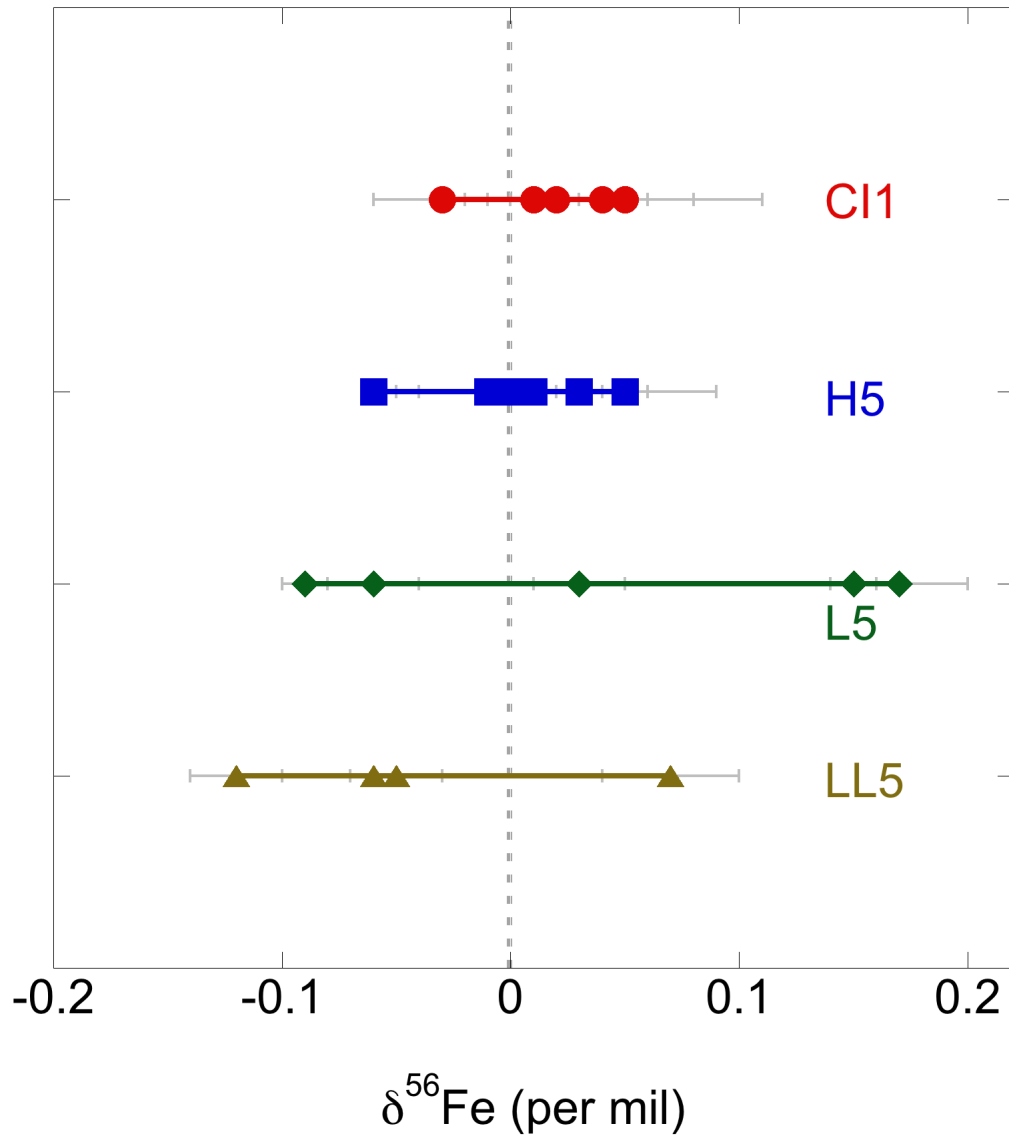


Figure 3-3. The ranges of iron isotope compositions of CI and ordinary chondrites from this study. Error bars (2SE) are shown as gray lines.

In contrast, the three ordinary chondrites show significantly larger Fe isotopic variations within the same stones (see Figure 3-3). Specifically, the different chips of LEW 85320 (H5), GRO 95540 (L5) and DOM 03194 (LL5) define ranges in $\delta^{56}\text{Fe}$ of 0.11‰, 0.26‰ and 0.19‰, respectively. However, the averages of the three ordinary chondrites ($\delta^{56}\text{Fe} = 0.00$) are indistinguishable from carbonaceous chondrites (see Figure 3-4), and agree with previous reports (Theis et al., 2008; Needham et al., 2009; Craddock et al., 2011). The Fe isotopic variations observed here between different chips of the same ordinary chondrites are as large as the Fe isotopic variation previously observed between different bulk ordinary chondrites (Theis et al., 2008; Needham et al., 2009). Therefore, this variation may be largely a matter of unrepresentative sampling of bulk meteorites and reflect the strongly Fe isotopic fractionated chondritic components (see discussion below). Caution should be taken when interpreting bulk ordinary chondrites when <1 g of homogeneous powder is used.

The three ordinary chondrites studied here are all Antarctic “finds”, however the Fe isotopic variations between different chips of one sample are unlikely to have been caused by terrestrial weathering effects. Firstly, the three samples used here are only minor to moderately weathered (see Table 3-1) and we carefully selected the “fresh” interior portions to avoid terrestrial contamination and weathering products. Secondly, terrestrial weathering effects have been observed only amongst the most weathered hot desert “finds”. Antarctic “finds” were preserved in ice during most of their terrestrial residence and have been less chemically altered compared to hot desert “finds” (Crozaz and Wadhwa, 2001; Saunier et al., 2010). Thirdly, no Fe isotopic fractionation due to weathering has been observed amongst Antarctic meteorites (Poitrasson et al., 2004; Saunier et al., 2010). Finally, Saunier et al. (2010) have studied the correlations between weathering condition and $\delta^{56}\text{Fe}$, and they show that even the most

weathered (W4 or W5) hot desert meteorites would only be enriched in the heavy Fe isotope by up to 0.07‰ ($\delta^{56}\text{Fe}$) due to the preferential loss of the lighter Fe isotopes to water in the Earth's environment. For the reasons above, we exclude the possibilities of terrestrial weathering/contamination from the following discussion.

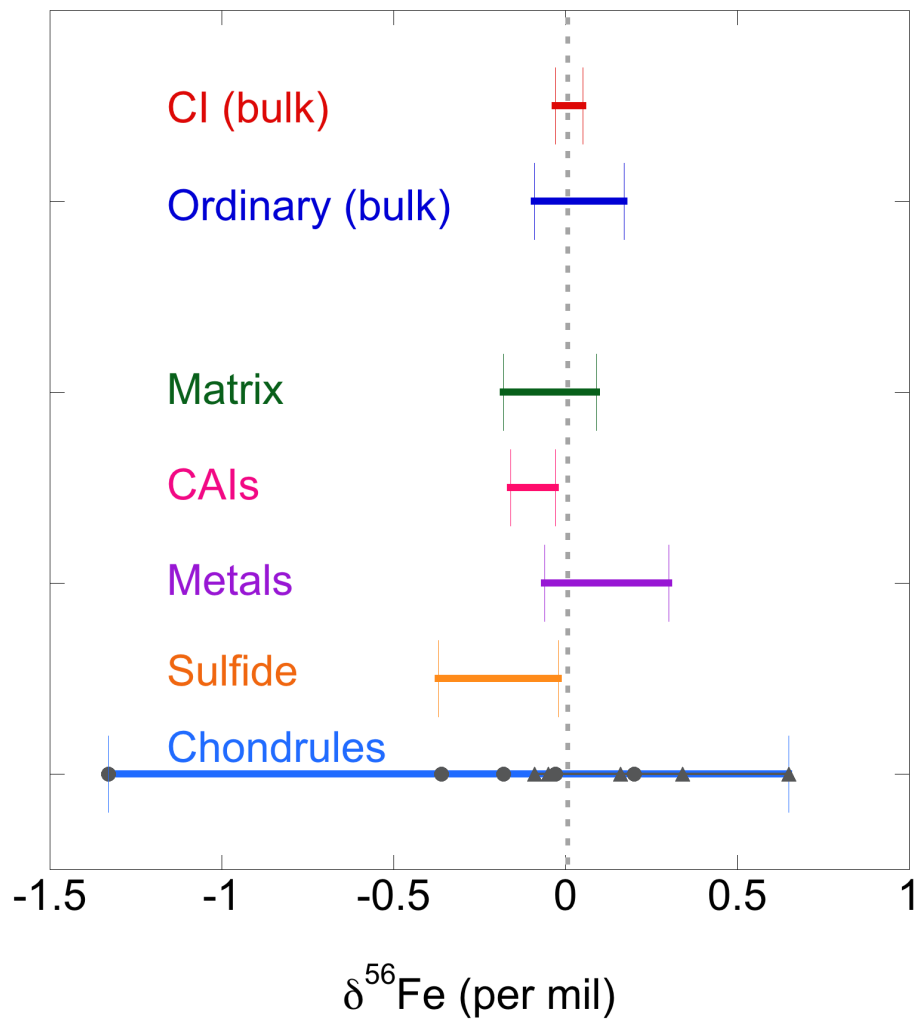


Figure 3-4. The ranges of iron isotope compositions of chondritic components (chondrules, matrix, CAIs and metals) and bulk chondrites. Only several studies report the types of the chondrules with their Fe isotopic values. These identified type I and II chondrules are highlighted as triangles and circles symbols, respectively. The data for bulk chondrites are from this study and the data for chondritic components are from literature sources: chondrules (Kehm et al., 2003; Mullane et al., 2005; Needham et al., 2009; Hezel et al., 2010), matrix (Mullane et al., 2005; Hezel et al., 2010), CAIs (Mullane et al., 2005), metals (Theis et al., 2008; Needham et al., 2009; Okabayashi et al., 2012) and sulfide (Needham et al., 2009).

Table 3-1. Iron isotope compositions of CI and ordinary chondrite

Sample Name	Type	Fall/find (weathering) ^a	Mass [mg] ^b	Fe [wt.%]	$\delta^{56}\text{Fe}$	2SE	$\delta^{57}\text{Fe}$	2SE	n ^d	Museum code ^e
Orgueil-1	CI1	Fall	23.2 (1000)	19.0 ^c	0.05	± 0.06	0.00	± 0.02	2	MNHN 219239
Orgueil-2	CI1	Fall	17.2 (620)	19.2 ^c	0.02	± 0.04	0.00	± 0.04	4	MNHN 222
Orgueil-3	CI1	Fall	17.5 (610)	20.9 ^c	-0.03	± 0.03	-0.08	± 0.04	5	MNHN 222
Orgueil-4	CI1	Fall	12.1 (840)	19.4 ^c	0.01	± 0.07	0.08	± 0.06	5	MNHN 234
Orgueil-5	CI1	Fall	12.2 (860)	19.2 ^c	0.01	± 0.03	0.04	± 0.05	5	MNHN 250
Orgueil-6	CI1	Fall	18.7 (1020)	18.7 ^c	0.07	± 0.02	0.09	± 0.05	5	MNHN 237
<i>Orgueil (average)^f</i>				19.5	0.01	± 0.04	0.01	± 0.04		
Alais	CI1	Fall	16.8 (330)	18.6 ^c	0.02	± 0.01	0.03	± 0.07	2	MNHN 24
Ivuna	CI1	Fall	12.6 (710)	18.9 ^c	0.04	± 0.02	0.10	± 0.06	2	MNHN 3578
<i>CI (average)^f</i>					0.02	± 0.04	0.02	± 0.05		
LEW 85320-1	H5	Find (Be)	14.7 (513)	10.7	-0.06	± 0.00	-0.10	± 0.03	3	JSC LEW 85320,45
LEW 85320-2	H5	Find (Be)	24.9 (584)	32.3	0.01	± 0.05	-0.01	± 0.03	3	JSC LEW 85320,45
LEW 85320-3	H5	Find (Be)	19.8 (267)	12.0	0.03	± 0.01	0.09	± 0.10	2	JSC LEW 85320,45
LEW 85320-4	H5	Find (Be)	17.6 (307)	21.7	0.00	± 0.04	0.00	± 0.04	3	JSC LEW 85320,45
LEW 85320-5	H5	Find (Be)	10.8 (410)	29.6	0.05	± 0.04	0.08	± 0.06	3	JSC LEW 85320,45
LEW 85320-6	H5	Find (Be)	17.8 (516)	24.6	0.01	± 0.01	0.00	± 0.02	3	JSC LEW 85320,45
LEW 85320-7	H5	Find (Be)	9.8 (498)	11.5	-0.01	± 0.04	-0.01	± 0.02	3	JSC LEW 85320,45
<i>LEW 85320 (average)</i>				20.3	0.00	± 0.03	0.01	± 0.05		
GRO 95540-1	L5	Find (A)	14.3 (657)	4.6	-0.09	± 0.01	-0.10	± 0.04	3	JSC GRO 95540,8
GRO 95540-2	L5	Find (A)	12.1 (387)	5.8	0.15	± 0.01	0.20	± 0.03	3	JSC GRO 95540,8
GRO 95540-3	L5	Find (A)	20.7 (652)	41.9	0.03	± 0.02	0.04	± 0.08	3	JSC GRO 95540,8
GRO 95540-4	L5	Find (A)	23.2 (961)	3.9	0.17	± 0.03	0.25	± 0.02	3	JSC GRO 95540,8
GRO 95540-5	L5	Find (A)	8.8 (492)	5.7	-0.06	± 0.02	-0.05	± 0.09	3	JSC GRO 95540,8
<i>GRO 95540 (average)</i>				12.4	0.04	± 0.11	0.07	± 0.14		
DOM 03194-1	LL5	Find (A)	14.2 (392)	10.4	-0.12	± 0.02	-0.18	± 0.03	3	JSC DOM 03194,5
DOM 03194-2	LL5	Find (A)	9.7 (563)	13.6	0.07	± 0.03	0.11	± 0.02	3	JSC DOM 03194,5
DOM 03194-3	LL5	Find (A)	13.1 (277)	9.5	-0.05	± 0.02	-0.07	± 0.04	3	JSC DOM 03194,5
DOM 03194-4	LL5	Find (A)	11.0 (450)	8.8	-0.06	± 0.01	-0.11	± 0.02	3	JSC DOM 03194,5
<i>DOM 03194 (average)</i>				10.6	-0.04	± 0.08	-0.06	± 0.12		
<i>Ordinary Chondrites (average)</i>					0.00	± 0.04	0.01	± 0.06		
BCR-2	Basalt				0.12	± 0.04	0.19	± 0.05	4	
BHVO-2	Basalt				0.10	± 0.02	0.12	± 0.04	5	

^a The weathering conditions are from MetBase (version 7.1) and references therein. Weathering index A, B or C represents “minor”, “moderate” or “severe” rustiness, respectively. Letter “e” represents evaporite minerals visible.

^b The numbers in the parentheses are the masses of the well-mixed powders.

^c Fe concentration data for the same CI chondrite solutions have been measured and reported by Barrat et al (2012).

^d Number of measurements; ^e MNHN =Muséum National d’Histoire Naturelle, Paris. JSC = NASA Johnson Space Center, Houston.

^f Orgueil-6 has different elemental compositions from those of other Orgueil samples (Barrat et al. 2012). It is not included in the calculation of the average.

3.4. Discussion

3.4.1. Fe Isotopic Homogeneity of the Early Solar Nebula

The four stable isotopes of Fe are formed by different nucleosynthesis processes in various stellar environments (Clayton, 2003). However, the Fe isotopic compositions of terrestrial and extraterrestrial samples all fall on the same mass-dependent fractionation line in a three-isotope diagram and no nucleosynthetic anomalies remain (see Figure 3-2; and Wang et al., 2011). This shows that the different stellar sources of Fe were well homogenized in the early solar nebula prior to the accretion of the parent bodies of the chondrites. Some presolar grains have survived such homogenization and have preserved large isotope anomalies for elements such as C, N, O, Si and noble gases (*e.g.*, Zinner, 2007). Preliminary reports have shown that some presolar grains have non-solar Fe isotopic compositions (Floss et al., 2008; Marhas et al., 2008; Ong et al., 2012). However, except for a few FUN (Fractionated and Unidentified Nuclear Effects) CAIs (Calcium Aluminum-rich Inclusions) from the Allende CV3 chondrite (Voelkening and Papanastassiou, 1989), Fe isotopic anomalies have not been observed in either bulk or stepwise leaching of primitive and differentiated meteorites (Dauphas et al., 2008; Wang et al., 2011). Furthermore, all of the carbonaceous and ordinary chondrites, including the data from this study (Zhu et al., 2001; Kehm et al., 2003; Poitrasson et al., 2004; Schoenberg and von Blanckenburg, 2006; Craddock and Dauphas, 2011) have the same average bulk Fe isotope compositions ($\delta^{56}\text{Fe} \sim 0.00\text{\textperthousand}$) within analytical error, even if they have different chemical compositions (CI, CM, CO, CV LL, L, and H) and have experienced distinct secondary alteration processes on parent bodies (petrological types 1 to 7). All of these pieces of evidence indicate an efficient mixing of Fe in the starting materials in the early solar nebula, without large secondary isotopic fractionation effects on parent bodies such as aqueous alteration and thermal

metamorphism. The average composition of CI chondrites, calculated from six different chips from Orgueil together with samples from Ivuna and Alais ($\delta^{56}\text{Fe} = 0.02 \pm 0.04\text{\textperthousand}$) represents the best estimate of the Fe isotopic composition of our Solar System.

3.4.2. Fe Isotope Fractionation between Chondritic Components

Even though on average CI and ordinary chondrites have indistinguishable Fe isotopic compositions ($0.02 \pm 0.04\text{\textperthousand}$ vs. $0.00 \pm 0.04\text{\textperthousand}$; see Table 3-1), ordinary chondrites show larger isotopic heterogeneity within one sample than CI. This is most likely due to variable contents of their different components (chondrules, metals and matrix, etc.), which are isotopically distinct for Fe. Chondrules and matrix are the two main components of chondrites; together they make up more than 90% of chondrites by volume (Scott and Krot, 2005) with CAIs, metals and sulfides as minor components in most chondrite groups. In detail, different groups of chondrites have variable amounts of these components. For example, CI chondrites are composed of more than 95 vol.% matrix and less than 5 vol.% chondrules, while ordinary chondrites comprise 60-80 vol.% chondrules, 10-15 vol.% matrix and ~ 10 vol.% metals (Scott and Krot, 2007). In early literature, due to the larger analytical uncertainties of ion microprobe techniques in comparison to MC-ICP-MS, no resolvable Fe isotopic variations between chondritic components were detectable (*e.g.*, Alexander and Wang, 2001). However, with the recent development of MC-ICP-MS and a large improvement in analytical precision, Fe isotopic variations between chondrules, matrix, CAIs and metals have since been resolved (Kehm et al., 2003; Mullane et al., 2005; Theis et al., 2008; Needham et al., 2009; Hezel et al., 2010; Okabayashi et al., 2012). The isotopic ranges of such components are as follows (all data are ‰): chondrules $-1.33 < \delta^{56}\text{Fe} < +0.65$, matrix $-0.18 < \delta^{56}\text{Fe} < +0.09$, CAIs $-0.16 < \delta^{56}\text{Fe} < -0.03$, metals $-0.06 < \delta^{56}\text{Fe} < +0.30$.

and sulfide $-0.37 < \delta^{56}\text{Fe} < +0.02$. As shown in Figure 3-4, the degree of isotopic variation within each chondritic component is significant.

Of the chondritic components, chondrules display the largest variation in Fe isotope compositions. The refractory Type I chondrules are isotopically heavier in Fe than the less refractory Type II chondrules (Mullane et al., 2005): Type I chondrules $\delta^{56}\text{Fe} = -0.05\text{\textperthousand}$ to $+0.65\text{\textperthousand}$; average $0.20 \pm 0.11\text{\textperthousand}$; Type II chondrules $\delta^{56}\text{Fe} = -1.33\text{\textperthousand}$ to $0.20\text{\textperthousand}$; average $-0.34 \pm 0.10\text{\textperthousand}$. Chondrules were formed by multiple stage heating events in the early solar nebula (Scott and Krot, 2005), wherein it has been proposed that refractory Type I chondrules represent partial evaporation residues of volatile Type II chondrules (Jones, 1990; Alexander, 1994); alternatively, Type I and II chondrules were formed as their precursors interacted (through evaporation/condensation) with surrounding nebular gas (Hewins and Zanda, 2012). Partial loss of Fe during a high-temperature heating event should enrich the surrounding gas in the lighter isotopes and enrich the residue in the heavier isotopes. Re-condensation of these Fe isotopically light vapors could therefore produce isotopically light chondrules (rims). Even though the degree of fractionation observed is still smaller than the expectation of free evaporation/condensation under traditional Rayleigh conditions (Alexander and Wang, 2001), nebular processing, evaporation and/or recondensation could modify the Fe isotopic composition of chondrules. The heterogeneous distribution of chondrules between chondrite groups should therefore result in larger isotopic heterogeneities within individual ordinary chondrites (which are chondrule rich), compared to CI chondrites (which are chondrule poor; see Figures 3-4 and 3-5).

The Fe isotopic variations in both metals and sulfides are not as large as those in chondrules, however, because metal and sulfide phases have the highest Fe concentrations in chondrites, the abundance of metals and sulfides have an important control on the bulk Fe

isotope compositions. Metals in chondrites are generally enriched in the heavier Fe isotopes (Theis et al., 2008; Needham et al., 2009; Okabayashi et al., 2012), while typically, sulfides in chondrites are lighter (Needham et al., 2009), which agrees well with the observation of metals and sulfides in iron meteorites and pallasites (Poitrasson et al., 2005; Williams et al., 2006) and also the theoretical prediction of preferential partitioning of heavy/light Fe isotopes into metal/sulfide phases (Polyakov and Mineev, 2000; Polyakov and Soultanov, 2011). The iron isotope compositions ($\delta^{56}\text{Fe}$) of metals separated from H, L and LL ordinary chondrites have been reported as 0.09‰, 0.20‰ and 0.28‰, respectively (Theis et al., 2008), while no systematic variation between metals in H, L and LL ordinary chondrites have been found in Needham et al. (2009).

Using mixing calculations of the various chondritic components, we can model the bulk Fe isotopic compositions of ordinary chondrites (see Figure 3-6). Chondrules, metals and matrix are the only three components considered in ordinary chondrites for the purpose of simplification. CAIs are minor components for ordinary chondrites (<0.1 vol%; Scott and Krot, 2007), and are poor in Fe; therefore they were neglected in our calculations. All the parameters and values used in our models are listed in Table 3-2 and the results are shown in Figure 3-6. Three major factors control the chondrite bulk Fe isotopic compositions of ordinary chondrites, which agrees with the discussion above, which are (1) chondrule abundance, (2) chondrule type and (3) metal abundance. Our calculations indicate that up to 0.1‰ $\delta^{56}\text{Fe}$ variations (between −0.05‰ and +0.05‰; see Figure 3-6) in bulk meteorites could be explained simply by these three factors. Chondrule abundance in ordinary chondrites can vary between 60 to 80 vol.% (Scott and Krot, 2007). Higher chondrule abundance is usually correlated with higher bulk $\delta^{56}\text{Fe}$ when other factors are unchanged.

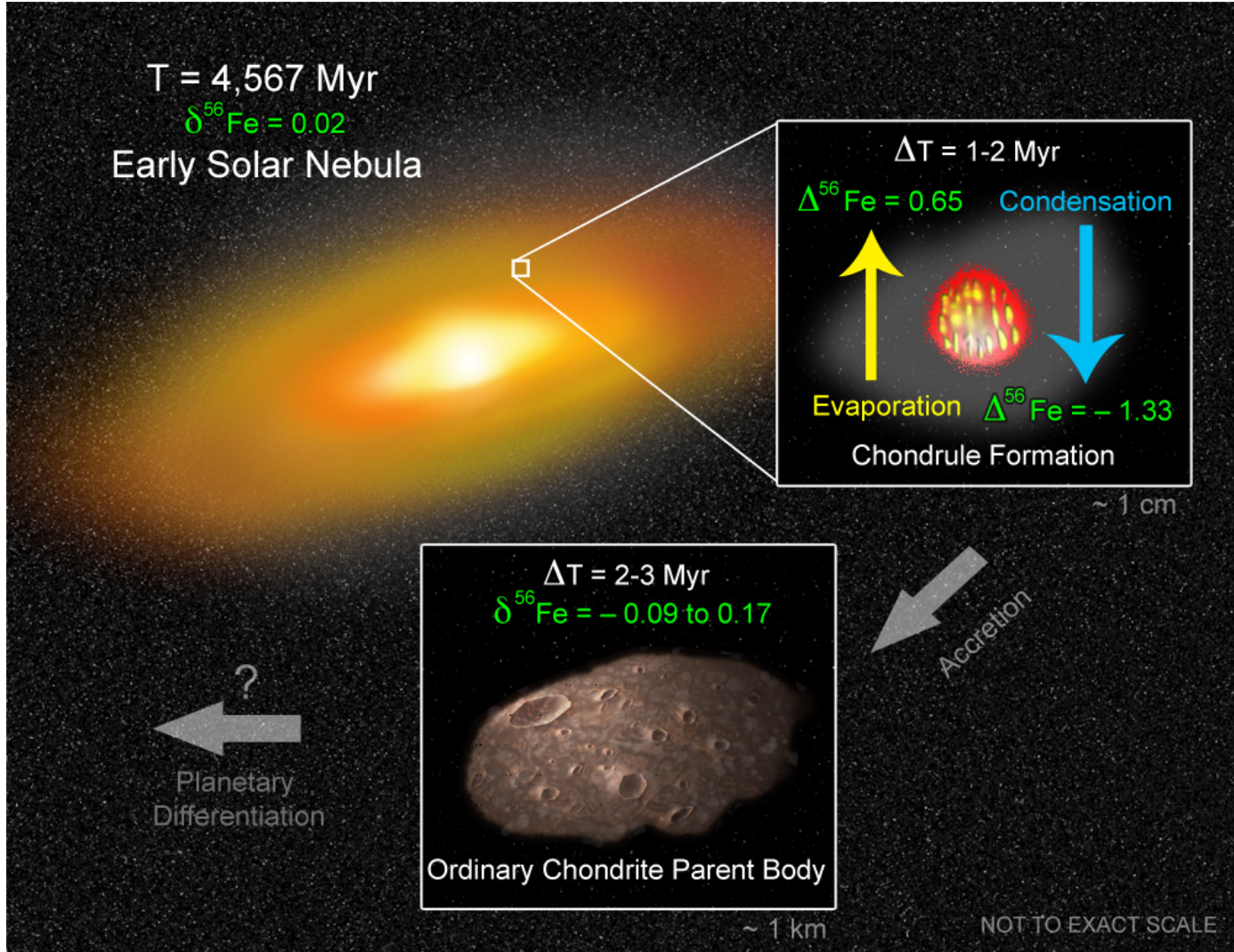


Figure 3-5. Cartoon showing iron isotope composition evolution in the early Solar System.

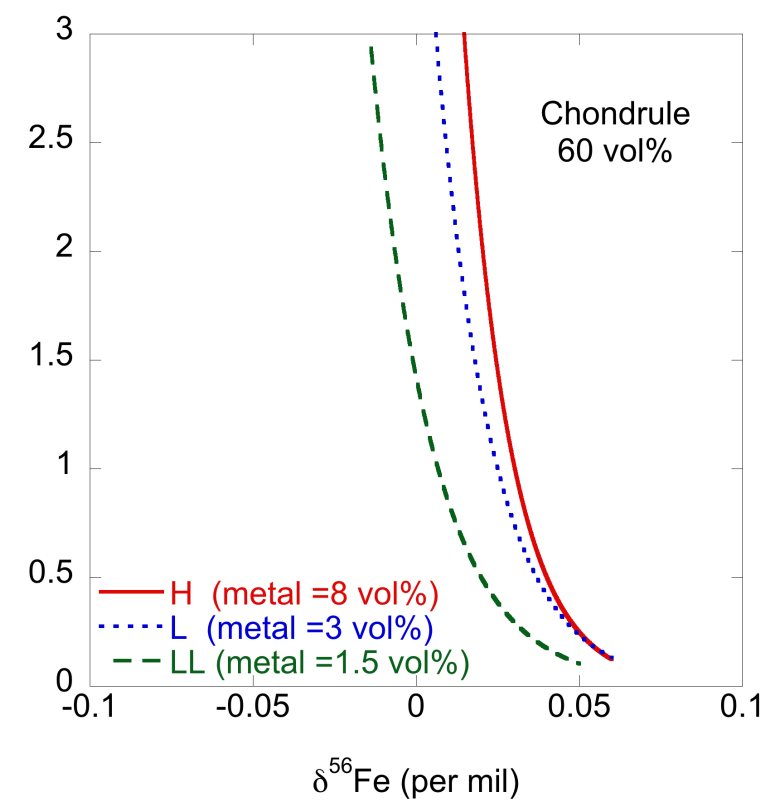
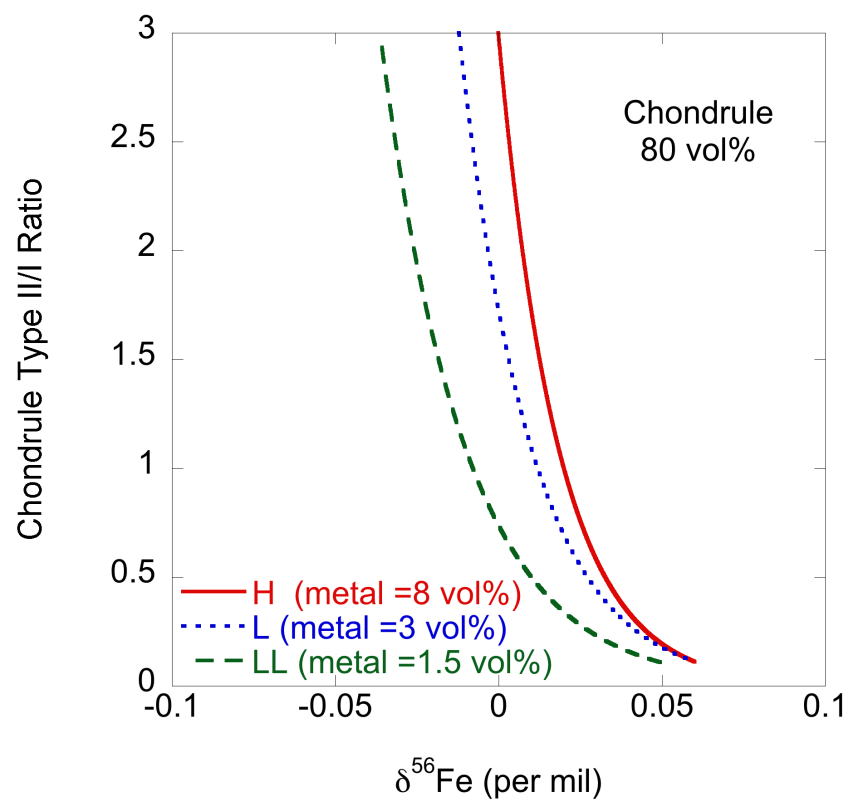


Figure 3-6. Modeling of the bulk iron isotope compositions of ordinary chondrites by mixing chondritic components with varying chondrule type II/I ratios.

Table 3-2. Parameters and values used in the modeling of the bulk iron isotope compositions of ordinary chondrites by mixing chondritic components

Parameter	Value	Reference
Type I chondrule $\delta^{56}\text{Fe}$ (‰)	+0.20	(Mullane et al., 2005)
Type II chondrule $\delta^{56}\text{Fe}$ (‰)	-0.34	(Mullane et al., 2005)
Metal $\delta^{56}\text{Fe}$ (‰) for H, L and LL	0.09, 0.20, 0.28	(Theis et al., 2008)
Matrix $\delta^{56}\text{Fe}$ (‰)	~0	(Mullane et al., 2005; Hezel et al., 2010)
Chondrule density (g/cm ³)	~3	(Hughes, 1980)
Pure iron density (g/cm ³)	7.875	(Lodders and Fegley, 1998)
Bulk density (g/cm ³) for H, L and LL	3.44, 3.40, 3.29	(Wilkison and Robinson, 2000)
Type I and II Chondrule Fe concentration (wt.%)	0.91, 9.87	(Jones and Scott, 1989)
Metal Fe concentration (wt.%)	~100%	Pure iron metal for simplification
Bulk Fe concentration (wt.%) for H, L and LL	27.2, 21.8, 19.8	(Lodders and Fegley, 1998)

Chondrule type proportion is another important variable controlling bulk isotopic compositions. Refractory Type I chondrules are enriched in Fe heavy isotopes while volatile Type II chondrules are depleted (Mullane et al., 2005). Type I chondrules are Fe-poor whereas Type II chondrules are very Fe-rich (Jones and Scott, 1989); although it has been recently found that the Fe content in chondrules is possibly a continuum rather than a bimodality (Berlin, 2009). A high proportion of Fe-rich Type II chondrules in chondrites could strongly affect bulk composition and efficiently drag bulk $\delta^{56}\text{Fe}$ to negative values (see high Type II/I ratio scenarios in Figure 3-6). The amounts of Type I and II chondrules are highly variable between H, L and LL ordinary chondrites. On average, the Type II/I ratios (v/v) are 0.8, 2.1 and 2.8 for H, L and LL ordinary chondrites respectively, but there is considerable overlap between each group (Zanda et al., 2006). By using the average ratios of Type II/I, we can predict the bulk Fe isotopic compositions for H (0.02‰ to 0.03‰), L (-0.01‰ to 0.01‰) and LL (-0.04‰ to -0.02‰).

These small differences between the three ordinary chondrite groups predicted by our model are at the limit of our current analysis precision, and have not yet been observed (*i.e.*, Needham et al., 2009).

In addition, metal abundance appears to play an important role in controlling bulk Fe isotope composition. From LL to L and H ordinary chondrites, metal abundance increases from 1.5 to 3 and 8 vol% (Scott and Krot, 2007). Because the metal abundances appear to correlate with chondrule Type II/I ratios (Zanda et al., 2006), these two factors are coupled in controlling bulk Fe isotope composition. For example, H ordinary chondrites have high metal abundances (high $\delta^{56}\text{Fe}$) and also high Type II/I chondrule ratios (low $\delta^{56}\text{Fe}$). This antithetic effect shown in our model is very important to the bulk Fe isotope composition and could explain why, on average, no resolvable systematic variations of bulk $\delta^{56}\text{Fe}$ between H, L, and LL ordinary chondrites have been observed in previous studies (*i.e.*, Needham et al., 2009) and also why on average ordinary chondrites have the same bulk Fe isotopic composition as CIs.

Given that the abundances of chondritic components can be highly variable between different samples and can significantly control bulk Fe isotope compositions, care should be taken when interpreting isotopic data acquired using small mass samples, as sampling bias could become an issue (isotopically light or heavy chondrules, or metal grains, etc.). Even large chips ($\sim 1\text{g}$) from the same ordinary chondrites have $\delta^{56}\text{Fe}$, which can vary up to 0.26‰ in $\delta^{56}\text{Fe}$. These isotopic variations within one individual sample are comparable to the bulk variations measured within the whole ordinary chondrite group (*e.g.*, Needham et al., 2009; Craddock and Dauphas, 2011). Nonetheless, this will not change the fact that on average ordinary and CIs have indistinguishable bulk Fe isotopic composition as observed in this and previous studies, which suggests that Fe isotopes were well homogenized in the early Solar System.

3.5. Conclusions

In this study, we report the most complete Fe isotope dataset of CI chondrites using large sample masses. Thus, we provide the best estimate of Fe isotopic composition for CI chondrites ($\delta^{56}\text{Fe} = 0.02 \pm 0.04\text{\textperthousand}$). We propose that this average represents the bulk Fe isotopic composition of our Solar System.

Different $\sim 1\text{g}$ chips of CI chondrites display a very limited range of Fe isotope compositions, while several $\sim 1\text{g}$ chips from the same ordinary chondrites show significantly larger variations. This appears to be the result of different modal proportions of chondritic components between CI and ordinary chondrites. Amongst all of the main chondritic components, chondrules have the largest Fe isotopic variation because of fractionation during evaporation and recondensation in the solar nebular setting. By employing mass balance calculations, we have shown that chondrule abundance and type, in addition to metal abundance are the main parameters controlling the bulk Fe isotopic compositions of the different ordinary chondrites. CI chondrites do not show large isotopic heterogeneity because they are composed mainly of matrix, with only a small (<5%) proportion of chondrules; this is not the case for ordinary chondrites, which have greater modal abundances of chondrules.

Ordinary chondrites exhibit large Fe isotopic heterogeneity within 1g chips of individual samples (up to $0.26\text{\textperthousand}$). This suggests that large samples are needed to obtain accurate bulk compositions, to avoid sampling bias (caused by natural, uneven distributions of large chondrules or metal grains, and/or by incomplete mixing during sample preparation). For CI chondrites, which contain dominantly matrix and lack chondrules and other chondritic components, small masses of samples should be enough to obtain a homogeneous bulk composition. This is serendipitous, given the low abundance of CI chondrites as a group.

References

- Alexander C. M. O'D. (1994) Trace element distributions within ordinary chondrite chondrules: Implications for chondrule formation conditions and precursors. *Geochim. Cosmochim. Acta* **58**, 3451–3467.
- Alexander C. M. O'D. and Wang J. (2001) Iron isotopes in chondrules: Implications for the role of evaporation during chondrule formation. *Meteorit. Planet. Sci.* **36**, 419–428.
- Anand M., Russell S. S., Blackhurst R. L. and Grady M. M. (2006) Searching for signatures of life on Mars: an Fe-isotope perspective. *Philos. Trans. R. Soc. Lond., B, Biol. Sci.* **361**, 1715–1720.
- Anders E. and Ebihara M. (1982) Solar-system abundances of the elements. *Geochim. Cosmochim. Acta* **46**, 2363–2380.
- Anders E. and Grevesse N. (1989) Abundances of the elements: Meteoritic and solar. *Geochim. Cosmochim. Acta* **53**, 197–214.
- Barrat J. A., Zanda B., Moynier F., Bollinger C., Liorzou C. and Bayon G. (2012) Geochemistry of CI chondrites: Major and trace elements, and Cu and Zn Isotopes. *Geochim. Cosmochim. Acta* **83**, 79–92.
- Berlin J. (2009) Mineralogy and bulk chemistry of chondrules and matrix in petrologic type 3 chondrites: Implications for early solar system processes. Ph.D. thesis, The University of New Mexico, Albuquerque, NM, USA.
- Clayton D.D. (2003) Handbook of Isotopes in the Cosmos: Hydrogen to Gallium. Cambridge: Cambridge University Press. 328 p.
- Craddock P. R. and Dauphas N. (2011) Iron isotopic compositions of geological reference materials and chondrites. *Geostand. Geoanal. Res.* **35**, 101–123.
- Crozaz G., and Wadhwa M. (2001) The terrestrial alteration of saharan shergottites dar al gani 476 and 489: a case study of weathering in a hot desert environment. *Geochim. Cosmochim. Acta* **65**, 971–977.
- Dauphas N., Cook D. L., Sacarabany A., Fröhlich C., Davis A. M., Wadhwa M., Pourmand A., Rauscher T. and Gallino R. (2008) Iron 60 evidence for early injection and efficient mixing of stellar debris in the protosolar nebula. *Astrophys. J.* **686**, 560–569.
- Dauphas N., Craddock P. R., Asimow P. D., Bennett V. C., Nutman A. P. and Ohnenstetter D. (2009a) Iron isotopes may reveal the redox conditions of mantle melting from Archean to Present. *Earth Planet. Sci. Lett.* **288**, 255–267.
- Dauphas N., Janney P. E., Mendybaev R. A., Wadhwa M., Richter F. M., Davis A. M., van Zuilen M., Hines R. and Foley C. N. (2004) Chromatographic separation and multicollection-ICPMS analysis of iron. Investigating mass-dependent and -independent isotope effects. *Anal. Chem.* **76**, 5855–5863.

- Dauphas N., Pourmand A. and Teng F.-Z. (2009b) Routine isotopic analysis of iron by HR-MC-ICPMS: How precise and how accurate? *Chem. Geol.* **267**, 175–184.
- Floss C., Stadermann F. J. and Bose M. (2008) Circumstellar Fe oxide from the Acfer 094 carbonaceous chondrite. *Astrophys. J.* **672**, 1266–1271.
- Grady M. M., Gibson E. K., Wright I. P. and Pillinger C. T. (1989) The formation of weathering products on the LEW-85320 ordinary chondrite - evidence from carbon and oxygen stable isotope compositions and implications for carbonates in SNC meteorites. *Meteoritics* **24**, 1–7.
- Hezel D. C., Needham A. W., Armytage R., Georg B., Abel R. L., Kurahashi E., Coles B. J., Rehkämper M. and Russell S. S. (2010) A nebula setting as the origin for bulk chondrule Fe isotope variations in CV chondrites. *Earth Planet. Sci. Lett.* **296**, 423–433.
- Hewins R. H., and Zanda B. (2012) Chondrules: Precursors and interactions with the nebular gas. *Meteorit. Planet. Sci.* **47**, 1120–1138.
- Hughes D. W. (1980) The dependence of chondrule density on chondrule size. *Earth Planet. Sci. Lett.* **51**, 26–28.
- Huss G. R., Rubin A. E. and Grossman J. N. (2006) Thermal metamorphism in chondrites. In *Meteorites and the early solar system II* (ed. Lauretta D. S. and McSween H. Y) Tucson: University of Arizona Press. pp. 567–586.
- Jones R. H., and Scott E. R. D. (1989) Petrology and thermal history of type IA chondrules in the Semarkona (LL3.0) chondrite. *Lunar Planet. Sci. Conf. Proc.* **19**, 523–536.
- Jones R. H. (1990) Petrology and mineralogy of Type II, FeO-rich chondrules in Semarkona (LL3.0): Origin by closed-system fractional crystallization, with evidence for supercooling. *Geochim. Cosmochim. Acta* **54**, 1785–1802.
- Jull A. J., Cheng S., Gooding J. L. and Velbel M. A. (1988) Rapid growth of magnesium-carbonate weathering products in a stony meteorite from antarctica. *Science* **242**, 417–419.
- Kehm K., Hauri E. H., Alexander C. M. O'D. and Carlson R. W. (2003) High precision iron isotope measurements of meteoritic material by cold plasma ICP-MS. *Geochim. Cosmochim. Acta* **67**, 2879–2891.
- Krot A. N., Keil K. and Scott E. R. D. (2007) Classification of Meteorites. In *Meteorites, Comets and Planets, Treatise on Geochemistry* (ed. A. M. Davis).
- Lodders K. (2003) Solar system abundances and condensation temperatures of the elements. *Astrophys. J.* **591**, 1220–1247.
- Lodders K., and Fegley B. (1998) *The planetary scientist's companion*, New York: Oxford University Press.

- Lodders K., Palme H. and Gail H.-P. (2009) Abundances of the elements in the solar system. In *Landolt-Bornstein (New Series)* (ed. J. E. Trumper). Springer Verlag, Berlin. pp. 560–630.
- Marhas K. K., Amari S., Gyngard F., Zinner E. and Gallino R. (2008) Iron and nickel isotopic ratios in presolar SiC grains. *Astrophys. J.* **689**, 622–645.
- Millet M.-A., Baker J. A and Payne C. E. (2012) Ultra-precise stable Fe isotope measurements by high resolution multiple-collector inductively coupled plasma mass spectrometry with a ^{57}Fe – ^{58}Fe double spike. *Chem. Geol.* **304–305**, 18–25.
- Mullane E., Russell S. S. and Gounelle M. (2005) Nebular and asteroidal modification of the iron isotope composition of chondritic components. *Earth Planet. Sci. Lett.* **239**, 203–218.
- Needham A. W., Porcelli D. and Russell S. S. (2009) An Fe isotope study of ordinary chondrites. *Geochim. Cosmochim. Acta* **73**, 7399–7413.
- Okabayashi S., Yokoyama T. and Hirata T. (2012) Iron isotopic signature for Fe-Ni metal of ordinary chondrite using newly developed technique; LAL-MC-ICPMS. *Lunar Planet. Sci. XLIII*. Lunar Planet. Inst., Woodlands. #1871(abstr.).
- Ong W. J., Floss C. and Gyngard F. (2012) Negative secondary ion measurements of ^{54}Fe / ^{56}Fe and ^{57}Fe / ^{56}Fe in presolar silicate grains from Acfer 094. *Lunar Planet. Sci. XLIII*. Lunar Planet. Inst., Woodlands. #1864(abstr.).
- Poirrasson F. (2009) Probes of the ancient and the inaccessible. *Science* **323**, 882–883.
- Poirrasson F. and Freydier R. (2005) Heavy iron isotope composition of granites determined by high resolution MC-ICP-MS. *Chem. Geol.* **222**, 132–147.
- Poirrasson F., Halliday A. N., Lee D. C., Levasseur S. and Teutsch N. (2004) Iron isotope differences between Earth, Moon, Mars and Vesta as possible records of contrasted accretion mechanisms. *Earth Planet. Sci. Lett.* **223**, 253–266.
- Poirrasson F., Levasseur S. and Teutsch N. (2005) Significance of iron isotope mineral fractionation in pallasites and iron meteorites for the core-mantle differentiation of terrestrial planets. *Earth Planet. Sci. Lett.* **234**, 151–164.
- Polyakov V. B. and Mineev S. D. (2000) The use of Mossbauer spectroscopy in stable isotope geochemistry. *Geochim. Cosmochim. Acta* **64**, 849–865.
- Polyakov V. B. and Soultanov D. M. (2011) New data on equilibrium iron isotope fractionation among sulfides: Constraints on mechanisms of sulfide formation in hydrothermal and igneous systems. *Geochim. Cosmochim. Acta* **75**, 1957–1974.
- Saunier G., Poirrasson F., Moine B., Gregoire M. and Seddiki A. (2010) Effect of hot desert weathering on the bulk-rock iron isotope composition of L6 and H5 ordinary chondrites. *Meteorit. Planet. Sci.* **45**, 195–209.
- Schoenberg R. and von Blanckenburg F. (2006) Modes of planetary-scale Fe isotope fractionation. *Earth Planet. Sci. Lett.* **252**, 342–359.

- Scott E. R. D. and Krot A. N. (2005) Chondritic Meteorites and the High-Temperature Nebular Origins of Their Components. In *Chondrites and the Protoplanetary Disk, ASP Conference Series, Vol. 341* (eds. A. N. Krot, E. R. D. Scott, and B. Reipurth). pp. 15–53.
- Scott E. R. D. and Krot A. N. (2007) Chondrites and Their Components. In *Meteorites, Comets and Planets, Treatise on Geochemistry* (ed. A. M. Davis).
- Theis K. J., Burgess R., Lyon I. C. and Sears D. W. (2008) The origin and history of ordinary chondrites: A study by iron isotope measurements of metal grains from ordinary chondrites. *Geochim. Cosmochim. Acta* **72**, 4440–4456.
- Velbel M., Long D. and Gooding J. (1991) Terrestrial weathering of Antarctic stone meteorites: Formation of Mg-carbonates on ordinary chondrites. *Geochim. Cosmochim. Acta* **55**, 67–76.
- Voelkening J. and Papanastassiou D. A. (1989) Iron isotope anomalies. *Astrophys. J.* **347**, L43.
- Wang K., Moynier F., Dauphas N., Barrat J.-A., Craddock P. and Sio C. K. (2012a) Iron isotope fractionation in planetary crusts. *Geochim. Cosmochim. Acta* **89**, 31–45.
- Wang K., Moynier F., Podosek F. A. and Foriel J. (2012b) An iron isotope perspective on the origin of the nanophase metallic iron in lunar regolith. *Earth Planet. Sci. Lett.* **337–338**, 17–24.
- Wang K., Moynier F., Podosek F. and Foriel J. (2011) ^{58}Fe and ^{54}Cr in early solar system materials. *Astrophys. J.* **739**, L58.
- Weyer S. (2008) What drives iron isotope fractionation in magma. *Science* **320**, 1600–1601.
- Weyer S., Anbar A. D., Brey G. P., Munker C., Mezger K. and Woodland A. B. (2005) Iron isotope fractionation during planetary differentiation. *Earth Planet. Sci. Lett.* **240**, 251–264.
- Weyer S. and Schwiters J.B. (2003) High precision Fe isotope measurements with high mass resolution MC-ICPMS. *Int. J. Mass Spectrom.* **226**, 355–368.
- Wilkinson S. L. and Robinson M. S. (2000) Bulk density of ordinary chondrite meteorites and implications for asteroidal internal structure. *Meteorit. Planet. Sci.* **35**, 1203–1213.
- Williams H. M., Markowski A., Quitte G., Halliday A. N., Teutsch N., and Levasseur S. 2006. Fe isotope fractionation in iron meteorites: New insights into metal-sulphide segregation and planetary accretion. *Earth Planet. Sci. Lett.* **250**, 486–500.
- Young E. D., Galy A. and Nagahara H. (2002) Kinetic and equilibrium mass-dependent isotope fractionation laws in nature and their geochemical and cosmochemical significance. *Geochim. Cosmochim. Acta* **66**, 1095–1104.
- Zanda B., Hewins R., Bourotdenise M., Bland P. and Albarede F. (2006) Formation of solar nebula reservoirs by mixing chondritic components. *Earth Planet. Sci. Lett.* **248**, 650–660.

Zhu X. K., Guo Y., O’Nions R. K., Young E. D. and Ash R. D. (2001) Isotopic homogeneity of iron in the early solar nebula. *Nature* **412**, 311–313.

Zinner E. (2007) Presolar Grains. In *Meteorites, Comets and Planets, Treatise on Geochemistry* (ed. A. M. Davis).

CHAPTER 4 :

THE FE ISOTOPE COMPOSITION OF ENSTATITE METEORITES: IMPLICATIONS FOR THEIR ORIGIN AND THE METAL/SULFIDE FE ISOTOPIC FRACTIONATION FACTOR

This chapter has been submitted to *Geochimica et Cosmochimica Acta* and is currently under review for the possibility of publication: Wang, K., Savage, P.S., Moynier, F. The Fe Isotope Composition of Enstatite Meteorites: Implications for Their Origin and the Metal/sulfide Fe Isotopic Fractionation Factor. *Geochimica et Cosmochimica Acta*, in review.

Abstract

Despite their unusual chemical composition, it is often proposed that the enstatite chondrites represent a significant component of Earth building materials, based on their terrestrial similarity for numerous isotope systems. In order to investigate a possible genetic relationship between the Fe isotope composition of enstatite chondrites and the Earth, we have analyzed 22 samples from different subgroups of the enstatite meteorites, including EH and EL chondrites, aubrites (main group and Shallowater) and the Happy Canyon impact melt. We have also analyzed the Fe isotopic compositions of separated (magnetic and non-magnetic) phases from both enstatite chondrites and achondrites.

On average, EH3-5 chondrites ($\delta^{56}\text{Fe} = 0.004 \pm 0.043\text{\textperthousand}$; 2 standard deviation; n=9; including previous literature data) as well as EL3 chondrites ($\delta^{56}\text{Fe} = 0.030 \pm 0.038\text{\textperthousand}$; 2SD; n=2) have identical and homogeneous Fe isotopic compositions, indistinguishable from those of the carbonaceous chondrites and average terrestrial peridotite. In contrast, EL6 chondrites display a larger range of isotopic compositions ($-0.180\text{\textperthousand} < \delta^{56}\text{Fe} < 0.181\text{\textperthousand}$; n=11), which show a good relationship with the reciprocal of their Fe concentrations. The correlation between Fe isotopic composition and $1/\text{[Fe]}$ for EL6 chondrites indicates a mixing relation between isotopically distinct mineral phases (metal, sulfide and silicate). The large Fe isotopic heterogeneity of EL6 is best explained by chemical/mineralogical fragmentation and brecciation during the complex impact history of the EL parent body.

Enstatite achondrites (aubrites) also exhibit a relatively large range of Fe isotope compositions: all main group aubrites are depleted in the heavy Fe isotopes ($\delta^{56}\text{Fe} = -0.170 \pm 0.189\text{\textperthousand}$; 2SD; n=6), while Shallowater is isotopically relatively heavy ($\delta^{56}\text{Fe} = 0.045 \pm 0.101\text{\textperthousand}$; 2SD; n=4; number of chips). We take this variation to suggest that the main group

aubrite parent body formed a discreet heavy Fe isotope-enriched core, whilst the Shallowater meteorite is most likely from a different parent body where core and silicate material remixed. This could be due to intensive impact-induced shearing stress, or the ultimate destruction of the Shallowater parent body.

Analysis of separated enstatite meteorite mineral phases show that the magnetic phase (mostly Fe metal) is systematically enriched in the heavier Fe isotopes when compared to non-magnetic phases (Fe hosted in sulfide and silicate), which agrees with previous experimental observations and theoretical calculations. Our data provide an equilibrium metal-sulfide Fe isotopic fractionation factor of $\Delta^{56}\text{Fe}_{\text{metal-sulfide}} = \delta^{56}\text{Fe}_{\text{metal}} - \delta^{56}\text{Fe}_{\text{sulfide}}$ of $0.129 \pm 0.065\text{\textperthousand}$ (1SD) at $1060 \pm 80\text{K}$, which is also in agreement with the prediction of previous theoretical calculations.

4.1. Introduction

Enstatite chondrites have received much attention due to their remarkable resemblance to the Earth with respect to various isotope systems, notably O, but also N, Ti, Cr, Ni, Sr, Mo, Ru, and Os (Javoy and Pineau, 1983; Clayton et al., 1984; Dauphas et al., 2004; Trinquier et al., 2007; Regelous et al., 2008; Trinquier et al., 2009; Chen et al., 2010; Moynier et al., 2012; Steele et al., 2012). This has led some authors to propose that enstatite chondrites comprised a substantial component of the “building blocks” of the proto-Earth (Javoy, 1995; Javoy et al., 2010; Kaminski and Javoy, 2013). However, it is difficult to reconcile the refractory lithophile element (*e.g.*, Al, Si, Mg) budget of enstatite chondrites with the current composition of the terrestrial mantle (Larimer and Anders, 1970; Baedecker and Wasson, 1975), in addition significant Si isotopic differences exist between the terrestrial mantle and enstatite chondrites which would require an unrealistic amount of Si in the Earth’s core (Fitoussi and Bourdon, 2012; Savage and Moynier, 2013). Finally, it is predicted that enstatite chondrites were formed under extremely reduced conditions (Keil and Fredriksson, 1963), which strongly contrast with the present state of the terrestrial mantle (Frost and McCammon, 2008).

After O, Fe is the most abundant element on Earth. Given this, understanding the relationship between the Fe isotopic compositions of enstatite chondrites and Earth may be important for testing the enstatite chondritic Earth model. The enstatite meteorites include both the enstatite chondrites and the differentiated enstatite achondrites, also known as aubrites. Enstatite chondrites can be further divided into two subgroups: the Fe-rich EH and the Fe-poor EL. Each of these groups is composed of several petrographic types according to their degree of thermal metamorphism: EH3-6 and EL3-6 (Huss et al., 2006), with 3 being the least altered. The genetic relationship between EL and EH is still debated. Based on the inverse variation of

moderately volatile element abundances with petrographic type between EH and EL groups, Kong et al. (1997) proposed that both meteorite families originated from a single parent body, while Keil et al. (1989) considered that they were derived from two separate parent bodies based on the absence of EL clasts in EH chondrites (and vice versa). Happy Canyon is an impact-melt breccia, probably of enstatite chondritic parentage, but the precise origin of the precursor is debated; it seems that material of EL3-chondrite composition is the most likely possibility (McCoy et al., 1995; Moynier et al., 2011a).

Enstatite achondrites (aubrites) are FeO-poor enstatite orthopyroxenites, which formed under very reducing conditions (Keil, 1989), comparable to those of the enstatite chondrites. All the aubrites (except Shallowater) are brecciated and appear to have formed on the same parent body (Keil, 1989). In contrast, the Shallowater aubrite is the only unbrecciated aubrite and probably comes from a distinct parent body (Keil, 1989; Moynier et al., 2011a). A comprehensive study of the Fe isotopic compositions of enstatite meteorites could provide some insights on the genetic relationships between these subgroups. To date, such an investigation has not been performed.

Even though the few existing Fe isotope data for enstatite chondrites appears, on average, similar to that of carbonaceous chondrites (*e.g.*, Craddock and Dauphas, 2011), some samples have shown large and intriguing variations. For example, the EL6 Blithfield shows a depletion by 140 ppm in $^{56}\text{Fe}/^{54}\text{Fe}$ (Dauphas et al., 2009) compared to the average $^{56}\text{Fe}/^{54}\text{Fe}$ ratio of enstatite chondrites, whereas another EL6, Daniel's Kuil, is enriched by 121 ppm in $^{56}\text{Fe}/^{54}\text{Fe}$ (Craddock and Dauphas, 2011). Due to the limited amount of Fe isotopic data available, no compositions of EL3 (unmetamorphosed EL6 precursors) have been reported; hence, the interpretation of the enrichment in both light and heavy isotopes is difficult.

In this study, we focus on the entire enstatite meteorite group, derived from at least four distinct parent bodies (EH, EL, aubrite-main group and aubrite-Shallowater), to systematically investigate their Fe isotopic variations using Multiple-Collector Inductively-Coupled-Plasma Mass-Spectrometry (MC-ICP-MS). In addition to bulk samples, we have also studied phase separates (magnetic and non-magnetic phases) to assess to what extent igneous processes such as metal/silicate/sulfide separation have affected the Fe isotopic compositions of the enstatite meteorites. The main goal of this study is to investigate the Fe isotopic composition of the enstatite meteorites, in terms of variations within this meteorite class, as well as in comparison to other meteorite groups and the terrestrial mantle. In addition, utilizing the mineral separate data, we aim to provide an empirical estimate of the equilibrium Fe isotope fractionation factor between metal and sulfide.

4.2. Samples and Method

4.2.1. Sample Description

We have studied twenty-two bulk meteorite samples, likely representative of four (EH, EL, aubrite-main group and aubrite-Shallowater) enstatite meteorite parent bodies. Fifteen enstatite chondrites include two EH3 (Kota-Kota and Qingzhen), two EH4 (Abee and Indarch), two EL3 (MAC 88184 and PCA 91020), eight EL6 (Atlanta, Blithfield, Eagle, Hvittis, Kairpur, LON 94100, North West Forrest, and Yilmia) and the Happy Canyon impact melt. Six aubrite samples were analyzed from the aubrite main group (ALH 84007, Aubres, Bustee, Cumberland Falls, Khor Temiki, and Norton County) and one from Shallowater. All the main group aubrites are brecciated: Bustee and Khor Temiki are regolith breccias, Cumberland Falls is a polymict breccia and the remaining main group aubrites are monomict fragmental breccias (Keil, 1989; Keil, 2010; Rubin, 2010). Shallowater is the only unbrecciated sample.

To test the degree of Fe isotopic heterogeneity within bulk enstatite meteorite samples, different chips of the same meteorites (Norton County - 3 chips; Shallowater - 3 chips; and Blithfield - 2 chips) were analyzed separately.

Finally, in order to test the accuracy of our measurements we analyzed the Fe isotopic composition of two previously well-characterized USGS geostandards: USGS GSP-1, a granodiorite from the Silver Plume Quarry, Colorado and USGS AGV-1, an andesite from Guano Valley, Oregon.

4.2.2. Analytical Methods

Meteorite chips of ~500-1000 mg were crushed into a fine powder in an agate pestle and mortar. For enstatite chondrites, ~10-20 mg were dissolved under pressure in Parr bombs in

concentrated HNO₃/HF for several days; the rest of the samples were dissolved in concentrated HNO₃/HF in closed Teflon beakers.

In addition to whole-rock dissolution, selected aubrites and enstatite chondrites were subjected to phase separation, whereby magnetic and non-magnetic phases were separated with a hand magnet. The magnetic phase (metal) was dissolved in aqua regia. The non-magnetic fraction (silicate and sulfide) was dissolved in concentrated HNO₃/HF. Fine silicates often adhere to the metal particles separated by hand-magnet (Torigoye and Shima, 1993). The isotopic compositions measured here for the different phases will therefore represent the minimum isotopic variations between the pure phases.

Iron was purified by anion-exchange chromatography using the same procedure employed in our previous studies (Wang et al., 2011; 2012a&b; 2013). The samples were loaded in 6N HCl on 1 ml AG-1X8 (200-400 mesh) chromatographic columns and Fe was extracted in 0.4N HCl. This process was repeated again to further purify Fe. Iron isotopic ratios were measured on either a Thermo Scientific Neptune or Neptune Plus MC-ICP-MS at the University of Chicago or Washington University in St. Louis (respectively). Isotopic ratios are expressed as parts per 1,000 deviations relative to the standard IRMM-014 in Eq. 4-1:

$$\delta^xFe = \left[\frac{(^xFe / ^{54}Fe)_{sample}}{(^xFe / ^{54}Fe)_{IRMM-014}} - 1 \right] \times 1000 \quad \text{Eq. 4-1}$$

where $x = 56$ or 57 . Every sample was measured 8 or 9 times. The analytical uncertainties are reported as 2 standard error (2SE), calculated as the 2 standard deviation divided by the square root of the total number of analyses. The 2SE values are typically better than $\delta^{56}\text{Fe} \pm 0.030\text{‰}$ for most of the samples (see the Table 4-1 and 4-2).

4.3. Results

Iron isotopic compositions are reported in Table 4-1 for bulk enstatite meteorites and geostandards, and in Table 4-2 for separated mineral phases from enstatite meteorites. The terrestrial standard GSP-1 ($\delta^{56}\text{Fe} = 0.143 \pm 0.023\text{\textperthousand}$) and 3 different dissolutions of AGV-1 ($\delta^{56}\text{Fe} = 0.101 \pm 0.023\text{\textperthousand}$; $0.115 \pm 0.024\text{\textperthousand}$ and $0.097 \pm 0.018\text{\textperthousand}$) are all in excellent agreement with previously published values for GSP-2 and AGV-2 which are different samples from the same outcrops (see Table 4-1).

Literature data for enstatite chondrites from Schoenberg and von Blanckenburg (2006) and Craddock and Dauphas (2011) are also included in Table 4-1 for comparison and are used in the group averages reported below. As expected for mass-dependent isotopic fractionation, all the data fall onto a straight line of slope ~ 1.5 on a three-isotope ($\delta^{57}\text{Fe}$ vs. $\delta^{56}\text{Fe}$) plot (Figure 4-1).

4.3.1. Iron Isotope Compositions of the Whole-rock Meteorites

The EH chondrites range from $-0.016 \pm 0.041\text{\textperthousand}$ to $0.009 \pm 0.020\text{\textperthousand}$. The EL3 are similar to EH chondrites with a range from $0.016 \pm 0.016\text{\textperthousand}$ to $0.043 \pm 0.025\text{\textperthousand}$. EL6 show more variability, with a range of $\delta^{56}\text{Fe}$ from $-0.180 \pm 0.023\text{\textperthousand}$ to $0.181 \pm 0.018\text{\textperthousand}$ and the impact melt Happy Canyon is enriched in the heavier isotopes with a $\delta^{56}\text{Fe}$ of $0.143 \pm 0.035\text{\textperthousand}$.

The absence of Fe isotopic fractionation in EH chondrites confirms previous observations (Schoenberg and von Blanckenburg, 2006; Dauphas et al., 2009; Craddock and Dauphas, 2011). However, our data for the EL6 and impact melt enstatite chondrites (which are possibly of EL parentage, see later) do not always agree with previous data (see Table 4-1). For example, one of our two chips of Blithfield ($\delta^{56}\text{Fe} = -0.122 \pm 0.016\text{\textperthousand}$) is in fairly good agreement with data

reported by Dauphas et al. (2009) ($\delta^{56}\text{Fe} = -0.140 \pm 0.030\text{\textperthousand}$) whereas the second chip ($\delta^{56}\text{Fe} = 0.030 \pm 0.027\text{\textperthousand}$) is markedly different. We attribute these disagreements to isotopic heterogeneity of EL6, and we will explore it in detail in the following discussion section.

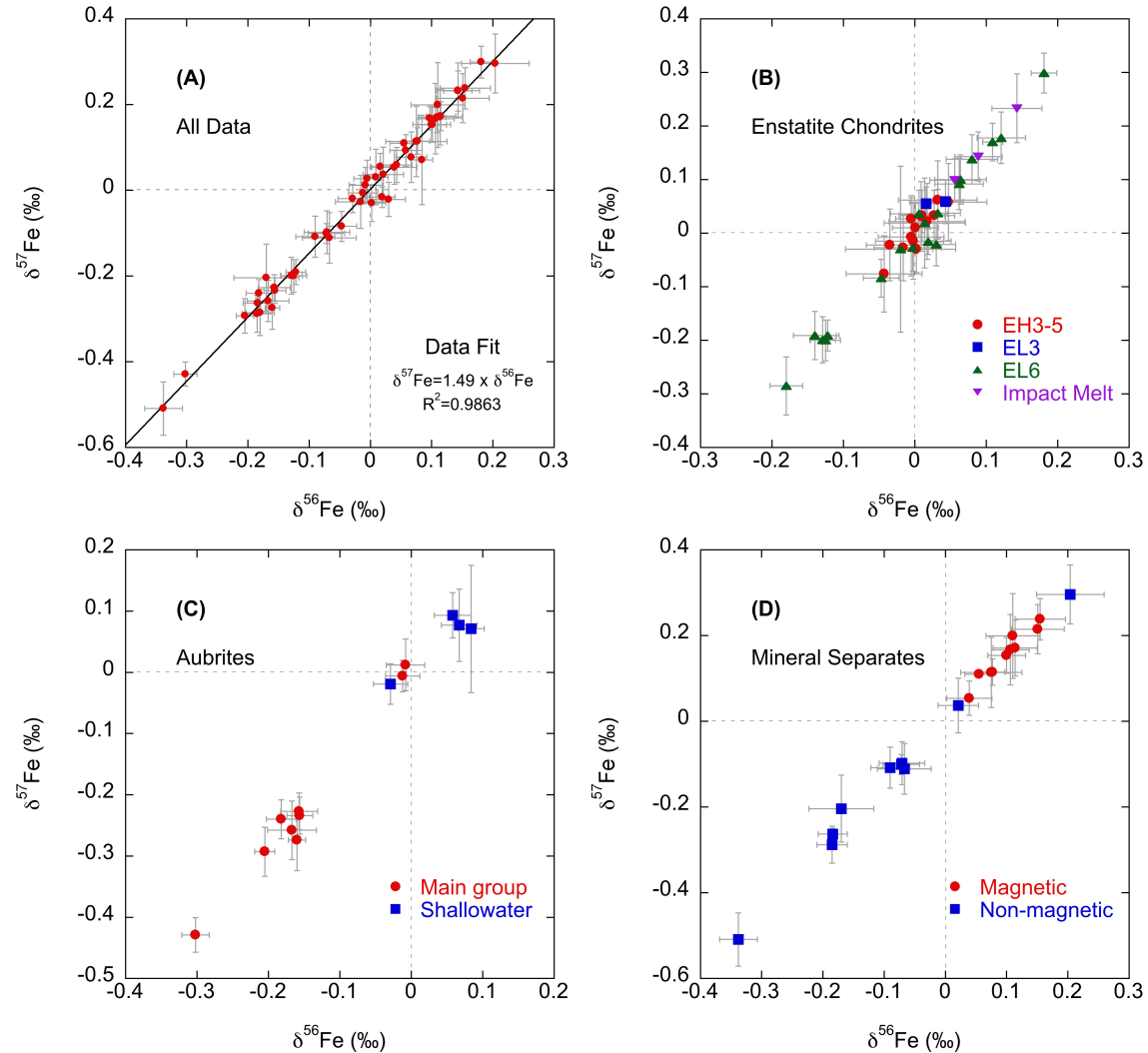


Figure 4-1. Iron isotope compositions of all samples analyzed in this study, shown in three-isotope ($\delta^{57}\text{Fe}$ vs. $\delta^{56}\text{Fe}$) space. All data fall onto the mass-dependent fractionation line of slope ~ 1.5 . (A) All the data analyzed in this study including terrestrial geostandards; (B) enstatite chondrites from this study and from the literature (Schoenberg and von Blanckenburg, 2006; Craddock and Dauphas, 2010); (C) aubrites from this study; (D) mineral separates from this study. Each datum represents an independent analysis of a different chip of meteorite material (data for the same meteorites are not combined; see Table 4-1).

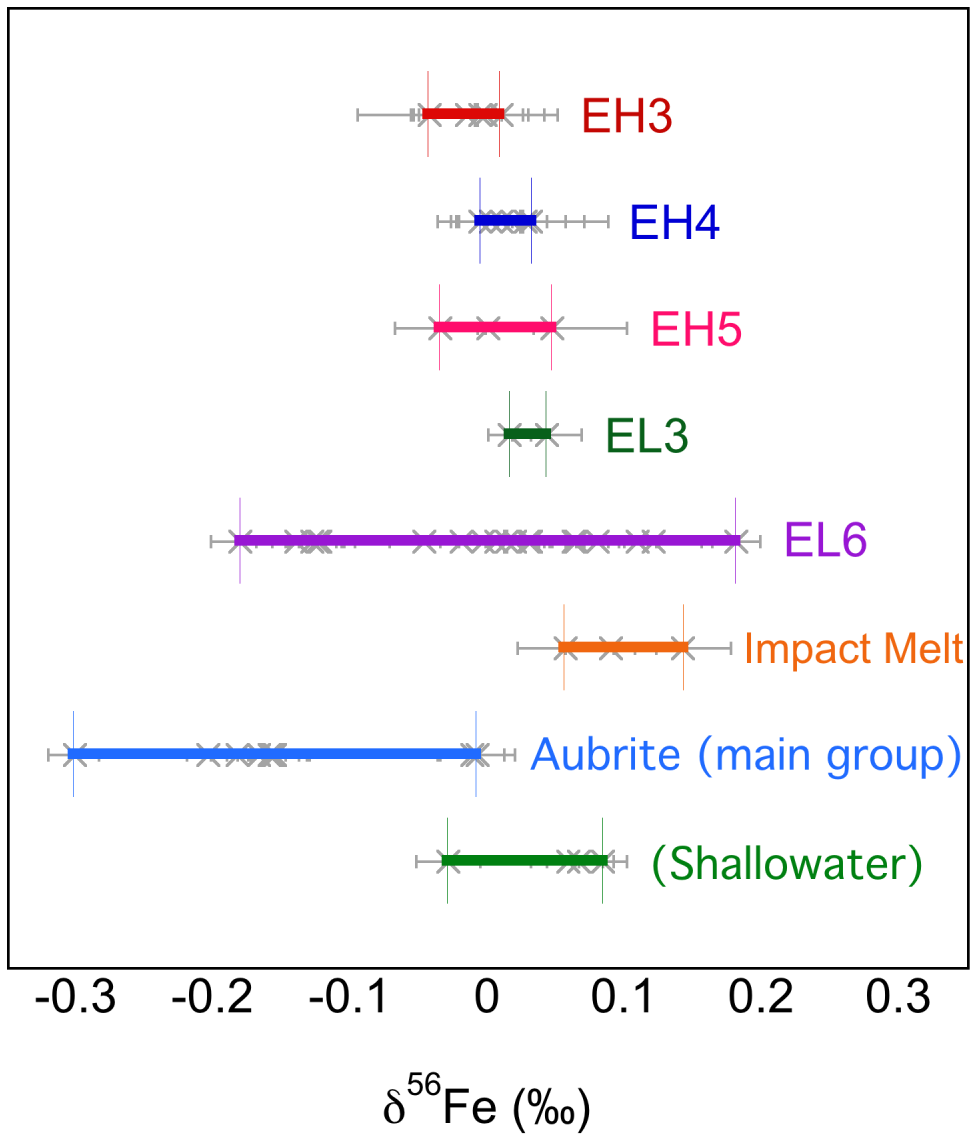


Figure 4-2. Iron isotope variations of different subgroups of enstatite meteorites. Each independent analysis from this and previous studies are plotted as grey crosses. Error bars (2SE in this study and reported uncertainties from literature) are shown as grey lines.

When combined with previous data, the different groups of enstatite meteorites give the following average values: EH3-5 ($\delta^{56}\text{Fe} = 0.004 \pm 0.043\text{‰}$; 2 standard deviation; n=9; number of individual meteorites); EL3 ($\delta^{56}\text{Fe} = 0.030 \pm 0.038\text{‰}$; 2SD; n=2); EL6 ($\delta^{56}\text{Fe} = 0.016 \pm 0.195\text{‰}$; 2SD; n=11); impact melt enstatite chondrites ($\delta^{56}\text{Fe} = 0.094 \pm 0.015\text{‰}$; 2SD; n=2) with both the

EL6 and impact melt groups defining non-Gaussian distributions; aubrite main group ($\delta^{56}\text{Fe} = -0.170 \pm 0.189\text{\textperthousand}$; 2SD; n=6); and the Shallowater aubrite ($\delta^{56}\text{Fe} = 0.045 \pm 0.101\text{\textperthousand}$; 2SD; n=4; number of chips). More importantly, EL6 chondrites ($-0.180\text{\textperthousand} < \delta^{56}\text{Fe} < 0.181\text{\textperthousand}$) and aubrites ($-0.302\text{\textperthousand} < \delta^{56}\text{Fe} < 0.084\text{\textperthousand}$) display a large range of isotopic compositions. The ranges of $\delta^{56}\text{Fe}$ variations in different groups are shown in both Figures 4-1 and 4-2. Except for the aubrite and impact melt enstatite chondrites, all enstatite meteorite groups have the same average Fe isotopic composition as carbonaceous chondrites ($\delta^{56}\text{Fe} = 0.02 \pm 0.04\text{\textperthousand}$; 2SE; Wang et al., 2013) and abyssal peridotites ($\delta^{56}\text{Fe}=0.010 \pm 0.007\text{\textperthousand}$; 95% confidence interval; Craddock et al., 2013).

4.3.2. Iron Isotope Compositions of the Separated Mineral Phases

The magnetic phases (mostly Fe from metal) from enstatite meteorites are all (with the exception of the impact melts) systematically enriched in heavy isotopes when compared to the non-magnetic phases (mostly Fe from sulfide and silicate). The average values of magnetic (metal) and non-magnetic (silicate+sulfide) are $0.101 \pm 0.076\text{\textperthousand}$ (2SD; n=8), and $-0.140 \pm 0.200\text{\textperthousand}$ (2SD; n=8), respectively (Figure 4-3) giving an average $\Delta^{56}\text{Fe}_{\text{magnetic}/\text{non-magnetic}}$ ($\delta^{56}\text{Fe}_{\text{magnetic}} - \delta^{56}\text{Fe}_{\text{non-magnetic}}$) of $0.241 \pm 0.125\text{\textperthousand}$ (1SD; n=8). No variations in fractionation magnitude between magnetic and non-magnetic phases in different subgroups are observed except for the enstatite chondrite impact melts, whereby both magnetic and non-magnetic portions of Happy Canyon impact melt are enriched in heavier Fe isotopes (see Section 4.4.4 for discussion).

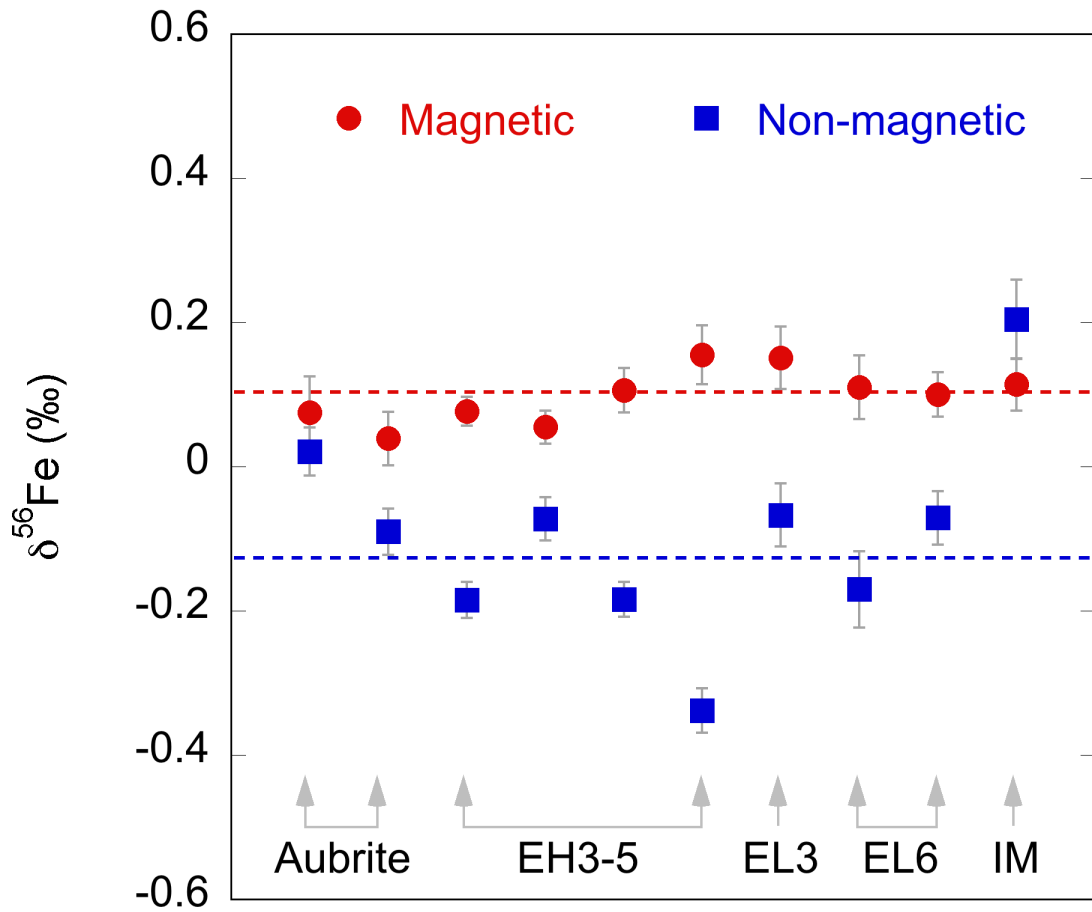


Figure 4-3. Iron isotope fractionation between magnetic (metal) and non-magnetic (silicate and sulfide) phases in enstatite chondrites and achondrites. IM: enstatite chondrite impact melt. The dashed lines are the averages of magnetic (red) and non-magnetic (blue) phases. Enstatite chondrite impact melt is not included in the average calculation.

Table 4-1. Iron isotope compositions of enstatite meteorites

<i>Sample</i>	<i>Type</i>	<i>Fall/find</i>	<i>Shock stage^a</i>	<i>Fe (wt.%)</i>	$\delta^{56}\text{Fe}$ (%)	\pm 2SE ^b	$\delta^{57}\text{Fe}$ (%)	\pm 2SE ^b	<i>n</i> ^c	<i>Museum code^d</i>
Kota-Kota	EH3	Find	S3	15.0	-0.016	\pm 0.041	-0.027	\pm 0.062	5	NHM 1905,355
Qingzhen	EH3	Fall	S3	27.4	0.009	\pm 0.020	0.031	\pm 0.065	9	
Qingzhen ^e	EH3	Fall	S3	28.5	-0.043	\pm 0.053	-0.076	\pm 0.071	9	
Sahara 97072 ^e	EH3	Find	S2	28.8	-0.002	\pm 0.053	-0.015	\pm 0.071	9	
Sahara ^f	EH3	Find	S2		-0.005	\pm 0.046	-0.007	\pm 0.073	4	
Abee	EH4	Fall	S2-S4	36.5	0.002	\pm 0.023	-0.030	\pm 0.043	9	
Abee ^f	EH4	Fall	S2-S4		0.032	\pm 0.055	0.062	\pm 0.073	3	
Adhi Kot ^e	EH4	Fall	S3	29.5	0.017	\pm 0.053	0.022	\pm 0.071	9	AMNH 3993
Indarch	EH4	Fall	S3	28.3	-0.005	\pm 0.022	0.027	\pm 0.043	8	FM 1404
Indarch ^e	EH4	Fall	S3	28.1	0.027	\pm 0.029	0.033	\pm 0.047	9	
Indarch ^e	EH4	Fall	S3	28.3	0.010	\pm 0.032	0.033	\pm 0.048	9	
St. Mark's ^e	EH5	Fall	S3	29.8	0.047	\pm 0.054	0.058	\pm 0.072	9	USNM 3027
Saint-Sauveur ^e	EH5	Fall	S3	29.1	-0.035	\pm 0.033	-0.022	\pm 0.067	9	
Saint-Sauveur ^e	EH5	Fall	S3	33.6	0.001	\pm 0.032	0.010	\pm 0.048	9	
MAC 88184	EL3	Find	S3	20.3 ^g	0.043	\pm 0.025	0.059	\pm 0.041	9	JSC
PCA 91020	EL3	Find	S5	27.2	0.016	\pm 0.016	0.055	\pm 0.031	9	JSC
Atlanta	EL6	Find	S2	25.9	0.019	\pm 0.021	-0.016	\pm 0.024	9	NHM 1959,1001
Atlanta ^f	EL6	Find	S2		-0.020	\pm 0.077	-0.030	\pm 0.155	4	
Blithfield chip 1	EL6	Find	S2	16.6	-0.122	\pm 0.016	-0.191	\pm 0.029	9	FM 1979
Blithfield chip 2	EL6	Find	S2	23.7	0.030	\pm 0.027	-0.021	\pm 0.040	9	FM 1979
Blithfield ^e	EL6	Find	S2	15.5	-0.140	\pm 0.030	-0.191	\pm 0.045	9	

Daniel's Kuil ^e	EL6	Fall	S2	20.0	0.121	\pm	0.034	0.178	\pm	0.048	9	FM 1500
Eagle	EL6	Fall	S2	11.8	-0.047	\pm	0.025	-0.084	\pm	0.035	9	USNM 6411
Eagle ^e	EL6	Fall	S2	13.4	-0.003	\pm	0.040	-0.027	\pm	0.044	9	
Eagle ^f	EL6	Fall	S2		0.014	\pm	0.057	0.019	\pm	0.084	4	
Hvittis	EL6	Fall	S2	19.2	-0.125	\pm	0.021	-0.200	\pm	0.038	8	FM 1470
Hvittis ^e	EL6	Fall	S2	22.2	0.032	\pm	0.032	0.037	\pm	0.045	9	FM 578
Jajh deh Kot Lalu ^e	EL6	Fall	S2	17.9	0.062	\pm	0.034	0.092	\pm	0.048	9	USNM 1260
Khairpur	EL6	Fall	S2	12.0	-0.180	\pm	0.023	-0.285	\pm	0.054	9	AMNH
Khairpur ^e	EL6	Fall	S2	21.3	0.006	\pm	0.040	0.036	\pm	0.044	9	FM 1538
LON 94100	EL6	Find	S2	12.3	-0.129	\pm	0.018	-0.199	\pm	0.043	9	
North West Forrest	EL6	Find	S2	14.7	0.181	\pm	0.018	0.299	\pm	0.037	9	WAM 13194
Pillistfer ^e	EL6	Fall	S2	34.7	0.080	\pm	0.036	0.138	\pm	0.046	9	FM 1647
Yilmia	EL6	Find	S2	38.1	0.109	\pm	0.014	0.170	\pm	0.035	9	WAM 12192
Yilmia ^e	EL6	Find	S2	18.9	0.064	\pm	0.036	0.100	\pm	0.046	9	FM 2740
Happy Canyon	Impact melt	Find	S2	8.7	0.143	\pm	0.035	0.233	\pm	0.064	8	ASU 1058f
Happy Canyon ^e	Impact melt	Find	S2	16.3	0.056	\pm	0.035	0.099	\pm	0.040	9	FM 2760
Ilafegh 009 ^e	Impact melt	Find	S4	23.2	0.089	\pm	0.033	0.143	\pm	0.046	9	
ALH 84007	Aubrite (main group)	Find	S4	0.3	-0.205	\pm	0.014	-0.293	\pm	0.040	9	JSC
Aubres	Aubrite (main group)	Fall		0.6	-0.182	\pm	0.021	-0.240	\pm	0.032	9	NHM 63552
Bustee	Aubrite (main group)	Fall		3.6	-0.008	\pm	0.027	0.012	\pm	0.042	9	NHM 32100
Bustee (replicates)	Aubrite (main group)	Fall		3.6	-0.012	\pm	0.024	-0.006	\pm	0.026	9	NHM 32100
Cumberland Falls	Aubrite (main group)	Fall	S5	0.2	-0.302	\pm	0.019	-0.429	\pm	0.028	9	USNM 2558
Khor Temiki	Aubrite (main group)	Fall		0.9	-0.160	\pm	0.012	-0.274	\pm	0.050	9	NHM 1934,781
Norton County chip 1	Aubrite (main group)	Fall		0.7	-0.156	\pm	0.018	-0.234	\pm	0.030	9	UNM
Norton County chip 2	Aubrite (main group)	Fall		0.8	-0.157	\pm	0.026	-0.227	\pm	0.030	9	UNM

Norton County chip 3	Aubrite (main group)	Fall		0.4	-0.167	\pm	0.034	-0.258	\pm	0.048	9	UNM
Shallowater chip 1	Aubrite (Shallowater)	Find	S2	14.0	-0.029	\pm	0.024	-0.019	\pm	0.033	9	USNM 1206
Shallowater chip 2	Aubrite (Shallowater)	Find	S2	7.0	0.067	\pm	0.025	0.077	\pm	0.059	9	USNM 1206
Shallowater chip 2 (replicates)	Aubrite (Shallowater)	Find	S2	7.0	0.084	\pm	0.018	0.071	\pm	0.104	9	USNM 1206
Shallowater chip 3	Aubrite (Shallowater)	Find	S2	18.2	0.058	\pm	0.026	0.093	\pm	0.037	9	ASU 318.9
AGV1	Geostandard				0.101	\pm	0.023	0.153	\pm	0.041	8	
AGV1	Geostandard				0.115	\pm	0.024	0.173	\pm	0.034	9	
AGV1	Geostandard				0.097	\pm	0.018	0.168	\pm	0.027	9	
AGV2 ^e	Geostandard				0.105	\pm	0.011	0.146	\pm	0.016	9	
GSP1	Geostandard				0.143	\pm	0.023	0.232	\pm	0.047	9	
GSP2 ^e	Geostandard				0.159	\pm	0.013	0.230	\pm	0.021	9	

^a Shock stage values are from Rubin et al. (1997; 2009; 2010), Izawa et al. (2011) and Grossman (1998). Values for Sahara 97072 and MAC 88184 are from those of their paired meteorites Sahara 97096 and MAC 88136, respectively.

^b The analytical uncertainties are 2 standard error (2SE) for data from this study or reported uncertainties for data from literatures.

^c Number of measurements.

^d Museum code: USNM=United States National Museum, Washington DC. NHM=The National History Museum, London. ASU=Arizona State University, Tempe. UNM= University of New Mexico, Albuquerque, NM. FM=The Field Museum, Chicago. AMNH=American Museum of Natural History, New York. JSC=Johnson Space Center, NASA, Houston. WAM=Western Australia Museum, Perth.

^e Data from Craddock and Dauphas (2010).

^f Data from Schoenberg and von Blanckenburg (2006).

^g Data from Zhang et al. (1995).

Table 4-2. Iron isotope compositions of mineral fractions of aubrites and enstatite chondrites

Sample	Mineral	Type	Fall/find	Fe (wt.%)	$\delta^{56}\text{Fe}$ (‰)	±	2SE	$\delta^{57}\text{Fe}$ (‰)	±	2SE	n ^a	Museum code ^b
Shallowater chip 1												
Magnetic	Metal	Aubrite	Find	30.1	0.075	±	0.050	0.114	±	0.082	8	USNM 1206
Non-magnetic	Silicate+sulfide	Aubrite	Find	1.5	0.021	±	0.033	0.037	±	0.064	6	USNM 1206
Shallowater chip 2												
Magnetic	Metal	Aubrite	Find	46.4	0.039	±	0.037	0.054	±	0.040	8	USNM 1206
Non-magnetic	Silicate+sulfide	Aubrite	Find	5.8	-0.090	±	0.032	-0.108	±	0.048	6	USNM 1206
Qingzhen												
Magnetic	Metal	EH3	Fall	43.0	0.077	±	0.020	0.115	±	0.031	7	
Non-magnetic	Silicate+sulfide	EH3	Fall	8.6	-0.185	±	0.025	-0.288	±	0.043	7	
Abee												
Magnetic	Metal	EH4	Fall	47.4	0.055	±	0.023	0.110	±	0.006	4	
Non-magnetic	Silicate+sulfide	EH4	Fall	14.3	-0.072	±	0.030	-0.101	±	0.023	4	
Indarch												
Magnetic	Metal	EH4	Fall	41.5	0.106	±	0.031	0.167	±	0.082	7	FM 1404
Non-magnetic	Silicate+sulfide	EH4	Fall	12.2	-0.184	±	0.024	-0.263	±	0.013	5	FM 1404
St. Mark's												
Magnetic	Metal	EH5	Fall	50.9	0.155	±	0.041	0.238	±	0.048	7	USNM 3027
Non-magnetic	Silicate+sulfide	EH5	Fall	5.8	-0.338	±	0.031	-0.509	±	0.062	5	USNM 3027
MAC 88184												
Magnetic	Metal	EL3	Find	48.8	0.151	±	0.043	0.215	±	0.057	8	JSC
Non-magnetic	Silicate+sulfide	EL3	Find	17.2	-0.067	±	0.044	-0.111	±	0.059	7	JSC
Blithfield												
Magnetic	Metal	EL6	Find	29.5	0.110	±	0.044	0.199	±	0.099	4	FM 1979
Non-magnetic	Silicate+sulfide	EL6	Find	10.9	-0.170	±	0.053	-0.204	±	0.078	4	FM 1979
Eagle												

Magnetic	Metal	EL6	Fall	33.3	0.100	\pm	0.031	0.154	\pm	0.042	4	USNM 6411
Non-magnetic	Silicate+sulfide	EL6	Fall	6.6	-0.071	\pm	0.037	-0.098	\pm	0.050	4	USNM 6411
Happy Canyon												
Magnetic	Metal	Impact melt	Find	33.5	0.114	\pm	0.036	0.171	\pm	0.065	6	ASU 1058f
Non-magnetic	Silicate+sulfide	Impact melt	Find	11.8	0.204	\pm	0.055	0.296	\pm	0.069	6	ASU 1058f

^a Number of measurements.

^b Museum code: USNM=United States National Museum, Washington DC. ASU=Arizona State University, Tempe. FM=The Field Museum, Chicago.

JSC=Johnson Space Center, NASA, Houston.

4.4. Discussion

4.4.1. The Homogeneous Iron Isotope Composition of Enstatite Chondrites

The different petrologic types of EH chondrites have identical (within error) Fe isotopic compositions ($\delta^{56}\text{Fe} = 0.004 \pm 0.043\text{\textperthousand}$; 2SD; n=9). Amongst EL chondrites, EL3 appear isotopically homogeneous ($\delta^{56}\text{Fe} = 0.030 \pm 0.038\text{\textperthousand}$; 2SD; n=2) and have the same isotopic composition as EH. Even though the highly metamorphosed EL6 chondrites are relatively heterogeneous ($-0.180\text{\textperthousand} < \delta^{56}\text{Fe} < 0.181\text{\textperthousand}$) (see Section 4.4.3), the average composition of EL6 is $0.016 \pm 0.195\text{\textperthousand}$ (2SD; n=11), indistinguishable with the EH and EL3 averages. As shown in Figure 4-4, EH, EL3 and the average value of EL6 share the same Fe isotopic composition (within error) with previously published carbonaceous, ordinary chondrites, HED and martian meteorites, and terrestrial abyssal peridotite samples, where $\delta^{56}\text{Fe} \sim 0.00\text{\textperthousand}$ (Dauphas et al., 2009a; Craddock and Dauphas, 2011; Wang et al. 2012a; Wang et al., 2013). All enstatite chondrites (except EL6 and impact melts) provide an extremely homogeneous Fe isotopic composition of $0.009 \pm 0.045\text{\textperthousand}$ (2SD; n=11), which we propose as the best estimate of the initial Fe isotopic composition of the bulk enstatite meteorite parent bodies. With respect to the enstatite chondrite Earth model (*e.g.*, Javoy et al., 2010), in terms of Fe isotopes we cannot rule out enstatite chondrites as building blocks of the proto-Earth, assuming no Fe isotope fractionation during core formation (Hin et al., 2012). In addition, it is important to note that both EL and EH chondrites have the same average Fe isotope composition. Hence, it is impossible, on the basis of Fe isotopes, to confirm whether or not EL and EH are from the same or separate parent bodies (Keil, 1989; Kong et al., 1997).

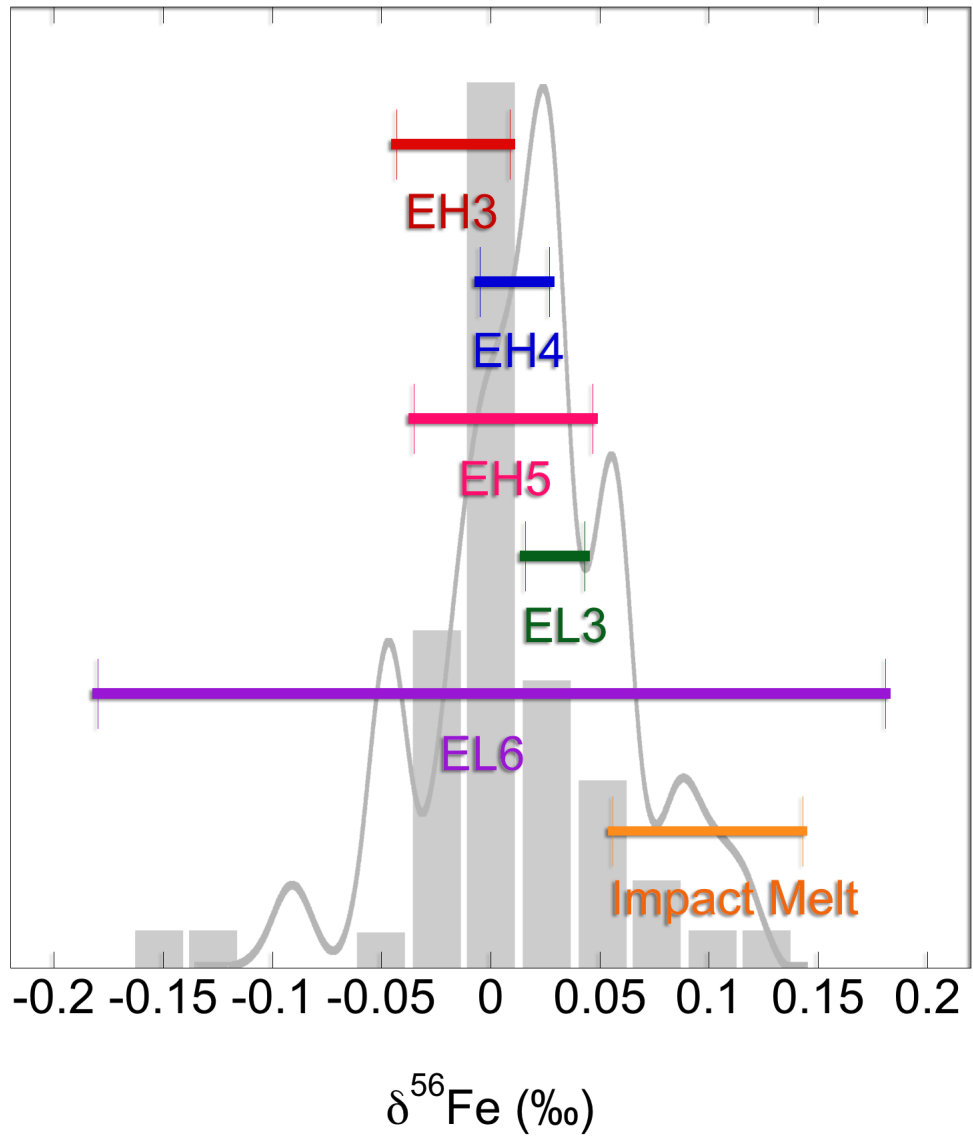


Figure 4-4. Iron isotope variations of the different subgroups of enstatite chondrites and comparison with the iron isotope frequency distributions of previously reported terrestrial peridotites and chondrites (including ordinary, carbonaceous and enstatite chondrites) from Craddock et al. (2013). Histogram: relative frequency distributions of ordinary, carbonaceous and enstatite chondrites from literature data (Craddock et al., 2013). Curved line: relative frequency distributions of abyssal peridotites and peridotite mylonites (Craddock et al., 2013).

Table 4-3. Mass-balance models of Fe isotopic compositions of the structures of the Earth

<i>Fe carriers</i>		<i>Mass (%)^a</i>	<i>[Fe] (%)^a</i>	<i>Fe (%)</i>	<i>Enstatite chondritic Earth (EE-1)</i>	<i>Enstatite chondritic Earth (EE-2)</i>	<i>Super-chondritic Earth (SE-1)</i>
Assumption					Bulk Earth = Enstatite chondrite; $\Delta^{56}\text{Fe}_{(\text{lower mantle-core})} = 0.00\text{\textperthousand}$	Bulk Earth = Enstatite chondrite; $\Delta^{56}\text{Fe}_{(\text{lower mantle-core})} = 0.48\text{\textperthousand}$ ^b	Bulk Earth \neq Enstatite chondrite; $\Delta^{56}\text{Fe}_{(\text{lower mantle-core})} = 0.00\text{\textperthousand}$
Crust	Pyroxene, olivine, magnetite, ilmenite	0.4	4.0	0.05	0.10‰	0.10‰	0.10‰
Upper mantle	Olivine, pyroxene, garnet	22.4	6.3	4.38	0.00‰	0.00‰	0.10‰
Lower mantle	Ferropericlase, post-perovskite	44.7	6.3	8.74	0.00‰	0.44‰	0.10‰
Core	Fe, FeS	32.5	85.6	86.83	0.00‰	-0.04‰	0.10‰
Bulk Earth		100	32.0	100	0.00‰	0.00‰	0.10‰

^a Data from Lodders and Fegley (1998).

^b Data from Williams et al. (2012).

4.4.2. Implications on Bulk Earth Fe Isotope Composition

This homogenous Fe isotope composition of enstatite meteorites is indistinguishable from the average Fe isotope composition ($\delta^{56}\text{Fe} \sim 0.00\text{\textperthousand}$) of various terrestrial peridotites values (Weyer et al., 2005; Weyer and Ionov, 2007; Dauphas et al., 2009a; Dauphas et al., 2010; Zhao et al., 2010; Huang et al., 2011; Zhao et al., 2012; Hibbert et al., 2012; Craddock et al., 2013), and are significantly different from the $\delta^{56}\text{Fe} \sim 0.10\text{\textperthousand}$ value of terrestrial basalts (Beard and Johnson, 1999; Beard et al., 2003; Poitrasson et al., 2004; Weyer et al., 2005; Schoenberg and von Blanckenburg, 2006; Dauphas et al., 2009a; Teng et al., 2013). This 0.10‰ difference between enstatite meteorite $\delta^{56}\text{Fe}$ and the terrestrial basalt value can be explained by 1) non-enstatite chondritic precursor of the Earth; 2) isotopic fractionation between metal and perovskite at high-pressure core-mantle boundary (Polyakov, 2009; Rustad and Yin, 2009; Williams et al., 2012); 3) preferential evaporation of light Fe isotopes during the Moon-forming giant impact (Poitrasson et al., 2004); and/or 4) fractionation during partial melting of their mantle sources at oxidized environments (Weyer and Ionov, 2007; Williams et al., 2009; Dauphas et al., 2009a; Wang et al., 2012a). The important and still unsettled question lies on whether the Fe isotopic composition of the peridotites (highly scattered $\delta^{56}\text{Fe}$ with an average $\sim 0.00\text{\textperthousand}$) or basalts (clustered at $\delta^{56}\text{Fe} \sim 0.10\text{\textperthousand}$) represent the current bulk silicate Earth composition. One argument is that peridotites represent the upper mantle lithosphere and their Fe isotopes have been highly altered by local metasomatism, while basalts have sampled a deeper source of mantle which is well mixed through mantle convections (Poitrasson et al., 2013).

We modeled the Fe isotopic compositions of the main terrestrial Fe reservoirs and assessed depth profiles for $\delta^{56}\text{Fe}$ (see Table 4-3 and Figure 4-5). We considered two enstatite chondritic Earth models (EE-1 and EE-2), and one super-chondritic Earth scenario (SE-1). In the

EE-1 model, we assume an enstatite chondritic value for the bulk Earth ($\delta^{56}\text{Fe} \sim 0.00\text{\textperthousand}$), and that Fe isotopes fractionate during partial melting of their mantle sources; however no high-pressure core-mantle reservoirs' fractionation is considered. EE-2 is similar with to EE-1, but the fractionation between metal and perovskite at the core-mantle boundary is added into the model (Polyakov, 2009; Rustad and Yin, 2009; Williams et al., 2012). SE-1 is the only non-enstatite chondritic model. In this scenario, the Earth is either built on super-chondritic precursors ($\delta^{56}\text{Fe} \sim 0.10\text{\textperthousand}$), or has been enriched in heavy Fe isotopes through preferential evaporation of light Fe isotopes during the Moon-forming giant impact (Poitrasson et al., 2004).

As shown by mass balance calculation in Table 4-3, the core is the largest Fe reservoir in the Earth, and contains 86.83% of total Fe of the whole Earth. The outer core of the Earth is mainly composed of molten iron and nickel, however it also includes substantial amounts of light elements (*e.g.*, Badro et al., 2007). Recent high-temperature-pressure experiments suggest that the metal-silicate Fe isotopic fractionation factor could be affected by the amount of S added in the metal (Shahar et al., 2013). However, the species and abundances of light elements proposed in the core vary significantly based on numerous models (Allègre et al., 1995; Alfè et al., 2002; Badro et al., 2007; McDonough, 2007; Rubie et al., 2011); and isotopic measurements (Georg et al., 2007; Moynier et al., 2011b; Savage and Moynier, 2013). The influence of these light elements on the metal/silicate Fe isotopic fractionation is still uncertain. Here as a result, and to simplify discussion, we ignored the possible effects of these light elements on the core/mantle Fe isotopic fractionation.

The Fe isotopic composition of the core could be estimated by two different approaches. First, magmatic iron meteorites are believed to be the remnants of the cores of differentiated planetary bodies (*e.g.*, Haack and McCoy, 2007). The $\delta^{56}\text{Fe}$ values of bulk iron meteorites range

from 0.02 to 0.08‰ (Moynier et al., 2007) and the $\delta^{56}\text{Fe}$ values of the metal fraction separated from magmatic iron meteorites range from -0.05 to $0.23\text{\textperthousand}$ (Williams et al., 2006). In Schoenberg and von Blanckenburg (2006)'s Fe isotopic model of the Earth, the $\delta^{56}\text{Fe}$ of bulk iron meteorites is used to represent the Earth's core. However, in such situation the silicate Earth would have an extremely negative $\delta^{56}\text{Fe}$ ($-0.43\text{\textperthousand}$), which contradicts both observations on natural samples and results from experiments. Alternatively Schoenberg and von Blanckenburg (2006) used the $\delta^{56}\text{Fe}$ of iron meteorites as the $\delta^{56}\text{Fe}$ of the inner core rather than that of the whole core. However, this assumption brought more problems than solve them since there are no theoretical or experimental constraints on the Fe isotopic fractionations between inner and outer cores. Williams et al. (2006) also show that it is not correct to simply use the Fe isotopic composition of the metal fractions of iron meteorites to represent the one of the core. In addition, theoretical calculations and high-temperature-pressure experiments have shown that equilibrium Fe isotopic fractionation between silicate and metal is pressure dependent and that, at extremely high pressure (~ 120 GPa), the degree of isotopic fractionation is different from the fractionation in small planetary bodies such as the parent bodies of iron meteorites (Polyakov, 2009; Rustad and Yin, 2009; Williams et al., 2012). In conclusion, it is problematic to use the Fe isotopic composition of iron meteorites to represent the composition of the inner core or of the whole core.

The second approach to assess the Fe isotopic composition of the core is by assuming the composition of the bulk Earth and the metal/silicate Fe isotopic fractionation based on theoretical/experimental studies. This is the approach we used here. In EE-1, we assume the enstatite chondritic value obtained in this study as the bulk Earth value ($\delta^{56}\text{Fe} \sim 0.00\text{\textperthousand}$) and no Fe isotopic fractionation is considered between core and mantle. This model will lead to a core

practically with the same Fe isotopic composition as the bulk Earth ($\delta^{56}\text{Fe} \sim 0.00\text{\textperthousand}$). In EE-2, we use the experimentally calibrated fractionation factor ($\Delta^{56}\text{Fe}_{\text{lower-mantle}/\text{core}} = 0.48\text{\textperthousand}$) determined by Williams et al (2012) and we estimated the Fe isotopic composition of the core as $-0.04\text{\textperthousand}$. In the SE-1 model, the Fe isotopic composition of the core is equal to the bulk Earth value ($\delta^{56}\text{Fe} \sim 0.10\text{\textperthousand}$), which has been either inherited from non-chondritic building blocks at the origin of the Earth or fractionated during the Moon-forming giant impact (Poitrasson et al., 2004). Nevertheless, under all the three models considered here, the Fe isotopic composition of the core does not depend on the Fe isotopic compositions of the crusts and upper mantle, since they only store 4.43 wt.% (weight percentage) of total Fe of the Earth. The Fe isotopic composition of the core is only a function of the bulk Earth value and the isotopic fractionation factor between core and mantle.

The lower mantle is the second largest reservoir of Fe in the Earth and stores 8.74% of total Earth Fe. As shown in Table 4-3 and Figure 4-5, the Fe isotopic composition of the lower mantle does not depend on the Fe isotopic compositions of the crusts and upper mantle rocks (where we have samples measured), but depend on the bulk Earth value and the fractionation factor between core and mantle (where we have to make assumptions). For both EE-1 and SE-1 models, the Fe isotopic compositions of the lower mantle is equal to those of the core and the bulk Earth value ($\delta^{56}\text{Fe} \sim 0.00\text{\textperthousand}$ for EE-1 and $\sim 0.10\text{\textperthousand}$ for SE-1). In the EE-2 model, the lower mantle has a heavy Fe isotopic composition ($\delta^{56}\text{Fe} = 0.44\text{\textperthousand}$) based on the recent experimentally equilibrated metal and perovskite fractionation factor measured by Williams et al. (2012). As shown in Figure 4-5, the EE-2 profile line exhibits a sharp change between upper and lower mantles. Mixing of the heavy Fe isotopic composition of perovskite through the entire mantle via convection would yield a $\delta^{56}\text{Fe} = 0.29\text{\textperthousand}$ for whole mantle, which is significantly higher than

what have been observed in mantle samples such as peridotites (Weyer et al., 2005; Weyer and Ionov, 2007; Dauphas et al., 2009a; Dauphas et al., 2010; Zhao et al., 2010; Huang et al., 2011; Zhao et al., 2012; Hibbert et al., 2012; Craddock et al., 2013).

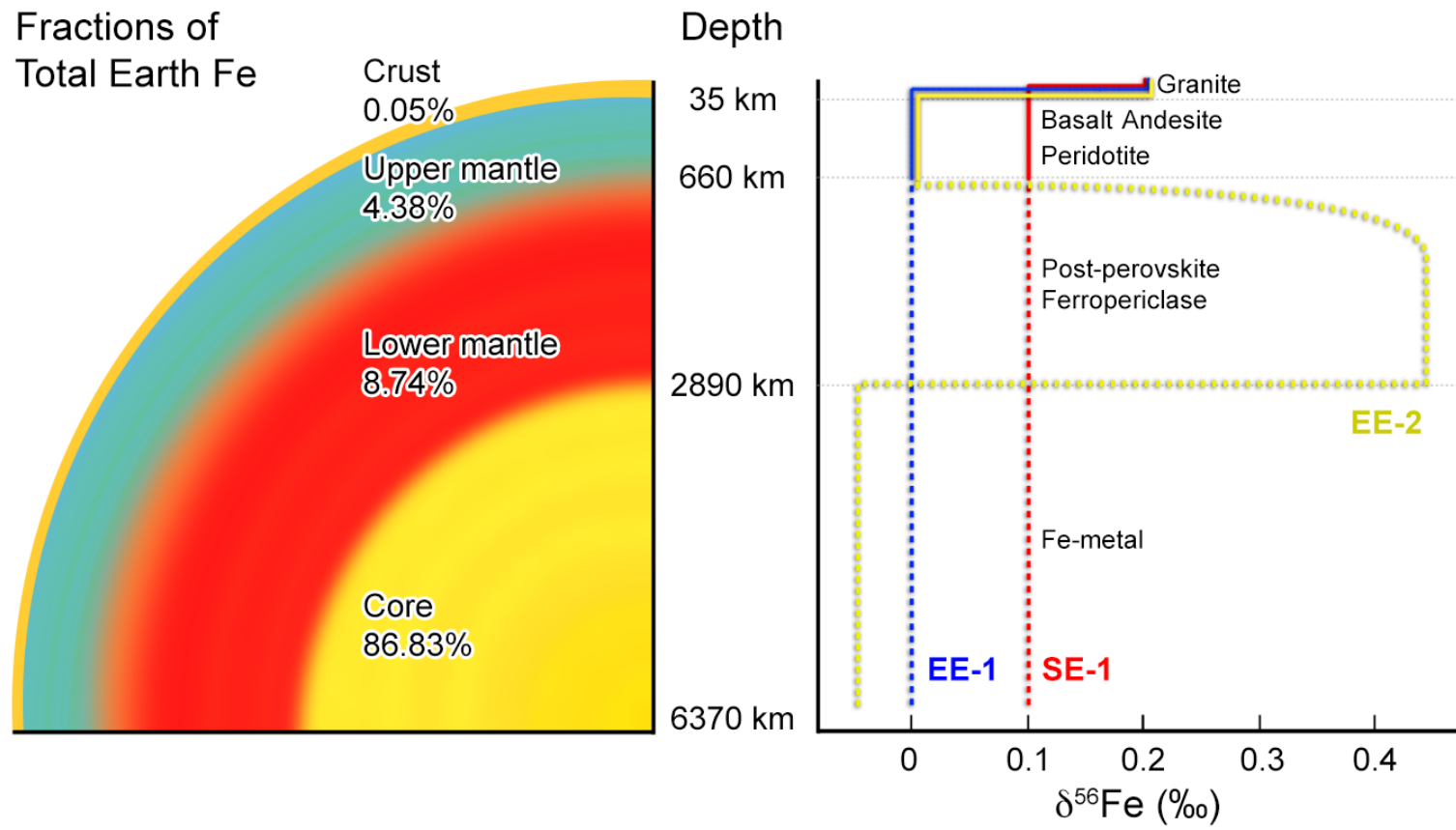


Figure 4-5. The $\delta^{56}\text{Fe}$ depth profiles of the Earth based on modeling

4.4.3. Iron Isotope Fractionation in EL6 Chondrites

In contrast to all other enstatite chondrites (EH3-5 and EL3), the EL6 chondrites show a large range of Fe isotope compositions ($-0.180\text{\textperthousand} < \delta^{56}\text{Fe} < 0.181\text{\textperthousand}$). The highly metamorphosed EL6 ([Fe]=21.3-21.9 %) are depleted in Fe when compared to EL3 ([Fe]=26.2-26.6 %; Kong et al., 1997), whereas among the different EH chondrite groups, there is no trend of Fe depletion with degree of metamorphism (EH3: [Fe]=26.7-30.7%; EH4: [Fe]=27.7-31.3%; EH5: [Fe]=28.7-31.2%). This suggests that increasing thermal metamorphism did not modify the chemical abundance and, as such, the isotopic composition of Fe on the EH parent body. Similarly, the unequilibrated EL3 share the same Fe concentration and isotopic composition as EH. In contrast, the highly metamorphosed EL6 have lost part of their Fe and are isotopically fractionated compared to EL3; therefore the more variable Fe isotopic compositions of EL6 are more likely a result of parent-body processing (rather than nebular processes).

To understand the mechanism(s) for the origin of the Fe isotopic variations observed in EL6, we will first consider possible evaporation-driven kinetic Fe isotopic fractionation. The EL6 chondrites have experienced both thermal metamorphism and also impact melting and/or brecciation (Rubin et al., 2009). Rubin and Wasson (2011) suggest that ~60% of EL6 meteorites were formed by impact melting. However, we can exclude evaporation-driven Fe isotopic fractionation for EL6 with confidence for the following reasons. Firstly, kinetic isotopic fractionation during vaporization would enrich the EL6 in the heavier isotopes. Enstatite chondrite impact melts Happy Canyon and Ilafegh 009 are such examples (see Section 4.4.4); however, EL6 chondrites scatter toward both light and heavy $\delta^{56}\text{Fe}$ values ($-0.180\text{\textperthousand} < \delta^{56}\text{Fe} < 0.181\text{\textperthousand}$). Secondly, there is no correlation between impact shock level and $\delta^{56}\text{Fe}$. Thirdly, a *negative* correlation between $\delta^{56}\text{Fe}$ and $1/\text{[Fe]}$ (the inverse of Fe concentration) is observed (see

Figure 4-6), which contrasts with the expected *positive* correlation for the Fe isotopic fractionation due to impact vaporization (see also Section 4.4.4). In summary, evaporation-driven kinetic Fe isotopic fractionation is unlikely to be the main contributor to the large $\delta^{56}\text{Fe}$ variations observed for EL6 meteorites.

The origin of the isotopic variation observed in EL6 is best explained by mixing between three isotopically distinct mineral phases (metal, sulfide and silicate), as suggested before for ordinary chondrites (Moynier et al., 2007). Theoretical calculations (Polyakov and Mineev, 2000; Schauble et al., 2001; Polyakov et al., 2007) suggest that, at equilibrium, metal should be enriched in the heavier isotopes of Fe compared to the coexisting sulfide and silicate phases. This is exactly what is observed in the mineral separate data (see Figure 4-3). The average values of magnetic (metal) and non-magnetic separates (silicate and sulfide) are $0.101 \pm 0.076\text{\textperthousand}$ (2SD; n=8), and $-0.140 \pm 0.200\text{\textperthousand}$ (2SD; n=8), respectively, which results in a $\delta^{56}\text{Fe}$ difference of $0.241 \pm 0.249\text{\textperthousand}$ (2SD; n=8). This value is in the same range as theoretical calculations made at 600K to 1200K (Polyakov and Mineev, 2000; Polyakov and Soultanov, 2011); this temperature range corresponds to that proposed for enstatite chondrites and aubrites formation and equilibration (Wasson et al., 1994; Zhang et al., 1995). Heavy Fe isotope enrichments in the metallic phase compared to the silicate and sulfide phases have previously been observed in pallasites (Zhu et al., 2002; Weyer et al., 2005; Poitrasson et al., 2005; Schoenberg and von Blanckenburg, 2006); ordinary chondrites (Theis et al., 2008; Okabayashi et al., 2012); iron metal-bearing terrestrial basalt from Disko island, Greenland (Sio et al., 2010) and during experimental reduction of metal at equilibrium (Roskosz et al., 2006).

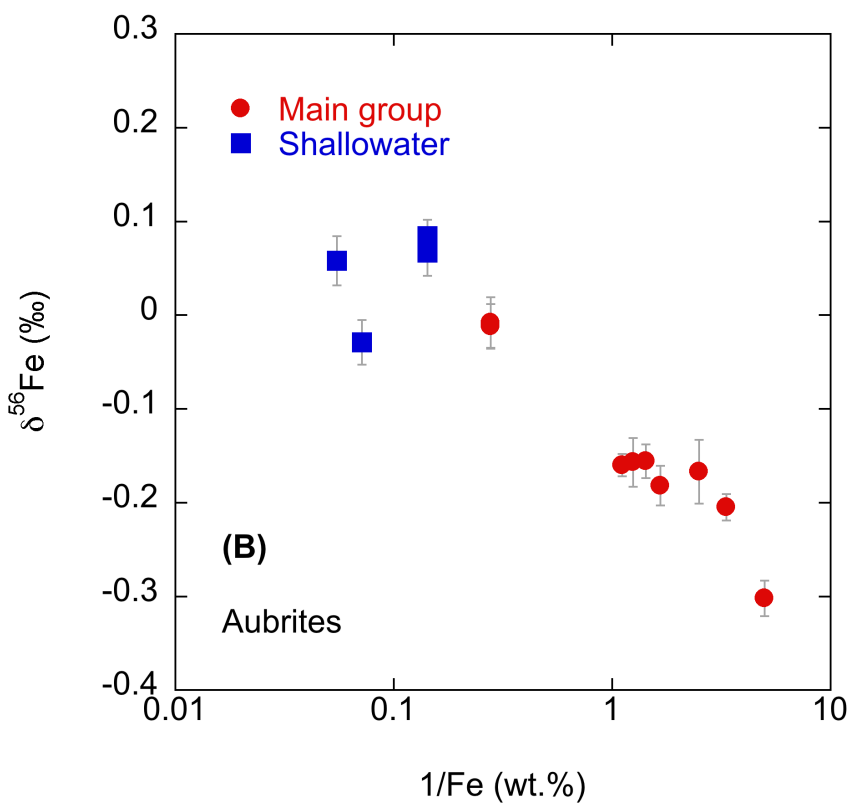
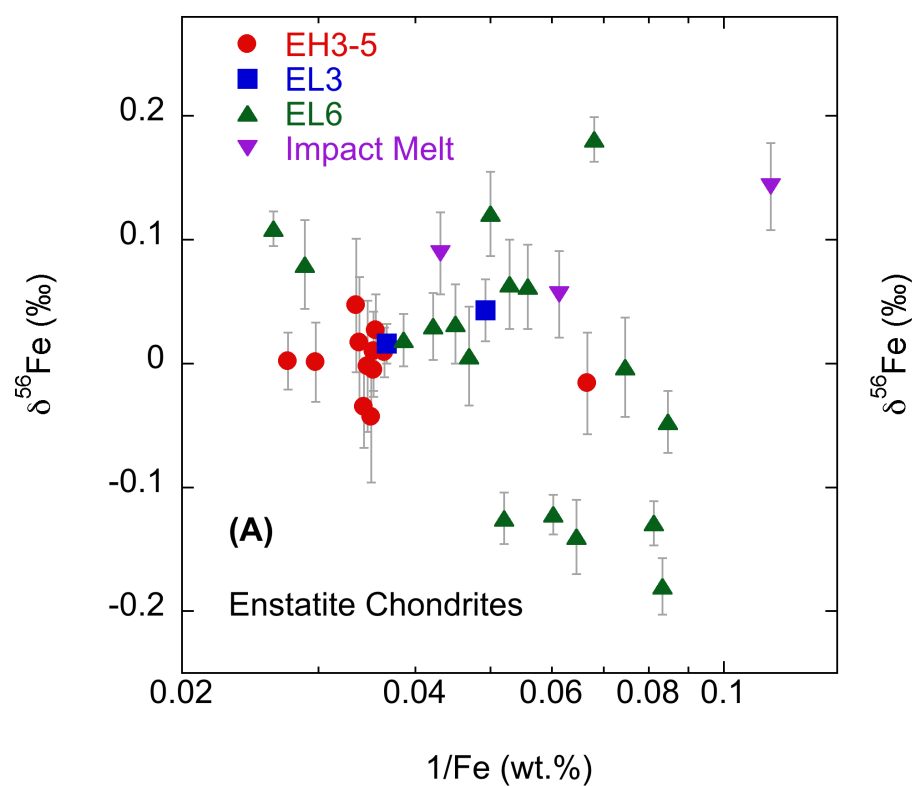


Figure 4-6. $\delta^{56}\text{Fe}$ vs. $1/\text{[Fe]}$ for (A) enstatite chondrites and (B) aubrites analyzed in this study and in the literature (Schoenberg and von Blanckenburg, 2006; Craddock and Dauphas, 2010). $[\text{Fe}]$ is the concentration of Fe in weight %. The linear correlation between $\delta^{56}\text{Fe}$ and the reciprocal of Fe concentration indicates a mixing relation between different sources of Fe with distinct isotopic compositions.

The variable mixing of metallic (isotopically heavy), sulfide (isotopically light) and silicate (isotopically light) phases is a viable explanation for the considerable Fe isotopic variations observed among EL6 (see Figure 4-6). A subsequent question is why then is it only EL6 chondrites that are heterogeneous with respect to Fe isotopes while EH and EL3 are homogeneous? We believe that the Fe isotopic heterogeneity of EL6 chondrites is closely associated with observed chemical/mineralogical fragmentation and brecciation due to their complex impact history (Rubin, 1983a&b; 1984; 2009; Rubin et al., 1997; 2009; Rubin and Wasson, 2011). For example, Hvittis consists of centimeter-sized impact-melt clast (Rubin, 1983a); Blithfield contains centimeter-sized metal-poor-sulfide-rich clasts and metal nodules in metal-rich matrix (Rubin, 1984); and Atlanta comprises centimeter-sized sulfide-rich clasts and centimeter-wide kamacite veins (Rubin, 1983b; Rubin et al., 1997). Keil and Bischoff (2008) suggested that small amounts of troilite and metal could be mobilized and dispersed during impact events. We hence propose that the considerable Fe isotopic variations observed among EL6 are due to this chemical/mineralogical heterogeneity that is unique for EL6. It reflects the intensive impact history suffered by the EL6 chondrites (as compared to EL3 and the EH chondrites) and it is consistent with the conclusions drawn from petrographic evidence (*e.g.*, Rubin et al., 1997), fractionated refractory lithophile elements patterns (Kallemeij and Wasson, 1986; Rubin et al., 2009; Barrat et al., 2013) and enrichment in heavy Zn isotopes (Moynier et al., 2011a).

4.4.4. Iron Isotope Fractionation in Enstatite Chondrite Impact Melts

Happy Canyon and Ilafegh 009 enstatite chondrite impact melts are the sole heavy Fe isotope-enriched group among all the enstatite chondrites (Ilafegh 009 was measured by Craddock and Dauphas, 2010). Happy Canyon contains up to 70 vol.% impact-melt material, which is intermixed with unmelted target clastic material (up to 30 vol.%). Ilafegh 009 crystallized from a total impact melt with no identified unmelted target clastic material (McCoy et al., 1995). The Fe isotopic compositions of Happy Canyon and Ilafegh 009 are both significantly heavier than those of the EH and EL3 and are within the upper range of the EL6. On a $\delta^{56}\text{Fe}$ vs. 1/Fe plot, the $\delta^{56}\text{Fe}$ of impact melts show a slight positive trend with 1/Fe (see Figure 4-6). This correlation of $\delta^{56}\text{Fe}$ and 1/Fe in impact melts suggests that the enriched Fe isotopic compositions were caused by partial loss of Fe during impact vaporization. In addition, the enstatite chondrite impact melts are the only group with both magnetic (metal) and non-magnetic (sulfide+silicate) portions enriched in heavy Fe isotopes (see Figure 4-3). More significantly, the non-magnetic phase has a *heavier* Fe isotopic composition than the magnetic phase. Since sulfides are more volatile than metal (Lodders, 2003), preferential evaporation of sulfides would lead to enrichment of the bulk in the heavy isotopes. This conclusion agrees with a previous study which showed that enstatite chondrite impact melts are also enriched in the heavy isotopes of Zn (a more volatile element than Fe) compared to EH and EL3 chondrites, again interpreted as a consequence of impact vaporization (Moynier et al., 2011a).

Evaporation-driven kinetic isotopic fractionation during impact has been proposed as one important mechanism of Fe isotopic fractionation (Davis and Richter, 2007; Richter et al., 2009), and it has been proposed to explain the enriched heavy Fe isotopic compositions in micrometeorite-impacted lunar regolith (Wang et al., 2012b). In the case of the enstatite

chondrite impact melts, their enriched heavy Fe isotopic compositions provide additional evidence for an impact origin.

It is important to note that impact-induced Fe isotopic fractionation is not observed in other heavily shocked enstatite chondrite samples. The impact metamorphism level of meteorites can be evaluated from their mineralogy and texture (Stöffler et al., 1991) and enstatite meteorites vary from S2 (very weakly shocked) to S5 (strongly shocked) on this scheme (Rubin et al., 1997). Table 4-1 lists all available shock levels for individual samples (Rubin et al., 1997; Grossman, 1998; Rubin, 2009; Rubin, 2010; Izawa et al., 2011). There is no correlation between shock level and Fe isotopic compositions. For example, EL3 chondrite PCA 91020 has been strongly shocked (S5) while EL3 chondrite MAC 88184 (paired with MAC 88136, whose shock stage is reported as S2) has only been very weakly shocked; however they have an identical Fe isotopic composition. The post-annealing shock stages for enstatite chondrite impact melts Happy Canyon and Ilafegh 009 are S2 and S4, respectively, which is also not consistent with their elevated $\delta^{56}\text{Fe}$ values. In conclusion, shock metamorphism does not play a major role in the Fe isotopic fractionation of enstatite chondrites except in those that have experienced extensive melting during impact, such as Happy Canyon and Ilafegh 009.

4.4.5. Iron Isotope Fractionation in Aubrites

All the aubrites (except Shallowater) have negative $\delta^{56}\text{Fe}$ (-0.302 to $-0.008\text{\textperthousand}$). If the aubrites started with a Fe isotopic composition similar to EH or EL3, the negative $\delta^{56}\text{Fe}$ of the aubrites implies that a reservoir enriched in heavy isotopes has been segregated from the source of the aubrite meteorites. The aubrite parent body most probably segregated a metallic core (Keil, 1989), however, the metal/silicate segregation was apparently incomplete, leaving nodules of

metals in the mantle (Casanova et al., 1993a). As shown in our mineral phases separation and in previous studies of ordinary chondrites, pallasites, terrestrial Disko Island metal-bearing basalts, and laboratory experiments (Zhu et al., 2002; Weyer et al., 2005; Poitrasson et al., 2005; Roskosz et al., 2006; Schoenberg and von Blanckenburg, 2006; Theis et al., 2008; Sio et al., 2010; Okabayashi et al., 2012), metallic iron is consistently isotopically heavier than accompanying silicate and/or sulfide phases. We hence suggest that the core of the aubrite parent body, which was enriched in the heavy isotopes of Fe, separated from the silicate (light Fe-enriched) mantle.

The correlation between $\delta^{56}\text{Fe}$ and the 1/Fe suggests that the isotopic variations among aubrites are due to mixing between isotopically distinct components (see Figure 4-6), possibly an incomplete segregation of core and mantle. Aubrites are mainly (~90%) composed of enstatite (MgSiO_3), and, although most of their Fe must have segregated into a core (Keil, 1989), some metallic blobs are found in the aubrite matrix (Casanova et al., 1993a; Casanova et al., 1993b). Based on the pattern of their siderophile elements, these metal grains are thought to be residual material trapped in the silicate magma during partial melting after incomplete core formation (Casanova et al., 1993a; 1993b).

As shown in Figure 4-6, the isotopic compositions of aubrites appear as mixtures of two isotopically distinct components (metal + sulfide, and silicate). The isotopic composition of a mixture of two components (A and B) of different isotopic compositions and concentrations is given by Eq. 4-2:

$$\delta^{56}Fe_{mix} = \delta^{56}Fe_A + (\delta^{56}Fe_A - \delta^{56}Fe_B) \times \frac{[Fe]_B}{[Fe]_A - [Fe]_B} \times (1 - \frac{[Fe]_B}{[Fe]_{mix}})$$

Eq. 4-2

where $[Fe]$ is the concentration of Fe in the different components (A, B and the mixture).

If we assume that the Fe concentration is $\sim 90\%$ in the metal and $\sim 0.1\%$ in the enstatite; and if we use $\delta^{56}Fe_{mix} = 0.00\text{\textperthousand}$, the isotopic compositions of two isotopically distinct components (presumably core and mantle) are $0.14 \pm 0.13\text{\textperthousand}$ and $\delta^{56}Fe = -0.31 \pm 0.13\text{\textperthousand}$, respectively.

Shallowater is an anomalous aubrite and is also the only unbrecciated aubrite. Keil (1989) proposed that Shallowater is derived from a separate parent body to the main group aubrites and other enstatite chondrites. The Shallowater parent body is thought to have experienced a severe impact history whereby the original parent body, which likely consisted of partially or completely molten enstatite covered with a solid carapace, was disrupted by a low-velocity impact with a solid body of enstatite chondrite-like material (Keil, 1989). Such impacts have the potential to fractionate Fe isotopes with loss of light isotopes during vaporization generated by impacts leaving an isotopically heavy residue (see Section 4.4.4). This could be an explanation for the heavy enrichment in Fe isotopes in the Shallowater samples. In addition, Shallowater is enriched in Zn heavy isotopes compared to other aubrites, also interpreted as a result of impact vaporization (Moynier et al., 2011a). However, on a $\delta^{56}Fe$ vs. $1/[Fe]$ plot (Figure 4-6), Shallowater plots on the same *negative* correlation line defined by the other aubrites. Therefore, an alternative explanation could be that Shallowater parent body and main group aubrite parent body have the same Fe isotopic composition and that core formation occurred at similar temperatures. Remaking of core material with silicate portions during the destruction of Shallowater parent body, or core material draw-back into the mantle caused by impact-induced

shearing stress (Rushmer et al., 2005; van Acken et al., 2012) should both lead to the enrichment of metal in Shallowater samples and to their enrichment in the heavier isotopes.

4.4.6. Iron Isotope Fractionation between Metal and Sulfide in Enstatite Meteorites

It is not possible to precisely determine the abundances of metal, sulfide and silicate phases as well as the Fe concentration of each phase in any given sample by our separation procedure, however, it is possible to estimate the Fe inventory in enstatite meteorites through a mass-balance calculation based on the data compilation of previous studies (Keil, 2010; Javoy et al., 2010). On average, in enstatite chondrites, the metal, sulfide and silicate phases contain 49.53, 49.41 and 1.06 wt.% of all the Fe in the sample. Similarly for aubrites, average metal, sulfide and silicate phases carry 49.83, 46.26 and 3.92 wt.% of all the Fe in the sample. For both enstatite chondrites and achondrites, metal and sulfides are the main (and almost equally important) carriers of Fe. Therefore in term of Fe budget, the magnetic separates are dominated by Fe-metal, while the non-magnetic portions are dominated by sulfides. In addition, theoretical calculations show that $\Delta^{56}\text{Fe}_{\text{metal-sulfide}}$ and $\Delta^{56}\text{Fe}_{\text{metal-enstatite}}$ are very close at high temperatures (Polyakov and Mineev, 2000; Polyakov et al., 2007), for example, $\Delta^{56}\text{Fe}_{\text{metal-sulfide}} = 0.11\text{\textperthousand}$ and $\Delta^{56}\text{Fe}_{\text{metal-enstatite}} = 0.08\text{\textperthousand}$ at 1000°C. It is hence reasonable to use the $\delta^{56}\text{Fe}$ difference between magnetic and non-magnetic separates to estimate the metal-sulfide Fe isotopic fractionation factor where $\Delta^{56}\text{Fe}_{\text{metal-sulfide}} = \delta^{56}\text{Fe}_{\text{metal}} - \delta^{56}\text{Fe}_{\text{sulfide}} \approx \Delta^{56}\text{Fe}_{\text{magnetic/non-magnetic}} = \delta^{56}\text{Fe}_{\text{magnetic}} - \delta^{56}\text{Fe}_{\text{non-magnetic}}$.

As discussed above, the average difference ($\Delta^{56}\text{Fe}_{\text{metal-sulfide}}$) of metal-dominated magnetic phases and sulfide-dominated non-magnetic phases for aubrites and enstatite chondrites is $0.242 \pm 0.125\text{\textperthousand}$ (1SD). In detail, however, the $\delta^{56}\text{Fe}$ differences between magnetic and non-magnetic separates in enstatite chondrites ($\Delta^{56}\text{Fe}_{\text{metal-sulfide}} = 0.127 - 0.493\text{\textperthousand}$; average at $0.263 \pm 0.118\text{\textperthousand}$;

1SD) are significantly larger than those in Shallowater aubrites ($\Delta^{56}\text{Fe}_{\text{metal-sulfide}} = 0.054 - 0.129\text{\textperthousand}$; average at $0.091 \pm 0.053\text{\textperthousand}$; 1SD). Isotopic fractionation factors are functions of the equilibration temperatures between phases; therefore, do the different $\Delta^{56}\text{Fe}$ values between aubrites and enstatite chondrites reflect their different equilibration temperatures? The equilibration temperatures of EL chondrites are estimated to be between 1200 – 1400K, averaging at $1220 \pm 80\text{K}$ (Wasson et al., 1994). Zhang et al. (1995) demonstrated that EH and EL have experienced a similar range of equilibration temperatures based on their mineral compositions. For aubrites, Ziegler et al. (2010) calculated final equilibration temperatures for two aubrites at between 1200 and $1130 \pm 80\text{K}$. Here, we follow Ziegler et al. (2010) and apply the temperature calibration provided by Wasson et al. (1994; using the relationship between mole fraction of Si in the metal and mole fraction of Fe in the enstatite) to the Shallowater aubrite. An equilibration temperature of $1060 \pm 80\text{K}$ for Shallowater is hence calculated from the mole fraction of Si (2 mol.%) in the metal and mole fraction (0.005 mol.%) of Fe in the enstatite (Wasson and Wai, 1970). This value represents the final equilibration temperature after melting and thermal metamorphism events (Ziegler et al., 2010).

As shown in a $\Delta^{56}\text{Fe}_{\text{metal-sulfide}}$ vs. temperature plot (Figure 4-7), the maximum value measured between Fe-metal and sulfide in Shallowater agrees very well with the fractionation factors predicted by theoretical calculations (Polyakov et al., 2007; Polyakov and Soultanov, 2011), as defined in Eq. 4-3:

$$\Delta^{56}\text{Fe}_{\text{metal-troilite}} = \frac{0.1774 \times 10^6}{T^2} + \frac{5.6912 \times 10^9}{T^4} + \frac{0.2605 \times 10^{12}}{T^6} \quad \text{Eq. 4-3}$$

In contrast, enstatite chondrites exhibit larger $\Delta^{56}\text{Fe}_{\text{metal-sulfide}}$ fractionations ($\Delta^{56}\text{Fe}_{\text{metal-sulfide}} = 0.127 - 0.493\text{\textperthousand}$) than those expected in Eq. 4-3. The origins of metal and sulfide in

chondrites have been suggested as direct condensation products from solar nebula or sulfurization of Fe/desulfurization of FeS in later stages (*e.g.*, Campbell et al., 2005). This larger $\Delta^{56}\text{Fe}_{\text{metal-sulfide}}$ than expected during high temperature equilibrium implies that the metal and sulfide is unlikely to be in Fe isotopic equilibrium, or metal and sulfide obtained isotopic equilibrium at a lower temperature reached by later thermal alteration events on parent bodies. Alternatively, we have only considered kamacite as the metal phase and troilite as the major phase of sulfides. Enstatite chondrites contain many additional Fe-bearing phases (*e.g.*, alabandite, daubreelite, niningerite, and perryite) that would contribute to the Fe isotopic budgets of the different samples. Currently, there are no experimental data or theoretical calculations for these mineral phases.

A previous study by Williams et al. (2006) has reported a large range of $\Delta^{56}\text{Fe}$ fractionations ($0.03 \pm 0.03\text{\textperthousand}$ – $0.53 \pm 0.06\text{\textperthousand}$) between metal and troilite phases separated from magmatic iron meteorites. The Fe isotopic fractionation factor $0.129 \pm 0.065\text{\textperthousand}$ at $1060 \pm 80\text{K}$ obtained in this study falls in this range. Williams et al. (2006) proposed their maximum $\Delta^{56}\text{Fe}$ value ($0.53 \pm 0.06\text{\textperthousand}$) as the best estimate of the equilibrium metal-sulfide Fe isotopic fractionation factor for temperature range of 773 – 1263 K. At 773K and 1263K, our measurement as well as theoretical calculations (Polyakov et al., 2007; Polyakov and Soltanov, 2011) predicts a $\Delta^{56}\text{Fe} \sim 0.31\text{\textperthousand}$ and $\sim 0.11\text{\textperthousand}$, respectively, which is a factor two or five smaller than the $0.53 \pm 0.06\text{\textperthousand}$ observed by Williams et al. (2006). This inconsistency between laboratory measurements and theoretical calculations needs to be further investigated.

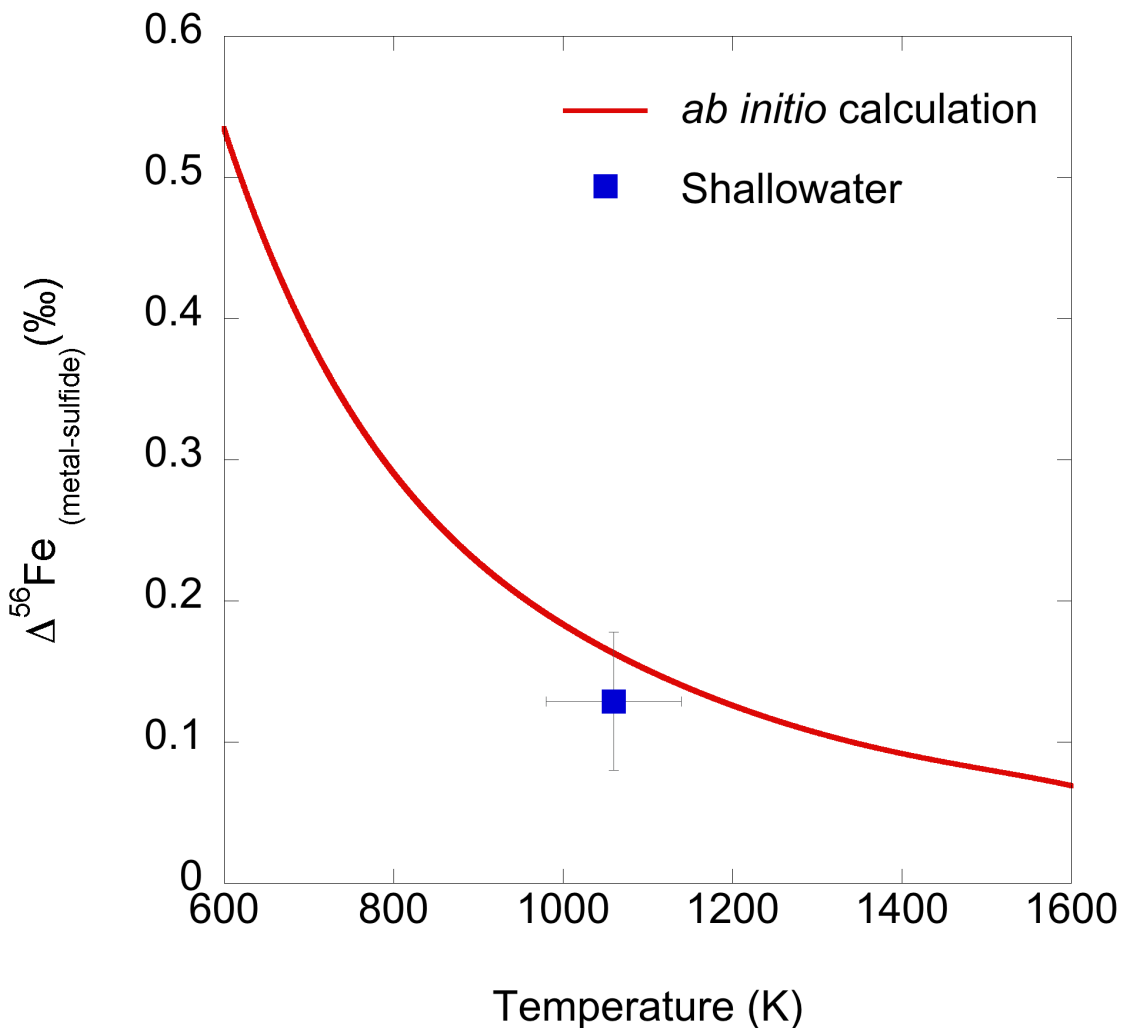


Figure 4-7. $\Delta^{56}\text{Fe}_{\text{(metal-sulfide)}}$ vs. temperature (K). The dashed line is the theoretical calculation of Fe isotopic fractionation between iron-metal and troilite (Polyakov et al., 2007; Polyakov and Soultanov, 2011). The $\Delta^{56}\text{Fe}_{\text{(metal-sulfide)}}$ of Shallowater is the maximum value measured in the magnetic and non-magnetic portions separated from Shallowater aubrites.

4.5. Conclusions

We measured the bulk Fe isotopic composition of 22 samples from the different enstatite meteorite groups: EH and EL chondrites, aubrites (main group and Shallowater) and Happy Canyon impact melt as well as in separated phases (magnetic and non-magnetic phases) from these meteorites, by high precision MC-ICP-MS. The main conclusions from this study are described below.

EH3-5 and EL3 chondrites all have the same homogeneous Fe isotopic composition $0.009 \pm 0.045\text{\textperthousand}$ (2SD; n=11), which is identical to the averages of ordinary, carbonaceous chondrites, terrestrial mantle rocks, martian and HED meteorites. Therefore, in terms of the enstatite chondrite Earth model, Fe is yet another isotopic system that shows a remarkable resemblance to terrestrial materials.

The EL6 chondrites have a large range of Fe isotopic compositions ($-0.180\text{\textperthousand} < \delta^{56}\text{Fe} < 0.181\text{\textperthousand}$), which are well correlated with $1/\text{[Fe (wt.\%)]}$. We propose that these Fe isotopic variations are due to the mixing between metallic Fe (isotopically heavy), sulfide (isotopically light) and silicate (isotopically light) components in different proportions. Our mineral separation experiments have shown that, in enstatite meteorites, magnetic (metal; $0.101 \pm 0.076\text{\textperthousand}$) and non-magnetic (silicate+sulfide; $-0.140 \pm 0.200\text{\textperthousand}$) phases have distinct Fe isotopic compositions, which agrees with previous experimental observations and theoretical calculations. The extreme heterogeneity of Fe isotopes is unique to EL6 chondrites likely due to the chemical/mineralogical fragmentation and brecciation as a result of the complex and intense impact history experienced during their formation.

The enstatite chondrite impact melts (Happy Canyon and Ilafegh 009) are the only heavy Fe isotope-enriched group, on average, among all the enstatite chondrites. This enrichment is most likely caused by kinetic fractionation during impact vaporization and is consistent with their impact-melt origin, previously implied by mineralogical, compositional and Zn isotopic studies.

Like the EL6, aubrites exhibit a wide range of Fe isotopic compositions ($-0.302\text{\textperthousand} < \delta^{56}\text{Fe} < 0.084\text{\textperthousand}$). All the main group aubrites are depleted in heavy Fe isotopes, while the anomalous aubrite Shallowater is enriched in heavy Fe isotopes. The correlation between the Fe isotopic composition and $1/\text{Fe}$ suggests a mixing relation between two isotopically distinct reservoirs of Fe that we believe are the core and mantle of the aubrite parent body. Our Fe isotopic study of aubrites indicates the separation of a heavy Fe isotope-rich core on the aubrite parent body. If we assume that Shallowater has the same Fe isotope composition as main group aubrites, our data suggest that core material remixed with silicate portions during the destruction of the Shallowater parent body, or alternatively the core material draw-back into the mantle occurred due to intensive impact-induced shearing stress.

We have obtained an empirical metal-sulfide Fe isotopic fractionation factor ($\Delta^{56}\text{Fe}_{\text{metal-sulfide}}$) of $0.129 \pm 0.065\text{\textperthousand}$ (1SD) at $1060 \pm 80\text{K}$. This value agrees well with previously theoretical calculations of equilibrium fractionation data between Fe-metal and troilite.

References

- Baedecker P. A. and Wasson J. T. (1975) Elemental fractionations among enstatite chondrites. *Geochim. Cosmochim. Acta* **39**, 735–765.
- Alfè D., Gillan M. J. and Price G. D. (2002) Composition and temperature of the Earth's core constrained by combining ab initio calculations and seismic data. *Earth Planet. Sci. Lett.* **195**, 91–98.
- Allègre C. J., Poirier J.-P., Humler E. and Hofmann A. W. (1995) The chemical composition of the Earth. *Earth Planet. Sci. Lett.* **134**, 515–526.
- Badro J., Fiquet G., Guyot F., Gregoryanz E., Occelli F., Antonangeli D. and d'Astuto M. (2007) Effect of light elements on the sound velocities in solid iron: Implications for the composition of Earth's core. *Earth Planet. Sci. Lett.* **254**, 233–238.
- Barrat J.-A., Zanda B., Jambon A. and Bollinger C. (2013) The “not so lithophile” trace elements in enstatite chondrites and the Nb budget of the bulk silicate Earth. *Geochim. Cosmochim. Acta* **in review**.
- Beard B. L. and Johnson C. M. (1999) High precision iron isotope measurements of terrestrial and lunar materials. *Geochim. Cosmochim. Acta* **63**, 1653–1660.
- Beard B. L., Johnson C. M., Skulan J. L., Nealson K. H., Cox L. and Sun H. (2003) Application of Fe isotopes to tracing the geochemical and biological cycling of Fe. *Chem. Geol.* **195**, 87–117.
- Campbell A. J., Zanda B., Perron C., Meibom A. and Petaev M. I. (2005) Origin and Thermal History of Fe-Ni Metal in Primitive Chondrites. In *Chondrites and the Protoplanetary Disk* (eds. Alexander N. Krot, E. R. D. Scott, and B. Reipurth). Astronomical Society of the Pacific, San Francisco. p. 407.
- Casanova I., Keil K. and Newsom H. E. (1993a) Composition of metal in aubrites: Constraints on core formation. *Geochim. Cosmochim. Acta* **57**, 675–682.
- Casanova I., McCoy T. J. and Keil K. (1993b) Metal-rich meteorites from the aubrite parent body. *Lunar Planet. Sci. XXIV*. Lunar Planet. Inst., Houston. 259–260.
- Chen J. H., Papanastassiou D. A. and Wasserburg G. J. (2010) Ruthenium endemic isotope effects in chondrites and differentiated meteorites. *Geochim. Cosmochim. Acta* **74**, 3851–3862.
- Clayton R. N., Mayeda T. K. and Rubin A. E. (1984) Oxygen isotopic compositions of enstatite chondrites and aubrites. *J. Geophys. Res.* **89**, C245.
- Craddock P. R. and Dauphas N. (2011) Iron isotopic compositions of geological reference materials and chondrites. *Geostand. Geoanal. Res.* **35**, 101–123.

- Craddock P. R., Warren J. M. and Dauphas N. (2013) Abyssal peridotites reveal the near-chondritic Fe isotopic composition of the Earth. *Earth Planet. Sci. Lett.* **365**, 63–76.
- Dauphas N., Craddock P. R., Asimow P. D., Bennett V. C., Nutman A. P. and Ohnenstetter D. (2009) Iron isotopes may reveal the redox conditions of mantle melting from Archean to Present. *Earth Planet. Sci. Lett.* **288**, 255–267.
- Dauphas N., Davis A. M., Marty B. and Reisberg L. (2004) The cosmic molybdenum–ruthenium isotope correlation. *Earth Planet. Sci. Lett.* **226**, 465–475.
- Dauphas N., Teng F.-Z. and Arndt N. T. (2010) Magnesium and iron isotopes in 2.7 Ga Alexo komatiites: Mantle signatures, no evidence for Soret diffusion, and identification of diffusive transport in zoned olivine. *Geochim. Cosmochim. Acta* **74**, 3274–3291.
- Davis A. M. and Richter F. M. (2007) Condensation and evaporation of solar system materials. In *Treatise on Geochemistry* (eds. A. M. Davis, H. D. Holland, and K. K. Turekian). Elsevier-Pergamon, Oxford. pp. 407–430.
- Fitoussi C. and Bourdon B. (2012) Silicon isotope evidence against an enstatite chondrite Earth. *Science* **335**, 1477–80.
- Frost D. J. and McCammon C. A. (2008) The redox state of Earth's mantle. *Annu. Rev. Earth Planet. Sci.* **36**, 389–420.
- Georg R. B., Halliday A. N., Schauble E. A. and Reynolds B. C. (2007) Silicon in the Earth's core. *Nature* **447**, 1102–1106.
- Grossman J. N. (1998) The Meteoritical Bulletin, No. 82, 1998 July. *Meteorit. Planet. Sci.* **33**, A221–A239.
- Haack H. and McCoy T. J. (2007) Iron and Stony-iron Meteorites. In *Treatise on Geochemistry* (eds. A. M. Davis, H. D. Holland, and K. K. Turekian). Elsevier-Pergamon, Oxford. pp. 325–345.
- Hin R.C., Schmidt M.W., and Bourdon B. (2012) Experimental evidence for the absence of iron isotope fractionation between metal and silicate liquids at 1 GPa and 1250–1300°C and its cosmochemical consequences. *Geochim. Cosmochim. Acta* **93**, 164–181
- Hibbert K. E. J., Williams H. M., Kerr A. C. and Puchtel I. S. (2012) Iron isotopes in ancient and modern komatiites: Evidence in support of an oxidised mantle from Archean to present. *Earth Planet. Sci. Lett.* **321–322**, 198–207.
- Huang F., Zhang Z., Lundstrom C. C. and Zhi X. (2011) Iron and magnesium isotopic compositions of peridotite xenoliths from Eastern China. *Geochim. Cosmochim. Acta* **75**, 3318–3334.

- Huss G. R., Rubin A. E. and Grossman J. N. (2006) Thermal Metamorphism in Chondrites. In *Meteorites and the Early Solar System II* (eds. D. S. Lauretta and H. Y. McSween). University of Arizona Press, Tucson. pp. 567–586.
- Izawa M. R. M., Flemming R. L., Banerjee N. R. and McCausland P. J. A. (2011) Micro-X-ray diffraction assessment of shock stage in enstatite chondrites. *Meteorit. Planet. Sci.* **45**, 638–651.
- Javoy M. (1995) The integral enstatite chondrite model of the Earth. *Geophys. Res. Lett.* **22**, 2219–2222.
- Javoy M., Kaminski E., Guyot F., Andrault D., Sanloup C., Moreira M., Labrosse S., Jambon A., Agrinier P., Davaille A. and Jaupart C. (2010) The chemical composition of the Earth: Enstatite chondrite models. *Earth Planet. Sci. Lett.* **293**, 259–268.
- Javoy M. and Pineau F. (1983) Stable isotope constraints on a model Earth from a study of mantle nitrogen. *Meteoritics* **18**, 320.
- Kallemeyn G. W. and Wasson J. T. (1986) Compositions of enstatite (EH3, EH4,5 and EL6) chondrites: Implications regarding their formation. *Geochim. Cosmochim. Acta* **50**, 2153–2164.
- Kaminski E. and Javoy M. (2013) A two-stage scenario for the formation of the Earth's mantle and core. *Earth Planet. Sci. Lett.* **365**, 97–107.
- Keil K. (2010) Enstatite achondrite meteorites (aubrites) and the histories of their asteroidal parent bodies. *Chem. Erde* **70**, 295–317.
- Keil K. (1989) Enstatite meteorites and their parent bodies. *Meteoritics* **24**, 195–208.
- Keil K. and Bischoff A. (2008) Northwest Africa 2526: A partial melt residue of enstatite chondrite parentage. *Meteorit. Planet. Sci.* **43**, 1233–1240.
- Keil K. and Fredriksson K. (1963) Electron microprobe analysis of some rare minerals in the Norton County achondrite. *Geochim. Cosmochim. Acta* **27**, 939–947.
- Kong P., Mori T. and Ebihara M. (1997) Compositional continuity of enstatite chondrites and implications for heterogeneous accretion of the enstatite chondrite parent body. *Geochim. Cosmochim. Acta* **61**, 4895–4914.
- Larimer J. and Anders E. (1970) Chemical fractionations in meteorites—III. Major element fractionations in chondrites. *Geochim. Cosmochim. Acta* **34**, 367–387.
- Lodders K. (2003) Solar system abundances and condensation temperatures of the elements. *Astrophys. J.* **591**, 1220–1247.
- McCoy T. J., Keil K., Bogard D. D., Garrison D. H., Casanova I., Lindstrom M. M., Brearley A. J., Kehm K., Nichols R. H. and Hohenberg C. M. (1995) Origin and history of impact-melt rocks of enstatite chondrite parentage. *Geochim. Cosmochim. Acta* **59**, 161–175.

- McDonough W. F. (2007) Compositional Model for the Earth's Core. In *Treatise on Geochemistry* (eds. R. W. Carlson, H. D. Holland, and K. K. Turekian). Elsevier-Pergamon, Oxford. pp. 547–568.
- Moynier F., Blichert-Toft J., Telouk P., Luck J. M. and Albarede F. (2007) Comparative stable isotope geochemistry of Ni, Cu, Zn, and Fe in chondrites and iron meteorites. *Geochim. Cosmochim. Acta* **71**, 4365–4379.
- Moynier F., Day J. M. D., Okui W., Yokoyama T., Bouvier A., Walker R. J. and Podosek F. A. (2012) Planetary-scale strontium isotopic heterogeneity and the age of volatile depletion of early solar system materials. *Astrophys. J.* **758**, 45.
- Moynier F., Paniello R. C., Gounelle M., Albarède F., Beck P., Podosek F. and Zanda B. (2011a) Nature of volatile depletion and genetic relationships in enstatite chondrites and aubrites inferred from Zn isotopes. *Geochim. Cosmochim. Acta* **75**, 297–307.
- Moynier F., Yin Q.-Z. and Schauble E. (2011b) Isotopic evidence of Cr partitioning into Earth core. *Science* **331**, 1417–1420.
- Okabayashi S., Yokoyama T. and Hirata T. (2012) Iron isotopic signature for Fe-Ni metal of ordinary chondrite using newly developed technique; LAL-MC-ICPMS. *Lunar Planet. Sci. XLIII*. Lunar Planet. Inst., Woodlands. #1871(abstr.).
- Poirrasson F., Delpech G. and Grégoire M. (2013) On the iron isotope heterogeneity of lithospheric mantle xenoliths: implications for mantle metasomatism, the origin of basalts and the iron isotope composition of the Earth. *Contrib. Mineral. Petrol.* **165**, 1243–1258.
- Poirrasson F., Halliday A. N., Lee D. C., Levasseur S. and Teutsch N. (2004) Iron isotope differences between Earth, Moon, Mars and Vesta as possible records of contrasted accretion mechanisms. *Earth Planet. Sci. Lett.* **223**, 253–266.
- Poirrasson F., Levasseur S. and Teutsch N. (2005) Significance of iron isotope mineral fractionation in pallasites and iron meteorites for the core-mantle differentiation of terrestrial planets. *Earth Planet. Sci. Lett.* **234**, 151–164.
- Polyakov V. B. (2009) Equilibrium iron isotope fractionation at core-mantle boundary conditions. *Science* **323**, 912–914.
- Polyakov V. B., Clayton R. N., Horita J. and Mineev S. D. (2007) Equilibrium iron isotope fractionation factors of minerals: Reevaluation from the data of nuclear inelastic resonant X-ray scattering and Mössbauer spectroscopy. *Geochim. Cosmochim. Acta* **71**, 3833–3846.
- Polyakov V. B. and Mineev S. D. (2000) The use of Mossbauer spectroscopy in stable isotope geochemistry. *Geochim. Cosmochim. Acta* **64**, 849–865.

- Polyakov V. B. and Soultanov D. M. (2011) New data on equilibrium iron isotope fractionation among sulfides: Constraints on mechanisms of sulfide formation in hydrothermal and igneous systems. *Geochim. Cosmochim. Acta* **75**, 1957–1974.
- Regelous M., Elliott T. and Coath C. D. (2008) Nickel isotope heterogeneity in the early Solar System. *Earth Planet. Sci. Lett.* **272**, 330–338.
- Richter F. M., Dauphas N. and Teng F.-Z. (2009) Non-traditional fractionation of non-traditional isotopes: Evaporation, chemical diffusion and Soret diffusion. *Chem. Geol.* **258**, 92–103.
- Roskosz M., Luais B., Watson H. C., Toplis M. J., Alexander C. M. O. and Mysen B. O. (2006) Experimental quantification of the fractionation of Fe isotopes during metal segregation from a silicate melt. *Earth Planet. Sci. Lett.* **248**, 851–867.
- Rubie D. C., Frost D. J., Mann U., Asahara Y., Nimmo F., Tsuno K., Kegler P., Holzheid A. and Palme H. (2011) Heterogeneous accretion, composition and core–mantle differentiation of the Earth. *Earth Planet. Sci. Lett.* **301**, 31–42.
- Rubin A. E. (1983a) Impact melt-rock clasts in the Hvittis Enstatite chondrite breccia: Implications for a genetic relationship between El chondrites and aubrites. *J. Geophys. Res.* **88**, B293.
- Rubin A. E. (2010) Impact melting in the Cumberland Falls and Mayo Belwa aubrites. *Meteorit. Planet. Sci.* **45**, 265–275.
- Rubin A. E. (2009) Shock effects in EH6 chondrites and aubrites: Implications for collisional heating of asteroids. *Lunar Planet. Sci. XL*. Lunar Planet. Inst., Woodlands. #1353 (abstr.).
- Rubin A. E. (1983b) The Atlanta enstatite chondrite breccia. *Meteoritics* **18**, 113–121.
- Rubin A. E. (1984) The Blithfield meteorite and the origin of sulfide-rich, metal-poor clasts and inclusions in brecciated enstatite chondrites. *Earth Planet. Sci. Lett.* **67**, 273–283.
- Rubin A. E., Huber H. and Wasson J. T. (2009) Possible impact-induced refractory-lithophile fractionations in EL chondrites. *Geochim. Cosmochim. Acta* **73**, 1523–1537.
- Rubin A. E., Scott E. R. D. and Keil K. (1997) Shock metamorphism of enstatite chondrites. *Geochim. Cosmochim. Acta* **61**, 847–858.
- Rubin A. E. and Wasson J. T. (2011) Shock effects in “EH6” enstatite chondrites and implications for collisional heating of the EH and EL parent asteroids. *Geochim. Cosmochim. Acta* **75**, 3757–3780.
- Rushmer T., Petford N., Humayun M. and Campbell A. J. (2005) Fe-liquid segregation in deforming planetesimals: Coupling core-forming compositions with transport phenomena. *Earth Planet. Sci. Lett.* **239**, 185–202.

- Rustad J. R. and Yin Q. Z. (2009) Iron isotope fractionation in the Earth's lower mantle. *Nat. Geosci.* **2**, 514–518.
- Savage P. S. and Moynier F. (2013) Silicon isotopic variation in enstatite meteorites: Clues to their origin and Earth-forming material. *Earth Planet. Sci. Lett.* **361**, 487–496.
- Schauble E. A., Rossman G. R. and Taylor H. P. (2001) Theoretical estimates of equilibrium Fe-isotope fractionations from vibrational spectroscopy. *Geochim. Cosmochim. Acta* **65**, 2487–2497.
- Schoenberg R. and von Blanckenburg F. (2006) Modes of planetary-scale Fe isotope fractionation. *Earth Planet. Sci. Lett.* **252**, 342–359.
- Shahar A., Hillgren V. J., Mesa-Garcia J., Horan M. F., Mock T. D. and Deng L. (2013) Iron isotope fractionation in an Fe-S alloy: Implications for core formation. *Lunar Planet. Sci. XLIV*. Lunar Planet. Inst., Woodlands. #2351(abstr.)
- Sio C. K., Dauphas N. and Roskosz M. (2010) Can core formation in planetesimals fractionate iron isotopes? Clues from a study of metal-silicate assemblages in Disko basalt, Greenland. *Lunar Planet. Sci. XLI*. Lunar Planet. Inst., Woodlands. #1467(abstr.).
- Steele R. C. J., Coath C. D., Regelous M., Russell S. and Elliott T. (2012) Neutron-poor nickel isotope anomalies in meteorites. *Astrophys. J.* **758**, 59.
- Stöffler D., Keil K. and Edward R.D S. (1991) Shock metamorphism of ordinary chondrites. *Geochim. Cosmochim. Acta* **55**, 3845–3867.
- Teng F.-Z., Dauphas N., Huang S. and Marty B. (2013) Iron isotopic systematics of oceanic basalts. *Geochim. Cosmochim. Acta* **107**, 12–26.
- Theis K. J., Burgess R., Lyon I. C. and Sears D. W. (2008) The origin and history of ordinary chondrites: A study by iron isotope measurements of metal grains from ordinary chondrites. *Geochim. Cosmochim. Acta* **72**, 4440–4456.
- Torigoye N. and Shima M. (1993) Evidence for a late thermal event of unequilibrated enstatite chondrites: A Rb-Sr study of Qingzhen and Yamato 6901 (EH3) and Khairpur (EL6). *Meteoritics* **28**, 515–527.
- Trinquier A., Birck J. and Allègre C. J. (2007) Widespread ^{54}Cr heterogeneity in the inner solar system. *Astrophys. J.* **655**, 1179–1185.
- Trinquier A., Elliott T., Ulfbeck D., Coath C., Krot A. N. and Bizzarro M. (2009) Origin of nucleosynthetic isotope heterogeneity in the solar protoplanetary disk. *Science* **324**, 374–6.
- van Acken D., Brandon A. D. and Lapen T. J. (2012) Highly siderophile element and osmium isotope evidence for postcore formation magmatic and impact processes on the aubrite parent body. *Meteorit. Planet. Sci.* **47**, 1606–1623.

- Wang K., Moynier F., Barrat J.-A., Zanda B., Paniello R. C. and Savage P. S. (2013) Homogeneous distribution of Fe isotopes in the early solar nebula. *Meteorit. Planet. Sci.* **48**, 354–364.
- Wang K., Moynier F., Dauphas N., Barrat J.-A., Craddock P. and Sio C. K. (2012a) Iron isotope fractionation in planetary crusts. *Geochim. Cosmochim. Acta* **89**, 31–45.
- Wang K., Moynier F., Podosek F. A. and Foriel J. (2012b) An iron isotope perspective on the origin of the nanophase metallic iron in lunar regolith. *Earth Planet. Sci. Lett.* **337-338**, 17–24.
- Wang K., Moynier F., Podosek F. and Foriel J. (2011) ^{58}Fe and ^{54}Cr in early solar system materials. *Astrophys. J.* **739**, L58.
- Wasson J. T., Kallemeyn G. W. and Rubin A. E. (1994) Equilibration temperatures of EL chondrites: A major downward revision in the ferrosilite contents of enstatite. *Meteoritics* **29**, 658–662.
- Wasson J. T. and Wai C. M. (1970) Composition of the metal, schreibersite and perryite of enstatite achondrites and the origin of enstatite chondrites and achondrites. *Geochim. Cosmochim. Acta* **34**, 169–184.
- Weyer S., Anbar A. D., Brey G. P., Munker C., Mezger K. and Woodland A. B. (2005) Iron isotope fractionation during planetary differentiation. *Earth Planet. Sci. Lett.* **240**, 251–264.
- Weyer S. and Ionov D. A. (2007) Partial melting and melt percolation in the mantle: The message from Fe isotopes. *Earth Planet. Sci. Lett.* **259**, 119–133.
- Williams H. M., Markowski A., Quitte G., Halliday A. N., Teutsch N. and Levasseur S. (2006) Fe isotope fractionation in iron meteorites: New insights into metal-sulphide segregation and planetary accretion. *Earth Planet. Sci. Lett.* **250**, 486–500.
- Williams H. M., Nielsen S. G., Renac C., Griffin W. L., O'Reilly S. Y., McCammon C. A., Pearson N., Viljoen F., Alt J. C. and Halliday A. N. (2009) Fractionation of oxygen and iron isotopes by partial melting processes: Implications for the interpretation of stable isotope signatures in mafic rocks. *Earth Planet. Sci. Lett.* **283**, 156–166.
- Williams H. M., Wood B. J., Wade J., Frost D. J. and Tuff J. (2012) Isotopic evidence for internal oxidation of the Earth's mantle during accretion. *Earth Planet. Sci. Lett.* **321-322**, 54–63.
- Zhang Y., Benoit P. H. and Sears D. W. G. (1995) The classification and complex thermal history of the enstatite chondrites. *J. Geophys. Res.* **100**, 9417.
- Zhao X., Zhang H., Zhu X., Tang S. and Tang Y. (2010) Iron isotope variations in spinel peridotite xenoliths from North China Craton: implications for mantle metasomatism. *Contrib. Mineral. Petrol.* **160**, 1–14.

Zhao X., Zhang H., Zhu X., Tang S. and Yan B. (2012) Iron isotope evidence for multistage melt–peridotite interactions in the lithospheric mantle of eastern China. *Chem. Geol.* **292-293**, 127–139.

Zhu X. K., Guo Y., Williams R. J. P., O’Nions R. K., Matthews A., Belshaw N. S., Canters G. W., de Waal E. C., Weser U., Burgess B. K. and Salvato B. (2002) Mass fractionation processes of transition metal isotopes. *Earth Planet. Sci. Lett.* **200**, 47–62.

Ziegler K., Young E. D., Schauble E. A. and Wasson J. T. (2010) Metal–silicate silicon isotope fractionation in enstatite meteorites and constraints on Earth’s core formation. *Earth Planet. Sci. Lett.* **295**, 487–496.

CHAPTER 5 :

FE ISOTOPE FRACTIONATION IN PLANETARY CRUSTS

This chapter has been published in *Geochimica et Cosmochimica Acta*: Wang, K., Moynier, F., Dauphas, N., Barrat, J-A., Craddock, P. and Sio, C.K. (2012) Iron Isotope Fractionation in Planetary Crusts. *Geochimica et Cosmochimica Acta*, **89**, 31-45.

Abstract

We present new high precision iron isotope data ($\delta^{56}\text{Fe}$ vs. IRMM-014 in per mil) for four groups of achondrites: one lunar meteorite, eleven martian meteorites, thirty-two Howardite-Eucrite-Diogenite meteorites (HEDs), and eight angrites. Angrite meteorites are the only planetary materials, other than Earth/Moon system, significantly enriched in the heavy isotopes of Fe compared to chondrites (by an average of +0.12 ‰ in $\delta^{56}\text{Fe}$). While the reason for such fractionation is not completely understood, it might be related to isotopic fractionation by volatilization during accretion or more likely magmatic differentiation in the angrite parent-body. We also report precise data on martian and HED meteorites, yielding an average $\delta^{56}\text{Fe}$ of 0.00 ± 0.01 ‰. Stannern-trend eucrites are isotopically heavier by +0.05 ‰ in $\delta^{56}\text{Fe}$ than other eucrites. We show that this difference can be ascribed to the enrichment of heavy iron isotopes in ilmenite during igneous differentiation. Preferential dissolution of isotopically heavy ilmenite during remelting of eucritic crust could have generated the heavy iron isotope composition of Stannern-trend eucrites. This supports the view that Stannern-trend eucrites are derived from main-group eucrite source magma by assimilation of previously formed asteroidal crust.

These new results show that iron isotopes are not only fractionated in terrestrial and lunar basalts, but also in two other differentiated planetary crusts. We suggest that igneous processes might be responsible for the iron isotope variations documented in planetary crusts.

5.1. Introduction

Iron is the ninth most abundant element in the Solar System, and the second most abundant element in the Earth and other terrestrial planetary bodies. Iron can behave as a siderophile (metal-loving), lithophile (rock-loving) and chalcophile (sulfur-loving) element and is ubiquitous in Solar System planetary bodies. On Earth, it is a major element in the core, the mantle and the crust (Allègre et al., 1995; Rudnick and Gao, 2003). In the past decade, the development of high-resolution Multi-Collector Inductively-Coupled-Plasma Mass-Spectrometers (MC-ICP-MS) has allowed measurements of iron isotope composition at high precision (Belshaw et al., 2000; Zhu et al., 2001; Weyer and Schwiters, 2003; Dauphas et al., 2009b; Millet et al., 2012). Following this improvement, small yet resolvable iron isotopic variations in igneous rocks have been discovered (Poitrasson et al., 2004; Weyer et al., 2005; Schoenberg and von Blanckenburg, 2006; Weyer and Ionov, 2007; Heimann et al., 2008; Teng et al., 2008; Dauphas et al., 2009a; Teng et al., 2011; Weyer and Seitz, 2012).

Mid-ocean ridge basalts (MORBs), oceanic island basalts (OIBs), and continental basalts are enriched in heavy iron isotopes by $\sim +0.1\text{‰}$ when compared to chondrites; while martian and 4-Vesta (HED) meteorites all have similar iron isotope compositions to chondrites (Zhu et al., 2001; Poitrasson et al., 2004; Weyer et al., 2005; Anand et al., 2006; Schoenberg and von Blanckenburg, 2006; Craddock and Dauphas, 2011). Three mechanisms have been proposed to explain this difference: (1) *Planetary accretion*: Heavy iron isotopes were enriched on the Earth and Moon by evaporative kinetic isotope fractionation during the giant impact that formed the Moon (Poitrasson et al., 2004). In this context, one of the difficulties is to explain why potassium, which is highly volatile, is not isotopically fractionated in the Earth-Moon system (Humayun and Clayton, 1995). Poitrasson et al. (2004) proposed that Fe was evaporated from core material as

metal while K was evaporated as oxides. In that case, Fe would be more volatile than K and could be isotopically more fractionated. However, lunar mare basalts (low-Ti vs. high-Ti) have large variable iron isotope compositions and the $\delta^{56}\text{Fe}$ value of the bulk Moon is not well known (Liu et al., 2010), which provides little constraint on the evaporative isotope fractionation hypothesis. (2) *Core-mantle segregation*: At ultra high-pressure (>100 GPa) relevant to terrestrial core-mantle boundary conditions, Polyakov (2009) suggested based on nuclear resonant inelastic X-ray scattering data that a detectable fractionation between metallic and silicate phases should be present, which could explain the heavy iron isotope composition of terrestrial silicate rocks. While the approach used by Polyakov (2009) is sound, the results are highly dependent on the high-energy tails of the phonon density of states, which are highly uncertain for high-pressure minerals. In contrast to this hypothesis, laboratory experiments at temperatures and pressures applicable to differentiation of parent bodies to achondrites have shown no iron isotope fractionation between metal and silicate minerals (Poitrasson et al., 2009; Hin et al., 2010). (3) *Crust formation*: It has been widely observed that iron isotopes could be fractionated during various magmatic differentiation processes of the terrestrial crust, such as partial melting, mineral fractionation and fluids exsolution (Williams et al., 2004; Poitrasson and Freydier, 2005; Weyer and Ionov, 2007; Teng et al., 2008; Schuessler et al., 2009). Island arc basalts also show iron isotope fractionation that may be related to the degree of partial melting (Dauphas et al., 2009a). During partial melting, Fe(III) is more incompatible in olivine and pyroxene than Fe(II) is. Both theoretical calculations and experimental determinations show that Fe(III)-bearing phases tend to be enriched in the heavy isotopes of iron compared to Fe(II)-bearing phases (Polyakov and Mineev, 2000; Schauble et al., 2001; Schuessler et al., 2007; Shahar et al., 2008). Such equilibrium isotope fractionation between Fe(III) and Fe(II) may

explain, at least in part, the heavy iron isotope composition of MORBs and OIBs relative to that of chondrites and other planetary basalts (Dauphas et al., 2009a). Indeed, terrestrial basalts are formed under more oxidizing conditions than martian meteorites or HEDs (McCammon, 2005; Wadhwa, 2008).

Achondrites are samples from differentiated planetary bodies formed under a variety of conditions. Here, we report high-precision iron isotope compositions of several classes of achondrites from at least four different parent bodies, including a lunar meteorite, martian meteorites, Howardite-Eucrite-Diogenite meteorites (HEDs) and angrites, and discuss the implications regarding the conditions relevant to the differentiation of the parent-bodies of these meteorites.

5.2. Samples and Method

5.2.1. Sample Descriptions

All samples, their classifications and weathering conditions (if available) are listed in Table 5-1. Well-characterized terrestrial geostandards were analyzed to assess the quality of the measurements and to provide a basis for inter-laboratory comparisons. BCR-2 is a continental flood basalt from the Columbia River, Oregon. BIR-1 is a basalt from Iceland. BHVO-2 is a Hawaiian lava basalt. AGV-1 and 2 are andesites from the Guano Valley, Oregon. GSP-1 is a granodiorite from Silver Plume, Colorado. AC-E is a granite from Ailsa Craig Island, Scotland. In addition, three modern island arc basalts (IABs) from New Britain (NMNH 116852-1, 116852-3 and 116852-11) were also analyzed here to test the accuracy of the measurements (see Dauphas et al., 2009a for a detailed discussion about IABs).

Lunar highland meteorite, MAC88105, is a polymict breccia. It is dominated by ferroan anorthosite lithology and contains small low-Ti basaltic clasts (Jolliff et al., 1991; Neal et al., 1991). The bulk composition of this lunar highland meteorite is different from those of highland rocks sampled by Apollo project (Koeberl et al., 1991; Lindstrom et al., 1991) and might represent a different feldspathic highlands terrane (Warren et al., 1989). Orbital remote sensing composition data shows that lunar highland meteorites are reasonably representative of lunar surface (Korotev et al., 2003).

The martian meteorites studied include eight shergottites, two nakhlites and ALH84001. Shergottites are basaltic or lherzolitic rocks. Basaltic shergottites (*e.g.*, Zagami, EETA79001) mainly consist of clinopyroxene and plagioclase (Mittlefehldt et al., 1998). Lherzolitic shergottites (*e.g.*, ALHA77005) are cumulates, consisting of magnesian olivine, clinopyroxene

and chromite (Mittlefehldt et al., 1998). Nakhlites are clinopyroxenites made of augite and a small amount of olivine (Mittlefehldt et al., 1998). ALH84001 is a cumulate orthopyroxenite.

The HED meteorites reported in this study include twenty eucrites, three howardites and nine diogenites. Based on spectroscopic observations, HED meteorites are generally recognized as being derived from asteroid 4-Vesta (McCord et al., 1970; Drake, 2001). Diogenites are orthopyroxenites, consisting chiefly of ~90 vol% coarse-grained orthopyroxene, and accessory minerals including olivine, chromite, troilite, and metal (Mittlefehldt et al., 1998). Eucrites are basalts (non-cumulates) or cumulate gabbros. Basaltic eucrites contain pigeonite, plagioclase and a minor amount of silica, ilmenite and chromite (Duke and Silver, 1967). Basaltic eucrites can be subdivided based on geochemical characteristics: “Main Group” (MG), “Nuevo Laredo Trend” (NL), and “Stannern Trend” (ST) (Stolper, 1977; Reid and Barnard, 1979; Yamaguchi et al., 2009). These three groups are very similar in major element compositions, however they are different in trace element abundances. The Stannern Trend shows a significant increase in incompatible trace elements without changes in Mg# compared to the Main Group; while the Nuevo Laredo Trend shows a slight increase in incompatible trace elements and a decrease in Mg# compared to the Main Group. Cumulate eucrites have mineral assemblages similar to basaltic eucrites, but they display cumulate textures and their pyroxenes are Mg-rich. Howardites are polymict breccias and are mixtures primarily of diogenite and eucrite clasts. In addition, we have analyzed Pasamonte and NWA 1240, two ungrouped eucrites recently found to have oxygen isotope compositions distinct from all other HEDs (Scott et al., 2009). Pasamonte is a polymict breccia that displays highly unequilibrated basaltic clasts (Takeda et al., 1978), and possibly records fluid-rock interactions (Schwartz and McCallum, 2005). NWA 1240 is an unbreciated stone, with unique features. It displays a porphyritic texture consisting of skeletal

hollow low-Ca pyroxene phenocrysts set in a variolitic (fan-spherulitic) mesostasis of fine elongate pyroxene and plagioclase crystals. Pyroxenes are highly unequilibrated and their compositions range from En₇₆ to En_{0.6}. Although its texture indicates a rock formed from a rapidly-cooled melt, its composition is more akin to cumulate eucrites and led Barrat et al. (2003) to propose an impact-melt origin. Nevertheless, these ungrouped eucrites are probably not from asteroid 4-Vesta, but from Vesta-like asteroid parent-bodies (Scott et al., 2009).

Angrites are among the oldest basaltic rocks in the Solar System (Baker et al., 2005; Nyquist et al., 2009; Dauphas and Chaussidon, 2011). Only nineteen angrites are recognized. Eight representative ones were analyzed here: D'Orbigny, NWA1296 and Sahara99555 consist of mainly Al-Ti-diopside-hedenbergite, Ca-rich olivine, anorthite and spinel olivine; they are also similar in bulk chemistry (Jambon et al., 2005); LEW86010 consists of ~58 vol% Al-Ti-diopside-hedenbergite, 21 vol% plagioclase, 20 vol% olivine and minor amount of spinel, troilite, and Fe-Ni metal (Prinz et al., 1988); NWA1670 consists of large olivine xenocrysts, and fine-grained groundmass with pyroxene, anorthite and olivine (Jambon et al., 2008); NWA4801 is composed of Al-Ti-diopside-hedenbergite and pure anorthite (Irving and Kuehner, 2007); NWA2999 contains 64 vol% Ca-rich olivine, 23 vol% Al-Ti-diopside-hedenbergite, 4 vol% spinel, 1 vol% plagioclase and 8 vol% metal (Kuehner et al., 2006); NWA6291 is the most recently found angrite and is possibly paired with NWA2999 (Bouvier et al., 2011).

5.2.2. Analytical Methods

Several hundred milligrams of meteorite was crushed in an agate mortar to ensure representative sampling. Between 5 and 10 mg of crushed material was fully digested by sequential mixtures of HF-HNO₃ and HNO₃-HCl. Iron in the dissolved samples was then purified

using anion-exchange chromatography (see Table 5-2 for the detailed procedure; Strelow, 1980; Dauphas et al., 2004; Dauphas et al., 2009b). The purification was repeated twice, thus ensuring the removal of all the matrix elements. Most separation chemistries were carried out in the clean laboratory at Washington University in St. Louis (WUSTL) and supplemented by chemistries for selected samples at the University of Chicago (UofC) to confirm inter-laboratory concordance and reproducibility. Most iron isotope analyses were performed with a Thermo Scientific Neptune MC-ICP-MS at the UofC and some were done with a Thermo Scientific Neptune Plus MC-ICP-MS at WUSTL, both following identical protocol described in Dauphas et al. (2009b).

In order to further confirm the validity of the iron separation technique used in this study (marked as “routine” chemistry), two other Fe separation techniques were applied to selected samples (marked as “long” and “UTEVA” chemistry in Table 5-2). The “long” column method uses long Teflon columns (10.5 cm) filled with 3 ml AG1-X8 anion-exchange resin (Dauphas et al., 2009b; Craddock and Dauphas, 2011). The “UTEVA” column method uses pre-packaged 1 mL Eichrom UTEVA resin cartridges (Horwitz et al., 1992; Tissot and Dauphas, 2011). All samples measured following purification by the three chemistry protocols yield identical iron isotope compositions within analytical uncertainty (Figure 5-1; Table 5-1).

All data are reported in $\delta^{56}\text{Fe}$ and $\delta^{57}\text{Fe}$ notations relative to the isotopic reference IRMM-014, defined as:

$$\delta^x\text{Fe} = \left[\frac{(^x\text{Fe}/^{54}\text{Fe})_{sample}}{(^x\text{Fe}/^{54}\text{Fe})_{IRMM-014}} - 1 \right] \times 1000 \quad \text{Eq. 5-1}$$

where $x = 56$ or 57 . In a three-isotope plot ($\delta^{56}\text{Fe}$ vs. $\delta^{57}\text{Fe}$), all samples define a straight line of slope 1.48 (Figure 5-2), consistent with mass-dependent isotope fractionation. Note that

during measurements, IRMM-524a was used as bracketing standard because it has identical isotope composition to IRMM-014 and it is more readily available. The analytical uncertainties reported here for each sample are 95 % confidence intervals (see Dauphas et al., 2009b for a detailed account on how error bars are calculated). Weighted averages and uncertainties are calculated for replicate analyses of meteorites using the following two equations:

$$\bar{x} = \frac{\sum_{i=1}^n (x_i / e_i^2)}{\sum_{i=1}^n (1/e_i^2)}$$
Eq. 5-2

$$\sigma^2 = \frac{1}{\sum_{i=1}^n (1/e_i^2)}$$
Eq. 5-3

where e_i is the standard deviation for each independent analysis. The uncertainties of previously published $\delta^{56}\text{Fe}$ data cited in this paper are typically 2 standard deviation (2SD) or 2 standard error (2SE). Caution should be taken when comparing these weighted average uncertainties to the 2SD or 2SE in previous studies because in most instances, accuracy of the measurements has not been tested below $\pm 0.03\text{‰}$.

Table 5-1. Iron isotope compositions of Earth/Moon rocks and martian, HED and angrite meteorites

Sample	Type	Fall/find (weathering)	Chemistry	Fe wt.%	$\delta^{56}Fe$	95 % c.i. ^a	$\delta^{57}Fe$	95 % c.i. ^a	n
Earth/Moon									
AGV-1 #1	Andesite	Routine ^b		0.081	0.034	0.133	0.049	8	
AGV-1 #2	Andesite	Routine ^b		0.077	0.045	0.105	0.058	8	
AGV-1 #3	Andesite	Routine ^b		0.081	0.046	0.134	0.066	9	
AGV-1 #4	Andesite	Routine ^c		0.106	0.031	0.157	0.039	11	
AGV-1 (average)				0.089	0.019	0.138	0.025		
AGV-2 #1	Andesite	Routine ^b	4.6	0.094	0.038	0.137	0.057	9	
AGV-2 #2	Andesite	Routine ^b		0.083	0.035	0.094	0.057	8	
AGV-2 #3	Andesite	Routine ^c		0.100	0.031	0.167	0.040	10	
AGV-2 (average)				0.093	0.020	0.141	0.028		
BCR-2 #1	Basalt	Routine ^b	11.0	0.063	0.032	0.080	0.046	9	
BCR-2 #2	Basalt	Routine ^b	11.0	0.052	0.033	0.110	0.058	9	
BCR-2 #3	Basalt	Routine ^c		0.089	0.031	0.110	0.039	11	
BCR-2 (average)				0.069	0.018	0.100	0.026		
BHVO-2 #1	Basalt	Routine ^c		0.116	0.038	0.164	0.057	4	
BHVO-2 #2-1	Basalt	Routine ^d	6.3	0.099	0.030	0.155	0.044	9	
BHVO-2 #2-2	Basalt	Long ^d	7.9	0.096	0.030	0.160	0.053	9	
BHVO-2 #2-3	Basalt	UTEVA ^d	8.7	0.101	0.030	0.166	0.044	9	
BHVO-2 #3-1 (+V+Cr) ^j	Basalt	Routine ^d	6.7	0.108	0.030	0.161	0.044	9	
BHVO-2 #3-2 (+V+Cr) ^j	Basalt	Long ^d	8.5	0.098	0.030	0.154	0.044	9	
BHVO-2 #3-3 (+V+Cr) ^j	Basalt	UTEVA ^d	9.0	0.098	0.030	0.154	0.044	9	
BHVO-2 (average)				0.102	0.012	0.159	0.018		
BIR-1 #1	Basalt	Routine ^b		0.044	0.030	0.070	0.049	9	
BIR-1 #2	Basalt	Routine ^b	7.7	0.038	0.038	0.047	0.075	8	
BIR-1 #3	Basalt	Routine ^b	7.7	0.020	0.032	0.019	0.059	8	
BIR-1 #4	Basalt	Routine ^c		0.068	0.031	0.070	0.040	10	
BIR-1 (average)				0.043	0.016	0.058	0.026		
NMNH 116852-1 #1-1	Basalt	Routine ^d	3.7	-0.148	0.035	-0.223	0.050	9	
NMNH 116852-1 #1-2	Basalt	UTEVA ^d	6.4	-0.081	0.035	-0.134	0.050	9	
NMNH 116852-1 (average)				-0.115	0.025	-0.179	0.035		
NMNH 116852-3 #1-1	Basalt	Routine ^d	5.6	0.061	0.027	0.096	0.042	9	
NMNH 116852-3 #1-2	Basalt	Long ^d	7.6	0.062	0.027	0.088	0.042	9	
NMNH 116852-3 #1-3	Basalt	UTEVA ^d	7.7	0.052	0.027	0.094	0.042	9	

NMNH 116852-3 (average)					0.058	0.016	0.093	0.024	
NMNH 116852-11 #1-1	Basalt		Routine ^d	5.5	0.134	0.027	0.190	0.035	9
NMNH 116852-11 #1-2	Basalt		Long ^d	7.1	0.133	0.027	0.200	0.035	9
NMNH 116852-11 #1-3	Basalt		UTEVA ^d	7.3	0.121	0.027	0.169	0.035	9
NMNH 116852-11 (average)					0.129	0.016	0.186	0.020	
GSP-1 #1	Granodiorite		Routine ^b		0.126	0.038	0.174	0.057	9
GSP-1 #2	Granodiorite		Routine ^b		0.141	0.046	0.204	0.066	9
GSP-1 #3	Granodiorite		Routine ^c		0.156	0.031	0.170	0.040	10
GSP-1 (average)					0.143	0.021	0.178	0.029	
AC-E #1-1	Granite		Routine ^d	1.2	0.314	0.030	0.452	0.044	9
AC-E #1-2	Granite		Long ^d	1.6	0.330	0.033	0.480	0.063	9
AC-E #1-3	Granite		UTEVA ^d	1.7	0.298	0.030	0.452	0.044	9
AC-E (average)					0.313	0.018	0.457	0.028	
MAC88105	Lunar meteorite	Find (A/Be) ⁱ	Routine ^b	3.4 ^h	0.086	0.034	0.132	0.049	8

Martian Meteorites

ALHA77005	Shergottite	Find (A) ⁱ	Routine ^b	15.6 ^h	-0.008	0.033	-0.026	0.058	9
EETA79001	Shergottite	Find (A/Ae) ⁱ	Routine ^b	14.3 ^h	-0.003	0.038	-0.038	0.075	8
Los Angeles	Shergottite	Find	Routine ^b	16.6 ^h	0.008	0.032	0.010	0.046	9
NWA1669	Shergottite	Find	Routine ^b		-0.016	0.032	-0.030	0.046	9
NWA1950	Shergottite	Find	Routine ^b	16.8 ^h	0.010	0.032	0.023	0.046	9
NWA5029	Shergottite	Find	Routine ^b		0.016	0.032	0.012	0.046	9
SaU008	Shergottite	Find	Routine ^b		-0.023	0.038	-0.042	0.075	8
Zagami	Shergottite	Fall	Routine ^b	16.0	0.016	0.031	0.064	0.055	9
		<i>Wt. Ave. of Shergottite</i>			<i>0.001</i>	<i>0.012</i>	<i>0.002</i>	<i>0.019</i>	
Mil03346	Nakhelite	Find (B) ⁱ	Routine ^b	14.8 ^h	0.025	0.032	0.027	0.046	9
Nakhla	Nakhelite	Fall	Routine ^b	16.0 ^h	0.031	0.032	0.033	0.046	9
		<i>Wt. Ave. of Nakhelite</i>			<i>0.028</i>	<i>0.023</i>	<i>0.030</i>	<i>0.033</i>	
ALH84001	Orthopyroxenite	Find (A/B) ⁱ	Routine ^b	13.6 ^h	-0.033	0.032	-0.034	0.046	9

		<i>Wt. Ave. of Mars</i>				0.003	0.010	0.004	0.015
HED									
ALHA77256	Diogenite	Find (A/B) ⁱ	Routine ^c	14.2 ^h	-0.008	0.034	0.013	0.049	6
GRO95555	Diogenite	Find (A/B) ⁱ	Routine ^b	12.7 ^h	0.019	0.034	0.042	0.049	8
MET00424	Diogenite	Find (B) ⁱ	Routine ^c	15.8 ^h	-0.034	0.034	-0.074	0.049	6
MET00436	Diogenite	Find (B/C) ⁱ	Routine ^c	16.5 ^h	-0.032	0.032	-0.077	0.045	8
Mil07001	Diogenite	Find (A/B) ⁱ	Routine ^c		-0.017	0.032	-0.036	0.045	8
NWA1461	Diogenite	Find	Routine ^c	7.5 ^h	0.027	0.038	0.009	0.057	4
NWA5480	Diogenite	Find	Routine ^b		0.015	0.034	0.040	0.049	8
Shalka	Diogenite	Fall	Routine ^c	12.7 ^h	-0.011	0.038	-0.034	0.057	4
Tatahouine	Diogenite	Fall	Routine ^b	9.0	0.013	0.030	0.036	0.049	9
	<i>Wt. Ave. of Diogenite</i>				-0.004	0.011	-0.011	0.016	
Frankfort	Howardite	Fall	Routine ^b	12.4	-0.002	0.038	-0.015	0.057	9
Kapoeta	Howardite	Fall	Routine ^b	8.7	0.026	0.030	0.042	0.049	9
Petersburg	Howardite/polymict eucrite	Fall	Routine ^b	8.3	0.035	0.038	0.056	0.057	9
	<i>Wt. Ave. of Howardite</i>				0.021	0.020	0.029	0.031	
NWA1240	Eucrite (Ungrouped)	Find	Routine ^d	15.7 ^h	0.016	0.031	-0.026	0.043	6
Pasamonte	Eucrite (Ungrouped)	Fall	Routine ^b	11.5	0.019	0.030	0.063	0.045	8
EET87548 #1	Eucrite (Cumulate)	Find (B/C) ⁱ	Routine ^d	15.1	-0.023	0.034	-0.029	0.051	9
EET87548 #2	Eucrite (Cumulate)	Find (B/C) ⁱ	Routine ^b	15.4	-0.017	0.034	-0.030	0.049	8
EET87548 #3	Eucrite (Cumulate)	Find (B/C) ⁱ	Routine ^d		-0.014	0.030	-0.024	0.059	9
EET87548 (average)					-0.018	0.019	-0.028	0.030	
Moore County #1	Eucrite (Cumulate)	Fall	Routine ^b		-0.004	0.038	-0.008	0.057	9

Moore County #2	Eucrite (Cumulate)	Fall	Routine ^b	7.4	0.010	0.030	0.040	0.049	9
Moore County (average)					0.005	0.024	0.020	0.037	
Serra de Magé #1	Eucrite (Cumulate)	Fall	Routine ^d	12.3	0.001	0.034	0.026	0.051	9
Serra de Magé #2-1	Eucrite (Cumulate)	Fall	Routine ^d	12.0	0.017	0.028	0.025	0.039	9
Serra de Magé #2-2	Eucrite (Cumulate)	Fall	Long ^d	16.1	0.019	0.028	0.032	0.039	9
Serra de Magé #2-3	Eucrite (Cumulate)	Fall	UTEVA ^d	16.6	0.006	0.028	0.009	0.039	9
Serra de Magé (average)					0.012	0.015	0.023	0.021	
	<i>Wt. Ave. of Eucrite (Cumulate)</i>				0.001	0.010	0.009	0.015	
Cachari	Eucrite (MG) ^e	Find	Routine ^b	15.9 ^h	0.002	0.030	0.011	0.045	8
Camel Donga	Eucrite (MG) ^e	Find	Routine ^d	15.3	0.019	0.034	0.034	0.051	9
Jonzac #1	Eucrite (MG) ^e	Fall	Routine ^b	15.0	0.025	0.035	0.031	0.057	8
Jonzac #2	Eucrite (MG) ^e	Fall	Routine ^b	11.5	0.007	0.034	0.051	0.049	8
Jonzac #3-1	Eucrite (MG) ^e	Fall	Routine ^d	9.8	0.008	0.032	0.028	0.045	9
Jonzac #3-2	Eucrite (MG) ^e	Fall	Long ^d	14.8	-0.006	0.032	-0.007	0.045	9
Jonzac #3-3	Eucrite (MG) ^e	Fall	UTEVA ^d	14.6	0.010	0.032	0.035	0.045	9
Jonzac (average)					0.008	0.015	0.026	0.021	
Juvinas #1	Eucrite (MG) ^e	Fall	Routine ^b		0.015	0.038	0.035	0.057	9
Juvinas #2-1	Eucrite (MG) ^e	Fall	Routine ^d	9.9	-0.025	0.028	-0.019	0.040	9
Juvinas #2-2	Eucrite (MG) ^e	Fall	Long ^d	14.0	-0.022	0.028	-0.024	0.040	9
Juvinas #2-3	Eucrite (MG) ^e	Fall	UTEVA ^d	13.6	-0.017	0.028	-0.021	0.040	9
Juvinas #3-1	Eucrite (MG) ^e	Fall	Routine ^d	9.9	-0.026	0.035	-0.038	0.050	9
Juvinas #3-2	Eucrite (MG) ^e	Fall	Long ^d	14.0	-0.023	0.035	-0.036	0.050	9
Juvinas #3-3	Eucrite (MG) ^e	Fall	UTEVA ^d	13.6	-0.037	0.035	-0.059	0.050	9
Juvinas (average)					-0.020	0.012	-0.024	0.017	
NWA049	Eucrite (MG) ^e	Find	Routine ^b	15.4 ^h	0.023	0.029	0.033	0.047	9
	<i>Wt. Ave. of Eucrite (MG)^e</i>				-0.004	0.008	0.001	0.012	
Agoult	Eucrite (Residual)	Find	Routine ^b	15.2 ^h	0.033	0.034	0.039	0.049	8
Dag945	Eucrite (Residual)	Find (W1) ⁱ	Routine ^c	15.6 ^h	0.028	0.036	0.037	0.052	5

		<i>Wt. Ave. of Eucrite (Residual)</i>				0.031	0.025	0.038	0.036
Nuevo Laredo	Eucrite (NL) ^f	Find	Routine ^c	16.2 ^h	0.031	0.036	0.056	0.052	5
Sahara02501	Eucrite (NL) ^f	Find	Routine ^c	16.3	0.037	0.029	0.053	0.049	8
	<i>Wt. Ave. of Eucrite (NL)^f</i>				0.035	0.023	0.054	0.036	
Bouvante #1	Eucrite (ST) ^g	Find	Routine ^d	15.1	0.049	0.034	0.096	0.051	9
Bouvante #2-1	Eucrite (ST) ^g	Find	Routine ^d	10.7	0.032	0.028	0.036	0.036	9
Bouvante #2-2	Eucrite (ST) ^g	Find	Long ^d	16.6	0.038	0.028	0.054	0.036	9
Bouvante #2-3	Eucrite (ST) ^g	Find	UTEVA ^d	15.9	0.026	0.028	0.054	0.036	9
Bouvante (average)					0.035	0.015	0.055	0.019	
NWA2061	Eucrite (ST) ^g	Find	Routine ^b	14.4	0.018	0.029	0.031	0.047	9
NWA4523 #1	Eucrite (ST) ^g	Find	Routine ^b	13.3 ^h	0.077	0.034	0.118	0.049	8
NWA4523 #2	Eucrite (ST) ^g	Find	Routine ^d		0.071	0.034	0.097	0.051	9
NWA4523 #3-1	Eucrite (ST) ^g	Find	Routine ^d		0.056	0.027	0.071	0.039	9
NWA4523 #3-2	Eucrite (ST) ^g	Find	Long ^d		0.052	0.027	0.095	0.039	9
NWA4523 #3-3	Eucrite (ST) ^g	Find	UTEVA ^d		0.060	0.027	0.095	0.039	9
NWA4523 (average)					0.061	0.013	0.093	0.019	
Pomozdino	Eucrite (ST) ^g	Find	Routine ^d	15.2	0.034	0.034	0.060	0.051	9
Stannern #1	Eucrite (ST) ^g	Fall	Routine ^b	14.2	0.072	0.035	0.095	0.057	8
Stannern #2	Eucrite (ST) ^g	Fall	Routine ^d	13.7	0.036	0.045	0.079	0.065	9
Stannern #3	Eucrite (ST) ^g	Fall	Routine ^d		0.049	0.045	0.102	0.065	9
Stannern #4	Eucrite (ST) ^g	Fall	Routine ^d	14.5	0.053	0.045	0.071	0.065	9
Stannern #5-1	Eucrite (ST) ^g	Fall	Routine ^d	12.0	0.047	0.026	0.078	0.032	9
Stannern #5-2	Eucrite (ST) ^g	Fall	Long ^d	12.5	0.035	0.026	0.073	0.032	9
Stannern #5-3	Eucrite (ST) ^g	Fall	UTEVA ^d	15.6	0.037	0.026	0.059	0.032	9
Stannern (average)					0.045	0.012	0.074	0.016	
Yamato75011	Eucrite (ST) ^g	Find (A) ⁱ	Routine ^b	15.2	0.043	0.029	0.092	0.047	9
	<i>Wt. Ave. of Eucrite (ST)^g</i>				0.045	0.007	0.073	0.010	
Angrite									
D'Orbigny	Angrite	Find	Routine ^d	19.2 ^h	0.139	0.030	0.193	0.062	9
LEW86010	Angrite	Find(A/B) ⁱ	Routine ^b	14.2 ^h	0.139	0.043	0.179	0.059	9

NWA1670 #1	Angrite	Find	Routine ^b	14.4 ^h	0.167	0.033	0.253	0.058	9
NWA1670 #2	Angrite	Find	Routine ^d		0.125	0.036	0.210	0.058	9
NWA1670 #3-1	Angrite	Find	Routine ^d		0.148	0.030	0.225	0.038	9
NWA1670 #3-2	Angrite	Find	Long ^d		0.113	0.030	0.172	0.038	9
NWA1670 #3-3	Angrite	Find	UTEVA ^d		0.154	0.030	0.223	0.038	9
NWA1670 (average)					0.142	0.014	0.212	0.019	
NWA1296	Angrite	Find	Routine ^b	19.4 ^h	0.104	0.033	0.185	0.058	9
NWA6291	Angrite	Find	Routine ^d		0.052	0.030	0.116	0.062	9
NWA2999	Angrite	Find	Routine ^d	24.2 ^h	0.124	0.030	0.183	0.062	9
NWA4801	Angrite	Find	Routine ^d		0.135	0.030	0.219	0.062	9
Sahara99555 #1	Angrite	Find	Routine ^d	18.0 ^h	0.116	0.040	0.165	0.081	9
Sahara99555 #2	Angrite	Find	Routine ^b		0.107	0.033	0.136	0.058	9
Sahara99555 #3	Angrite	Find	Routine ^d		0.110	0.030	0.141	0.062	9
Sahara99555 (average)					0.110	0.019	0.144	0.038	
<i>Wt. Ave. of Angrite</i>					0.123	0.009	0.192	0.014	

^a Uncertainties are 95 % confidence intervals (see Dauphas et al., 2009b for details).

^b Samples chemically prepared at the Washington University in St. Louis and measured at the University of Chicago.

^c Samples both chemically prepared and measured at Washington University in St. Louis.

^d Samples both chemically prepared and measured at the University of Chicago.

^e Eucrite (MG)=Eucrite main group.

^f Eucrite (NL)=Eucrite Nuevo Laredo trend.

^g Eucrite (ST)=Eucrite Stannern trend.

^h Reference data: MAC88105 (Jarosewich, 1990); NWA1950 (Gillet et al., 2005); Los Angeles (Warren et al., 2000); EETA79001, ALHA77005, Nakhla, ALH84001 (Lodders, 1998); Mil03346 (Day et al., 2006); GRO95555, MET00436, MET00424 (Barrat et al., 2008); NWA1461 (Warren et al., 2009); Shalaka (McCarthy et al., 1972); ALHA77256 (Sack et al., 1991); NWA1240, NWA049 (Barrat et al., 2003); Cachari (Barrat et al., 2000); Agoult, Dag945 (Yamaguchi et al., 2009); Nuevo Laredo, NWA4523 (Barrat et al., 2007b); D'Orbigny, Sahara99555 (Mittlefehldt et al., 2002); LEW86010 (McKay et al., 1988); NWA1670 (Jambon et al., 2008); NWA1296 (Jambon et al., 2005); NWA2999 (Gellissen et al., 2007).

ⁱ Weathering conditions are from MetBase (version 7.1). Weathering index A, B or C represents “minor”, “moderate” or “severe” rustiness, respectively. Letter “e” represents evaporite minerals visible. Weathering grade W0 (fresh) to W6 (most weathered) is also shown if available.

^j These samples have been added V and Cr to double-check the purification of iron during chemistry.

Table 5-2. Comparison of the three iron purification chromatography protocols used in this study

	<i>Routine column</i>	<i>Long column</i>	<i>UTEVA column</i>
Column	Disposable Bio-Rad Poly Prep Polyethylene column (9 cm length)	Reusable Savillex PFA column (10.5 cm length, 0.62 cm diameter)	Pre-packaged Eichrom U/Teva cartridges
Resin	1 mL AG1-X8 200-400 mesh anion-exchange resin	3 mL AG1-X8 200-400 mesh anion-exchange resin	1 mL Eichrom U/Teva resin
Conditioning	10 mL 6 M HCl	4 mL 10 M HCl	6 mL 4 M HCl
Matrix Elution	8 mL 6 M HCl (0.5 + 0.5 + 1 + 2 + 4 mL increments)	5 mL 10 M HCl (0.5 + 0.5 + 1 + 3 mL increments)	25 mL 4M HCl (0.5 + 0.5 + 1 + 5 + 8 + 10 mL increments) 22 mL 4 M HCl (0.5 + 0.5 + 1 + 5 + 5 + 10 mL increments)
Iron Collecting	9 mL 0.4 M HCl (0.5 + 0.5 + 1 + 3 + 4 mL increments)	8 mL 0.4 M HCl (0.5 + 0.5 + 1 + 2 + 4 mL increments)	12 mL 0.4 M HCl (0.5 + 0.5 + 1 + 5 + 5 mL increments)

5.3. Results

Our iron isotope data are reported in Table 5-1, and illustrated in Figures 5-2 and 5-3.

The iron isotope compositions are compared to those of chondrites and terrestrial basalts, for which ten carbonaceous chondrites define an average $\delta^{56}\text{Fe}$ value of -0.010 ‰ and Earth basalts define an average value of $\sim+0.1\text{ ‰}$ relative to IRMM-014 (Craddock and Dauphas, 2011).

5.3.1. Earth and Moon

The terrestrial geostandards measured here (BIR-1, BCR-2, BHVO-2, AGV-1, AGV-2, GSP-1 and AC-E) give iron isotope compositions that are consistent with previous reports (see Craddock and Dauphas, 2011 for a data compilation). The composition of BCR-2 measured here is slightly lighter than that reported by Craddock and Dauphas (2011). Three modern island arc basalts (IABs) treated with different techniques (routine, long and UTEVA chemistries) also agree with the data in a previous study (Dauphas et al., 2009a).

The iron isotope composition of the lunar highland meteorite MAC88105 is $\delta^{56}\text{Fe} = +0.09 \pm 0.03\text{ ‰}$, which is consistent with previously reported Apollo lunar highland rocks (Poitrasson et al., 2004; Weyer et al., 2005). Other lunar lithologies have variable iron isotope compositions that encompass this value, from $\delta^{56}\text{Fe} = +0.03\text{ ‰}$ for low-Ti mare basalts (Weyer et al., 2005) to $+0.27\text{ ‰}$ for high-Ti mare basalts (Moynier et al., 2006). The formation of these highly fractionated iron isotope compositions in lunar samples has been discussed in several recent papers (Poitrasson et al., 2004; Weyer et al., 2005; Poitrasson, 2007; Weyer et al., 2007; Liu et al., 2010), and will not be further addressed here.

5.3.2. Martian meteorites

The eight shergottites studied have uniform $\delta^{56}\text{Fe}$ equal to $0.00 \pm 0.01\text{‰}$. These new and more precise data are in agreement with previous reports (average $+0.01\text{‰}$; Poitrasson et al., 2004; Weyer et al., 2005; Anand et al., 2006), and confirm that shergottites have an iron isotope composition identical to chondrites. The $\delta^{56}\text{Fe}$ of two nakhlites ($+0.03 \pm 0.02\text{‰}$) and ALH84001 ($-0.03 \pm 0.03\text{‰}$) are also very similar to shergottites (within analytical precision). A close look at the data hints at the presence of possibly different iron isotope compositions among different groups of martian meteorites. However, these differences are at the limits of current analytical precision.

5.3.3. HED Meteorites

Our new data confirm the findings of previous reports that most eucrites (cumulate eucrites, Main Group, Nuevo Laredo trend and residual eucrites) have a chondritic iron isotope composition (average $\delta^{56}\text{Fe} = 0.00 \pm 0.01\text{‰}$). However, it is significant that Stannern trend (ST) eucrites (average $\delta^{56}\text{Fe} = +0.05 \pm 0.01\text{‰}$) are isotopically heavier than other eucrites. Our results for six individual ST eucrites are more precise than the four previous measurements, which were limited to two different ST eucrites samples: Stannern ($\delta^{56}\text{Fe} = 0.00 \pm 0.05\text{‰}$, Schoenberg and von Blanckenburg 2006; $+0.01 \pm 0.02\text{‰}$, Weyer et al. 2005; $-0.06 \pm 0.06\text{‰}$, Zhu et al. 2001) and Bouvante ($\delta^{56}\text{Fe} = +0.03 \pm 0.04\text{‰}$, Weyer et al. 2005; $+0.03 \pm 0.05$, Poitrasson et al. 2004). To confirm the heavier iron isotope composition of ST eucrites measured, we independently processes and analyzed the same splits at UofC using three independent chemistry methods (Table 5-2). All these replicated measurements of ST eucrites show consistent results (Figure 5-1; Table 5-1). ST eucrites are enriched in heavy iron isotopes compared to other classes of

eucrites. Ungrouped eucrites, Pasamonte ($+0.02 \pm 0.03 \text{ ‰}$) and NWA1240 ($+0.02 \pm 0.03 \text{ ‰}$), have iron isotope compositions identical to other eucrites. Three howardites (average $\delta^{56}\text{Fe} = +0.02 \pm 0.02 \text{ ‰}$) and nine diogenites ($0.00 \pm 0.01 \text{ ‰}$) are isotopically identical to all classes of eucrites, excluding ST. Hence, iron isotopes, unlike oxygen isotopes, cannot distinguish ungrouped eucrites from other HEDs.

5.3.4. Angrites

The eight samples of angrites (average $\delta^{56}\text{Fe} = +0.12 \pm 0.01 \text{ ‰}$) are isotopically heavier than chondrites, but similar to terrestrial basalts. To ensure that these data were correct, we again processed samples independently at WUSTL and UofC using three chemistry methods. All replicate measurements of the same samples processed by different methods gave the same iron isotope compositions within analytical uncertainty (Table 5-1; Figure 5-1) and confirm that angrites have heavy fractionated iron isotope compositions.

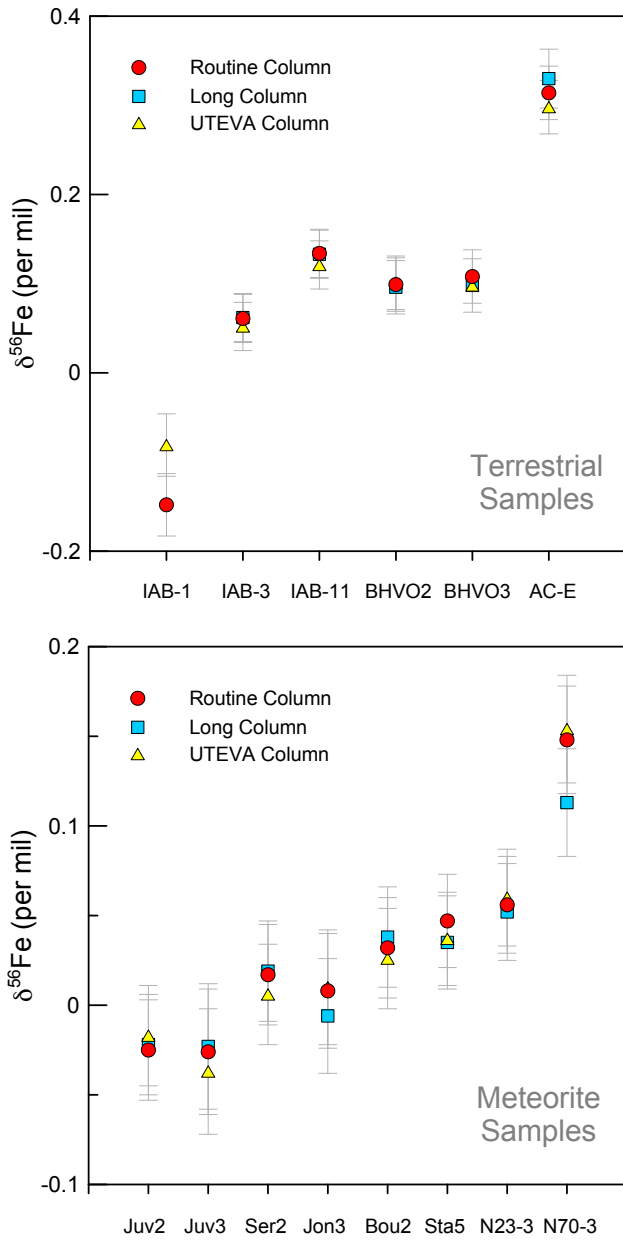


Figure 5-1. Iron isotope results of the samples that were purified independently by three different purification chemistries, namely “Routine Columns”, “Long Columns” and “UTEVA Columns”. For a detailed description of these purification chemistry protocols, please see Table 5-2 and text. Top panel: terrestrial samples. IAB-1=NMNH 116852-1, IAB-3=NMNH 116852-3, IAB-11=NMNH 116852-11, BHVO2=BHVO-2 #2, BHVO3=BHVO-2 #3, AC-E= AC-E #1. Bottom panel: meteorite samples. Juv2=Juvinas #2, Juv3=Juvinas #3, Ser2=Serra de Magé #2, Jon3=Jonzac #3, Bou2=Bouvante #2, Sta5=Stannern #5, N23-3=NWA4523 #3, N70-3=NWA1670 #3.

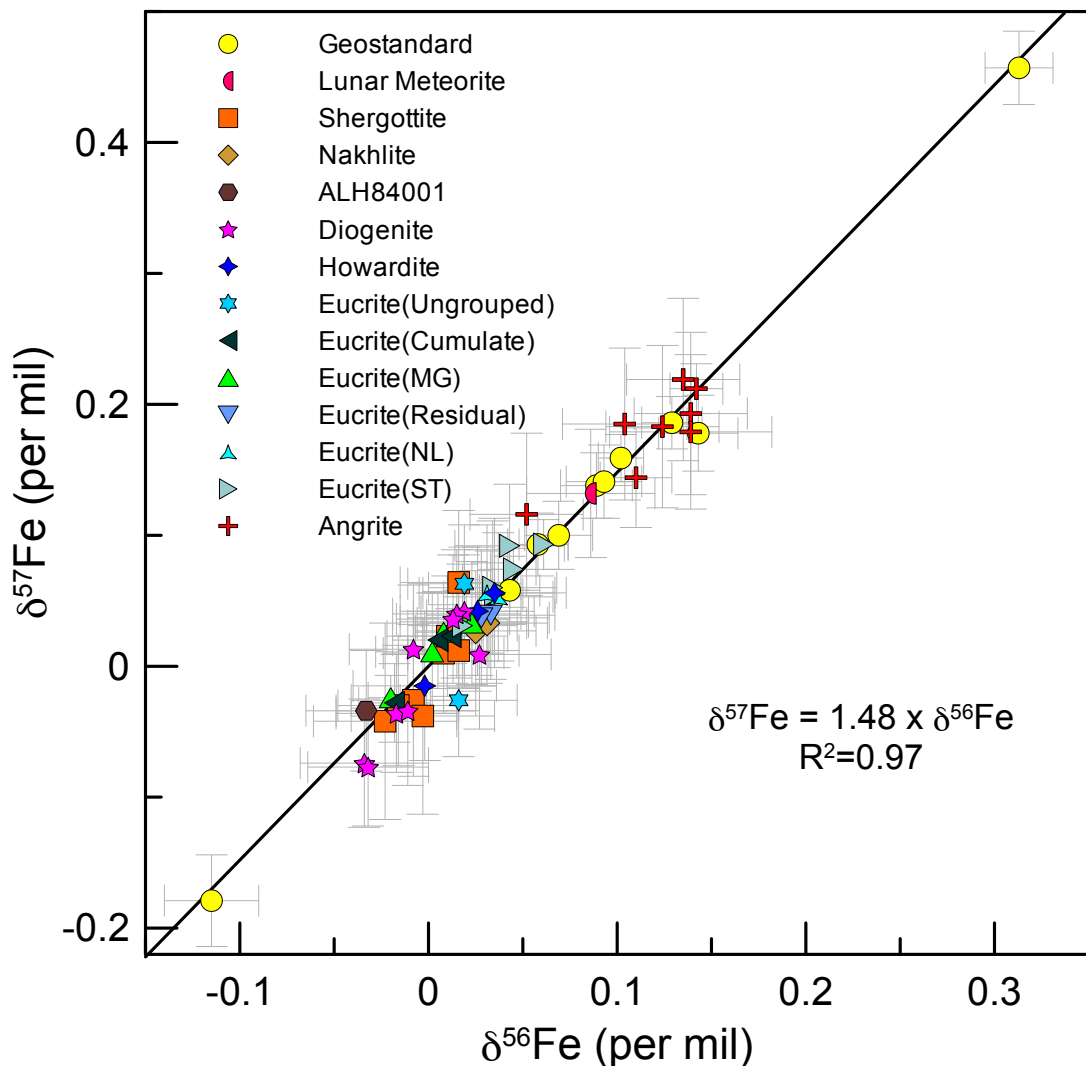


Figure 5-2. Mass-dependent isotope fractionation of all samples in this study, shown in a $\delta^{56}\text{Fe}$ - $\delta^{57}\text{Fe}$ space. Eucrite (MG)=Eucrite Main Group, Eucrite (NL)=Eucrite Nuevo Laredo Trend, Eucrite (ST)=Eucrite Stannern Trend. Each point represents one meteorite/geostandard. For replicate measurements in Table 5-1, only the average is plotted.

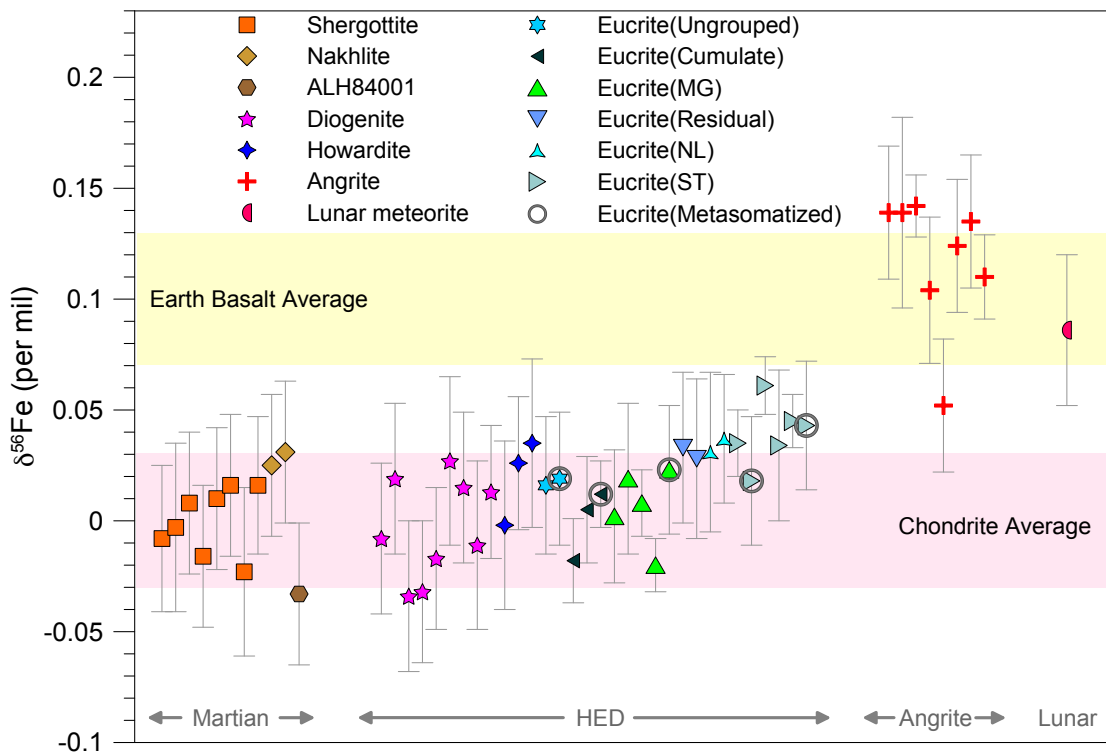


Figure 5-3. Iron isotope compositions of martian meteorites, HEDs, and angrites. Colored shadow areas schematically show “Earth Basalt Average” and “Chondrite Average,” established by a compilation of literature data (Dauphas and Rouxel, 2006; Dauphas et al., 2009a). Eucrite (MG)=Eucrite Main Group, Eucrite (NL)=Eucrite Nuevo Laredo Trend, Eucrite (ST)=Eucrite Stannern Trend. Each point represents one meteorite. For replicate measurements in Table 5-1, only the average is plotted.

5.4. Discussion

In the following section, we discuss the implications of the enrichment in the heavy isotopes of Fe observed in angrites and Stannern trend (ST) eucrites in terms of the redox state of the parent bodies and magmatic differentiation.

5.4.1. Redox-controlled Iron Isotope Fractionation on the Angrite Parent-body

Several processes can be considered in order to explain the fractionated iron isotope composition of basaltic angrites compared to other basaltic meteorites, including fractionation during low temperature terrestrial alteration, metal-silicate segregation, mineral fractionation, volatilization during impact, and partial silicate mantle melting. All angrites studied here are finds from the Sahara desert, Antarctica or Argentina. Leaching of isotopically light iron during terrestrial weathering can raise the $\delta^{56}\text{Fe}$ value of the residual rock up to +0.06 ‰ (Saunier et al., 2010). This process, however, is an unlikely candidate to explain the enrichment of heavy isotopes in angrites because all the angrites have a very narrow range of $\delta^{56}\text{Fe}$ (+0.12 ±0.01 ‰). These samples were found across a wide range of environments (from icy to hot desert) and have been subject to different exposure histories, which would not fractionate iron isotopes during alteration to an almost identical extent. In addition, for all other achondrite groups measured in this study, there is no difference in iron isotope composition between meteorite falls and finds indicating that terrestrial exposure has not affected isotope behavior for the samples in this study.

Equilibrium iron isotope fractionation between metal core and mantle is also not a viable explanation for the fractionated iron isotope compositions of angrites. High temperature (2000 °C) and high pressure (7.7 GPa) equilibrium melting experiments of chondritic materials show no iron isotope fractionation between metal alloy and silicate melt (Poitrasson et al., 2009).

Low-temperature, low-pressure metal silicate segregation would enrich the metal in heavy isotopes and the silicates in lighter isotopes (as seen in pallasites by Poitrasson et al., 2005). Campbell and Humayun (2005) proposed that IVB iron meteorites, enriched in heavy iron isotopes (Williams et al., 2006), could be the core of the angrite parent-body. If this is the case, angrite is expected to be enriched in light iron isotopes, which is the inverse of what is observed in angrites. Only at extremely high pressures (>100 GPa) encountered at the core-mantle boundary of the Earth, metallic core could be enriched in light iron isotopes while silicate mantle could be enriched heavy iron isotopes according to theoretical calculations (Polyakov, 2009). Although the parent-body of angrites is still unidentified; there is little doubt that these meteorites come from a small-scale asteroid (Burbine et al., 2006; Rivkin et al., 2007; Trilling et al., 2007).

Preferential evaporation of lighter Fe during impact events (and enrichment in the heavier in the residue) is a mechanism that has been proposed to explain the difference between terrestrial and lunar basalts (Poitrasson et al. 2004). All angrites (except Angra dos Reis and NWA2999) are unshocked and do not show particular impact features (Scott and Bottke, 2011). In addition, angrites are depleted in moderately volatile elements, but they are not notably more depleted in moderately volatile elements (*e.g.*, Zn, Cd) than eucrites (Weisberg et al., 2006). If volatilization due to impacts was the origin of the fractionation observed in angrites, similar effects should be found in eucrites, which is not the case. Therefore the enrichment in the heavier iron isotopes of angrites is unlikely caused by volatilization during impact processing, although this cannot be definitely ruled out.

Redox-controlled iron isotope fractionation through partial mantle melting provides one possible explanation for the fractionated iron isotope compositions of angrites. Redox proxies

indicate that angrites probably formed in a relatively oxidized environment (IW +1 to +2; Jurewicz et al., 1991, 1993; McKay et al., 1994), even though the exact redox conditions are difficult to quantify. Dauphas et al. (2009a) devised a quantitative model of iron isotope fractionation between source and melt as a function of Fe(III)/Fe(II) ratio. According to this model, given the low Fe(III)/Fe(II) ratio of angrites, little Fe isotope fractionation would be expected during partial melting. However, the exact redox condition of the mantle of angrite's parent body remains poorly known and it is also uncertain whether redox conditions can affect iron equilibrium isotope fractionation factors by modifying the structure of the melt even in systems with little Fe(III). Further work remains to be done to understand iron isotopic fractionation in angrites.

5.4.2. Iron Isotope Fractionation on the HED Parent-body

Petrological arguments indicate that HED meteorites were formed in a low oxygen fugacity environment, close to the IW buffer, with Fe(III) absent (Stolper, 1977; Hewins and Ulmer, 1984). The chondritic $\delta^{56}\text{Fe}$ values of diogenites, howardites, cumulate eucrites, MG-NL eucrites, and residual eucrites are consistent with a chondritic iron isotope composition of the HED parent-body mantle that has not been modified by core segregation or partial melting, as is also seen on Mars (Poitrasson et al., 2004).

The $\delta^{56}\text{Fe}$ values of ST eucrites are higher than those of other eucrites. ST eucrites do not show any particular depletion in volatile elements or impact features when compared to other eucrites (Barrat et al. 2007b). Therefore, volatilization of light isotopes of Fe due to impact is a very unlikely origin for iron isotope difference between ST eucrites and other eucrites. Iron isotope fractionation is also observed in lunar basalts where redox state is extremely low (IW-2

to -1 ; Liu et al., 2010). It has been proposed that ilmenite fractionation controls the 0.1‰ difference in $\delta^{56}\text{Fe}$ between low-Ti and high-Ti lunar mare basalts (Craddock et al., 2010). Ilmenite is enriched in the heavy isotopes of iron between 0.16 up to 0.42‰ in $\delta^{56}\text{Fe}$ (Craddock et al., 2010). ST eucrites are richer in Ti than the other eucrites and petrographic studies have also shown there is relatively more ilmenite in ST eucrites than in other eucrites ($0.93\text{-}1.20\text{ vol\%}$ vs. trace- 1.00 vol\% , respectively; Delaney et al., 1984; Warren et al., 1990). By mixing ilmenite with $\delta^{56}\text{Fe} = +0.42\text{‰}$ (the maximum fractionation) to main-group or cumulate eucrites ($\delta^{56}\text{Fe} \approx 0$), we obtained a $\delta^{56}\text{Fe} = 0.02\text{‰}$ (see Appendix for the mixing calculation; the calculation results are plotted as the shaded area in Figure 5-4). This could be enough to explain the observed ST eucrites values within analytical errors ($\pm 0.03\text{‰}$). If the ilmenites have a lower $\delta^{56}\text{Fe}$, only a fraction of the isotopic effect observed in ST eucrites can be explained by ilmenites and other source of isotope fractionation cannot be excluded. It is possible that other Fe-bearing minerals also controlled the iron isotope composition of eucrites, and further work is needed to characterize Fe isotope fractionation between minerals in eucrite meteorites.

The origin of ST eucrites is debated (see review by McSween et al., 2010). ST eucrites are petrographically and geochemically similar to MG eucrites, but are enriched in incompatible elements (Figure 5-4). Their origin was first explained as smaller degrees of partial melting of the same source as other eucrites (Consolmagno and Drake, 1977; Stolper, 1977; Hsu and Crozaz, 1996). However, this model is not consistent with the growing database for trace lithophile and siderophile elements (Mittlefehldt and Lindstrom, 2003; Barrat et al., 2007b). It has been proposed recently that ST eucrites are derived from the same parent magma to MG eucrites and have been modified by the assimilation of the asteroidal crust (Barrat et al., 2007b). This model is supported by our iron isotope data. It is observed in this study that $\delta^{56}\text{Fe}$ is correlated with Ti

and other incompatible elements (Figure 5-4). Non-modal re-melting of previously formed asteroidal crust would preferentially consume ilmenite (Barrat et al., 2007b). Partial melts formed from the eucritic crust will be rich not only in Ti, but also in the heavy isotopes of Fe because ilmenite in the case of the Moon has been demonstrated to be consistently heavy by up to 0.42 ‰ in $\delta^{56}\text{Fe}$ (Craddock et al., 2010). Contamination of ordinary basaltic eucrites by such components could explain the origin of ST eucrites with fractionated iron isotope compositions.

5.4.3. Iron Isotopes and Fluid-rock Interactions on Asteroidal Bodies

A few eucrites display pre-terrestrial secondary minerals, which may have recorded interactions with fluids. Serra de Magé contains quartz veinlets, which have been ascribed by Treiman et al. (2004) to the circulation of water. A few other eucrites display Fe-enrichment along the cracks that crosscut the pyroxenes, and sometimes deposits of Fe-rich olivine and anorthitic plagioclase inside the fractures (Barrat et al., 2011). The origin of these phases is a matter of debate. Barrat et al. (2011) have proposed that this Fe-enrichment is the result of a metasomatic event. The nature of the metasomatic agent is not clear, but could have been an aqueous fluid. Subsequently, Roszjar et al. (2011) proposed that Fe-olivine and anorthite were formed by incongruent *in situ* melting of pyroxene at a temperature slightly above the temperature of formation of the primary pyroxenes, at about 1150 °C.

Fluid-rock interaction and exsolution of aqueous fluids could preferentially remove light iron isotopes from bulk rock and is an important mechanism for iron chemical and isotope fractionation in both low- and high-temperature processes on Earth (Rouxel et al., 2003; Poitrasson and Freydier, 2005; Chapman et al., 2009). Thus, the fingerprint of aqueous fluid interaction in eucritic rocks could be detected using Fe isotopes. Among our samples, five

eucrites have been suspected to interact with aqueous fluids: Serra de Magé, Pasamonte, NWA 049, NWA 2061 and Y-75011 (circled points in Figures 5-3 and 5-4). None of these samples show iron isotope compositions fractionated relative to other similarly grouped eucrites. These results do not rule out definitively the involvement of fluids during eucrite evolution, but imply that fluid interactions on eucritic parent-bodies had negligible impact on iron isotope compositions. These results exclude the possibility that secondary processes on HED parent-body are the reason for the fractionated iron isotope compositions of ST eucrites.

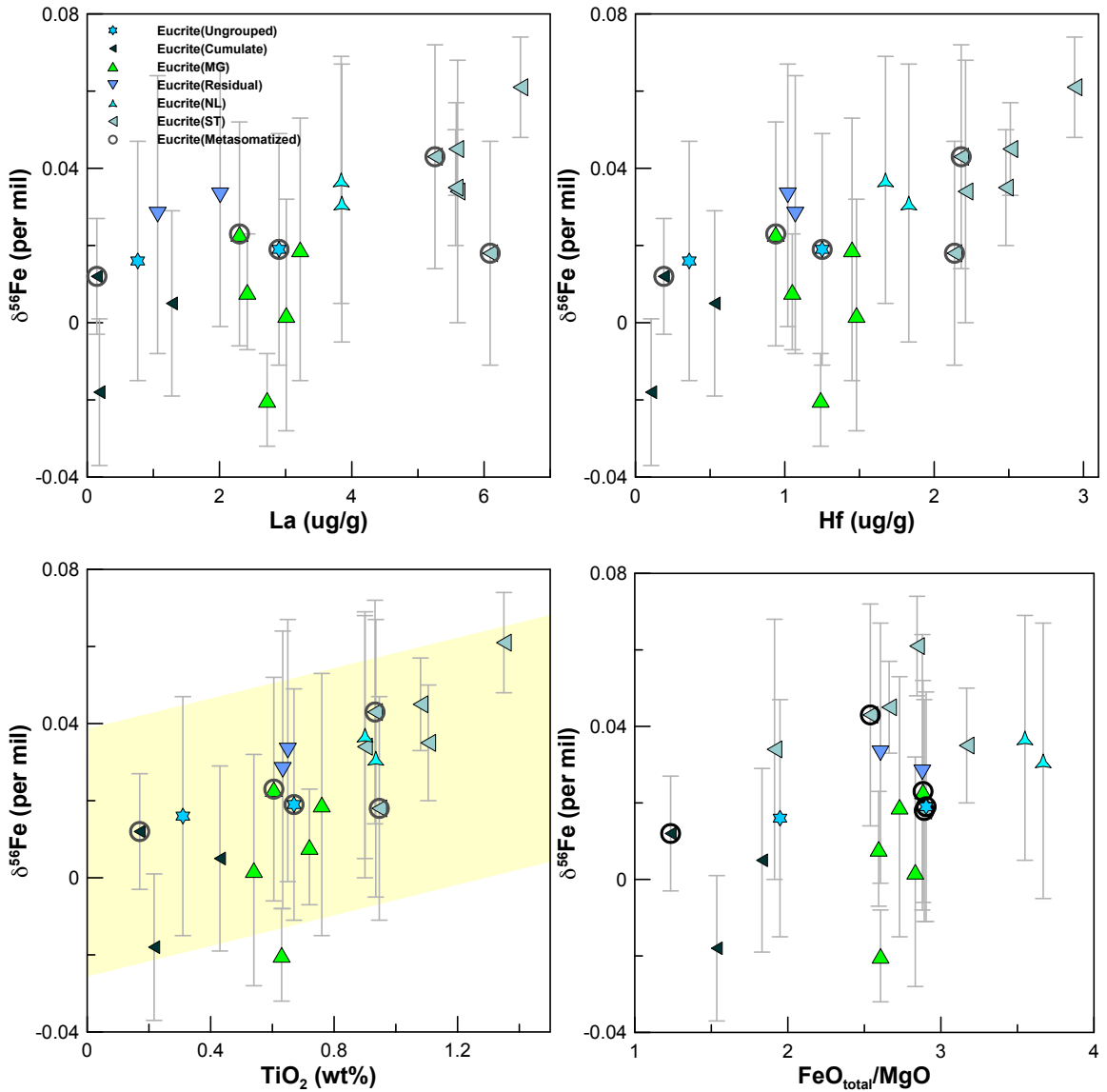


Figure 5-4. $\delta^{56}\text{Fe}$ vs. La, Hf, TiO_2 and $\text{FeO}_{\text{total}}/\text{MgO}$. The yellow shaded area represents ilmenite-controlled iron isotope fractionation (see text for details). Eucrite (MG)=Eucrite Main Group, Eucrite (NL)=Eucrite Nuevo Laredo Trend, Eucrite (ST)=Eucrite Stannern Trend. Each point represents one meteorite. For replicate measurements in Table 5-1, only the average is plotted. Data sources: The concentration data of Pasamonte, Moore County, Cachari, Jonzac, Serra de Magé, and Camel Donga come from Barrat et al. (2000); Nuevo Laredo, Juvinas, Stannern, NWA4523, and Bouvante from Barrat et al. (2007b); NWA049 and NWA1240 from Barrat et al. (2003); Sahara 02501 from Barrat et al. (2007a); NWA2061 from Barrat et al. (2011); Yamato75011 from Fukuoka and Ikeda (1983); Agoult and Dag945 from Yamaguchi et al. (2009); EET87548 comes from Warren et al. (2009); Pomozdino from Kitts and Lodders (1998).

5.5. Conclusion

We have found that Fe is enriched in the heavier isotopes in angrites (by $+0.12 \pm 0.01\text{‰}$; similar to terrestrial basalts) and in Stannern Trend eucrites (by $+0.05 \pm 0.01\text{‰}$). Martian and HEDs (except Stannern Trend) meteorites have iron isotope compositions identical to chondrites. Isotope fractionations during magmatic processes (partial melting, mineral fractionation and fluid exsolution) under different redox conditions are the best explanations to explain iron isotope variations in planetary crusts. However, further work remains to be done to document experimentally equilibrium iron isotope fractionation between melts and minerals to understand iron isotope variations in magmatic rocks. Our results show that not only terrestrial and lunar basalts are isotopically fractionated in iron but also crustal rocks from at least two asteroids with different sizes and volatilization histories.

References

- Allègre, C.J., Poirier, J.-P., Humler, E. and Hofmann, A.W. (1995) The chemical composition of the Earth. *Earth Planet. Sci. Lett.* **134**, 515-526.
- Anand, M., Russell, S.S., Blackhurst, R.L. and Grady, M.M. (2006) Searching for signatures of life on Mars: An Fe-isotope perspective. *Philos. Trans. R. Soc. Lond. B Biol. Sci.* **361**, 1715-1720.
- Baker, J., Bizzarro, M., Wittig, N., Connelly, J. and Haack, H. (2005) Early planetesimal melting from an age of 4.5662 Gyr for differentiated meteorites. *Nature* **436**, 1127-1131.
- Barrat, J.A., Blichert-Toft, J., Gillet, P. and Keller, F. (2000) The differentiation of eucrites: The role of in situ crystallization. *Meteorit. Planet. Sci.* **35**, 1087-1100.
- Barrat, J.A., Jambon, A., Bohn, M., Blichert-Toft, J., Sautter, V., Göpel, C., Gillet, P., Boudouma, O. and Keller, F. (2003) Petrology and geochemistry of the unbreciated achondrite Northwest Africa 1240 (NWA 1240): An HED parent body impact melt. *Geochim. Cosmochim. Acta* **67**, 3959-3970.
- Barrat, J.A., Yamaguchi, A., Bunch, T.E., Bohn, M., Bollinger, C. and Ceuleneer, G. (2011) Possible fluid-rock interactions on differentiated asteroids recorded in eucritic meteorites. *Geochim. Cosmochim. Acta* **75**, 3839-3852.
- Barrat, J.A., Yamaguchi, A., Greenwood, R.C., Benoit, M., Cotten, J., Bohn, A. and Franchi, I.A. (2008) Geochemistry of diogenites: Still more diversity in their parental melts. *Meteorit. Planet. Sci.* **43**, 1759-1775.
- Barrat, J.A., Yamaguchi, A., Greenwood, R.C., Bohn, M., Cotten, J., Benoit, M. and Franchi, I.A. (2007a) Could Stannern-trend eucrites be crustal-contaminated melts? *Lunar Planet. Sci. XXXVIII*. Lunar Planet. Inst., Houston. #1558 (abstr.).
- Barrat, J.A., Yamaguchi, A., Greenwood, R.C., Bohn, M., Cotten, J., Benoit, M. and Franchi, I.A. (2007b) The Stannern trend eucrites: Contamination of main group eucritic magmas by crustal partial melts. *Geochim. Cosmochim. Acta* **71**, 4108-4124.
- Belshaw, N.S., Zhu, X.K., Guo, Y. and O'Nions, R.K. (2000) High precision measurement of iron isotopes by plasma source mass spectrometry. *Int. J. Mass Spectrom.* **197**, 191-195.
- Bouvier, A., Brennecke, G.A., Sanborn, M.E. and Wadhwa, M. (2011) The formation of the angritic crust. *Goldschmidt Conf.* (abstr.).
- Burbine, T.H., McCoy, T.J., Hinrichs, J.L. and Lucey, P.G. (2006) Spectral properties of angrites. *Meteorit. Planet. Sci.* **41**, 1139-1145.
- Campbell, A.J. and Humayun, M. (2005) Compositions of group IVB iron meteorites and their parent melt. *Geochim. Cosmochim. Acta* **69**, 4733-4744.

- Chapman, J.B., Weiss, D.J., Shan, Y. and Lemberger, M. (2009) Iron isotope fractionation during leaching of granite and basalt by hydrochloric and oxalic acids. *Geochim. Cosmochim. Acta* **73**, 1312-1324.
- Consolmagno, G.J. and Drake, M.J. (1977) Composition and evolution of the eucrite parent body: evidence from rare earth elements. *Geochim. Cosmochim. Acta* **41**, 1271-1282.
- Craddock, P.R. and Dauphas, N. (2011) Iron isotopic compositions of geological reference materials and chondrites. *Geostand. Geoanal. Res.* **35**, 101-123.
- Craddock, P.R., Dauphas, N. and Clayton, R.N. (2010) Mineralogical control on iron isotopic fractionation during lunar differentiation and magmatism. *Lunar Planet. Sci. XLI*. Lunar Planet. Inst., Woodlands. #1230 (abstr.).
- Dauphas, N. and Chaussidon, M. (2011) A perspective from extinct radionuclides on a young stellar object: the Sun and its accretion disk. *Annu. Rev. Earth Planet. Sci.* **39**, 351-386.
- Dauphas, N., Craddock, P.R., Asimow, P.D., Bennett, V.C., Nutman, A.P. and Ohnenstetter, D. (2009a) Iron isotopes may reveal the redox conditions of mantle melting from Archean to Present. *Earth Planet. Sci. Lett.* **288**, 255-267.
- Dauphas, N., Janney, P.E., Mendybaev, R.A., Wadhwa, M., Richter, F.M., Davis, A.M., van Zuilen, M., Hines, R. and Foley, C.N. (2004) Chromatographic separation and multicollection-ICPMS analysis of iron. Investigating mass-dependent and -independent isotope effects. *Anal. Chem.* **76**, 5855-5863.
- Dauphas, N., Pourmand, A. and Teng, F.Z. (2009b) Routine isotopic analysis of iron by HR-MC-ICPMS: How precise and how accurate? *Chem. Geol.* **267**, 175-184.
- Dauphas, N. and Rouxel, O. (2006) Mass spectrometry and natural variations of iron isotopes. *Mass Spectrom. Rev.* **25**, 515-550.
- Day, J.M.D., Taylor, L.A., Floss, C. and McSween, H.Y. (2006) Petrology and chemistry of MIL 03346 and its significance in understanding the petrogenesis of nakhlites on Mars. *Meteorit. Planet. Sci.* **41**, 581-606.
- Delaney, J.S., Prinz, M. and Takeda, H. (1984) The polymict eucrites. *J Geophys. Res.* **89**, C251-C288.
- Drake, M.J. (2001) The eucrite/Vesta story. *Meteorit. Planet. Sci.* **36**, 501-513.
- Duke, M.B. and Silver, L.T. (1967) Petrology of eucrites, howardites and mesosiderites. *Geochim. Cosmochim. Acta* **31**, 1637-1665.
- Gellissen, M., Palme, H., Korotev, R.L. and Irving, A.J. (2007) NWA2999, a unique angrite with a large chondritic component. *Lunar Planet. Sci. XXXVIII*. Lunar Planet. Inst., Houston. #1612 (abstr.).

- Gillet, P., Barrat, J.A., Beck, P., Marty, B., Greenwood, R.C., Franchi, I.A., Bohn, M. and Cotten, J. (2005) Petrology, geochemistry, and cosmic-ray exposure age of lherzolitic shergottite Northwest Africa 1950. *Meteorit. Planet. Sci.* **40**, 1175-1184.
- Heimann, A., Beard, B.L. and Johnson, C.M. (2008) The role of volatile exsolution and subsolidus fluid/rock interactions in producing high $^{56}\text{Fe}/^{54}\text{Fe}$ ratios in siliceous igneous rocks. *Geochim. Cosmochim. Acta* **72**, 4379-4396.
- Hewins, R.H. and Ulmer, G.C. (1984) Intrinsic oxygen fugacities of diogenites and mesosiderite clasts. *Geochim. Cosmochim. Acta* **48**, 1555-1560.
- Hin, R.C., Schimidt, M.W., Wiederhold, J.G. and Bourdon, B. (2010) Constraints on Fe isotope fractionation between liquid metal and liquid silicate from experiments at 1 GPa and 1250-1300°C. *AGU Fall Meeting*, #V44B-03 (abstr.).
- Horwitz, E.P., Dietz, M.L., Chiarizia, R., Diamond, H., Essling, A.M. and Graczyk, D. (1992) Separation and preconcentration of uranium from acidic media by extraction chromatography. *Anal. Chim. Acta* **266**, 25-37.
- Hsu, W.B. and Crozaz, G. (1996) Mineral chemistry and the petrogenesis of eucrites. I. Noncumulate eucrites. *Geochim. Cosmochim. Acta* **60**, 4571-4591.
- Humayun, M. and Clayton, R.N. (1995) Potassium isotope cosmochemistry - genetic-implications of volatile element depletion. *Geochim. Cosmochim. Acta* **59**, 2131-2148.
- Irving, A.J. and Kuehner, S.M. (2007) Plutonic angrite NWA 4801 and a model for the angrite parent body consistent with petrological and chronological constraints. *Workshop on the chronology of meteorites and the early Solar System*, #4050 (abstr.).
- Jambon, A., Barrat, J.A., Boudouma, O., Fonteilles, M., Badia, D., Göpel, C. and Bohn, M. (2005) Mineralogy and petrology of the angrite Northwest Africa 1296. *Meteorit. Planet. Sci.* **40**, 361-375.
- Jambon, A., Boudouma, O., Fonteilles, M., Guillou, C.L., Badia, D. and Barrat, J.A. (2008) Petrology and mineralogy of the angrite Northwest Africa 1670. *Meteorit. Planet. Sci.* **43**, 1783-1795.
- Jarosewich, E. (1990) Chemical-analyses of meteorites - a compilation of stony and iron meteorite analyses. *Meteoritics* **25**, 323-337.
- Jolliff, B.L., Korotev, R.L. and Haskin, L.A. (1991) A ferroan region of the lunar highlands as recorded in meteorites MAC88104 and MAC88105. *Geochim. Cosmochim. Acta* **55**, 3051-3071.
- Jurewicz, A.J.G., Mittlefehldt, D.W. and Jones, J.H. (1991) Partial melting of the Allende (CV3) meteorite - implications for origins of basaltic meteorites. *Science* **252**, 695-698.
- Jurewicz, A.J.G., Mittlefehldt, D.W. and Jones, J.H. (1993) Experimental partial melting of the Allende (CV) and Murchison (CM) chondrites and the origin of asteroidal basalts. *Geochim. Cosmochim. Acta* **57**, 2123-2139.

- Kitts, K. and Lodders, K. (1998) Survey and evaluation of eucrite bulk compositions. *Meteorit. Planet. Sci.* **33**, A197-A213.
- Koeberl, C., Kurat, G. and Brandstatter, F. (1991) MAC88105 - A regolith breccia from the lunar highlands: Mineralogical, petrological, and geochemical studies. *Geochim. Cosmochim. Acta* **55**, 3073-3087.
- Korotev, R.L., Jolliff, B.L., Zeigler, R.A., Gillis, J.J. and Haskin, L.A. (2003) Feldspathic lunar meteorites and their implications for compositional remote sensing of the lunar surface and the composition of the lunar crust. *Geochim. Cosmochim. Acta* **67**, 4895-4923.
- Kuehner, S.M., Irving, A.J., Bunch, T.E., Wittke, J.H., Hupé, G.M. and Hupé, A.C. (2006) Coronas and symplectites in plutonic angrite NWA 2999 and implications for Mercury as the angrite parent body. *Lunar Planet. Sci. XXXVII*. Lunar Planet. Inst., Houston. #1344 (abstr.).
- Lindstrom, M.M., Wentworth, S.J., Martinez, R.R., Mittlefehldt, D.W., McKay, D.S., Ming-Sheng, W. and Lipschutz, M.E. (1991) Geochemistry and petrography of the MacAlpine Hills lunar meteorites. *Geochim. Cosmochim. Acta* **55**, 3089-3103.
- Liu, Y., Spicuzza, M.J., Craddock, P.R., Day, J.M.D., Valley, J.W., Dauphas, N. and Taylor, L.A. (2010) Oxygen and iron isotope constraints on near-surface fractionation effects and the composition of lunar mare basalt source regions. *Geochim. Cosmochim. Acta* **74**, 6249-6262.
- Lodders, K. (1998) A survey of shergottite, nakhlite and chassigny meteorites whole-rock compositions. *Meteorit. Planet. Sci.* **33**, A183-A190.
- Lodders, K. and Fegley, B. (1998) *The Planetary Scientist's Companion*. Oxford University Press, New York.
- McCammon, C. (2005) The paradox of mantle redox. *Science* **308**, 807-808.
- McCarthy, T.S., Ahrens, L.H. and Erlank, A.J. (1972) Further evidence in support of the mixing model for howardite origin. *Earth Planet. Sci. Lett.* **15**, 86-93.
- McCord, T.B., Adams, J.B. and Johnson, T.V. (1970) Asteroid Vesta: spectral reflectivity and compositional implications. *Science* **168**, 1445-1447.
- McKay, G., Le, L., Wagstaff, J. and Crozaz, G. (1994) Experimental partitioning of rare-earth elements and strontium - constraints on petrogenesis and redox conditions during crystallization of Antarctic angrite Lewis Cliff-86010. *Geochim. Cosmochim. Acta* **58**, 2911-2919.
- McKay, G., Lindstrom, D., Yang, S.-R. and Wagstaff, J. (1988) Petrology of unique achondrite Lewis Cliff 86010. *Lunar Planet. Sci. XIX*. Lunar Planet. Inst., Houston. #762 (abstr.).
- McSween, H., Mittlefehldt, D., Beck, A., Mayne, R. and McCoy, T. (2010) HED meteorites and their relationship to the geology of Vesta and the Dawn mission. *Space Sci. Rev.*, 1-34.

- Millet, M.-A., Baker, J.A. and Payne, C.E. (2012) Ultra-precise stable Fe isotope measurements by high resolution multiple-collector inductively coupled plasma mass spectrometry with a ^{57}Fe - ^{58}Fe double spike. *Chem. Geol.* **304-305**, 18-25.
- Mittlefehldt, D.W., Killgore, M. and Lee, M.T. (2002) Petrology and geochemistry of D'Orbigny, geochemistry of Sahara 99555, and the origin of angrites. *Meteorit. Planet. Sci.* **37**, 345-369.
- Mittlefehldt, D.W. and Lindstrom, M.M. (2003) Geochemistry of eucrites: Genesis of basaltic eucrites, and Hf and Ta as petrogenetic indicators for altered Antarctic eucrites. *Geochim. Cosmochim. Acta* **67**, 1911-1934.
- Mittlefehldt, D.W., McCoy, T.J., Goodrich, C.A. and Kracher, A. (1998) Non-chondritic meteorites from asteroidal bodies. In *Planetary Materials*. (eds. Papike, J.J.). Mineralogical Society of America. *Reviews in Mineralogy* **36**, p. 195.
- Moynier, F., Albarède, F. and Herzog, G.F. (2006) Isotopic composition of zinc, copper, and iron in lunar samples. *Geochim. Cosmochim. Acta* **70**, 6103-6117.
- Neal, C.R., Taylor, L.A., Lui, Y.-G. and Schmitt, R.A. (1991) Paired lunar meteorites MAC88104 and MAC88105: A new "fan" of lunar petrology. *Geochim. Cosmochim. Acta* **55**, 3037-3049.
- Nyquist, L.E., Kleine, T., Shih, C.Y. and Reese, Y.D. (2009) The distribution of short-lived radioisotopes in the early solar system and the chronology of asteroid accretion, differentiation, and secondary mineralization. *Geochim. Cosmochim. Acta* **73**, 5115-5136.
- Poirrasson, F. (2007) Does planetary differentiation really fractionate iron isotopes? *Earth Planet. Sci. Lett.* **256**, 484-492.
- Poirrasson, F. and Freydier, R. (2005) Heavy iron isotope composition of granites determined by high resolution MC-ICP-MS. *Chem. Geol.* **222**, 132-147.
- Poirrasson, F., Halliday, A.N., Lee, D.C., Levasseur, S. and Teutsch, N. (2004) Iron isotope differences between Earth, Moon, Mars and Vesta as possible records of contrasted accretion mechanisms. *Earth Planet. Sci. Lett.* **223**, 253-266.
- Poirrasson, F., Levasseur, S. and Teutsch, N. (2005) Significance of iron isotope mineral fractionation in pallasites and iron meteorites for the core-mantle differentiation of terrestrial planets. *Earth Planet. Sci. Lett.* **234**, 151-164.
- Poirrasson, F., Roskosz, M. and Corgne, A. (2009) No iron isotope fractionation between molten alloys and silicate melt to 2000 degrees C and 7.7 GPa: Experimental evidence and implications for planetary differentiation and accretion. *Earth Planet. Sci. Lett.* **278**, 376-385.
- Polyakov, V.B. (2009) Equilibrium iron isotope fractionation at core-mantle boundary conditions. *Science* **323**, 912-914.

- Polyakov, V.B. and Mineev, S.D. (2000) The use of Mossbauer spectroscopy in stable isotope geochemistry. *Geochim. Cosmochim. Acta* **64**, 849-865.
- Prinz, M., Weisberg, M.K. and Nehru, C.E. (1988) LEW 86010, A Second Angrite: Relationship to CAI's and Opaque Matrix. *Lunar Planet. Sci. XIX*. Lunar Planet. Inst., Houston. #949 (abstr.).
- Reid, A.M. and Barnard, B.M. (1979) Unequilibrated and equilibrated eucrites. *Lunar Planet. Sci. X*. Lunar Planet. Inst., Houston. #1019 (abstr.).
- Rivkin, A.S., Trilling, D.E., Thomas, C.A., DeMeo, F., Spahr, T.B. and Binzel, R.P. (2007) Composition of the L5 Mars Trojans: Neighbors, not siblings. *Icarus* **192**, 434-441.
- Roszjar, J., Metzler, K., Bischoff, A., Barrat, J., Geisler, T., Greenwood, R.C., Franchi, I.A. and Klemme, S. (2011) Thermal history of Northwest Africa (NWA) 5073 - a coarse-grained Stannern-trend eucrite containing cm-sized pyroxenes and large zircon grains. *Meteorit. Planet. Sci.* **46**, 1754-1773.
- Rouxel, O., Dobbek, N., Ludden, J. and Fouquet, Y. (2003) Iron isotope fractionation during oceanic crust alteration. *Chem. Geol.* **202**, 155-182.
- Rudnick, R.L. and Gao, S. (2003) The composition of the continental crust. In *Treatise on Geochemistry*. (eds. Holland, H.D., Turekian, K.K.). Elsevier-Pergamon.
- Sack, R.O., Azeredo, W.J. and Lipschutz, M.E. (1991) Olivine Diogenites - the Mantle of the Eucrite Parent Body. *Geochim. Cosmochim. Acta* **55**, 1111-1120.
- Saunier, G., Poitrasson, F., Moine, B., Gregoire, M. and Seddiki, A. (2010) Effect of hot desert weathering on the bulk-rock iron isotope composition of L6 and H5 ordinary chondrites. *Meteorit. Planet. Sci.* **45**, 195-209.
- Schauble, E.A., Rossman, G.R. and Taylor, H.P. (2001) Theoretical estimates of equilibrium Fe-isotope fractionations from vibrational spectroscopy. *Geochim. Cosmochim. Acta* **65**, 2487-2497.
- Schoenberg, R. and von Blanckenburg, F. (2006) Modes of planetary-scale Fe isotope fractionation. *Earth Planet. Sci. Lett.* **252**, 342-359.
- Schuessler, J.A., Schoenberg, R., Behrens, H. and von Blanckenburg, F. (2007) The experimental calibration of the iron isotope fractionation factor between pyrrhotite and peralkaline rhyolitic melt. *Geochim. Cosmochim. Acta* **71**, 417-433.
- Schuessler, J.A., Schoenberg, R. and Sigmarsdottir, O. (2009) Iron and lithium isotope systematics of the Hekla volcano, Iceland - Evidence for Fe isotope fractionation during magma differentiation. *Chem. Geol.* **258**, 78-91.
- Schwartz, J.M. and McCallum, I.S. (2005) Comparative study of equilibrated and unequilibrated eucrites: Subsolidus thermal histories of Haraiya and Pasamonte. *Am. Mineral.* **90**, 1871-1886.

- Scott, E.R.D. and Bottke, W.F. (2011) Impact histories of angrites, eucrites, and their parent bodies. *Meteorit. Planet. Sci.* **46**, 1878-1887.
- Scott, E.R.D., Greenwood, R.C., Franchi, I.A. and Sanders, I.S. (2009) Oxygen isotopic constraints on the origin and parent bodies of eucrites, diogenites, and howardites. *Geochim. Cosmochim. Acta* **73**, 5835-5853.
- Shahar, A., Young, E.D. and Manning, C.E. (2008) Equilibrium high-temperature Fe isotope fractionation between fayalite and magnetite: An experimental calibration. *Earth Planet. Sci. Lett.* **268**, 330-338.
- Stolper, E. (1977) Experimental petrology of eucritic meteorites. *Geochim. Cosmochim. Acta* **41**, 587-611.
- Strelow, F.W.E. (1980) Improved separation of iron from copper and other elements by anion-exchange chromatography on a 4-percent cross-linked resin with high-concentrations of hydrochloric-acid. *Talanta* **27**, 727-732.
- Takeda, H., Ishii, T., Miyamoto, M. and Duke, M.B. (1978) Crystallization of pyroxenes in lunar KREEP basalt 15386 and meteoritic basalts. *Lunar Planet. Sci. IX*. Lunar Planet. Inst., Houston. #1157 (abstr.).
- Teng, F.-Z., Dauphas, N., Helz, R.T., Gao, S. and Huang, S. (2011) Diffusion-driven magnesium and iron isotope fractionation in Hawaiian olivine. *Earth Planet. Sci. Lett.* **308**, 317-324.
- Teng, F.Z., Dauphas, N. and Helz, R.T. (2008) Iron isotope fractionation during magmatic differentiation in Kilauea Iki Lava Lake. *Science* **320**, 1620-1622.
- Tissot, F. and Dauphas, N. (2011) Development of high precision $^{238}\text{U}/^{235}\text{U}$ ratio measurements for cosmochemical applications. *Lunar Planet. Sci. XLII*. Lunar Planet. Inst., Woodlands. #1082 (abstr.).
- Treiman, A.H., Lanzirotti, A. and Xirouchakis, D. (2004) Ancient water on asteroid 4 Vesta: evidence from a quartz veinlet in the Serra de Mage eucrite meteorite. *Earth Planet. Sci. Lett.* **219**, 189-199.
- Trilling, D.E., Rivkin, A.S., Stansberry, J.A., Spahr, T.B., Crudo, R.A. and Davies, J.K. (2007) Albedos and diameters of three Mars Trojan asteroids. *Icarus* **192**, 442-447.
- Wadhwa, M. (2008) Redox conditions on small bodies, the Moon and Mars. In *Oxygen in the Solar System*. (eds. MacPherson, G.J., Mittlefehldt, D.W., Jones, J.H., Simon, S.B.) *Reviews in Mineralogy & Geochemistry* **68**, pp. 493-510.
- Warren, P.H., Greenwood, J.P., Richardson, J.W., Rubin, A.E. and Verish, R.S. (2000) Geochemistry of Los Angeles, a Ferroan, La- and Th-rich Basalt from Mars. *Lunar Planet. Sci. XXXI*. Lunar Planet. Inst., Houston. #2001 (abstr.).
- Warren, P.H., Jerde, E.A. and Kallemeyn, G.W. (1989) Lunar meteorites: siderophile element contents, and implications for the composition and origin of the Moon. *Earth Planet. Sci. Lett.* **91**, 245-260.

- Warren, P.H., Jerde, E.A., Migdisova, L.F. and Yaroshevsky, A.A. (1990) Pomozdino - an anomalous, high-MgO/FeO, yet REE-rich eucrite. *Proc. Lunar Planet. Sci. Conf.* **20**, 281-297.
- Warren, P.H., Kallemeyn, G.W., Huber, H., Ulff-Moller, F. and Choe, W. (2009) Siderophile and other geochemical constraints on mixing relationships among HED-meteoritic breccias. *Geochim. Cosmochim. Acta* **73**, 5918-5943.
- Weisberg, M.K., McCoy, T.J. and Krot, A.N. (2006) Systematics and evaluation of meteorite classification. In *Meteorites and the Early Solar System II*. (eds. Lauretta, D.S., McSween, H.Y.J.). University of Arizona Press.
- Weyer, S., Anbar, A.D., Brey, G.P., Munker, C., Mezger, K. and Woodland, A.B. (2005) Iron isotope fractionation during planetary differentiation. *Earth Planet. Sci. Lett.* **240**, 251-264.
- Weyer, S., Anbar, A.D., Brey, G.P., Munker, C., Mezger, K. and Woodland, A.B. (2007) Fe-isotope fractionation during partial melting on Earth and the current view on the Fe-isotope budgets of the planets - (reply to the comment of F. Poitrasson and to the comment of B.L. Beard and C.M. Johnson on "Iron isotope fractionation during planetary differentiation" by S. Weyer, A.D. Anbar, G.P. Brey, C. Munker, K. Mezger and A.B. Woodland). *Earth Planet. Sci. Lett.* **256**, 638-646.
- Weyer, S. and Ionov, D.A. (2007) Partial melting and melt percolation in the mantle: The message from Fe isotopes. *Earth Planet. Sci. Lett.* **259**, 119-133.
- Weyer, S. and Schwiters, J.B. (2003) High precision Fe isotope measurements with high mass resolution MC-ICPMS. *Int. J. Mass Spectrom.* **226**, 355-368.
- Weyer, S. and Seitz, H.M. (2012) Coupled lithium- and iron isotope fractionation during magmatic differentiation. *Chem. Geol.* **294-295**, 42-50.
- Williams, H.M., Markowski, A., Quitte, G., Halliday, A.N., Teutsch, N. and Levasseur, S. (2006) Fe isotope fractionation in iron meteorites: New insights into metal-sulphide segregation and planetary accretion. *Earth Planet. Sci. Lett.* **250**, 486-500.
- Williams, H.M., McCammon, C.A., Peslier, A.H., Halliday, A.N., Teutsch, N., Levasseur, S. and Burg, J.P. (2004) Iron isotope fractionation and the oxygen fugacity of the mantle. *Science* **304**, 1656-1659.
- Yamaguchi, A., Barrat, J.A., Greenwood, R.C., Shirai, N., Okamoto, C., Setoyanagi, T., Ebihara, M., Franchi, I.A. and Bohn, M. (2009) Crustal partial melting on Vesta: Evidence from highly metamorphosed eucrites. *Geochim. Cosmochim. Acta* **73**, 7162-7182.
- Zhu, X.K., Guo, Y., O'Nions, R.K., Young, E.D. and Ash, R.D. (2001) Isotopic homogeneity of iron in the early solar nebula. *Nature* **412**, 311-313.

Appendix

Ilmenite is enriched in the heavy isotopes of iron between 0.16 and up to 0.42 ‰ in $\delta^{56}\text{Fe}$ (Craddock et al., 2010). By using the $\delta^{56}\text{Fe}$ value of separated ilmenite and the modal abundance of ilmenite in ST eucrites, we can construct a simplified mixing model of ilmenite-controlled iron isotope fractionation (Eq. 5-A1).

$$\delta^{56}\text{Fe}_{ST} = \delta^{56}\text{Fe}_{cumulate_MG} + \Delta_{ilmenite} \cdot \delta^{56}\text{Fe}_{ilmenite} \quad \text{Eq. 5-A1}$$

$\delta^{56}\text{Fe}_{ST}$ is the iron isotope composition of ST eucrites; $\delta^{56}\text{Fe}_{cumulate_MG}$ is the iron isotope composition of cumulate or MG eucrites; $\delta^{56}\text{Fe}_{ST}$ is the iron isotope composition of mineral ilmenite. $\Delta_{ilmenite}$ is the enrichment of ilmenite in ST eucrites compared to cumulate or MG eucrites; $\Delta_{ilmenite}$ is a function of the abundance of ilmenite in ST and in cumulate or MG eucrites. Considering the conversion of volume percentage reported in references to weight percentage, and iron concentration in mineral ilmenite and in bulk eucrites, we could write:

$$\Delta_{ilmenite} = (A_{ST} - A_{cumulate_MG}) \cdot \frac{\rho_{ilmenite}}{\rho_{eucrite}} \cdot \frac{C_{ilmenite}}{C_{ST}} \quad \text{Eq. 5-A2}$$

The meanings and values of the parameters used in Eq. 5-A2 are listed in Table 5-A1.

Hence, Eq. 5-A1 can be developed into Eq. 5-A3.

$$\delta^{56}\text{Fe}_{ST} = \delta^{56}\text{Fe}_{cumulate_MG} + (A_{ST} - A_{cumulate_MG}) \cdot \frac{\rho_{ilmenite}}{\rho_{eucrite}} \cdot \frac{C_{ilmenite}}{C_{ST}} \cdot \delta^{56}\text{Fe}_{ilmenite} \quad \text{Eq. 5-A3}$$

By using the maximum fractionation value ($\delta^{56}\text{Fe}=0.42\text{ ‰}$) measured in ilmenite (Craddock et al., 2010), we obtained a $\delta^{56}\text{Fe}=0.02$ for ST eucrites, which could largely explain the difference between ST eucrites and cumulate or MG eucrites within analytical errors

($\pm 0.03\text{\textperthousand}$). However, if we use the minimum fractionation value ($\delta^{56}\text{Fe}=0.16\text{\textperthousand}$) measured in ilmenite (Craddock et al., 2010), we obtained a $\delta^{56}\text{Fe} = 0.01$ for ST eucrites. In this case, other minerals might also contribute to the enrichment of iron isotope in ST eucrites. Due to the lack of iron isotope data of relevant minerals, there is no further constraint on this problem.

Table 5-A1. Parameters of the mass-balance used in Eq. 5-A1 to calculate the ilmenite-controlled iron isotope fractionation

Parameter	Meaning	Value	Reference
$A_{\text{cumulate_MG}}$	Ilmenite abundance in eucrite (cumulate) and eucrite (MG) (vol%)	trace-1.00	(Delaney et al., 1984)
A_{ST}	Ilmenite abundance in eucrite (ST) (vol%)	0.93-1.20	(Delaney et al., 1984; Warren et al., 1990)
ρ_{ilmenite}	Ilmenite density (g/cm ³)	4.79	(Lodders and Fegley, 1998)
ρ_{eucrite}	Eucrite average density (g/cm ³)	3.20	(Kitts and Lodders, 1998)
C_{ilmenite}	Iron concentration in ilmenite (%)	36.81	Ilmenite (FeTiO ₃) stoichiometric value
C_{ST}	Iron concentration in eucrite (ST) (%)	13.72-15.27	(Kitts and Lodders, 1998)
$\delta^{56}\text{Fe}_{\text{ilmenite}}$	Iron isotope composition of separated ilmenite	0.16-0.42	(Craddock et al., 2010)
$\delta^{56}\text{Fe}_{\text{cumulate_MG}}$	Average iron isotope composition of eucrite (cumulate) and eucrite (MG)	~ 0.00	This study and previous references (Poitrasson et al., 2004; Weyer et al., 2005; Schoenberg and von Blanckenburg, 2006)

Notes: Eucrite (MG)=Eucrite Main Group, Eucrite (ST)=Eucrite Stannern Trend

CHAPTER 6 :

IRON ISOTOPE FRACTIONATION DURING SULFIDE-RICH FELSIC PARTIAL MELTING ON EARLY PLANETESIMALS

This chapter has been submitted to Earth and Planetary Sciences Letters and is currently under review for the possibility of publication: Wang, K., Day, J.M.D., Korotev, R.L., Zeigler, R.A., Moynier, F. Iron Isotope Fractionation during Sulfide-rich Felsic Partial Melting on Early Planetesimals. *Earth and Planetary Sciences Letters*, in review.

Abstract

Feldspar-rich meteorites, Graves Nunataks 06128 and 06129 (GRA 06128/9) and olivine-rich brachinites represent the first known examples of crust and mantle compliments of a partially differentiated planetesimal. GRA 06128/9 are sulfide-rich felsic melts and brachinites are mantle residues after inefficient melt extraction of such a melt. Here we report Fe isotope data for GRA 06128/9 showing that they are the only known examples of crustal materials with isotopically light Fe isotope compositions ($\delta^{56}\text{Fe} = -0.08 \pm 0.06\text{\textperthousand}$; $\delta^{56}\text{Fe}$ is defined as the *per mille* deviation of a sample's $^{56}\text{Fe}/^{54}\text{Fe}$ ratio from the IRMM-14 standard). In contrast, associated brachinites, as well as brachinite-like achondrites have Fe isotope compositions ($\delta^{56}\text{Fe} = +0.01 \pm 0.02\text{\textperthousand}$) that are isotopically similar to carbonaceous chondrites and the bulk terrestrial mantle.

In order to understand the cause of Fe isotope variations in the GRA 06128/9 and brachinite parent body, we also report the Fe isotope compositions of metal, silicate and sulfide fractions from three ordinary chondrites (Semarkona, Kernouve, Saint-Séverin). Metals from ordinary chondrites are enriched in the heavier isotopes of Fe (average $\delta^{56}\text{Fe} = 0.15\text{\textperthousand}$), sulfide fractions are enriched in the lighter isotopes of Fe (average $\delta^{56}\text{Fe} = -0.14\text{\textperthousand}$), and the $\delta^{56}\text{Fe}$ values of the silicates are coincident with that of the bulk rock (average $\delta^{56}\text{Fe} = 0.03\text{\textperthousand}$). The enrichment of light isotopes of Fe isotopes in GRA 06128/9 is consistent with preferential melting of sulfides in precursor chondritic source materials leading to the formation of Fe-S-rich felsic melts. Melt generation (<1000°C) occurred prior to the onset of higher temperature basaltic melting and led to the generation of buoyant felsic melt with a strong Fe-S signature. This model not only explains the enrichment in light isotopes of Fe for GRA 06128/9, but is also entirely consistent with petrological and geochemical observations, experimental studies for the origin of Fe-S-rich felsic melts, and for the cessation of early melting on some asteroidal parent

bodies because of the effective removal of the major radioactive heat-source, ^{26}Al . The mode of origin for GRA 06128/9 contrasts strongly with crust formation on Earth, the Moon, Mars and other asteroids, where mantle differentiation and/or oxygen fugacity are the major controls on crustal Fe isotope compositions.

6.1. Introduction

Planet formation studies rely on a robust understanding of how the outermost solid crust of a planet is formed. Most planetary bodies are currently only studied remotely, or from meteorites that originate from the crust of the body, and thus most of the chemical and physical information obtained on the planets formation, differentiation and cooling history is obtained from its crust. Direct study of terrestrial crust has shown a fundamental dichotomy of dense basaltic crust in the ocean basins formed at mid-ocean ridges through adiabatic decompression, and evolved more buoyant feldspar-rich (felsic) continental crust (Rudnick and Gao, 2003). Unlike oceanic crust, felsic continental crust cannot be formed by single-stage melting of peridotite. Many processes have been proposed for continental crust formation, all of which require complex multi-stage melting of primary or recycled materials since at least 3 Ga ago (*e.g.*, Rudnick and Gao, 2003; Rudnick, 1995; Taylor and McLennan, 2009).

By contrast, although it has been proposed that felsic melts may have formed early on some planetesimals (Cohen et al., 2004; Keil, 2010), the preponderance of crust formed in the early Solar System appears to have been basaltic (Taylor and McLennan, 2009). Among all differentiated asteroidal meteorites, angrite and howardite-eucrite-diogenite (HED) meteorites are the only known crustal materials to have formed within 3 to 8 Ma of calcium-aluminium-rich inclusions (CAIs); the first solid materials condensed from the solar nebula (Amelin, 2008; Blichert-Toft et al., 2002; Trinquier et al., 2008). These two meteorite groups are broadly basaltic in composition and likely formed early during global-scale differentiation (magma ocean) events (*e.g.*, Greenwood et al., 2005) and subsequent to core formation on their parent bodies (Riches et al., 2012; Day et al., 2012b).

The identification of the paired achondrite meteorites GRA 06128/9 as evolved felsic crustal materials (Day et al., 2009a, 2012a; Shearer et al., 2010) has challenged the canonical view that the earliest planetary crusts were dominantly basaltic in composition. As rocks containing >70 modal percent sodic plagioclase, GRA 06128/9 represent a primordial felsic crust formed early in Solar System history - no later than 4517 ± 60 Ma (^{207}Pb - ^{206}Pb age; Day et al., 2009a) - and before metallic core formation within their parent body. The bulk chemistry of GRA 06128/9 reflects broadly andesitic compositions, similar to the composition of bulk terrestrial continental crust (Day et al., 2009a, 2009b).

Geochemical and petrological evidence indicates that GRA 06128/9 represent the crustal differentiation complements to olivine-dominated brachinites that represent melt-depleted mantle restites within a planetesimal (Day et al., 2012a). These similarities include overlap in oxygen mass-dependent isotope compositions, complementary petrology and trace-element geochemistry, similar oxidation conditions, and crystallization model ages of 2-3 Ma after the first Solar System solids (Arai et al., 2008; Day et al., 2009a, 2012a; Shearer et al., 2010; Zeigler et al., 2008). Brachinite-like achondrites, which have more magnesian compositions than brachinites, appear to be related by similar melt-depletion processes to brachinites, but are unlikely to derive from the same parent body, but point to similar processes acting on more than one asteroid (Day et al., 2012a).

Despite detailed petrological, geochemical and experimental studies on GRA 06128/9 (e.g., Day et al., 2009a; 2012a; Gardner-Vandy et al., 2013; Shearer et al., 2010), uncertainties remain in the formation mechanisms for GRA 06128/9, brachinites and brachinite-like achondrites. In particular, inter-element fractionations of highly siderophile elements in GRA 06128/9 and brachinites indicate complex melting processes and, possibly, more than a single-

stage process in their formation. Elucidating the mode of formation of asteroidal felsic crust is important not only for comparison with continental crust formation on Earth, but because early formation of felsic asteroidal crust offers a potential mechanism for the loss of radioactively generated heat within planetary bodies early in their history (Day et al., 2012a). This process would occur through the direct loss of ^{26}Al , a short-lived radioisotope (half life of 7.17×10^5 yrs) and likely the major source of heat during the initial stages of planetary melting (Mittlefehldt, 2007).

Iron isotopes have the potential to allow discrimination between models for asteroidal crust formation because of their potential to be fractionated during various magmatic differentiation processes, such as partial melting, mineral fractionation and fluid exsolution (Dauphas et al., 2009; Heimann et al., 2008; Liu et al., 2010; Poitrasson and Freydier, 2005; Schoenberg and von Blanckenburg, 2006; Schuessler et al., 2009; Sossi et al., 2012; Telus et al., 2012; Teng et al., 2008; Wang et al., 2012a; Weyer et al., 2005). In particular, iron isotopes can provide rigorous constraints on the origins of melts and melt residues from chondritic precursor materials because of the distinct Fe isotope fractionations observed between sulfide and metal phases (Needham et al., 2009). We show how Fe isotopes are powerful tracers of planetesimal differentiation processes and provide rigorous constraints on the style of partial melting responsible for GRA 06128/9, brachinites and brachinite-like achondrites.

6.2. Samples and Method

6.2.1. Sample Description

Iron isotope compositions for ungrouped achondrite stones GRA 06128, GRA 06129, six brachinites, three brachinite-like achondrites, and phase separates (metal, silicate and sulfide) from three ordinary chondrites (Tables 6-1 and 6-2) were analyzed in this study. Two geostandards, AGV-2 and BCR-2, were prepared and measured during the same analytical sessions with meteorite samples and are also reported.

Ungrouped achondrites GRA 06128/9 are paired feldspathic stony meteorites. They are coarse-grained stones with granoblastic textures and are dominated by sodic plagioclase (oligoclase; ~80 vol%), orthopyroxene and clinopyroxene (~10 vol%), Fe-rich olivine (~10 vol%), and minor amounts of Ca-phosphate (apatite and merrilite), sulfide (troilite and pentlandite) and FeNi metal (Arai et al., 2008; Day et al., 2012a, 2009a; Shearer et al., 2010; Zeigler et al., 2008). Their oxygen isotope and major/minor element bulk compositions show complementarity with brachinites, and are distinct from lunar anorthosites (Day et al., 2009a; Shearer et al., 2010; Zeigler et al., 2008). GRA 06128/9 was formed early in Solar System history, with a metamorphic age of 4517 ± 60 Ma (Day et al., 2009a), which is consistent with the 4565.9 ± 0.3 Ma age inferred from ^{26}Al - ^{26}Mg chronology (Shearer et al., 2008). The oxygen fugacity ($f\text{O}_2$) is estimated to be between iron-wüstite buffer (IW) -0.1 and IW +1.1 (Shearer et al., 2010). GRA 06128/9 is hypothesized to have formed by small degree (<30%) Fe-S bearing partial melting of a primitive, volatile-rich source region from an asteroid that had not fully differentiated a metallic core (Day et al., 2009a; Shearer et al., 2010).

Six brachinites were studied here: Brachina, Elephant Moraine (EET) 99402, Northwest Africa (NWA) 1500, NWA 3151, NWA 4872 and NWA 4882. Brachinites are dunitic wehrlites and they contain a majority of olivine (usually >80 vol%), with variable amounts of augite, chromite, Fe-sulfide, phosphate, and Fe-Ni metal (Day et al., 2012a; Mittlefehldt et al., 1998). Like GRA 06128/9, brachinites are ancient, with a ^{53}Mn - ^{53}Cr age of 4563.7 ± 0.9 Ma for Brachina (Wadhwa et al., 1998). It has previously been suggested that brachinites represent igneous cumulates (Mittlefehldt et al., 2003), but recent work indicates that they are partial melt residues (Day et al., 2012a).

Three ungrouped meteorites NWA 5400, NWA 6077 and Zag (b) (referred to as brachinite-like achondrites; Table 6-1) were also analyzed for their bulk Fe isotope compositions. They are all olivine dominated ultramafic achondrites, with similar mineralogy and geochemical composition to brachinites (Day et al., 2012a). NWA 5400 and NWA 6077 are possibly paired and they have an oxygen isotope composition close to the terrestrial fractionation line and are clearly distinct from brachinites (Day et al., 2012a). These differences in the oxygen isotope composition, as well as differences in the absolute and relative highly siderophile element abundances compared with brachinites, indicate that they were probably formed on different parent-bodies, but formed by similar partial melting processes (Day et al., 2012a).

Phase separations (metal, sulfide, silicate) were done on three extensively studied ordinary chondrite falls of various chemical class and petrologic type. Semarkona (LL3.0) is recognized as one of the least metamorphosed ordinary chondrites (Huss et al., 1981; Sears et al., 1980). Kernouve (H6) and Saint-Séverin (LL6) are two equilibrated ordinary chondrites.

6.2.2. Experimental and Analytical Method

Chemical purifications were undertaken in the clean laboratories at Washington University in St. Louis, or at the University of Chicago. The Fe isotope compositions were measured using a *Thermo Scientific Neptune* (in Chicago), or using a *Thermo Scientific Neptune Plus* (in St. Louis) multi-collector inductively-coupled-plasma mass-spectrometer (MC-ICP-MS; Tables 6-1 and 6-2). Data acquired for the same samples in both laboratories have identical values within the analytical uncertainties.

All samples were first ground to a fine powder with an agate pestle and mortar. The powders of GRA 06128/9, the brachinites, the brachinite-like meteorites, and the geostandards were then directly digested with a concentrated 4:1 acid mixture of HF and HNO₃ for three days at 180°C. For the three ordinary chondrites, the metals were first separated from the bulk powder with a hand magnet and then were digested with aqua regia. The non-magnetic fractions (which is mainly composed of silicates and sulfide) were first treated with cold 3N HCl for 6 hours to ensure dissolution of sulfides with a minimum dissolution of silicates (we cannot exclude the possibility that a minor fraction of the silicates were dissolved at this stage). This is a procedure adapted from Luck et al. (2005) and that was used in Moynier et al. (2011) to separate metal, sulfide and silicate from enstatite chondrites. The sulfide-bearing solutions were separated from the silicate residue and the residue was rinsed several times with water, dried and digested with concentrated HF/HNO₃. The bulk samples, dry metal and silicate fractions were weighed, and the masses of sulfide fractions were calculated by difference (Table 6-2). The masses represent the relative abundances of metals, silicates and sulfides in each ordinary chondrite (see Table 6-3). We note that this phase separation procedure is not perfect. Torigoye and Shima (1993) have examined phases separated by hand-magnet using binocular microscope and observed fine

silicate grains attached to metals. Hence, Fe isotope fractionation effects between metal, silicate and sulfide in chondrites are likely to be more extreme than the reported values.

All samples (bulk and mineral separate fractions) were re-digested with 6N HCl before being loaded onto chemical separation columns. We followed the same Fe purification and mass-spectrometer procedure that we used in Wang et al. (2011, 2012a, 2012b; 2013). Iron was separated from matrix elements in 6N HCl with 1 mL AG1-X8 200-400 mesh anion-exchange resin. Fe was then eluted from the resin in 0.4N HCl. This chemical separation procedure was done twice for each sample to maximize removal of matrix elements.

Samples were introduced into the MC-ICP-MS with a 100 μ L/min PFA MicroFlow nebulizer and a cyclonic spray chamber. The intensities of ^{54}Fe , ^{56}Fe and ^{57}Fe were measured on the peak shoulders with Faraday cups L2, C, and H1, respectively, to avoid the Ar-based polyatomic interferences. Isobaric interferences from ^{54}Cr were monitored as ^{53}Cr on Faraday cup L3. We used medium mass resolution and the resolving power ($M/\Delta M$) was ~ 8500 . To circumvent the instrumental bias, we used a sample-standard technique with IRMM-014 as the reference standard. Data are reported as $\delta^{56}\text{Fe}$ and $\delta^{57}\text{Fe}$, where $\delta^{56/57}\text{Fe} = [({}^{56/57}\text{Fe}/{}^{54}\text{Fe})_{\text{sample}}/({}^{56/57}\text{Fe}/{}^{54}\text{Fe})_{\text{IRMM-014}} - 1] \times 1000$ and are reported as *per mille* units (‰). Errors in this study are reported as 2 standard errors, which are calculated as the standard deviation divided by the square root of the total number of analyses and multiplied by the Student's *t*-value for the relevant degree of freedom at the 95% confidence level. All data fall on the mass dependent fractionation line, within total analytical uncertainties (Figure 6-1).

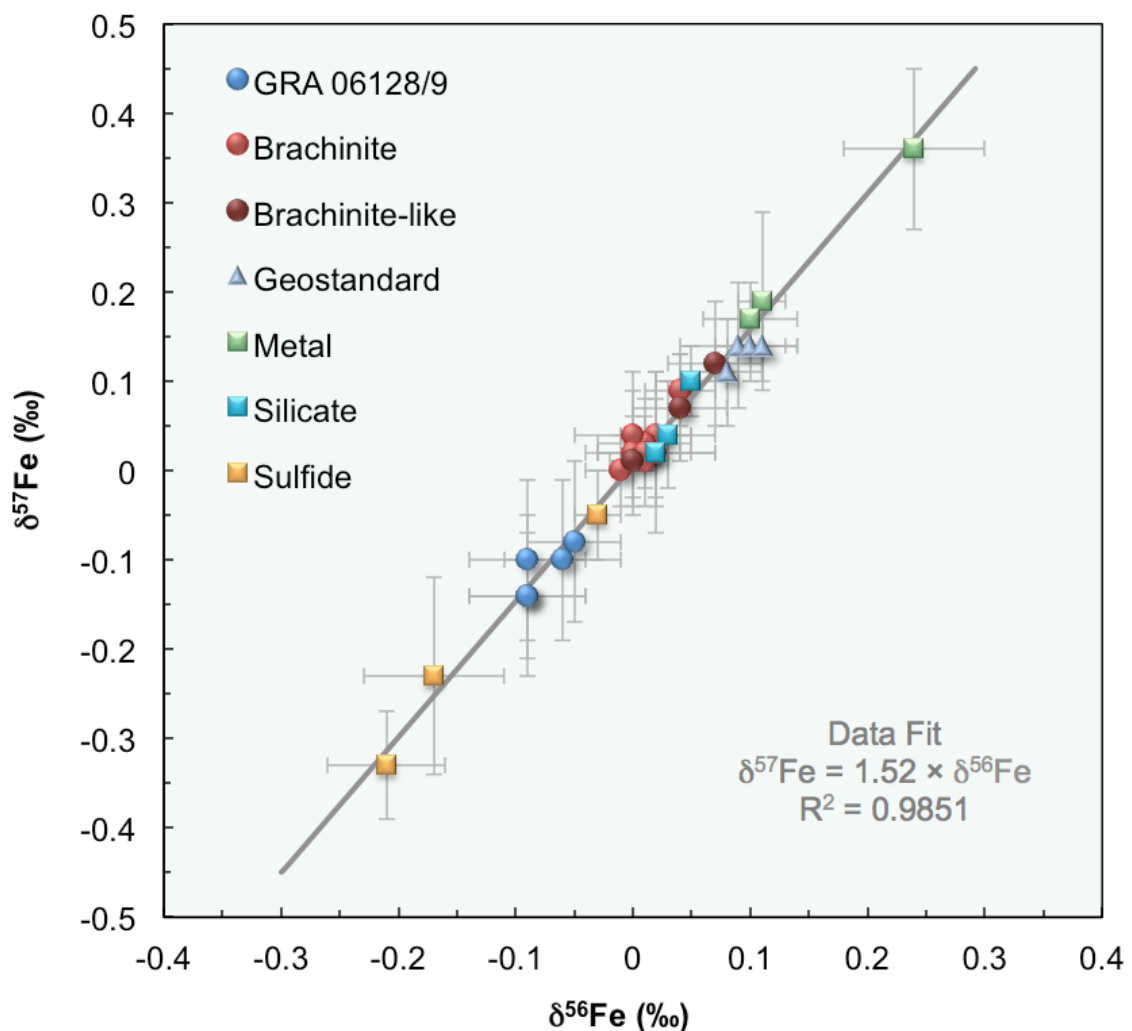


Figure 6-1. Iron isotope compositions of all samples analyzed in this study, shown in three-isotope ($\delta^{57}\text{Fe}$ vs. $\delta^{56}\text{Fe}$) space. All data fall onto the mass-dependent fractionation line of slope ~ 1.5 .

Table 6-1. Iron isotope compositions of GRA 06128/9, brachinites and brachinite-like achondrites

Sample	Type	Fall/Find	Mass [mg]	Fe [wt.%]	$\delta^{56}\text{Fe}$	2SE ^a	$\delta^{57}\text{Fe}$	2SE ^a	n ^b	Laboratory ^c
GRA 06128 #1	Ungrouped	Find	1.8	3.2	-0.05	± 0.04	-0.08	± 0.09	7	Chicago
GRA 06128 #2	Ungrouped	Find			-0.09	± 0.05	-0.14	± 0.09	9	Chicago
GRA 06129 #1	Ungrouped	Find	13.3	5.6	-0.06	± 0.05	-0.10	± 0.09	9	Chicago
GRA 06129 #2	Ungrouped	Find			-0.09	± 0.05	-0.10	± 0.09	9	Chicago
GRA 06129 #3	Ungrouped	Find	4.0	5.4	-0.09	± 0.05	-0.14	± 0.07	9	Chicago
Average					-0.08	± 0.06	-0.11	± 0.05	2	
Range _(max-min)					0.04		0.06			
Brachina #1	Brachinite	Find			0.02	± 0.03	0.04	± 0.07	9	Chicago
Brachina #2	Brachinite	Find			0.02	± 0.05	0.02	± 0.09	9	Chicago
Brachina #3	Brachinite	Find	3.7	20.0 ^d	0.01	± 0.04	0.03	± 0.03	12	St. Louis
EET 99402 #1	Brachinite	Find	2.1	19.9	0.00	± 0.05	0.04	± 0.07	9	Chicago
EET 99402 #2	Brachinite	Find	4.0	20.8 ^d	-0.01	± 0.03	0.00	± 0.04	12	St. Louis
NWA 1500	Brachinite	Find	8.6	23.9 ^d	0.01	± 0.02	0.01	± 0.03	11	St. Louis
NWA 3151	Brachinite	Find	4.0	29.2 ^d	0.00	± 0.04	0.02	± 0.07	13	St. Louis
NWA 4872	Brachinite	Find	9.5	25.6 ^d	0.04	± 0.03	0.09	± 0.04	11	St. Louis
NWA 4882	Brachinite	Find	3.1	23.5 ^d	0.01	± 0.04	0.02	± 0.06	14	St. Louis
Average					0.01	± 0.02	0.03	± 0.03	6	
Range _(max-min)					0.05		0.09			
NWA 5400	Brachinite-like	Find	4.6	19.6 ^d	0.00	± 0.02	0.01	± 0.05	10	St. Louis
NWA 6077	Brachinite-like	Find	4.7	20.9 ^d	0.04	± 0.04	0.07	± 0.06	12	St. Louis
Zag (b)	Brachinite-like	Find	6.0	20.9 ^d	0.07	± 0.04	0.12	± 0.07	13	St. Louis
AGV-2	Andesite	Geostandard	15.3		0.09	± 0.05	0.14	± 0.07	9	Chicago
AGV-2	Andesite	Geostandard	9.9		0.10	± 0.03	0.14	± 0.04	13	St. Louis
BCR-2	Basalt	Geostandard	5.1		0.11	± 0.03	0.14	± 0.04	13	St. Louis

^a Standard errors (2SE = standard deviation divided by the square root of the total number of analyses and multiplied by Student's *t*-value for the relevant degree of freedom at the 95% confidence level).

^b The number of analyses or number of individual meteorite samples for the group means.

^c Chicago = University of Chicago; St. Louis = Washington University in St. Louis.

^d These samples are from the same digestions of Day et al. (2012) and the concentrations have been reported therein.

Table 6-2. Iron isotope compositions of magnetic (metal), non-magnetic (sulfide) and non-magnetic (silicate) fractions of three ordinary chondrites

<i>Sample</i>	<i>Type</i>	<i>Fall/Find</i>	<i>Mass [mg]</i>	<i>Fe [wt.%]</i>	$\delta^{56}\text{Fe}$	<i>2SE^a</i>	$\delta^{57}\text{Fe}$	<i>2SE^a</i>	<i>n^b</i>	<i>Laboratory^c</i>		
Semarkona												
Magnetic (metal)	LL3.0	Fall	8.1	24.1	0.11	±	0.02	0.19	±	0.10	9	St. Louis
Non-magnetic (silicate)	LL3.0	Fall	16.8	5.6	0.03	±	0.04	0.04	±	0.06	8	St. Louis
Non-magnetic (sulfide)	LL3.0	Fall	6.2	18.0	-0.17	±	0.06	-0.23	±	0.11	8	St. Louis
Kernouve												
Magnetic (metal)	H6	Fall	15.8	35.8	0.10	±	0.04	0.17	±	0.04	6	St. Louis
Non-magnetic (silicate)	H6	Fall	25.6	8.0	0.02	±	0.05	0.02	±	0.06	7	St. Louis
Non-magnetic (sulfide)	H6	Fall	3.6	25.3	-0.21	±	0.05	-0.33	±	0.06	8	St. Louis
Saint-Séverin												
Magnetic (metal)	LL6	Fall	3.4	25.0	0.24	±	0.06	0.36	±	0.09	7	St. Louis
Non-magnetic (silicate)	LL6	Fall	28.4	11.6	0.05	±	0.03	0.10	±	0.04	6	St. Louis
Non-magnetic (sulfide)	LL6	Fall	19.6	27.8	-0.03	±	0.02	-0.05	±	0.05	7	St. Louis
BCR-2	Basalt	Geostandard	10.5	7.6	0.08	±	0.03	0.11	±	0.06	10	St. Louis

^a Standard errors (2SE = standard deviation divided by the square root of the total number of analyses and multiplied by Student's *t*-value for the relevant degree of freedom at the 95% confidence level).

^b Number of analyses.

^c St. Louis = Washington University in St. Louis.

Table 6-3. The modal bulk iron isotope compositions of ordinary chondrites

<i>Sample</i>	<i>Type</i>	<i>Metal [wt.%]</i>	<i>Silicate [wt.%]</i>	<i>Sulfide [wt.%]</i>	<i>Fe in Metal [%]</i>	<i>Fe in Silicate [%]</i>	<i>Fe in Sulfide [%]</i>	<i>Modal Bulk $\delta^{56}\text{Fe}$</i>	<i>Literature</i>
Seemarkona	LL3.0	26.1	54.0	19.9	48.8	23.4	27.9	0.01	$0.02 \pm 0.06^{\text{a}}$
Kernouve	H6	35.1	56.9	8.0	65.6	23.8	10.6	0.05	or $-0.14 \pm 0.02^{\text{b}}$
Saint-Séverin	LL6	6.6	55.3	38.1	8.9	34.4	56.8	0.02	$0.01 \pm 0.04^{\text{a}}$

^a From Dauphas et al. (2009)

^b From Needham et al. (2009)

6.3. Results

6.3.1. Iron Isotope Compositions of GRA 06128/9, Brachinites and Brachinite-Like Achondrites

The average $\delta^{56}\text{Fe}$ of brachinites and brachinite-like achondrites is $+0.01 \pm 0.02\text{\textperthousand}$ (range from -0.01 to $0.04\text{\textperthousand}$), similar to values obtained for bulk chondrites, a variety of planetary achondrites, and terrestrial mantle peridotites (Figure 6-2). Brachinite-like achondrites NWA 5400 and NWA 6077 have indistinguishable Fe isotope compositions from brachinites, within analytical errors, whereas Zag (b) is slightly isotopically heavier ($\delta^{56}\text{Fe} = 0.07 \pm 0.04\text{\textperthousand}$). GRA 06128/9 are the first crustal samples from any planetary body in the Solar System that are depleted in the heavy isotopes of Fe compared to chondrites ($\delta^{56}\text{Fe} = -0.08 \pm 0.06\text{\textperthousand}$; range from -0.09 to -0.05). GRA 06128/9 also show a difference in Fe isotope composition with brachinites that is well resolved within analytical uncertainty (see Table 6-1 and Figure 6-2).

6.3.2. Iron Isotope Compositions of Metal, Sulfide and Silicate Fractions of Ordinary Chondrites

Phase separations from three ordinary chondrites (LL3.0, L6, and H6) all show the same Fe isotope fractionation behavior: $\delta^{56}\text{Fe}_{\text{metal}} > \delta^{56}\text{Fe}_{\text{silicate}} > \delta^{56}\text{Fe}_{\text{sulfide}}$ (see Table 6-2 and Figure 6-3) and $\delta^{56}\text{Fe}_{\text{metal}} - \delta^{56}\text{Fe}_{\text{sulfide}} \approx 0.3\text{\textperthousand}$. The average $\delta^{56}\text{Fe}$ value of the metals, sulfides and silicates separated from the three ordinary chondrites is $0.15\text{\textperthousand}$ (range from 0.10 to $0.24\text{\textperthousand}$), $-0.14\text{\textperthousand}$ (range from -0.21 to $-0.03\text{\textperthousand}$) and $0.03\text{\textperthousand}$ (range from 0.02 to $0.05\text{\textperthousand}$), respectively. These average values are consistent with the ranges observed in previous studies of mineral phases in ordinary chondrites (Needham et al., 2009; Okabayashi et al., 2012; Theis et al., 2008). Needham et al. (2009) reported micro-drilling experiments on the Parnallae LL3.6 ordinary chondrite,

obtaining more extreme isotopic fractionation between mineral phases than reported in this study (Figure 6-3). This difference likely reflects the imperfect nature of the magnetic and leaching separation procedure used in this study. However, the method that we employed has the advantage that it is possible to perform a precise gravimetric mass-balance to understand the total Fe isotope budget of samples (Table 6-3).

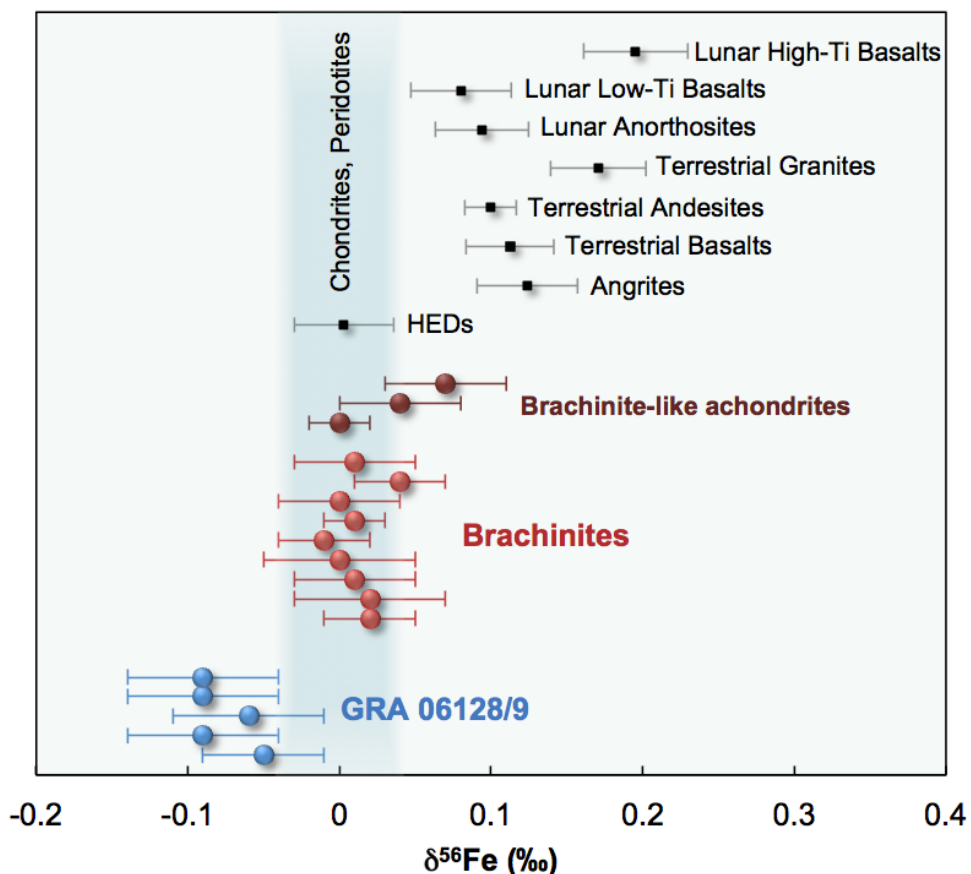


Figure 6-2. Iron isotope compositions (as $\delta^{56}\text{Fe}$) for GRA 06128/9, brachinites and brachinitelike achondrites. The chondritic and terrestrial mantle value, and its associated uncertainty, is shown in blue shade and average values for typical terrestrial, lunar rocks, HED and angrite meteorites are also plotted for comparison. All uncertainties in this study are reported as two standard errors, and those in literatures are reported as two sigma standard deviations. Published data are from: carbonaceous chondrites (Wang et al., 2013); terrestrial peridotites (Craddock and Dauphas, 2011; Craddock et al., 2013; Weyer and Ionov, 2007); terrestrial basalts and andesites (Craddock and Dauphas, 2011; Dauphas et al., 2009; Poitrasson et al., 2004; Schoenberg and von Blanckenburg, 2006; Weyer and Ionov, 2007; Weyer et al., 2005); terrestrial granites (Poitrasson and Freyder, 2005; Telus et al., 2012); lunar basalts and anorthosites (Liu et al., 2010; Poitrasson et al., 2004; Weyer et al., 2005); HED and angrite meteorites (Wang et al., 2012a).

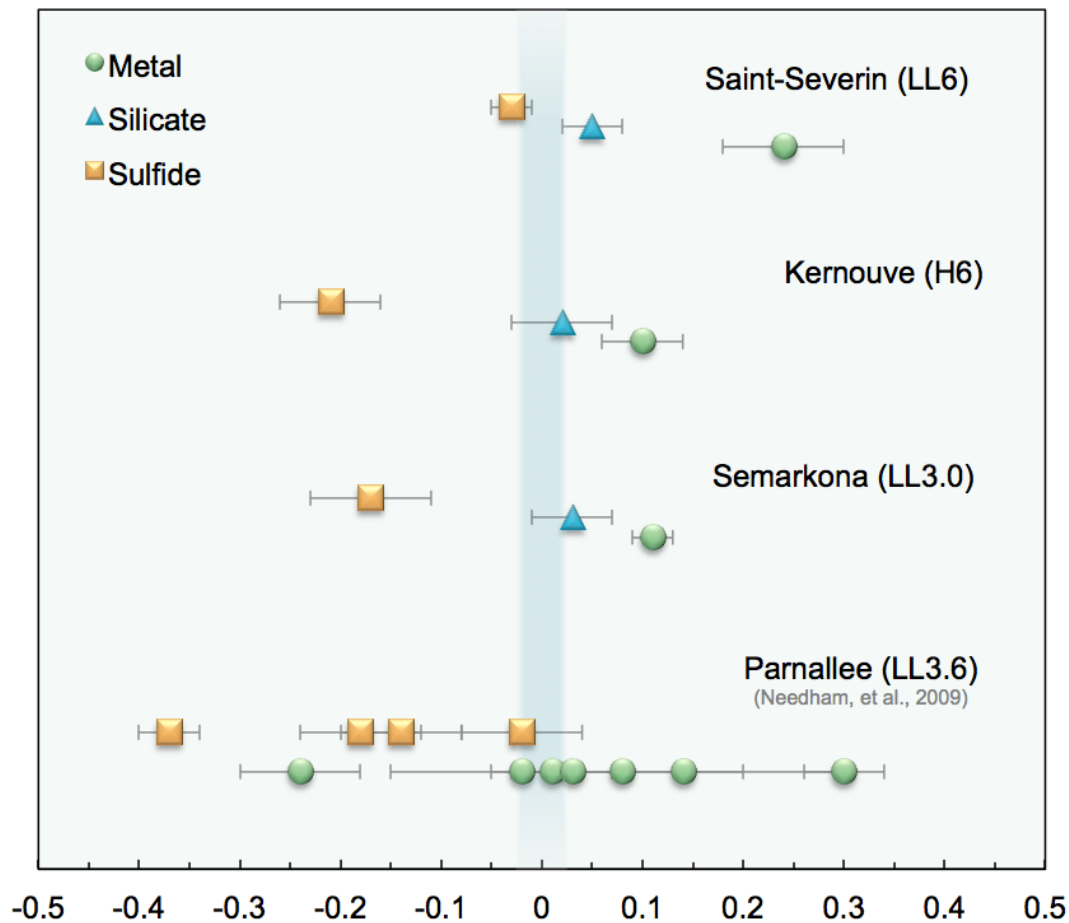


Figure 6-3. Iron isotope compositions for magnetic (metal), non-magnetic (sulfide) and non-magnetic (silicate) fractions of three ordinary chondrites measured in this study. Literature data from Needham et al. (2009) are plotted for comparison.

6.4. Discussion

6.4.1. Sulfide Control on Enrichment of Light Iron Isotopes in GRA 06128/9

GRA 06128/9 have the only negative $\delta^{56}\text{Fe}$ value ($-0.08 \pm 0.06\text{\textperthousand}$) among all known planetary crust materials (see Figure 6-2). In comparison, terrestrial felsic crustal materials (*e.g.*, andesites and granitoids) all have heavy Fe isotope enrichments ($\delta^{56}\text{Fe} = >0.1\text{\textperthousand}$; *e.g.*, Craddock and Dauphas, 2011; Poitrasson and Freydier, 2005; Telus et al., 2012). Basaltic crustal rocks from Mars and the majority of HED meteorites (excluding the incompatible enriched Stannern-trend eucrites) have Fe isotope compositions identical to carbonaceous chondrites ($\delta^{56}\text{Fe} \sim 0.0\text{\textperthousand}$; *e.g.*, Poitrasson et al., 2004; Wang et al., 2012a, 2013) and basaltic crustal materials from the Moon, the angrite parent body and from terrestrial mid-ocean ridges are enriched in the heavier isotopes of Fe with $\delta^{56}\text{Fe}$ values of $\sim 0.1\text{\textperthousand}$, or higher (Dauphas et al., 2009; Liu et al., 2010; Poitrasson et al., 2004; Teng et al., 2013; Wang et al., 2012a).

Negative $\delta^{56}\text{Fe}$ isotope compositions have previously been reported in sulfide phases (troilite and pentlandite) separated from ordinary chondrites ($\delta^{56}\text{Fe}: -0.02$ to $-0.37\text{\textperthousand}$; Theis et al., 2008; Needham et al., 2009), pallasites ($\delta^{56}\text{Fe}: -0.21\text{\textperthousand}$ to $-0.30\text{\textperthousand}$; Weyer et al., 2005) and iron meteorites ($\delta^{56}\text{Fe}: -0.10\text{\textperthousand}$ to $-0.45\text{\textperthousand}$; Williams et al., 2006). The new Fe isotope results for ordinary chondrites of various Fe-content and metamorphic grade (LL3.0, L6, and H6) confirm prior observations, with an Fe isotope fractionation pattern of: $\delta^{56}\text{Fe}_{\text{metal}} > \delta^{56}\text{Fe}_{\text{silicate}} > \delta^{56}\text{Fe}_{\text{sulfide}}$ (Figure 6-3), and sulfide compositions ranging from -0.03 to $-0.21\text{\textperthousand}$. The new result lie within the extremes of Fe isotope fractionation observed by micro-drilling and hand-separation from crushed samples by Needham et al. (2009). Therefore, different phase separation procedures (*c.f.*, this study and Needham et al., 2009) do not induce detectable Fe isotope effects.

To further test the validity of the ordinary chondrite phase separate data, we calculated modal bulk Fe isotope compositions based on the abundances, Fe concentrations and Fe isotope compositions of the metal, silicate and sulfide fractions (Table 6-3). Two of these three calculated modal compositions are consistent with previous measurements of the bulk samples (Dauphas et al., 2009), however the Kernouve value differs from that reported by Needham et al. (2009). Wang et al. (2013) have observed that individual ordinary chondrites can exhibit large Fe isotopic variations, probably due to the phase distribution effect, where uneven distributions of phases in bulk-rock fragments leads to different apparent Fe isotope ratios.

The new and published data for sulfides (mainly troilites) in chondrites are also consistent with theoretical calculations of Fe isotope fractionation. Equilibrium Fe isotope fractionation factors (*i.e.*, reduced partition function ratios β -factors) can be evaluated from Mössbauer spectroscopy data or synchrotron inelastic nuclear resonant X-ray scattering data (Polyakov et al., 2007; Polyakov and Soltanov, 2011). These theoretical calculations have extended the temperature-pressure range and species over existing limitations of laboratory experiments, and have confirmed that troilite is enriched in the lighter Fe isotopes compared with metal and silicate minerals.

6.4.2. Formation of Sulfide-rich Felsic Partial-melts in Planetesimals

It has been proposed that GRA06128/9 was formed from Fe-S- and felsic-rich low-degree (<30%) partial melting of a chondritic parent body prior to any core formation event (Day et al., 2009a, 2012a; Garner-Vandy et al., 2013). The light Fe isotope enrichment of GRA 06128/9 provides strong support for this mechanism, where sulfide-rich melt (negative $\delta^{56}\text{Fe}$ signature) formed during partial melting of chondritic precursor materials. In order to approximate this

process, we have calculated the initial melt reservoir generated from preferential consumption of sulfide minerals from chondritic precursors (Figure 6-4; see Table 6-4 for modeling parameters used). Since the separation procedure for metal, sulfide and silicate in chondrites is imperfect and the measured fractionation can only represent the minimum value, we use the largest Fe isotope fractionations of metals ($\delta^{56}\text{Fe} = 0.24\text{\textperthousand}$) and sulfides ($\delta^{56}\text{Fe} = -0.21\text{\textperthousand}$) observed in this study.

Table 6-4. Parameters and values used in the non-modal melting modeling of ordinary chondrites

	Sulfide	Metal	Silicate
Mineral	Troilite	Kamacite	Olivine + enstatite
Density (g/cm ³)	4.6	7.9	3.3
[Fe] wt.%	63.53	89.54	10
$\delta^{56}\text{Fe}$	-0.21	0.24	0

To obtain the Fe isotope composition of GRA 06128/9, preferential melting of sulfide relative to metal (sulfide to metal ratio varies from 5:1 to 10:1 in volume) is required (Figure 6-4). The invoked sulfide-preferential melting model is in agreement with low-temperature and low-degree partial melting experiments of chondritic materials (*e.g.*, Keil, 2000; McCoy et al., 1997). These experiments have shown that low-degrees of melting form Fe-S-rich melts, whereas higher degrees of melting at higher temperatures form basaltic melts (McCoy et al., 1997). For example, at $\sim 980\text{ }^{\circ}\text{C}$, the melts of low-degree partial melting of chondritic precursor materials consist of 85 wt.% sulfide and 15 wt.% metal, while silicate melt (basaltic) does not occur until $\sim 1050\text{ }^{\circ}\text{C}$ (Keil, 2000). This 85:15 ratio ($\sim 9:1$ in volume) of sulfide and metal from experiments agrees well with the predictions from our model. Our model is also consistent with the bulk felsic composition of the GRA 06128/9. A highly siliceous (up to ~ 95 vol.% silicate) melt can form a Fe isotopic composition identical to those of GRA 06128/9 if the sulfide is significantly enriched compared to metal in the melt (Figure 6-4). Melt generation ($< 1000\text{ }^{\circ}\text{C}$)

occurred prior to the onset of higher temperature, basaltic melting and led to the generation of buoyant felsic melt with a strong Fe-S signature. This model is also consistent with elevated highly siderophile element abundances in GRA 06128/9, as well as the cessation of melting in some planetesimals because of the effective removal of the major radioactive heat-source, ^{26}Al .

Since our model has emphasized the importance of the preferential consumption of sulfide minerals over Fe metals from chondritic precursors, it provides no constraint on the absolute proportion of sulfide minerals. Previous work has shown that melting in planetesimals is inefficient, with brachinites exhibiting a large range in rare earth element abundances due to variable retention of melts (Day et al., 2012a). In order to assess density constraints on the generation of sulfide-rich felsic melts in low gravity environments, such as planetesimals, we have also estimated the average density of Fe-S-rich melts (see Figure 6-5). The average densities of common ordinary and carbonaceous chondrites have been plotted as reference lines on Figure 6-4 (Consolmagno et al., 2008). Areas on the right of the chondritic reference lines are the forbidden zones according to simple density considerations, while areas on the left are the maximum sulfide/metal allowed with only consideration of density. These simple calculations indicate low maximum proportions of metal and sulfide assuming a carbonaceous or metal-poor R chondrite precursor composition (*e.g.*, Gardner-Vandy et al., 2013).

The light Fe isotopic composition of GRA 06128/9 can be explained as the result of crystallizing and/or plagioclase accumulation from a Fe-S-rich felsic melt with similar composition to the 10-15% degree partial melting of an ordinary or R-type chondrite (Feldstein et al., 2001; Gardner-Vandy et al., 2013). By mixing 60% of the melt composition provided in Feldstein et al. (2001) with 40% plagioclase measured by Day et al. (2012a), we can reproduce the major element composition of GRA 06128/9 (Table 6-5). Since plagioclase is nominally Fe

free (in reality, very low Fe; see Table 6-5), the Fe isotopic composition (negative $\delta^{56}\text{Fe}$) of GRA 06128/9 is largely inherited from the melt. Our new mixing model is entirely consistent with estimates of partial melting from rare earth elements (13-30%), to form GRA 06128/9 (Day et al., 2012a). Simple mass balance (*c.f.*, a preponderance of silicate) means that low-degree partial melting will not significantly change the Fe concentration or isotopic composition of the source. Therefore, the residual mantle of the GRA 06128/9 parent-body would not be isotopically fractionated compared to chondrites ($\delta^{56}\text{Fe} \sim 0$), as is observed for brachinites ($\delta^{56}\text{Fe} = 0.01 \pm 0.02\text{\%}$).

Table 6-5. Major element mixing model of GRA 06128/9

	<i>Melt^a</i>	<i>Plagioclase^b</i>	<i>60% Melt +40% Plagioclase</i>	<i>Bulk^b</i>	<i>2SD^b</i>
SiO ₂	51.73	65.22	57.12	55.98	\pm 1.93
TiO ₂	0.44	0.00	0.26	0.11	\pm 0.16
Al ₂ O ₃	12.75	21.49	16.25	16.29	\pm 3.14
Cr ₂ O ₃	0.30	0.00	0.18	0.09	\pm 0.10
MgO	8.13	0.03	4.89	3.28	\pm 2.46
CaO	8.36	2.94	6.19	6.07	\pm 1.25
MnO	0.32	0.00	0.19	0.11	\pm 0.08
FeO	16.30	0.13	9.83	9.74	\pm 3.06
Na ₂ O	0.97	9.86	4.53	5.95	\pm 1.41
K ₂ O	0.28	0.33	0.30	0.23	\pm 0.03
P ₂ O ₅	0.40	0.00	0.24	2.12	\pm 0.99
Cl	0.01	0.00	0.01	0.04	\pm 0.13
<i>Sum</i>	99.99	100.00	99.99	100.01	

^a 12.6% degree partial melting product of Leedey L6 chondrites from Feldstein et al. (2001)

^b From Day et al. (2012)

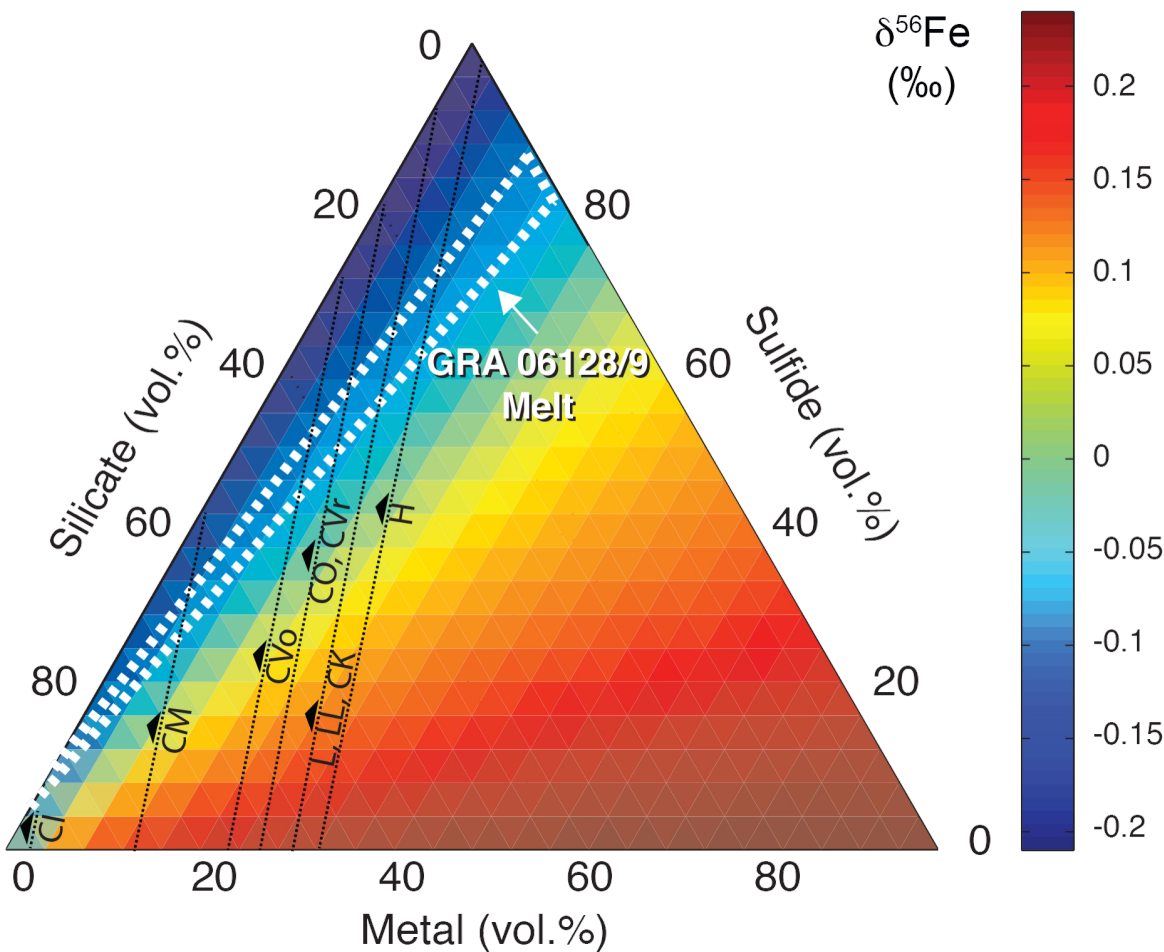


Figure 6-4. Ternary diagram showing the Fe isotope compositions of melts composed of varying proportions of silicate, metal and sulfide phases from chondritic precursors. This mass-balance diagram shows the composition of initial melt, and the sulfide/metal ratio; while the felsic composition reflects silicate melt segregation to form GRA 06128/9. The density considerations are also plotted for different types of ordinary and carbonaceous chondrites. Please refer to main text for details.

6.4.3. Implications for Highly Siderophile Element Fractionation during Melting

As demonstrated by the models above, initial melts from chondritic precursors can be enriched in the light isotopes of Fe due to preferential melting of sulfides. Sulfide minerals, such as troilite and pentlandite, are the main carriers of highly siderophile elements (HSE: Os, Ir, Ru,

Rh, Pt, Pd, Re, Au) in GRA 06128/9 (Day et al., 2012a). The elevated HSE contents of GRA 06128/9, brachinites and brachinite-like achondrites - within factors of approximately one to three of chondritic abundances - are consistent with partial melting processes prior to core formation (Day et al., 2009a; 2012a) and contrast strongly with the low HSE abundances of early-formed felsic and basaltic materials from the Moon and other planetesimal bodies (*e.g.*, Day et al., 2010; 2012b; Riches et al., 2012).

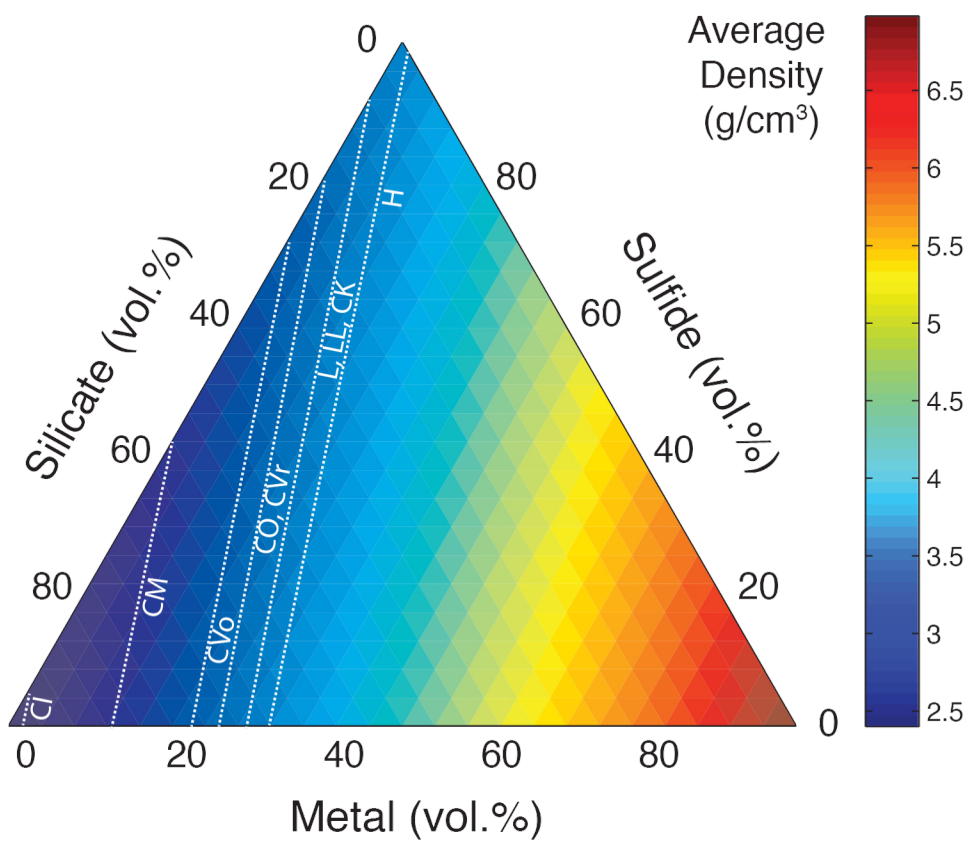


Figure 6-5. Average density of Fe-S-rich melts.

A unique aspect of the HSE abundances for GRA 06128/9 and brachinites is their strongly fractionated patterns, with low Ir, Pt and Pd relative to Ru (Day et al., 2012a). This unusual fractionation cannot be modeled with standard liquid metal-solid metal partitioning in

Fe-S systems (*e.g.*, Chabot & Jones, 2003), but instead requires either: (1) multiple phases in the residue; (2) two-stage melt fractionation; (3) fractional fusion, or (4) a non-chondritic starting composition (Day et al., 2012a). The new iron isotope data has some bearing on this conundrum. The new Fe isotope results do not indicate a non-chondritic starting composition or two-stage melt fractionation. Instead, the new data can most simply be explained by preferential consumption of sulfide and processes more akin to fractional fusion or inefficient melt removal and metal/sulfide retention in the GRA 06128/9 melt source regions. This is because the Fe isotope composition of GRA 06128/9 only requires a single-stage melting process where sulfide-rich felsic melt is inefficiently extracted from the melt region. Similarly, the HSE and REE patterns of both GRA 06128/9 and brachinites indicate inefficient melt extraction and complex liquid metal/sulfide-solid metal/sulfide partitioning behavior.

6.4.4. Planetary Crust Comparisons

GRA 06128/9 and brachinites are currently the only extra-terrestrial felsic crust/mantle materials considered to come from the same parent body (Day et al., 2012a). Therefore they represent a key sample suite for inter-planetary comparison to understand early crust formation. Other early asteroidal crusts formed at a comparable time period, such as basaltic angrites or HEDs. However these samples show completely different Fe isotopic fractionation behavior. Partial melting experiments of carbonaceous chondrites have shown that HEDs-like melts are formed at low f_{O_2} while angrite-like melts are formed at high f_{O_2} (Jurewicz et al., 1991, 1993). Primitive chondritic materials, including carbonaceous, ordinary and enstatite chondrites all have a bulk $\delta^{56}\text{Fe}$ value of $\sim 0\text{\textperthousand}$ (Craddock and Dauphas, 2011; Needham et al., 2009; Wang et al., 2013). While HEDs meteorites (except Stannern-trend eucrites) have an Fe isotope composition indistinguishable from chondrites; angrites are enriched in heavy Fe isotopes, up to $\delta^{56}\text{Fe} \sim$

+0.12‰ (Wang et al., 2012a). These differences of Fe isotopic composition between angrite and HEDs basaltic crustal samples are principally controlled by the oxygen fugacities prevailing at the time of formation. Oxidation state is the main parameter, which controls the Fe isotopic fractionation during higher degree ‘basaltic’ partial melting conditions (Wang et al., 2012a).

In contrast, we show that for low-degree partial melting of chondritic precursors, preferential segregation of isotopically fractionated sulfides controls the Fe isotope composition of the melt and therefore of the accumulated crust. The Fe-S rich melt is characterized not only by a significantly negative $\delta^{56}\text{Fe}$ signature, but also with HSE abundances similar to chondritic abundances, where both features are closely linked with their compatibilities within sulfide minerals. Our results indicate that iron isotopes, in conjunction with other isotopic and elemental tracers (*e.g.*, HSE abundances) have the potential to record mechanisms of early crust formation processes with fidelity (see Figure 6-6).

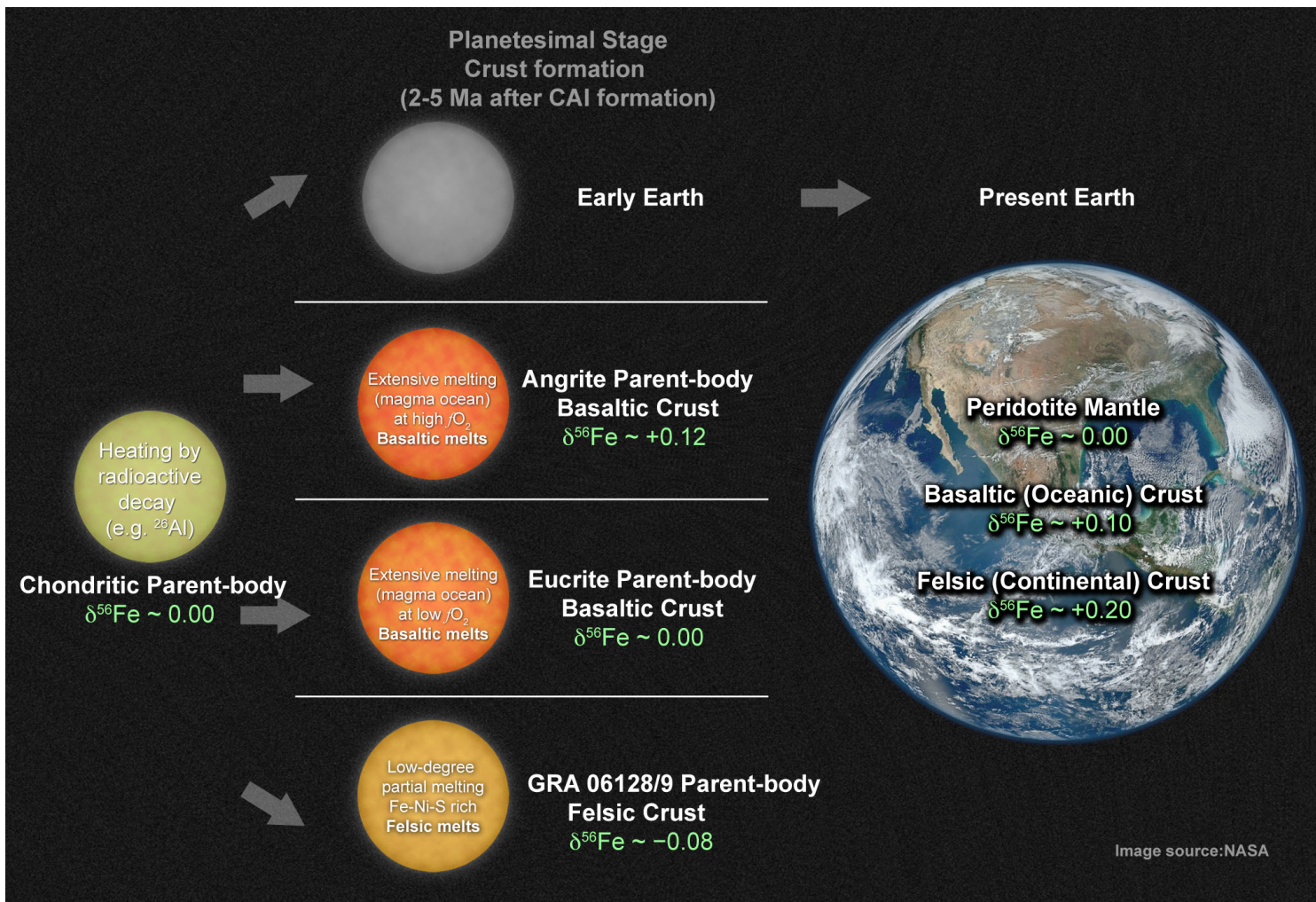


Figure 6-6. Schematic diagram showing iron isotope fractionations in three different types of early Solar System planetary crusts.

6.5. Conclusions

The paired meteorites GRA 06128 and 06129 (GRA 06128/9) are the only example of evolved felsic crust-type materials outside of Earth's continental crust. Remarkably, GRA 06128/9 are also the first example of crust with isotopically light Fe ($\delta^{56}\text{Fe} = -0.08 \pm 0.06\text{\textperthousand}$). We also report the Fe isotope compositions of brachinites and brachinite-like achondrite meteorites that are considered to represent mantle residuum after felsic crustal melt extraction to form GRA 06128/9-like melt compositions on asteroidal parent bodies. The new results show that: 1) even though GRA 06128/9 and brachinites have similar oxygen isotope compositions, they have different Fe isotope compositions and 2) GRA 06128/9 is enriched in the lighter isotopes compared to chondrites, while brachinites have $\delta^{56}\text{Fe} = 0.01 \pm 0.02\text{\textperthousand}$, similar to chondrites.

New metal, silicate and sulfide phase separations reinforce previous studies and show that sulfide phases are universally enriched in lighter Fe isotopes ($\delta^{56}\text{Fe} = -0.14\text{\textperthousand}$) compared with metals ($\delta^{56}\text{Fe} = 0.15\text{\textperthousand}$) and silicates ($\delta^{56}\text{Fe} = 0.03\text{\textperthousand}$). The unique negative Fe isotope composition of GRA 06128/9 can be best explained as being inherited from preferential melting of sulfide phases from chondritic precursors, forming an Fe-S-rich felsic melt by low-degree (<30%) partial melting. This conclusion is consistent with previous studies of highly siderophile elements (HSE) in GRA 06128/9 and brachinites.

References

- Amelin Y. (2008) U–Pb ages of angrites. *Geochim. Cosmochim. Acta* **72**, 221–232.
- Arai T., Tomiyama T., Saiki K. and Takeda H. (2008) Unique achondrites GRA 06128/06129: Andesitic partial melt from a volatile-rich parent body. *Lunar Planet. Sci. XXXIX*. Lunar Planet. Inst., Houston. #2465 (abstr.).
- Blichert-Toft J., Boyet M., Télouk P. and Albarède F. (2002) ^{147}Sm – ^{143}Nd and ^{176}Lu – ^{176}Hf in eucrites and the differentiation of the HED parent body. *Earth Planet. Sci. Lett.* **204**, 167–181.
- Chabot, N.L. and Jones, J.H. (2003) The parameterization of solid metal–liquid metal partitioning of siderophile elements. *Meteorit. Planet. Sci.* **38**, 1425–1436.
- Cohen B. A., Goodrich C. A. and Keil K. (2004) Feldspathic clast populations in polymict ureilites: Stalking the missing basalts from the ureilite parent body. *Geochim. Cosmochim. Acta* **68**, 4249–4266.
- Consolmagno, G.J., Britt, D.T. and Macke, R.J. (2008) The significance of meteorite density and porosity. *Chemie der Erde* **68**, 1–29.
- Craddock P. R. and Dauphas N. (2011) Iron isotopic compositions of geological reference materials and chondrites. *Geostand. Geoanal. Res.* **35**, 101–123.
- Craddock P. R., Warren J. M. and Dauphas N. (2013) Abyssal peridotites reveal the near-chondritic Fe isotopic composition of the Earth. *Earth Planet. Sci. Lett.* **365**, 63–76.
- Dauphas N., Craddock P. R., Asimow P. D., Bennett V. C., Nutman A. P. and Ohnenstetter D. (2009) Iron isotopes may reveal the redox conditions of mantle melting from Archean to Present. *Earth Planet. Sci. Lett.* **288**, 255–267.
- Day J. M. D., Ash R. D., Liu Y., Bellucci J. J., Rumble D. I., McDonough W. F., Walker R. J. and Taylor L. A. (2009a) Asteroids and andesites - reply. *Nature* **459**, E1–E2.
- Day J. M. D., Ash R. D., Liu Y., Bellucci J. J., Rumble D., McDonough W. F., Walker R. J. and Taylor L. A. (2009b) Early formation of evolved asteroidal crust. *Nature* **457**, 179–182.
- Day J.M.D., Walker R.J., James O.B. and Puchtel I.S. (2010) Osmium isotope and highly siderophile element systematics of the lunar crust. *Earth Plant. Sci. Lett.* **289**, 595–605.
- Day J. M. D., Walker R. J., Ash R. D., Liu Y., Rumble D. I., Irving A. J., Goodrich C. A., Tait K., McDonough W. F. and Taylor L. A. (2012a) Origin of felsic achondrites Graves Nunataks 06128 and 06129, and ultramafic brachinites and brachinite-like achondrites by partial melting of volatile-rich primitive parent bodies. *Geochim. Cosmochim. Acta* **81**, 94–128.
- Day J.M.D., Walker R.J., Qin L., Rumble D. and (2012b) Late accretion as a natural consequence of planetary growth. *Nature Geosci.* **5**, 614–617.

- Feldstein S. N., Jones R. H. and Papike J. J. (2001) Disequilibrium partial melting experiments on the Leedey L6 chondrite: Textural controls on melting processes. *Meteorit. Planet. Sci.* **36**, 1421–1441.
- Gardner-Vandy, K.G., Lauretta, D.S. and McCoy, T.J. (2013) A petrologic, thermodynamic and experimental study of brachinites: Partial melt residues of an R chondrite-like precursor. *Geochim. Cosmochim. Acta* **122**, 36-57.
- Greenwood R. C., Franchi I. A., Jambon A. and Buchanan P. C. (2005) Widespread magma oceans on asteroidal bodies in the early Solar System. *Nature* **435**, 916–918.
- Heimann A., Beard B. L. and Johnson C. M. (2008) The role of volatile exsolution and subsolidus fluid/rock interactions in producing high $^{56}\text{Fe}/^{54}\text{Fe}$ ratios in siliceous igneous rocks. *Geochim. Cosmochim. Acta* **72**, 4379–4396.
- Huss G. R., Keil K. and Taylor G. J. (1981) The matrices of unequilibrated ordinary chondrites: Implications for the origin and history of chondrites. *Geochim. Cosmochim. Acta* **45**, 33–51.
- Jurewicz A. J. G., Mittlefehldt D. W. and Jones J. H. (1993) Experimental partial melting of the allende (CV) and murchison (CM) chondrites and the origin of asteroidal basalts. *Geochim. Cosmochim. Acta* **57**, 2123–2139.
- Jurewicz A. J. G., Mittlefehldt D. W. and Jones J. H. (1991) Partial melting of the Allende (CV3) meteorite - implications for origins of basaltic meteorites. *Science* **252**, 695–698.
- Keil K. (2010) Enstatite achondrite meteorites (aubrites) and the histories of their asteroidal parent bodies. *Chem. Erde* **70**, 295–317.
- Keil K. (2000) Thermal alteration of asteroids: evidence from meteorites. *Planet. Space Sci.* **48**, 887–903.
- Liu Y., Spicuzza M. J., Craddock P. R., Day J. M. D., Valley J. W., Dauphas N. and Taylor L. A. (2010) Oxygen and iron isotope constraints on near-surface fractionation effects and the composition of lunar mare basalt source regions. *Geochim. Cosmochim. Acta* **74**, 6249–6262.
- Luck J.-M., Othman D. Ben and Albarède F. (2005) Zn and Cu isotopic variations in chondrites and iron meteorites: Early solar nebula reservoirs and parent-body processes. *Geochim. Cosmochim. Acta* **69**, 5351–5363.
- McCoy T. J., Keil K., Muenow D. W. and Wilson L. (1997) Partial melting and melt migration in the acapulcoite-lodranite parent body. *Geochim. Cosmochim. Acta* **61**, 639–650.
- Mittlefehldt D. W. (2007) Achondrites. In *Treatise on Geochemistry* (eds. H. D. Holland and K. K. Turekian). Elsevier-Pergamon, Oxford. pp. 1–40.
- Mittlefehldt D. W., McCoy T. J., Goodrich C. A. and Kracher A. (1998) Non-chondritic meteorites from asteroidal bodies. In *Planetary Materials* (ed. J. J. Papike). Mineralogical Society of America, Washington, DC. p. 195.

- Moynier F., Paniello R. C., Gounelle M., Albarède F., Beck P., Podosek F. and Zanda B. (2011) Nature of volatile depletion and genetic relationships in enstatite chondrites and aubrites inferred from Zn isotopes. *Geochim. Cosmochim. Acta* **75**, 297–307.
- Needham A. W., Porcelli D. and Russell S. S. (2009) An Fe isotope study of ordinary chondrites. *Geochim. Cosmochim. Acta* **73**, 7399–7413.
- Okabayashi S., Yokoyama T. and Hirata T. (2012) Iron isotopic signature for Fe-Ni metal of ordinary chondrite using newly developed technique; LAL-MC-ICPMS. *Lunar Planet. Sci. XLIII*. Lunar Planet. Inst., Houston. #1871 (abstr.).
- Poirrasson F. and Freydier R. (2005) Heavy iron isotope composition of granites determined by high resolution MC-ICP-MS. *Chem. Geol.* **222**, 132–147.
- Poirrasson F., Halliday A. N., Lee D. C., Levasseur S. and Teutsch N. (2004) Iron isotope differences between Earth, Moon, Mars and Vesta as possible records of contrasted accretion mechanisms. *Earth Planet. Sci. Lett.* **223**, 253–266.
- Polyakov V. B., Clayton R. N., Horita J. and Mineev S. D. (2007) Equilibrium iron isotope fractionation factors of minerals: Reevaluation from the data of nuclear inelastic resonant X-ray scattering and Mössbauer spectroscopy. *Geochim. Cosmochim. Acta* **71**, 3833–3846.
- Polyakov V. B. and Soultanov D. M. (2011) New data on equilibrium iron isotope fractionation among sulfides: Constraints on mechanisms of sulfide formation in hydrothermal and igneous systems. *Geochim. Cosmochim. Acta* **75**, 1957–1974.
- Riches A.J.V., Day J.M.D., Walker R.J., Simonetti A., Liu Y., Neal C.R. and Taylor L.A., 2012. Rhenium-osmium isotope and highly siderophile element abundance systematics of angrite meteorites. *Earth Planet. Sci. Lett.* **353–354**, 208–218.
- Rudnick R. L. (1995) Making continental crust. *Nature* **378**, 571–578.
- Rudnick R. L. and Gao S. (2003) The composition of the continental crust. In *Treatise on Geochemistry* (eds. H. D. Holland and K. K. Turekian). Elsevier-Pergamon, Oxford.
- Schoenberg R. and von Blanckenburg F. (2006) Modes of planetary-scale Fe isotope fractionation. *Earth Planet. Sci. Lett.* **252**, 342–359.
- Schuessler J. A., Schoenberg R. and Sigmarsson O. (2009) Iron and lithium isotope systematics of the Hekla volcano, Iceland - Evidence for Fe isotope fractionation during magma differentiation. *Chem. Geol.* **258**, 78–91.
- Sears D. W., Grossman J. N., Melcher C. L., Ross L. M. and Mills A. A. (1980) Measuring metamorphic history of unequilibrated ordinary chondrites. *Nature* **287**, 791–795.
- Shearer C. K., Burger P. V., Neal C., Sharp Z., Spivak-Birndorf L., Borg L., Fernandes V. A., Papike J. J., Karner J., Wadhwa M., Gaffney A., Shafer J., Geissman J., Atudorei N. V., Herd C., Weiss B. P., King P. L., Crowther S. A. and Gilmour J. D. (2010) Non-basaltic asteroidal magmatism during the earliest stages of solar system evolution: A view from

Antarctic achondrites Graves Nunatak 06128 and 06129. *Geochim. Cosmochim. Acta* **74**, 1172–1199.

Shearer C. K., Burger P. V., Neal C. R., Sharp Z., Borg L. E., Spivak-Birndorf L., Wadhwa M., Papike J. J., Karner J. M., Gaffney A. M., Shafer J., Weiss B. P., Geissman J. and Fernandes V. A. (2008) A unique glimpse into asteroidal melting processes in the early solar system from the Graves Nunatak 06128/06129 achondrites. *Am. Mineral.* **93**, 1937–1940.

Sossi P. A., Foden J. D. and Halverson G. P. (2012) Redox-controlled iron isotope fractionation during magmatic differentiation: an example from the Red Hill intrusion, S. Tasmania. *Contrib. Mineral. Petrol.* **164**, 757–772.

Taylor S. R. and McLennan S. M. (2009) *Planetary Crusts: Their Composition, Origin and Evolution*. Cambridge University Press.

Telus M., Dauphas N., Moynier F., Teng F.-Z., Nabelek P. I., Craddock P. R. and Groat L. A. (2012) Iron, zinc and magnesium isotopic fractionation during continental crust differentiation: The tale from migmatites, granites and pegmatites. *Geochim. Cosmochim. Acta* **97**, 247–265.

Teng F.-Z., Dauphas N. and Helz R. T. (2008) Iron isotope fractionation during magmatic differentiation in Kilauea Iki lava lake. *Science* **320**, 1620–1622.

Teng F.-Z., Dauphas N., Huang S. and Marty B. (2013) Iron isotopic systematics of oceanic basalts. *Geochim. Cosmochim. Acta* **107**, 12–26.

Theis K. J., Burgess R., Lyon I. C. and Sears D. W. (2008) The origin and history of ordinary chondrites: A study by iron isotope measurements of metal grains from ordinary chondrites. *Geochim. Cosmochim. Acta* **72**, 4440–4456.

Torigoye N. and Shima M. (1993) Evidence for a late thermal event of unequilibrated enstatite chondrites: A Rb-Sr study of Qingzhen and Yamato 6901 (EH3) and Khairpur (EL6). *Meteoritics* **28**, 515–527.

Trinquier A., Birck J., Allègre C. J., Göpel C. and Ulfbeck D. (2008) ^{53}Mn - ^{53}Cr systematics of the early Solar System revisited. *Geochim. Cosmochim. Acta* **72**, 5146–5163.

Wadhwa M., Shukolyukov A. and Lugmair G. W. (1998) ^{53}Mn - ^{53}Cr systematics in Brachina: A record of one of the earliest phases of igneous activity on an asteroid. *Lunar Planet. Sci. XXIX*. Lunar Planet. Inst., Houston. #1480 (abstr.).

Wang K., Moynier F., Barrat J.-A., Zanda B., Paniello R. C. and Savage P. S. (2013) Homogeneous distribution of Fe isotopes in the early solar nebula. *Meteorit. Planet. Sci.* **48**, 354–364.

Wang K., Moynier F., Dauphas N., Barrat J.-A., Craddock P. and Sio C. K. (2012a) Iron isotope fractionation in planetary crusts. *Geochim. Cosmochim. Acta* **89**, 31–45.

- Wang K., Moynier F., Podosek F. A. and Foriel J. (2012b) An iron isotope perspective on the origin of the nanophase metallic iron in lunar regolith. *Earth Planet. Sci. Lett.* **337-338**, 17–24.
- Wang K., Moynier F., Podosek F. and Foriel J. (2011) ^{58}Fe and ^{54}Cr in early solar system materials. *Astrophys. J.* **739**, L58.
- Weyer S., Anbar A. D., Brey G. P., Munker C., Mezger K. and Woodland A. B. (2005) Iron isotope fractionation during planetary differentiation. *Earth Planet. Sci. Lett.* **240**, 251–264.
- Weyer S. and Ionov D. A. (2007) Partial melting and melt percolation in the mantle: The message from Fe isotopes. *Earth Planet. Sci. Lett.* **259**, 119–133.
- Williams H. M., Markowski A., Quitte G., Halliday A. N., Teutsch N. and Levasseur S. (2006) Fe isotope fractionation in iron meteorites: New insights into metal-sulphide segregation and planetary accretion. *Earth Planet. Sci. Lett.* **250**, 486–500.
- Zeigler, R.A., Jolliff, B.L., Korotev, R.L., Rumble D., I.I.I., Carpenter, P.K., Wang, A., 2008. Petrology, geochemistry, and likely provenance of unique achondrite Graves Nunataks 06128. *Lunar Planet. Sci. XXXIX*. Lunar Planet. Inst., Houston. #2456 (abstr.).

CHAPTER 7 :

IRON ISOTOPE FRACTIONATION DURING EVAPORATION AND THE ORIGIN OF THE NANOPHASE METALLIC IRON IN LUNAR REGOLITH

This chapter has been published in *Earth and Planetary Sciences Letters*: Wang, K., Moynier, F., Podosek, F., Foriel, J. (2012) An Iron Isotope Perspective on the Origin of the Nanophase Metallic Iron in Lunar Regolith. *Earth and Planetary Sciences Letters*, **337-338**, 17-24.

Abstract

The surfaces of the Moon and other airless planetary bodies are constantly weathered by meteorite impacts and sputtering by charged particles. One of the hallmarks of this “space weathering” is the presence of nanophase metallic Fe (npFe^0) at the surface of airless bodies. These npFe^0 grains alter the surface optical spectra of planetary bodies without an atmosphere and their concentration is used to estimate the degree of maturity of lunar regolith. The origin of npFe^0 has been debated between in situ reduction due to the solar wind, and evaporation generated by charged particle sputtering and/or micrometeorite impact followed by re-condensation of metallic Fe. These two mechanisms will impart completely different Fe isotopic fractionation effects on the npFe^0 . In this study we measure the Fe isotopic composition of npFe^0 using a step-by-step surface etching technique on lunar regolith plagioclase. Our results show that npFe^0 is highly enriched in the heavy isotopes of Fe ($\delta^{56}\text{Fe}$ up to $0.71\text{\textperthousand}$) compared to bulk plagioclase and other lunar materials such as regolith and igneous rocks. We suggest that the formation of npFe^0 in lunar regolith is responsible for the higher $\delta^{56}\text{Fe}$ in the lunar regolith compared to lunar igneous rocks. In addition, a thermal escape model shows that the heavy Fe isotopic composition of npFe^0 is best explained by the preferential escape of light Fe isotopes to space in the vaporization phase of Fe. The temperature of the vapor can be inferred from our model (2750-3000 K), which is compatible with those proposed by previous calculations and experiments. Therefore our results unambiguously support the vapor deposit origin of npFe^0 , explain the origin of the heavy Fe isotopic composition of the lunar regolith and provide a temperature estimate for the impact event at the origin of the npFe^0 .

7.1. Introduction

The Moon, as well as other small terrestrial bodies like Phobos and 4-Vesta have little to no atmosphere or magnetic field. All planetary bodies are under continuous bombardment by various events such as cosmic ray radiation, solar wind sputtering/implantation, and meteorite/micrometeorite impacts (Clark et al., 2002; Lucey et al., 2006). While both the atmosphere and magnetic field protect the Earth from the majority of these effects, these processes constantly alter the unprotected surface of airless bodies and/or the bodies absent of significant magnetic fields. The cumulative alteration effects of these events are loosely defined as “space weathering” (Hapke, 2001; Pieters et al., 2000). On these airless planetary bodies, space weathering has long been recognized as a key factor for the alteration of surface optical features by, for example, lowering the albedo, reddening the spectral slope, and subduing the absorption fine structures (Adams and Jones, 1970; Clark et al., 2002; Hapke, 2001). Space weathering complicates the interpretation of the composition of airless bodies’ surface materials (Chapman, 2004; Clark et al., 2002) and makes it almost impossible to spectrally match groups of meteorites with types of asteroids (Britt et al., 1992).

Lunar regolith samples provide the best available materials to study space weathering, and the knowledge learned about space weathering from these samples could be extended to other airless bodies (Taylor et al., 2001). Nanophase metallic Fe (npFe^0) is widely observed on the surface of lunar regolith minerals or inside agglutinates (Keller and McKay, 1993; 1997; Wentworth et al., 1999), and it has been thought to be the cause of alteration of optical spectra from the lunar surface (Hapke et al., 1975; Moroz et al., 1996; Sasaki et al., 2001; Tang et al., 2011). Understanding the origin and characteristics of npFe^0 is critical to the interpretation of remote sensing data from the Moon and other airless planetary bodies. In addition, the

characteristic ferromagnetic resonance of npFe⁰ has been used as the main index to evaluate the maturity of the lunar regolith (Cirlin et al., 1974; Housley et al., 1975; Morris, 1976; Pearce et al., 1974). Therefore understanding the origin and formation mechanism of npFe⁰ is also very important for explaining the exposure history of lunar regolith.

After the discovery of npFe⁰ on the surface of lunar regolith grains and inside agglutinates, two competing theories were proposed to explain its origin. The first and long-accepted one is that npFe⁰ is formed as the reduction of silicates/oxide in lunar regolith saturated with solar-wind-implanted hydrogen during impact melting (Housley et al., 1973). Concurrently, it was suggested that npFe⁰ was actually formed as the deposition of the solar wind sputtering/micrometeorite impact-generated vapors (Hapke, 1973; Hapke et al., 1975).

The model of Housley et al. (1973) was widely accepted. It is, however, problematic because (1) The reduction process would have formed by-product water ($\text{FeO} + 2\text{H} = \text{Fe} + \text{H}_2\text{O}\uparrow$), and the presence of water in lunar regolith is still not fully accepted (Taylor et al., 1995). Although many recent studies have described the detection of OH/H₂O at the lunar surface, however the source of water (indigenous, solar wind reduction, or meteoritic component) remains largely debated (Clark, 2009; Liu et al., 2012; McCord et al., 2011; Pieters et al., 2009; Sunshine et al., 2009); (2) Pulse laser irradiation experiments, simulating a high-velocity micrometeorite impacting environment, show that no solar wind hydrogen is needed to form npFe⁰ and to change the optical spectra (Sasaki et al., 2001); (3) Transmission electron microscopy (TEM) imaging has clearly shown that npFe⁰ is present in the rim of nominally Fe-free minerals such as plagioclase (Keller and McKay, 1993; 1997; Wentworth et al., 1999).

One method to differentiate between the two formation processes is to use an isotopic tracer, as the two proposed mechanisms should impart different isotopic effects on npFe⁰ in lunar regolith. In the solar wind hydrogen reduction scenario, the only possible source of Fe isotopic fractionation is the reduction of Fe(II) to Fe(0). As the solar wind hydrogen reduction process would have happened at high temperatures (*i.e.*, ~1500 K; Housley et al., 1973), and since equilibrium isotopic fractionation is proportional to $1/T^2$ as predicted by the classic equilibrium isotope fractionation theory (Urey, 1947), no measurable isotopic fractionation is expected. Recent theoretical calculations have shown no resolvable fractionation occurs between Fe metal and silicate/oxide at high temperatures (>1500 K), except at extremely high-pressure environments, such as at the Earth's core-mantle boundary (Polyakov, 2009). Experimental work has also observed no equilibrium fractionation between Fe metal and silicate at high temperatures (Poitrasson et al., 2009). Therefore the Fe isotopic composition of the npFe⁰ formed by solar wind hydrogen reduction would be expected to be unfractionated from the host lunar regolith. In the solar-wind-sputtering/micrometeorite-generated-vapor-deposit scenario (Hapke et al., 1975), kinetic effects could induce a preferential escape of the light isotopes of vaporized Fe to space. As a result, the remaining npFe⁰ should be enriched in heavy isotopes relative to host lunar regolith. The Fe isotopic compositions of npFe⁰ could therefore be used to distinguish which mechanism has dominated their formation.

Following this logic, Wiesli et al. (2003) and Moynier et al. (2006) both investigated the Fe isotopic compositions of bulk lunar regolith and found that it is enriched in the heavy isotopes of Fe when compared to lunar rocks by an average of 0.10 ‰/a.m.u. (atomic mass unit) and the most mature and finest lunar regolith samples have the most enriched heavy isotopes of Fe, up to 0.15 ‰/a.m.u. (Wiesli et al., 2003). Since the most mature and finest lunar regolith samples have

the largest surface-to-volume ratio and have had more time to accumulate npFe⁰, these investigations strongly suggest that the heavy-Fe-isotope-enrichment of the lunar regolith (relative to lunar rocks) is caused by the formation of npFe⁰, which was predicted to have a highly fractionated Fe isotopic composition (more enriched in heavy isotopes of Fe than the bulk regolith). If these suggestions were correct, it would favor the impact-produced-vapor-deposit origin of the npFe⁰. However, no direct isotopic investigation of the npFe⁰ in the lunar regolith has been reported so far, due to its submicroscopic size (from a few to hundreds of nanometers; Hapke, 2001).

Plagioclase is a stoichiometrically Fe-free mineral (up to 0.25 wt.% in bulk Apollo 16 regolith plagioclase; Bell and Mao, 1973; Taylor and Carter, 1973), so little intrinsic Fe from the host mineral could contaminate the npFe⁰ on the surface. The Apollo 16 regolith is very mature (relatively determined by the amounts of npFe⁰; Cirlin et al., 1974; Housley et al., 1975; Morris, 1976; Pearce et al., 1974), and hence contains large amounts of npFe⁰ (Heiken et al., 1991). Thus Apollo 16 lunar regolith plagioclase mineral separates are ideal samples to search for the Fe isotopic composition of npFe⁰. In order to access this npFe⁰ signature, we used a step-by-step etching technique (Kitts et al., 2003), preferentially dissolving the surface (from 0.1 to 0.8 μm) of handpicked pure lunar regolith plagioclase grains with a series of weak acids. We have successfully managed to isolate the Fe isotope signature of npFe⁰ using Multi-Collector Inductively Coupled Plasma Mass Spectrometer (MC-ICP-MS). We will discuss the origin of the npFe⁰ in lunar regolith from the perspective of Fe isotopic fractionation.

7.2. Material and Method

7.2.1. Sample Treatment

We used the same sample solutions previously treated by Kitts et al. (2003). Here we briefly repeat the rationale and main steps (a detailed preparation procedures could be found in Kitts et al. 2003). To maximize the proportion of nanophase Fe and limit the contamination from the intrinsic Fe of host minerals as much as possible, plagioclase from Apollo 16 regolith was chosen because (1) plagioclase stoichiometrically contains no Fe, and; (2) Apollo 16 regolith has long exposure ages and large surface-to-volume ratios (Heiken et al., 1991). Sample 60601 is from Apollo 16, station 10, 65m southwest surface. Sample 62281 is from Apollo 16, station 2, south slope of Buster crater surface. For both samples, about 50 g of bulk regolith were used. First, the fine and ultra fine particles of the regolith were removed as suspensions using electronic grade methanol. The remaining material was initially size-sorted (35-75 μm and 75-150 μm), then the plagioclase grains were isolated, first using a Frantz magnetic separator and finally by hand. The handpicked clean plagioclase grains represent about 1.5-2.0 % of the initial total mass of the regolith (Kitts et al., 2003).

The isolated plagioclase grains were first cleaned in MQ-e water ($18.2\text{M}\Omega\text{cm}$) in an ultrasonic bath for 60 seconds. The cleaned grains were then progressively etched by using 0.1 N HCl at room temperature. The first four etches (Etch1, 2, 3 and 4) each lasted for 1 hour, while the final one (Etch5) continued for 20 hours to consume as much sample as possible. The acid solution in each etching step was pipetted into cleaned PTFE beakers and used for the Fe purification. The Ca concentrations in the same solutions were previously measured by Kitts et al. (2003) and the etch depths were calculated therein (see Table 7-1). Each step was estimated to

etch about 0.1 μm of sample (see Figure 7-1; Kitts et al., 2003), which corresponds to the depth of the npFe⁰ rim of plagioclase reported by Keller and McKay (1997).

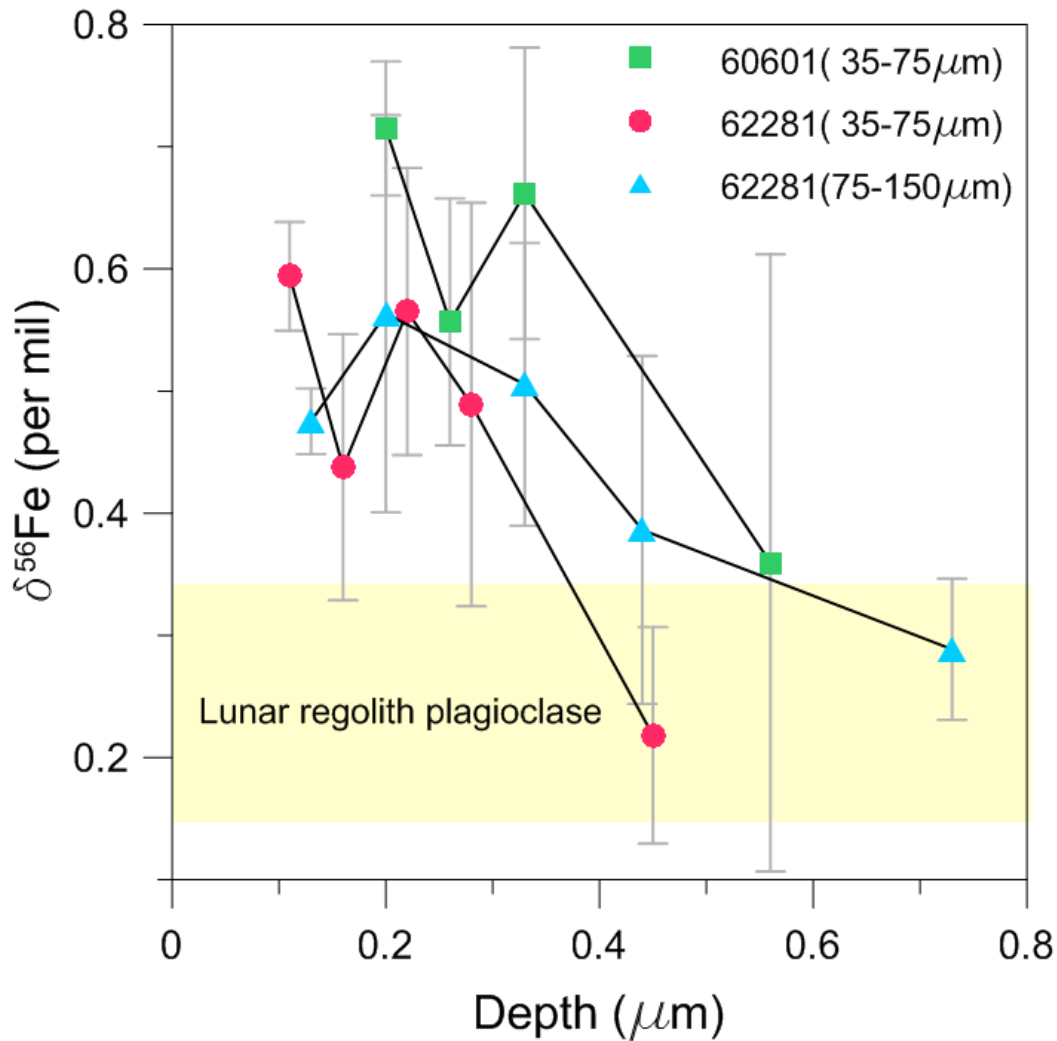


Figure 7-1. Iron isotope compositions expressed in delta notation ($\delta^{56}\text{Fe}$) relative to IRMM-014 vs. etching depth profile. Etching depth values are taken from Kitts (2003) derived from Ca concentrations. The yellow shaded area represents bulk plagioclase isotopic composition taken from lunar igneous rocks (Craddock et al., 2010).

7.2.2. Isotopic Measurements

Prior to the mass spectrometry analysis, Fe was purified by ion exchange chromatography following procedures described previously (Dauphas et al., 2004) and recently applied in Wang et al. (2011; 2012). Samples were dissolved in ~1 ml of 6N HCl and loaded into columns filled with 1 mL AG1-X8 200-400 mesh anion-exchange resin. The matrix was first eluted in 8 mL (0.5+0.5+1+2+4 mL increments) of 6 M HCl and the Fe was collected in 9 mL (0.5+0.5+1+3+4 mL increments) of 0.4 M HCl. These purifications were repeated twice to ensure removal of all interfering isobars and other matrix elements. The Fe isotopic measurements were performed using a standard-sample bracketing method on the Thermo Scientific Neptune Plus Multi-Collector Inductively Coupled Plasma Mass Spectrometer (MC-ICP-MS) at Washington University in St. Louis, running at medium resolution (resolving power $M/\Delta M \sim 8500$). Both samples and standards were analyzed at the same concentration (0.5 ppm \pm 10%) and were introduced into the MC-ICP-MS using a 100 μ L/min PFA MicroFlow nebulizer and with an Apex-Q+Spiro desolvator, which reduces ambient species interferences and results in a higher machine sensitivity. The intensities of the isotopes ^{54}Fe , ^{56}Fe , ^{57}Fe and ^{58}Fe were measured in the L2, center, H1 and H2 Faraday cups respectively. Possible interferences from ^{54}Cr and ^{58}Ni were assessed by monitoring ^{53}Cr (L3) and ^{60}Ni (H4) respectively. The measurements were made on the flat-topped peak shoulder (light mass side) to avoid the interferences of $^{40}\text{Ar}^{14}\text{N}^+$, $^{40}\text{Ar}^{16}\text{O}^+$, $^{40}\text{Ar}^{14}\text{OH}^+$ and $^{40}\text{Ar}^{18}\text{O}^+$. The results are reported as delta notation relative to IRMM-014, where $\delta^i\text{Fe} = [(^i\text{Fe}/^{54}\text{Fe})_{\text{sample}}/(^i\text{Fe}/^{54}\text{Fe})_{\text{IRMM014}} - 1] \times 10^3$, $i=56, 57$ and 58. Because $\varepsilon^{53}\text{Cr}$ and $\varepsilon^{54}\text{Cr}$ anomalies were previously found in the same solutions (Kitts et al., 2003), it is necessary to check the non-mass fractionation effects for Fe isotopes too. For this reason, to correct the instrumental and natural mass-dependent fractionations, all the data were

also normalized to $^{57}\text{Fe}/^{54}\text{Fe}=0.362566$ or $^{56}\text{Fe}/^{54}\text{Fe}=15.69786$ (Taylor et al., 1992) using the exponential law (Maréchal et al., 1999). The normalized data are reported in ϵ units, $\epsilon^i\text{Fe}=[(^i\text{Fe}/^{54}\text{Fe})_{\text{sample}}/(^i\text{Fe}/^{54}\text{Fe})_{\text{IRMM-014}}-1]\times 10^4$, $i=56, 57$ and 58 . The errors are reported as two standard errors (2SE) of the replicated measurements.

7.3. Results

The isotopic compositions of lunar regolith plagioclase etchings are presented in Table 7-1. For the three separate experiments (60601 35-75 μm ; 62281, 35-75 μm and 75-150 μm), the first three/four one-hour etching solutions all have significantly higher $\delta^{56}\text{Fe}$ values ($\delta^{56}\text{Fe} = 0.39\text{-}0.71\text{\textperthousand}$) than the last twenty-hour etching solutions ($\delta^{56}\text{Fe} = 0.22\text{-}0.36\text{\textperthousand}$). Figure 7-1 shows a clear trend of $\delta^{56}\text{Fe}$ decreasing from the surface to the core of plagioclase grains for the three independent experiments. The $\delta^{56}\text{Fe}$ values in the last etching solution fall into normal lunar plagioclase values ($\delta^{56}\text{Fe} = 0.15\text{-}0.34\text{\textperthousand}$; shown as the yellow shaded area in Figure 7-1; Craddock et al., 2010). The largest $\delta^{56}\text{Fe}$ offset from “average” lunar plagioclase Fe measured from surface etching is $0.71 \pm 0.05\text{\textperthousand}$, which we use as a possible end-member Fe isotopic composition of nanophase Fe, as discussed in the following section.

Because surface-related chromium isotopic anomalies have been previously found in the same etching solutions used in this study (Kitts et al., 2003), internally normalized Fe isotopic data for comparison, to check for non-mass dependent Fe isotopic signatures due to solar wind implantation (see Table 7-1 and Figure 7-2). After correction for mass-dependent fractionation, either by normalizing to the $^{57}\text{Fe}/^{54}\text{Fe}$ or $^{56}\text{Fe}/^{54}\text{Fe}$ ratio, all $\varepsilon^{56}\text{Fe}$, $\varepsilon^{57}\text{Fe}$ and $\varepsilon^{58}\text{Fe}$ are equal to zero within analytical uncertainty. Unlike Cr isotopes there are no isotopic anomalies observed in Fe isotopes (see Figure 7-2). Therefore, all the isotopic variations observed in our samples are caused by mass-dependent fractionation.

Table 7-1. Iron isotope compositions of etched plagioclase in Apollo 16 lunar regolith

Sample	Treatment	Etch Depth ^a	$\delta^{56}\text{Fe}$	\pm	2SE	$\delta^{57}\text{Fe}$	\pm	2SE	$\delta^{58}\text{Fe}$	\pm	2SE	$\varepsilon^{56}\text{Fe}^b$	\pm	2SE	$\varepsilon^{58}\text{Fe}^b$	\pm	2SE	$\varepsilon^{57}\text{Fe}^c$	\pm	2SE	$\varepsilon^{58}\text{Fe}^c$	\pm	2SE	n ^d	
60601, 50g, 35-75um																									
Etch2	0.1N HCl (1 hour)	0.20	0.71	\pm	0.05	1.05	\pm	0.05	1.34	\pm	0.12	0.11	\pm	0.21	-0.39	\pm	1.38	-0.16	\pm	0.31	-0.61	\pm	1.43	3	
Etch3	0.1N HCl (1 hour)	0.26	0.56	\pm	0.10	0.88	\pm	0.12	1.22	\pm	0.31	-0.37	\pm	0.23	0.56	\pm	1.61	0.55	\pm	0.34	1.29	\pm	1.16	3	
Etch4	0.1N HCl (1 hour)	0.33	0.66	\pm	0.12	1.00	\pm	0.08	1.23	\pm	0.03	-0.13	\pm	0.65	-0.96	\pm	1.12	0.19	\pm	0.97	-0.71	\pm	2.28	3	
Etch5	0.1N HCl (20 hour)	0.56	0.36	\pm	0.25	0.60	\pm	0.28	0.92	\pm	0.22	-0.47	\pm	0.67	1.25	\pm	1.96	0.70	\pm	0.99	2.18	\pm	3.25	3	
62281, 50g, 35-75um																									
Etch1	0.1N HCl (1 hour)	0.11	0.59	\pm	0.04	0.94	\pm	0.05	1.27	\pm	0.12	-0.38	\pm	0.17	0.24	\pm	1.23	0.57	\pm	0.26	0.99	\pm	1.41	6	
Etch2	0.1N HCl (1 hour)	0.16	0.44	\pm	0.11	0.71	\pm	0.12	0.87	\pm	0.11	-0.39	\pm	0.35	-0.69	\pm	1.03	0.57	\pm	0.52	0.07	\pm	1.57	6	
Etch3	0.1N HCl (1 hour)	0.22	0.57	\pm	0.12	0.82	\pm	0.11	0.98	\pm	0.10	0.12	\pm	0.42	-1.08	\pm	0.98	-0.18	\pm	0.62	-1.32	\pm	1.70	6	
Etch4	0.1N HCl (1 hour)	0.28	0.49	\pm	0.17	0.73	\pm	0.17	0.83	\pm	0.17	-0.01	\pm	0.53	-1.35	\pm	1.27	0.01	\pm	0.80	-1.34	\pm	2.21	6	
Etch5	0.1N HCl (20 hour)	0.45	0.22	\pm	0.09	0.33	\pm	0.09	0.20	\pm	0.17	-0.01	\pm	0.31	-2.31	\pm	1.79	0.01	\pm	0.47	-2.29	\pm	1.81	5	
62281, 50g, 75-150um																									
Etch1	0.1N HCl (1 hour)	0.13	0.48	\pm	0.03	0.77	\pm	0.03	0.83	\pm	0.09	-0.40	\pm	0.44	-1.86	\pm	0.57	0.60	\pm	0.66	-1.07	\pm	1.44	2	
Etch2	0.1N HCl (1 hour)	0.20	0.56	\pm	0.16	0.84	\pm	0.15	1.13	\pm	0.07	0.01	\pm	0.59	0.20	\pm	1.31	-0.01	\pm	0.88	0.19	\pm	2.47	2	
Etch3	0.1N HCl (1 hour)	0.33	0.51	\pm	0.12	0.78	\pm	0.11	1.06	\pm	0.05	-0.19	\pm	0.41	0.33	\pm	1.01	0.28	\pm	0.61	0.70	\pm	1.82	2	
Etch4	0.1N HCl (1 hour)	0.44	0.39	\pm	0.14	0.65	\pm	0.16	0.92	\pm	0.00	-0.53	\pm	0.38	0.53	\pm	2.02	0.78	\pm	0.56	1.56	\pm	2.76	2	
Etch5	0.1N HCl (20 hour)	0.73	0.29	\pm	0.06	0.46	\pm	0.08	0.68	\pm	0.10	-0.23	\pm	0.07	0.72	\pm	0.03	0.34	\pm	0.10	1.17	\pm	0.10	2	
Geostandard																									
BCR-2	(Bulk)		0.07	\pm	0.06	0.11	\pm	0.06	0.01	\pm	0.11	-0.05	\pm	0.22	-1.40	\pm	1.61	0.08	\pm	0.32	-1.30	\pm	1.99	4	

^a Etch depth is from Kitts et al. (2003) calculated from Ca concentration.

^b $i\text{Fe}^{54}\text{Fe}$ normalized to $^{57}\text{Fe}^{54}\text{Fe}=0.362566$. i=56 and 58 (Taylor et al., 1992).

^c $i\text{Fe}^{54}\text{Fe}$ normalized to $^{56}\text{Fe}^{54}\text{Fe}=15.69786$. i=57 and 58 (Taylor et al., 1992).

^d Number of sample measurement.

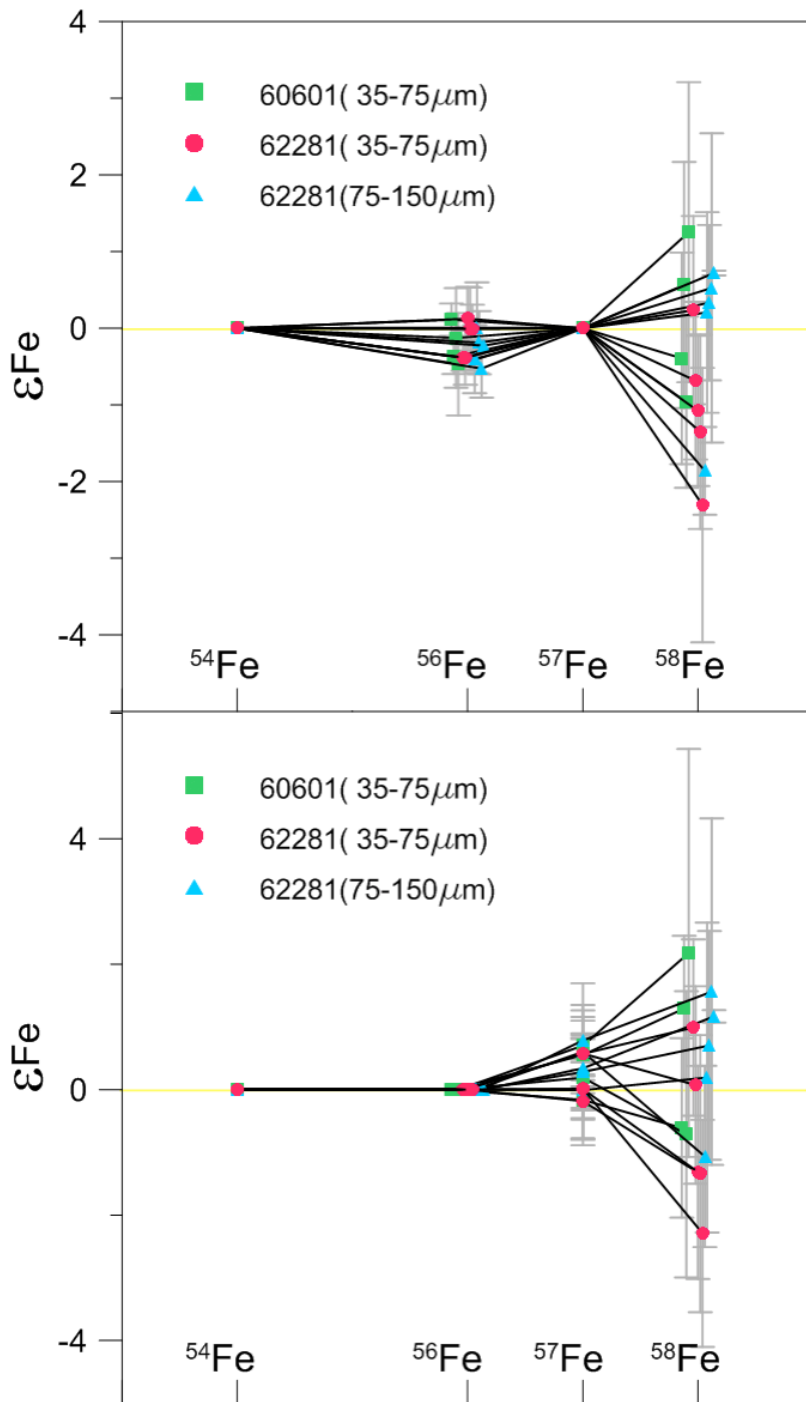


Figure 7-2. Iron isotope compositions expressed in epsilon notation ($\epsilon^{56}\text{Fe}$) after mass-dependent fractionation corrections, either normalized to $^{57}\text{Fe}/^{54}\text{Fe}=0.362566$ (Taylor et al., 1992; top panel) or to $^{56}\text{Fe}/^{54}\text{Fe}=15.69786$ (Taylor et al., 1992; bottom panel) using the exponential law (Maréchal et al., 1999). Both sets of data show no Fe isotopic anomalies within analytical uncertainty.

7.4. Discussion

Plagioclase is a nominally Fe-free mineral, and in Apollo 16 regolith plagioclase the bulk Fe concentration is only 0.14 – 0.25 wt.% (Bell and Mao, 1973; Taylor and Carter, 1973). The higher Fe concentration on the surface (<0.4 μm depth) of lunar regolith plagioclase implies that this extra Fe is probably not primary (Keller and McKay, 1997). Our study shows this secondary Fe has significant different isotopic compositions ($\delta^{56}\text{Fe}$ up to 0.71‰) from the host plagioclase (see Figure 7-1). Three possible sources of this extrinsic Fe have been suggested: contamination by meteoritic components, solar wind Fe implantation or vapor-deposit Fe coating (Keller and McKay, 1997; Kitts et al., 2003).

Meteoritic components could contribute between 0.7 and 1.7% by mass in a typical regolith from Apollo 16 (Korotev, 1987). Meteorites, especially chondrites, usually contain high amounts of Fe-Ni metal (up to 20% in H group ordinary chondrites; Lodders and Fegley, 1998). However, no types of meteorites thus far measured for Fe isotopes could provide such heavy Fe isotopic compositions as measured here ($\delta^{56}\text{Fe}$ up to 0.71‰). For example, chondrites are the most frequent falls (~80%; Bevan et al., 1998) on the Earth (probably also on the Moon), and the average $\delta^{56}\text{Fe}$ is only $0.01 \pm 0.01\text{\textperthousand}$ (Craddock and Dauphas, 2010). Iron meteorites have higher $\delta^{56}\text{Fe}$ (~0.1‰; Poitrasson et al., 2005; Schoenberg and von Blanckenburg, 2006; Williams et al., 2006) but are still too light to provide the $\delta^{56}\text{Fe} = 0.71\text{\textperthousand}$ end-member required here. Achondrites, such as Martian, HED, or angrite, have various Fe isotopic compositions, but their $\delta^{56}\text{Fe}$ are all less than 0.2‰ (Anand et al., 2006; Poitrasson et al., 2004; Schoenberg and von Blanckenburg, 2006; Wang et al., 2012; Weyer et al., 2005). Thus, meteoritic components are not a plausible source for these highly fractionated Fe isotopic composition in the step etching solutions of the Apollo 16 lunar regolith plagioclase.

Solar wind is dominated by hydrogen and helium; heavy elements comprise less than 1% (Anders and Grevesse, 1989; Lodders, 2003). However, solar wind-derived implanted elements other than hydrogen and helium, such as noble gases (Benkert et al., 1993; Eberhardt et al., 1972), lithium (Chaussidon and Robert, 1999), carbon (Hashizume et al., 2004), nitrogen (Hashizume et al., 2000; Jull et al., 1995), and oxygen (Hashizume and Chaussidon, 2005; Ireland et al., 2006) have long been recognized at the surface of lunar regolith grains. Calculations based on solar wind flux shows that up to 0.3 wt.% of the total Fe in lunar regolith could be implanted by solar wind (Shkuratov, 2012), which could therefore be a possible source for the secondary Fe found on the surface of lunar regolith plagioclase.

In addition, non-mass dependent Cr isotopic variations have been measured in the same etching used in our study. As with the heavy-Fe isotope-enriched etchings in this study, these anomalies were concentrated in the surface of lunar regolith plagioclases (Kitts et al., 2003). The origin of these Cr isotopic anomalies is still unclear, however, since these variations are definitively *non*-mass dependent, they can be best (if not only) explained by having formed by spallation in the solar atmosphere, transported to the Moon and implanted in lunar regolith by solar wind.

However, this conclusion based on Cr isotopes does not apply here for Fe, even though we have analyzed the same etching solutions. First, after correcting for mass dependent fractionation, within analytical uncertainty no non-mass dependent Fe isotopic anomalies ($\varepsilon^{56}\text{Fe}$, $\varepsilon^{57}\text{Fe}$ or $\varepsilon^{58}\text{Fe}$) are found (see Table 7-1 and Figure 7-2). This does not necessarily exclude the possibilities of solar wind origin for the secondary Fe (e.g., if the Sun has a chondritic Fe isotopic composition) but is not definitive evidence for a solar wind origin. Second, inefficient Coulomb drag theory predicts heavier isotopes are depleted in solar wind relative to the outer

convective zone (OCZ) of the Sun (Bochsler, 2000; Bodmer and Bochsler, 2000; Geiss et al., 1970; Wiens et al., 2004). This means that the implanted solar wind stable isotopic compositions should be enriched in light isotopes. Recent support for this theory comes from the isotopically light Mg isotopic composition (down to -2‰ /a.m.u.) of solar wind collected by the Genesis mission (Humayun et al., 2011). For the Fe isotopic composition of solar wind, the High-Resolution Mass Spectrometer (MASS) loaded on the Wind spacecraft and the Mass Time-of-Flight Spectrometer (MTOF) on the Solar and Heliospheric Observatory (SOHO) spacecraft have reported very negative Fe isotopic compositions (see Figure 7-3; Ipavich et al., 2001; Oetliker et al., 1997). The positive Fe isotopic compositions measured here ($\delta^{56}\text{Fe}$ up to 0.71‰) cannot therefore be attributed to solar wind implantation (see Figure 7-3).

Lastly, abundant nanophase metallic Fe (npFe^0) has long been found in the vapor-deposit coating which universally covers mature lunar regolith particles like the Apollo 16 regolith plagioclase studied here (see Hapke, 2001 for a review). Previous acid leaching experiments have shown the surface npFe^0 can be readily accessed with short-term acid exposure (Gold et al., 1970; Hapke et al., 1970). The etching depth in this study (see Figure 7-2; Kitts et al., 2003) is comparable with the appearance depth of the vapor-deposit npFe^0 observed by transmission electron microscope (Keller and McKay, 1993; 1997). This vapor-deposit Fe coating dominates the concentration of Fe on the rims of nominally Fe-free minerals such as plagioclase (Keller and McKay, 1997), hence controlling the Fe isotopic compositions measured in the surface etchings in this study. As such, the Fe of the surface ($<0.4\text{ }\mu\text{m}$) etching solutions of lunar Apollo 16 regolith plagioclases must represent the npFe^0 instead of meteorite components or solar wind implanted Fe.

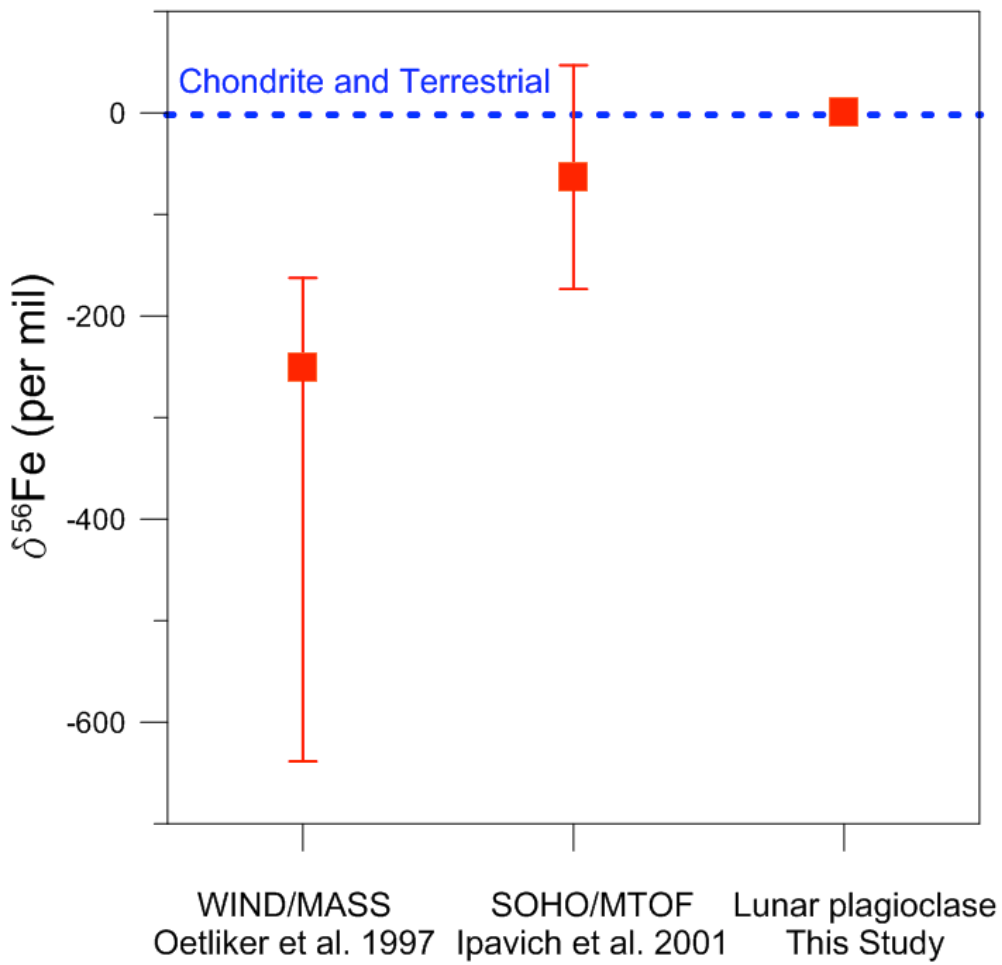


Figure 7-3. Solar wind Fe isotope compositions measured by spacecraft vs. Fe isotope compositions measured in lunar regolith plagioclase surface etching solutions. The error bars for the literature data are 2σ ; the error bars for this study are within the data symbols.

In this study we directly show that heavier $\delta^{56}\text{Fe}$ is only concentrated in the topmost part ($<0.4 \mu\text{m}$) of lunar regolith plagioclase (see Figure 7-1); the core has a “normal” $\delta^{56}\text{Fe}$, comparable to that of plagioclase separated from lunar igneous rock (Craddock et al., 2010). We propose that the heavy enriched Fe isotopic compositions of the lunar regolith are solely caused

by the formation of npFe⁰, and that the degree of isotopic enrichment is determined by the amount of npFe⁰ contained.

The highly fractionated Fe isotopic composition of npFe⁰ measured in this study does not only explain why lunar regolith has a higher $\delta^{56}\text{Fe}$ than lunar igneous rock, but also sheds light on the origin of the npFe⁰. As stated in the introduction, two competing formation mechanisms of npFe⁰ (reduction of FeO in lunar regolith by solar wind vs. thermal disassociation with oxygen in solar wind sputtering/micrometeorite impact generated hot vapor) would have distinct Fe isotopic fractionation effects. As shown in Figure 7-1 the npFe⁰ measured here have highly fractionated heavy Fe isotopic composition ($\delta^{56}\text{Fe}$ up to 0.71‰), more than twice that of average lunar regolith (~0.3‰; Wiesli et al., 2003). This highly fractionated Fe isotopic composition of npFe⁰ strongly disfavors the solar wind hydrogen reduction hypothesis. The fractionation can be best explained by the preferential loss of light Fe isotopes to space during the hot vaporization stage, as predicted by the classical thermal escape model (Wiesli et al., 2003).

Chemical fractionation between vapor deposits and source material during vapor transport has been previously reviewed in detail (Hapke et al., 1975; Hapke, 2001); here we will briefly discuss the possibility of isotopic fractionation. Following a classical thermal escape model (Jeans escape), atoms in the high-velocity-tail of the Maxwell-Boltzmann distribution may reach the planetary escape velocity and hence could be lost to space (Hunten, 1982; Jeans, 1925). Criss (1999) modeled the isotopic fractionation as a result of the preferential loss of lighter isotopes following this mechanism. The temperature of impact-produced vapor has been evaluated from both calculations and experiments (Anand et al., 2004; Cassidy and Hapke, 1975; Hapke et al., 1975; Tang et al., 2011; Yakovlev et al., 2011): depending on the natural variations of impact energy and source materials, the vapor temperature generally ranges from ~1500 to

3000 K or higher. At these high temperatures, a small but significant amount of Fe in the hot vapor would have velocity larger than the escape velocity of the Moon (2.38 km/s). As an example, at 2500 K (a reasonable vapor temperature) ~0.099% and ~0.077% of atoms of ^{54}Fe and ^{56}Fe respectively could be lost to space based on their different masses (see Figure 7-4). These results were calculated using Equation 7-1, after Criss (1999; see Appendix for the equation derivation), as such:

Eq. 7-1

$$\delta^{56}\text{Fe}_{\text{new}} = \frac{1 - \sqrt{\frac{2M^{56}}{\pi RT}} V_e e^{-M^{56}V_e^2/(2RT)} + \text{erf} \left(\sqrt{\frac{2M^{56}}{\pi RT}} V_e \right)}{1 - \sqrt{\frac{2M^{54}}{\pi RT}} V_e e^{-M^{54}V_e^2/(2RT)} + \text{erf} \left(\sqrt{\frac{2M^{54}}{\pi RT}} V_e \right)} \cdot (\delta^{56}\text{Fe}_{\text{source}} + 1000) - 1000$$

where M^{54} is the mass of ^{54}Fe (kg/mol), M^{56} is the mass of ^{56}Fe (kg/mol), \mathbf{R} is the gas constant ($\text{JK}^{-1}\text{mol}^{-1}$), V_e is the lunar escape velocity (m/s) and T is the temperature of the vapor. Equation 7-1 is plotted in Figure 7-5 as a function of vapor temperature. The data range of the npFe^0 measured in the first etching solutions (0.48‰ to 0.71‰) is plotted as the shaded region in the diagram.

As shown in Figure 7-5, the Fe isotope composition of npFe^0 in lunar plagioclase surface etchings can be explained as the condensation residue of material that has lost light Fe isotopes to space in a hot micrometeorite-impact-generated vapor (Hapke et al., 1975). The vapor temperature can be evaluated to between ~2500 and 2750 K if the fractionation starts from an average lunar regolith Fe isotope composition (~0.3‰; Wiesli et al., 2003). It is worth noting that the average lunar regolith $\delta^{56}\text{Fe}$ already includes the influence of the high $\delta^{56}\text{Fe}$ caused by the formation of npFe^0 . If the evaporating material has typical lunar igneous rock values ($\delta^{56}\text{Fe} =$

0.1-0.2‰; Liu et al., 2010; Poitrasson et al., 2004; Weyer et al., 2005; Wiesli et al., 2003), a higher temperature (~2750 to 3000 K) of the vapor is predicted. Considering the Fe isotope composition of npFe⁰ from this stepwise etching experiment can only represent the lower limit value, we further suggest that a higher temperature (>3000 K) is equally possible. These temperature estimates deduced from Equation 7-1 (see Figure 7-5) are compatible with the theoretical and experimental evaluations of the vapor temperature (~2000 to >3000 K; Anand et al., 2004; Basu, 2005; Cassidy and Hapke, 1975; Hapke et al., 1975; Tang et al., 2011; Yakovlev et al., 2011).

The Fe isotope data presented here indicate that the formation of npFe⁰ on the surface of lunar plagioclase is explained by the deposition of a solar wind sputtering/micrometeorite impact-generated vapor. Our results do not provide direct evidence for the origin of the npFe⁰ found in lunar agglutinates (glassy breccias formed at the surface of the Moon by micrometeorite impacts) as, unfortunately, the stepwise etching method used in this study would dissolve a lot of non-reduced Fe present in the agglutinate. Since the npFe⁰ associated within agglutinates are larger than the npFe⁰ found at the surface of regolith grains (Lucey et al., 2006), in-situ high precision measurements of Fe isotopes (*e.g.*, Nano Secondary Ion Mass Spectrometry; Ong et al., 2012) might provide a solution to this problem in the future.

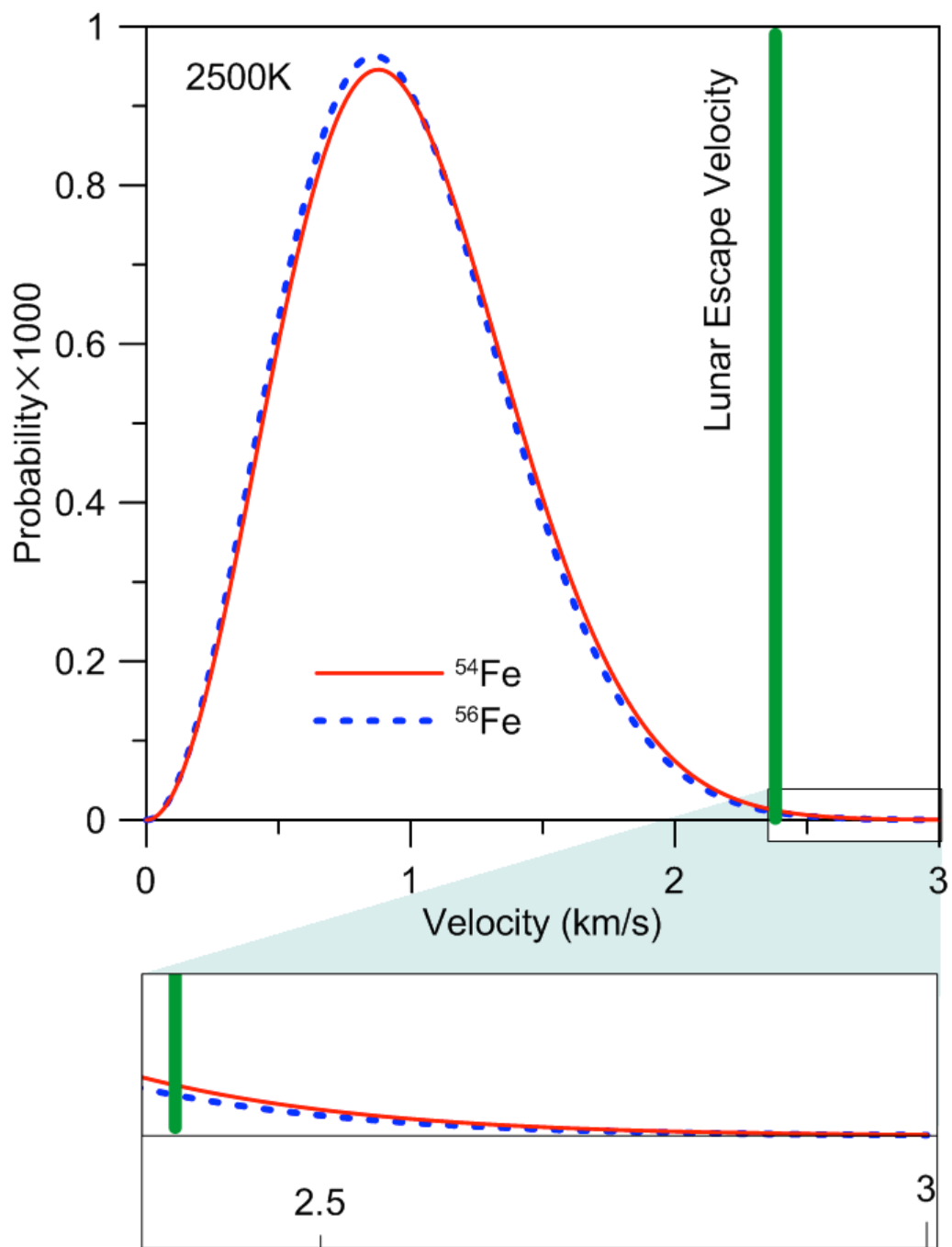


Figure 7-4. Iron isotope fractionation during thermal escape from the high-velocity-tail of Maxwell-Boltzmann distribution.

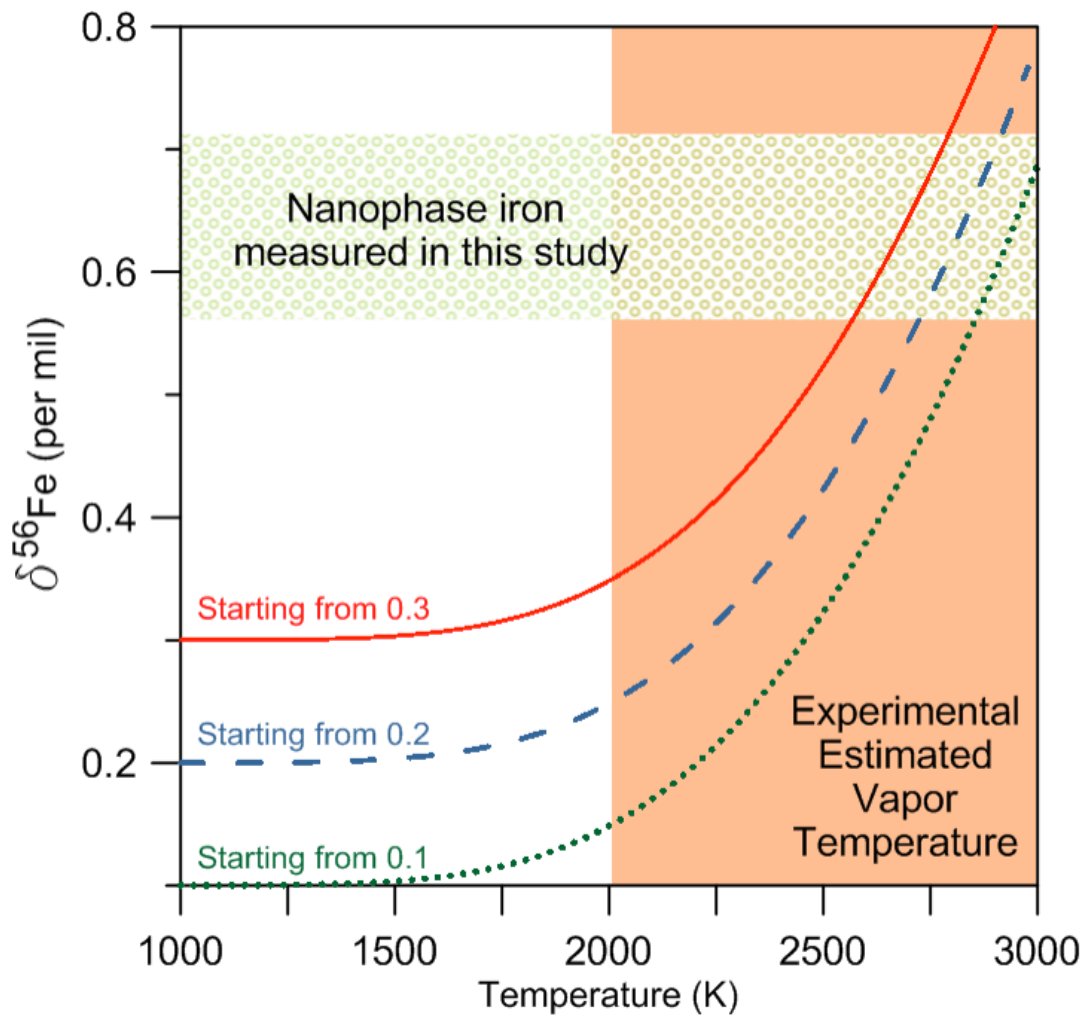


Figure 7-5. The Fe isotope compositions of nanophase Fe measured in this study could be explained by fractionation during preferential thermal escape (see Equation 7-1 in text) starting from a typical lunar regolith value (red solid line; $\delta^{56}\text{Fe} = 0.3\text{\textperthousand}$; Wiesli et al., 2003), a typical high-Ti lunar basalt value (blue dashed line; $\delta^{56}\text{Fe} = 0.2\text{\textperthousand}$; Liu et al., 2010; Poitrasson et al., 2004; Weyer et al., 2005) or a typical low-Ti lunar basalt/highland rock value (green dotted line; $\delta^{56}\text{Fe} = 0.1\text{\textperthousand}$; Liu et al., 2010; Poitrasson et al., 2004; Weyer et al., 2005). The experimentally estimated vapor temperature range is between ~2000 and 3000 K (Anand et al., 2004; Basu, 2005; Cassidy and Hapke, 1975; Hapke et al., 1975; Yakovlev et al., 2011).

7.5. Conclusions

In this study, the Fe isotopic composition of nanophase metallic Fe (npFe^0) from the surface of lunar regolith plagioclase grains has been directly measured. The npFe^0 show large enrichments in the heaviest Fe isotopes ($\delta^{56}\text{Fe}$ up to 0.71‰) compared to lunar regolith (~0.3‰; Wiesli et al., 2003, Moynier et al. 2006) or lunar igneous rocks (0.1-0.2‰; Liu et al., 2010; Poitrasson et al., 2004; Weyer et al., 2005; Wiesli et al., 2003). These results provide good evidence that the enrichment in heavy Fe isotopes of the lunar regolith compared to lunar igneous rocks is the result of the presence of npFe^0 in the regolith. This conclusion is supported by previous studies on the bulk lunar regolith (Moynier et al., 2006; Wiesli et al., 2003). In addition, the highly fractionated Fe isotopic composition of npFe^0 measured here strongly favors a solar-wind-sputtering/micrometeorite-impact generated vapor deposit origin (Hapke et al., 1975), which is in agreement with the study of npFe^0 by Transmission Electron Microscopy (Keller and McKay, 1997). A thermal escape model predicts that preferential loss of light Fe isotopes to space in the hot vapor generated by constant solar wind sputtering/micrometeorite impacts can explain the Fe isotopic compositions of npFe^0 . The temperature of the vapor can also be predicted from the model, and is inferred as between ~2750 to 3000 K. This is compatible with the temperature range proposed by previous theoretical or experimental studies (Anand et al., 2004; Cassidy and Hapke, 1975; Hapke et al., 1975; Tang et al., 2011; Yakovlev et al., 2011).

References

- Adams J.B. and Jones R.L. (1970) Spectral reflectivity of lunar samples. *Science* **167**, 737–739.
- Anand M., Russell S. S., Blackhurst R. L. and Grady M. M. (2006) Searching for signatures of life on Mars: an Fe-isotope perspective. *Philos. Trans. R. Soc. Lond., B, Biol. Sci.* **361**, 1715–1720.
- Anand M., Taylor L.A., Nazarov M.A., Shu J., Mao H.K. and Hemley R.J. (2004) Space weathering on airless planetary bodies: Clues from the lunar mineral hapkeite. *Proc. Natl. Acad. Sci.* **101**, 6847–6851.
- Anders E. and Grevesse, N. (1989) Abundances of the elements - meteoritic and solar. *Geochim. Cosmochim. Acta* **53**, 197–214.
- Basu A. (2005) Nanophase Fe⁰ in lunar soils. *J. Earth Syst. Sci.* **114**, 375–380.
- Bell P.M. and Mao, H.K. (1973) An analytical study of iron in plagioclase from Apollo 16 soils 64501, 64502, 64802, rock 66095 and Apollo 15 rock 15475. *Lunar Planet. Sci. IV*. Lunar Planet. Inst., Houston. #57(abstr.).
- Benkert J.-P., Baur H., Signer P. and Wieler, R. (1993) He, Ne, and Ar from the solar wind and solar energetic particles in lunar ilmenites and pyroxenes. *J. Geophys. Res.* **98**, 13147–13162.
- Bevan A.W.R., Bland P.A. and Jull, A.J.T. (1998) Meteorite flux on the Nullarbor Region, Australia. *Geol. Soc. Spec. Pub.* **140**, 59–73.
- Bochsler P. (2000) Abundances and charge states of particles in the solar wind. *Rev. Geophys.* **38**, 247–266.
- Bodmer R. and Bochsler P. (2000) Influence of Coulomb collisions on isotopic and elemental fractionation in the solar wind acceleration process. *J. Geophys. Res.* **105**, 47–60.
- Britt D.T., Tholen D.J., Bell J.F. and Pieters, C.M. (1992) Comparison of asteroid and meteorite spectra: Classification by principal component analysis. *Icarus* **99**, 153–166.
- Cassidy W. and Hapke, B. (1975) Effects of darkening processes on surfaces of airless bodies. *Icarus* **25**, 371–383.
- Chapman C.R. (2004) Space weathering of asteroid surfaces. *Annu. Rev. Earth Planet. Sci.* **32**, 539–567.
- Chaussidon M. and Robert F. (1999) Lithium nucleosynthesis in the Sun inferred from the solar-wind Li-7/Li-6 ratio. *Nature* **402**, 270–273.
- Cirlin E.H., Housley R.M., Goldberg I.B. and Paton N.E. (1974) Ferromagnetic resonance as a method for studying regolith dynamics and breccia formation. *Lunar Sci. Conf. V*. Lunar Planet. Inst., Houston. #121(abstr.).

- Clark B.E., Hapke B., Pieters C. and Britt, D. (2002) Asteroid space weathering and regolith evolution, in *Asteroids III* (eds. Bottke, W.F., Cellino, A., Paolicchi, P., Binzel, R.P.). University of Arizona Press, Tucson, AZ, pp. 585-599.
- Clark R.N. (2009) Detection of adsorbed water and hydroxyl on the Moon. *Science* **326**, 562–564.
- Craddock P. R. and Dauphas N. (2011) Iron isotopic compositions of geological reference materials and chondrites. *Geostand. Geoanal. Res.* **35**, 101–123.
- Craddock P.R., Dauphas N. and Clayton, R.N. (2010) Mineralogical control on iron isotopic fractionation during lunar differentiation and magmatism. *Lunar Planet. Sci. XLI*. Lunar Planet. Inst., Woodlands. #1230(abstr.).
- Criss R.E. (1999) *Principles of Stable Isotope Distribution*. Oxford University Press, New York.
- Dauphas N., Janney P. E., Mendybaev R. A., Wadhwa M., Richter F. M., Davis A. M., van Zijl M., Hines R. and Foley C. N. (2004) Chromatographic separation and multicollection-ICPMS analysis of iron. Investigating mass-dependent and -independent isotope effects. *Anal. Chem.* **76**, 5855–5863.
- Eberhardt P., Geiss J., Graf H., Grögler N., Mendoza M.D. and Mörgeli, M. (1972) Trapped solar wind gases in lunar fines and a breccia. *Lunar Planet. Sci. III*. Lunar Planet. Inst., Woodlands. #203(abstr.).
- Geiss J., Hirt P. and Leutwyler H. (1970) On acceleration and motion of ions in corona and solar wind. *Sol. Phys.* **12**, 458–483.
- Gold T., Campbell M.J. and O'Leary B.T. (1970) Optical and high-frequency electrical properties of the lunar sample. *Science* **167**, 707–709.
- Hapke B. (1973) Darkening of silicate rock powders by solar wind sputtering. *Moon* **7**, 342–355.
- Hapke B. (2001) Space weathering from Mercury to the asteroid belt. *J. Geophys. Res.* **106**, 10039–10073.
- Hapke B., Cassidy W. and Wells E. (1975) Effects of vapor-phase deposition processes on the optical, chemical, and magnetic properties of the lunar regolith. *Moon* **13**, 339–353.
- Hapke B., Cohen A.J., Cassidy W.A. and Wells E.N. (1970) Solar radiation effects on the optical properties of Apollo 11 samples. *Proc. Lunar Sci. Conf.* **3**, 2199–2212.
- Hashizume K. and Chaussidon M. (2005) A non-terrestrial (^{16}O -rich) isotopic composition for the protosolar nebula. *Nature* **434**, 619–622.
- Hashizume K., Chaussidon M., Marty B. and Robert F. (2000) Solar wind record on the moon: Deciphering presolar from planetary nitrogen. *Science* **290**, 1142–1145.
- Hashizume K., Chaussidon M., Marty B. and Terada K. (2004) Protosolar carbon isotopic composition: Implications for the origin of meteoritic organics. *Astrophys. J.* **600**, 480–484.

- Heiken G., Vaniman D. and French B.M. (1991) *Lunar Sourcebook: A User's Guide to the Moon*. Cambridge University Press.
- Housley R.M., Cirlin E.H., Goldberg I.B., Crowe H., Weeks R.A. and Perhac, R. (1975) Ferromagnetic resonance as a method of studying the micrometeorite bombardment history of the lunar surface. *Proc. Lunar Sci. Conf.* **6**, 3173–3186.
- Housley R.M., Grant R.W. and Paton N.E. (1973) Origin and characteristics of excess Fe metal in lunar glass welded aggregates. *Proc. Lunar Sci. Conf.* **4**, 2737–2749.
- Humayun M., Burnett D.S. and Jurewicz A.J.G. (2011) Preliminary magnesium isotopic composition of solar wind from Genesis SOS. *Lunar Planet. Sci. XLII*. Lunar Planet. Inst., Woodlands. #1211(abstr.).
- Hunten D.M. (1982) Thermal and nonthermal escape mechanisms for terrestrial bodies. *Planet. Space Sci.* **30**, 773–783.
- Ipavich F.M., Paquette J.A., Bochsler P., Lasley S.E. and Wurz P. (2001) Solar wind iron isotopic abundances: Results from SOHO/CELIAS/MTOF. *AIP Conf. Proc.* **598**, 121–126.
- Ireland T.R., Holden P., Norman M.D. and Clarke, J. (2006) Isotopic enhancements of O-17 and O-18 from solar wind particles in the lunar regolith. *Nature* **440**, 776–778.
- Jeans J.H. (1925) *The Dynamical Theory of Gases*. Cambridge University Press.
- Jull A.J.T., Lal D. and Donahue D.J. (1995) Evidence for a non-cosmogenic implanted C-14 component in lunar samples. *Earth Planet. Sci. Lett.* **136**, 693–702.
- Keller L.P. and McKay D.S. (1993) Discovery of vapor deposits in the lunar regolith. *Science* **261**, 1305–1307.
- Keller L.P. and McKay D.S. (1997) The nature and origin of rims on lunar soil grains. *Geochim. Cosmochim. Acta* **61**, 2331–2341.
- Kitts B.K., Podosek F.A., Nichols R.H., Brannon J.C., Ramezani J., Korotev R.L. and Jolliff B.L. (2003) Isotopic composition of surface-correlated chromium in Apollo 16 lunar soils. *Geochim. Cosmochim. Acta* **67**, 4881–4893.
- Korotev R.L. (1987) The nature of the meteoritic components of Apollo 16 soil, as inferred from correlations of iron, cobalt, iridium, and gold with nickel. *J. Geophys. Res.* **92**, E447–E461.
- Liu Y., Guan Y., Zhang Y., Rossman G.R., Eiler J.M. and Taylor L.A. (2012) Lunar surface water in agglutinates: origin and abundances. *Lunar Planet. Sci. XLIII*. Lunar Planet. Inst., Woodlands. #1864(abstr.).
- Liu Y., Spicuzza M.J., Craddock P.R., Day J.M.D., Valley J.W., Dauphas N. and Taylor L.A. (2010) Oxygen and iron isotope constraints on near-surface fractionation effects and the

composition of lunar mare basalt source regions. *Geochim. Cosmochim. Acta* **74**, 6249–6262.

Lodders K. (2003) Solar system abundances and condensation temperatures of the elements. *Astrophys. J.* **591**, 1220–1247.

Lodders K., and Fegley B. (1998) *The Planetary Scientist's Companion*, New York: Oxford University Press.

Lucey P., Korotev R.L., Gillis J.J., Taylor L.A., Lawrence D., Campbell B.A., Elphic R., Feldman B., Hood L.L., Hunten D., Mendillo M., Noble S., Papike J.J., Reedy R.C., Lawson S., Prettyman T., Gasnault O. and Maurice S. (2006) Understanding the lunar surface and space-moon interactions. *Rev. Mineral. Geochem.* **60**, 83–219.

Maréchal C.N., Télouk P. and Albarède F. (1999) Precise analysis of copper and zinc isotopic compositions by plasma-source mass spectrometry. *Chem. Geol.* **156**, 251–273.

McCord, T. B., Taylor, L. A., Combe, J. P., Kramer, G., Pieters, C. M., Sunshine, J. M. and Clark, R. N. (2011) Sources and physical processes responsible for OH/H₂O in the lunar soil as revealed by the Moon Mineralogy Mapper (M³). *J. Geophys. Res.* **116**, E00G05.

Moroz L.V., Fisenko A.V., Semjonova L.F., Pieters C.M. and Korotaeva N.N. (1996) Optical effects of regolith processes on S-asteroids as simulated by laser shots on ordinary chondrite and other mafic materials. *Icarus* **122**, 366–382.

Morris R.V. (1976) Surface exposure indices of lunar soils: a comparative FMR study. *Proc. Lunar Sci. Conf.* **7**, 315–335.

Moynier F., Albarède F. and Herzog G.F. (2006) Isotopic composition of zinc, copper, and iron in lunar samples. *Geochim. Cosmochim. Acta* **70**, 6103–6117.

Oetliker M., Hovestadt D., Klecker B., Collier M.R., Gloeckler G., Hamilton D.C., Ipavich F.M., Bochsler P. and Managadze G.G. (1997) The isotopic composition of iron in the solar wind: first measurements with the MASS sensor on the Wind spacecraft. *Astrophys. J.* **474**, L69.

Ong W. J., Floss C. and Gyngard F. (2012) Negative secondary ion measurements of ⁵⁴Fe/⁵⁶Fe and ⁵⁷Fe/⁵⁶Fe in presolar silicate grains from Acfer 094. *Lunar Planet. Sci. XLIII*. Lunar Planet. Inst., Woodlands. #1864(abstr.).

Pearce G.W., Strangway D.W. and Gose W.A. (1974) Magnetic properties of Apollo samples and implications for regolith formation. *Proc. Lunar Sci. Conf.* **5**, 2815–2826.

Pieters C.M., Goswami J.N., Clark R.N., Annadurai M., Boardman J., Buratti B., Combe J.P., Dyar M.D., Green R., Head J.W., Hibbitts C., Hicks M., Isaacson P., Klima R., Kramer G., Kumar S., Livo E., Lundein S., Malaret E., McCord T., Mustard J., Nettles J., Petro N., Runyon C., Staid M., Sunshine J., Taylor L.A., Tompkins S. and Varanasi P. (2009) Character and spatial distribution of OH/H₂O on the surface of the Moon seen by M³ on Chandrayaan-1. *Science* **326**, 568–572.

- Pieters C.M., Taylor L.A., Noble S.K., Keller L.P., Hapke B., Morris R.V., Allen C.C., McKay D.S. and Wentworth S. (2000) Space weathering on airless bodies: Resolving a mystery with lunar samples. *Meteorit. Planet. Sci.* **35**, 1101–1107.
- Poirras F., Halliday A. N., Lee D. C., Levasseur S. and Teutsch N. (2004) Iron isotope differences between Earth, Moon, Mars and Vesta as possible records of contrasted accretion mechanisms. *Earth Planet. Sci. Lett.* **223**, 253–266.
- Poirras F., Levasseur S. and Teutsch N. (2005) Significance of iron isotope mineral fractionation in pallasites and iron meteorites for the core-mantle differentiation of terrestrial planets. *Earth Planet. Sci. Lett.* **234**, 151–164.
- Poirras F., Roskosz M. and Corgne, A. (2009) No iron isotope fractionation between molten alloys and silicate melt to 2000 degrees C and 7.7 GPa: Experimental evidence and implications for planetary differentiation and accretion. *Earth Planet. Sci. Lett.* **278**, 376–385.
- Polyakov V.B. (2009) Equilibrium iron isotope fractionation at core-mantle boundary conditions. *Science* **323**, 912–914.
- Sasaki S., Nakamura K., Hamabe Y., Kurahashi E. and Hiroi, T. (2001) Production of iron nanoparticles by laser irradiation in a simulation of lunar-like space weathering. *Nature* **410**, 555–557.
- Schoenberg R. and von Blanckenburg F. (2006) Modes of planetary-scale Fe isotope fractionation. *Earth Planet. Sci. Lett.* **252**, 342–359.
- Shkuratov Y.G. (2012) Forgotten solar-wind iron implanted in lunar regolith. *Lunar Planet. Sci. XLIII*. Lunar Planet. Inst., Woodlands. #1286(abstr.).
- Sunshine J.M., Farnham T.L., Feaga L.M., Groussin O., Merlin F., Milliken R.E. and A'Hearn M.F. (2009) Temporal and spatial variability of lunar hydration as observed by the Deep Impact spacecraft. *Science* **326**, 565–568.
- Tang H., Wang S. and Li X. (2011) Simulation of nanophase iron production in lunar space weathering. *Planet. Space Sci.* **60**, 322–327.
- Taylor H.C.J. and Carter J.L. (1973) Silicate mineral chemistry of Apollo soils 15411, 15501, 66081, and 69941. *Lunar. Sci. IV*. Lunar Planet. Inst., Houston. #291(abstr.).
- Taylor L.A., Pieters C.M., Keller L.P., Morris R.V. and McKay D.S. (2001) Lunar mare soils: Space weathering and the major effects of surface-correlated nanophase Fe. *J. Geophys. Res.* **106**, 27985–27999.
- Taylor L.A., Rossman G.R. and Qi Q. (1995) Where has all the lunar water gone? *Lunar Planet. Sci. XXVI*. Lunar Planet. Inst., Woodlands. #1399(abstr.).
- Taylor P.D.P., Maeck R. and De Bièvre P. (1992) Determination of the absolute isotopic composition and atomic weight of a reference sample of natural iron. *Int. J. Mass Spectrom. Ion Processes* **121**, 111–125.

- Urey H.C. (1947) The thermodynamic properties of isotopic substances. *J. Chem. Soc.*, 562–581.
- Wang K., Moynier F., Dauphas N., Barrat J.-A., Craddock P. and Sio C. K. (2012) Iron isotope fractionation in planetary crusts. *Geochim. Cosmochim. Acta* **89**, 31–45.
- Wang K., Moynier F., Podosek F. and Foriel J. (2011) ^{58}Fe and ^{54}Cr in early solar system materials. *Astrophys. J.* **739**, L58.
- Wentworth S.J., Keller L.P., McKay D.S. and Morris R.V. (1999) Space weathering on the Moon: Patina on Apollo 17 samples 75075 and 76015. *Meteorit. Planet. Sci.* **34**, 593–603.
- Weyer S., Anbar A. D., Brey G. P., Munker C., Mezger K. and Woodland A. B. (2005) Iron isotope fractionation during planetary differentiation. *Earth Planet. Sci. Lett.* **240**, 251–264.
- Wiens R.C., Bochsler P., Burnett D.S. and Wimmer-Schweingruber R.F. (2004) Solar and solar-wind isotopic compositions. *Earth Planet. Sci. Lett.* **222**, 697–712.
- Wiesli R.A., Beard B.L., Taylor L.A., Johnson C.M. (2003) Space weathering processes on airless bodies: Fe isotope fractionation in the lunar regolith. *Earth Planet. Sci. Lett.* **216**, 457–465.
- Williams H. M., Markowski A., Quitte G., Halliday A. N., Teutsch N., and Levasseur S. (2006) Fe isotope fractionation in iron meteorites: New insights into metal-sulphide segregation and planetary accretion. *Earth Planet. Sci. Lett.* **250**, 486–500.
- Yakovlev O., Gerasimov M. and Dikov Y. (2011) Conditions of condensate rim formation on the surface of lunar regolith particles. *Geochem. Int.* **49**, 967–973

Appendix

DERIVATION OF EQUATION 1

Equation 1 describes iron isotopic fractionation during the classical thermal escape (Jeans escape). The derivation of equation 1 follows Criss (1999). Here briefly shows the development of this equation. Maxwell-Boltzmann distribution law describes the velocities of gas particles. The velocity probability p is defined as a function of temperature T , mass M , and velocity V .

$$p = 4\pi V^2 \left(\frac{M}{2\pi \mathbf{R}T} \right)^{3/2} e^{-MV^2/(2\mathbf{R}T)} \quad (\text{A.1})$$

where \mathbf{R} is the gas constant. The proportion of particles having velocities larger than the Moon escape velocity V_e (the high-velocity-tail of Maxwell-Boltzmann distribution visualized in Figure 4) can be calculated by integrating Equation A.1.

$$\Phi_{V>V_e} = \int_{V_e}^{\infty} p dV = \sqrt{\frac{2M}{\pi \mathbf{R}T}} V_e e^{-MV_e^2/(2\mathbf{R}T)} + 1 - \text{erf} \left(\sqrt{\frac{2M}{\pi \mathbf{R}T}} V_e \right) \quad (\text{A.2})$$

Consider half of the particles whose velocities larger than the Moon escape velocity have velocity directions toward the sky and could lose to the space (the rest half have directions toward the Moon and couldnot lose to the space). Then the particles stay on the Moon include both particles having velocities smaller than the Moon escape velocity and those having larger velocities but directions toward the Moon. The proportion of particles stays on the Moon could be written as following:

$$\Phi_{\text{stay}} = 1 - \frac{1}{2} \Phi_{V>V_e} \quad (\text{A.3})$$

For the two iron isotopes ^{54}Fe and ^{56}Fe , the isotopic ratio changed after loss to space because they have different mass M . The new isotopic ratio R_{new} can be written as following:

$$R_{\text{new}} = \frac{\Phi_{\text{stay}}^{56}}{\Phi_{\text{stay}}^{54}} R_{\text{source}} \quad (\text{A.4})$$

According to the definition of δ notation,

$$\delta^{56}\text{Fe}_{\text{new}} = \left(\frac{R_{\text{new}}}{R_{\text{referece}}} - 1 \right) \times 1000 \quad (\text{A.5})$$

$$\delta^{56}\text{Fe}_{\text{source}} = \left(\frac{R_{\text{source}}}{R_{\text{referece}}} - 1 \right) \times 1000 \quad (\text{A.6})$$

Hence,

$$\delta^{56}\text{Fe}_{\text{new}} = \frac{R_{\text{new}}}{R_{\text{source}}} \cdot (\delta^{56}\text{Fe}_{\text{source}} + 1000) - 1000 \quad (\text{A.7})$$

Substitute Equation A.4 and A.3 into Equation A.7,

$$\delta^{56}\text{Fe}_{\text{new}} = \frac{\Phi_{\text{stay}}^{56}}{\Phi_{\text{stay}}^{54}} \cdot (\delta^{56}\text{Fe}_{\text{source}} + 1000) - 1000 \quad (\text{A.8})$$

$$= \frac{\left(1 - \frac{1}{2}\Phi_{V>V_e}^{56}\right)}{\left(1 - \frac{1}{2}\Phi_{V>V_e}^{54}\right)} \cdot (\delta^{56}\text{Fe}_{\text{source}} + 1000) - 1000 \quad (\text{A.9})$$

$$= \frac{\left(2 - \Phi_{V>V_e}^{56}\right)}{\left(2 - \Phi_{V>V_e}^{54}\right)} \cdot (\delta^{56}\text{Fe}_{\text{source}} + 1000) - 1000 \quad (\text{A.10})$$

Finally, substitute Equation A.2 into Equation A.9,

$$\delta^{56}\text{Fe}_{\text{new}} = \frac{1 - \sqrt{\frac{2M^{56}}{\pi\mathbf{R}T}}V_e e^{-M^{56}V_e^2/(2\mathbf{R}T)} + \text{erf}\left(\sqrt{\frac{2M^{56}}{\pi\mathbf{R}T}}V_e\right)}{1 - \sqrt{\frac{2M^{54}}{\pi\mathbf{R}T}}V_e e^{-M^{54}V_e^2/(2\mathbf{R}T)} + \text{erf}\left(\sqrt{\frac{2M^{54}}{\pi\mathbf{R}T}}V_e\right)} \cdot (\delta^{56}\text{Fe}_{\text{source}} + 1000) - 1000 \quad (\text{A.11})$$

where M^{54} and M^{56} are the mass for the iron isotopes ^{54}Fe and ^{56}Fe , respectively.

CURRICULUM VITAE

Kun Wang

Department of Earth and Planetary Sciences
Washington University in St. Louis
1 Brookings Drive, Campus Box 1169
St Louis, MO 63130 (USA)

E-mail: wangkun@wustl.edu
Tel: (314)935-4023
Fax: (314)935-7361
cosmochem.wustl.edu

RESEARCH INTERESTS

- Origin of the Earth and of the Solar System
- Planetary differentiation: core-mantle segregation and crust formation
- Transition metal isotope geochemistry
- Analytical development and application of high precision isotopic measurements using Multi Collector Inductively Coupled Plasma Mass Spectrometry (MC-ICP-MS)

EDUCATION

2013 Ph.D. (Geochemistry)

Washington University in St. Louis

2011 A.M. (Geochemistry)

Washington University in St. Louis

2008 B.S. (Geology)

China University of Geosciences

EMPLOYMENT

2014 – Origins of Life Initiative Fellow

Harvard University

2009 – 2013 Research/Teaching Assistant

Washington University in St. Louis

2008 – 2009 Research Assistant

Chinese Academy of Sciences

HONORS AND AWARDS

- NASA Earth and Space Science Fellowship, 2012-2013
- Fifth LPI Career Development Award: Lunar and Planetary Institute, 2012
- Carl Tolman Prize for Outstanding Graduate Teaching Assistant: Washington University in St. Louis, 2011
- Graduating with Honors, Academic Record Outstanding Student, People's Scholarship, Tibet Zhongkai Mining Co. Ltd. Scholarship: China University of Geosciences, 2004-2008

PUBLICATION LIST

- Wang, K.**, Savage, P.S., Moynier, F. The Fe isotope composition of enstatite meteorites: implications for their origin and the metal/sulfide Fe isotopic fractionation factor. *Geochimica et Cosmochimica Acta*, in review.
- Wang, K.**, Day, J.M.D., Korotev, R.L., Zeigler, R.A., Moynier, F. Iron isotope fractionation during sulfide-rich felsic partial melting on early planetesimals. *Earth and Planetary Sciences Letters*, in review.
- Moynier, F., Fujii, T., **Wang, K.**, Foriel, J. Ab initio calculations of the Fe(II) and Fe(III) isotopic effects in citrates, nicotianamine, and phytosiderophore, and new Fe isotopic measurements in higher plants. *Comptes Rendus Geosciences*, **345**, 230-240.
- Wang, K.**, Moynier, F., Barrat, J-A., Zanda, B., Paniello, R.C., Savage, P.S. (2013) Homogeneous distribution of Fe isotopes in the early solar nebula. *Meteoritics & Planetary Sciences*, **48**, 354-364.
- Wang, K.**, Moynier, F., Podosek, F., Foriel, J. (2012) An iron isotope perspective on the origin of the nanophase metallic iron in lunar regolith. *Earth and Planetary Sciences Letters*, **337-338**, 17-24.
- Bishop, MC, Moynier F., Weinstein, C., Fraboulet, JG, **Wang, K.**, Foriel, J. (2012) The Cu isotopic composition of iron meteorites, *Meteoritics & Planetary Sciences*, **47**, 268–276.
- Wang, K.**, Moynier, F., Dauphas, N., Barrat, J.A., Craddock, P., Sio, C. (2012) Iron isotope fractionation in planetary crusts. *Geochimica et Cosmochimica Acta*, **89**, 31-45.
- Moynier, F., Blichert-Toft, J., **Wang, K.**, Herzog, G., Albarede, F. (2011) Elusive ^{60}Fe in the early solar system. *The Astrophysical Journal*, **741**, 71.
- Wang, K.**, Moynier, F., Podosek, F., Foriel, J. (2011) ^{58}Fe and ^{54}Cr in early solar system materials. *The Astrophysical Journal Letters*, **739**, L58.
- Weinstein, C., Moynier, F., **Wang, K.**, Paniello, R., Foriel, J., Catalano, J., Pichat, S. (2011) Isotopic fractionation of Cu in plants. *Chemical Geology*, **286**, 266-271.

CONFERENCE ABSTRACTS

- Wang, K.**, Moynier, F., Paniello, R.C. (2013) Iron isotopic fractionation during metal/silicate segregation in enstatite chondrite and aubrite parent bodies, *44th Lunar & Planetary Sci. Conf.* Abstract#: 2254.
- Wang, K.**, Moynier, F., Dauphas N., Barrat, J.-A., Day, J.M.D., Sio, C.K., Korotev, R.L., Zeigler, R.A. (2012) Iron isotopic fractionation in early planetary crusts, 2012 American Geophysical Union Fall Meeting. Abstract#: P44A-06.
- Wang, K.**, Moynier, F., Dauphas, N., Barrat, J-A., Craddock, P., Sio, C. (2012) Iron isotopic compositions of angrites and Stannern-trend eucrites, *43th Lunar & Planetary Sci. Conf.* Abstract#: 1146.
- Wang, K.**, Moynier, F., Podosek, F., Foriel, J. (2012) Iron isotope and the origin of nanophase iron in lunar regolith, *43th Lunar & Planetary Sci. Conf.* Abstract#: 1148.Huang, J., Xiao L., **Wang, K.** (2009) Xifeng circular basin: another failed potential crater in China, *40th Lunar & Planetary Sci. Conf.* Abstract#: 1035.